Durham E-Theses

The radio frequency and microwave dielectric properties of doped magnesium oxide

Enayati-Rad, Nasser

How to cite:

Use policy

THE RADIO FREQUENCY AND MICROWAVE

DIELECTRIC PROPERTIES OF DOPED

MAGNESIUM OXIDE

by

Nasser Enayati-Rad, B.Sc. (TABRIZ)

A Thesis submitted to the University of Durham

for the degree of

Doctor of Philosophy

Department of Applied Physics

and Electronics, Science Laboratories,

Durham City, England.

JUNE 1980

To my Wife

ABSTRACT

A study of the dielectric properties of pure magnesium oxide and MgO doped with iron or chromium is presented.   Measurements were carried out in the frequency range between 5×10^2 Hz and 9.3×10^9 Hz at room temperature using a.c. bridge, Q-meter, slotted-line and cavity methods.

The basic ideas and principles of each technique have been discussed individually in relation to their suitability for dielectric measurements on materials having particular characteristics. A major attempt has been made to develop the slotted-line technique (500 MHz-7.5 GHz) and the cavity resonator (9.3 GHz) method. Sources of possible error in these techniques have been investigated in detail and some suggestions made to minimize them. A new method for measuring the dielectric properties of low loss solids has been examined theoretically and some suggestions for its practical development pointed out.

The dielectric data obtained at room temperature has been analysed and interpreted in terms of the hopping theory involved in the "Universal Law" of dielectric response. The frequency variation of conductivity, followed $\sigma_{ac}(\omega) \propto \omega^n$ law   with $n = 0.98 \pm 0.02$ for pure MgO. The dielectric constant, ε', loss factor, ε'' and loss tangent, $\mathrm{Tan}\delta$, decrease slightly over the frequency range. Similar behaviour was also observed for Fe doped MgO and Cr doped MgO samples. The variation of ε' and ε'' both agree with the "Universal Law" showing that $\varepsilon'(\omega) \propto \omega^{n-1}$ and $\varepsilon''(\omega) \propto \omega^{n-1}$; the magnitude of n obtained was also 0.98. The data of ε' and ε'' approximately fit the Kramers-Kronig relation i.e.

$$\frac{\varepsilon''(\omega)}{\varepsilon'(\omega) - \varepsilon_\infty} = \cot \frac{n\pi}{2} = \text{constant} \quad \text{when } 0.5 < n < 1 .$$

Measurements were extended to higher temperatures (up to 700° C) using special apparatus which was designed for this purpose. The data obtained fit the Jonscher theory very well ; the exponent n decreases with increasing temperature and falls to a value of n = 0.5 at 700° C. In the high temperature range the Havinga proposal for the temperature dependence of dielectric constant was tested and the change of dielectric constant with temperature was found to agree well with the relation

$$\frac{1}{(\varepsilon'-1)(\varepsilon'+2)} \left\{ \frac{\partial \varepsilon'}{\partial T} \right\}_p = A + B + C$$

for MgO single crystal.

A detailed comparison is made of the effect of doping MgO with the trivalent ions Fe^{3+} and Cr^{3+}. The addition of either significantly increases the conductivity by an amount proportional to the concentration and this effect is explained in terms of an increase in the number of hopping sites available.

ACKNOWLEDGEMENTS

CONTENTS

CHAPTER 1

INTRODUCTION

1.1   OBJECTIVES

Magnesium oxide is of considerable importance as an electrical insulating material and its insulating properties have many various applications. It is widely used as an insulator in heating elements, and as the dielectric in mineral insulated cables. The study of the electrical conductivity of MgO as a function of the temperature and impurity content is also of considerable interest since this material is widely used in different branches of high temperature technology. It has been found that at high temperatures ($\sim 800^{\circ}$ C) the insulating behaviour of the MgO collapses ; consequently, it starts conducting and this effect leads rapidly to the failure of the heating element. For pure MgO the melting point is 2852° C and the boiling point is approximately, 3600° C.

Magnesia may be obtained in various forms and the material used here was single crystal which appeared to the eye to be of high quality even at the higher dopant concentrations. The pure single crystal is colourless and transparent while the powder of MgO is white. The addition of impurities causes colouration ; for example chromium doped crystals are green and iron doped crystals vary from light yellow-green to dark yellow-green, according to iron concentration.

In the present studies the dielectric properties, (and hence the electrical conductivity), of nominally pure magnesium oxide together with those of magnesium oxide doped with different concentrations of iron or chromium have been measured at room temperature over a very wide range of frequencies from 500 Hz to 9 GHz. The dopants Fe and Cr
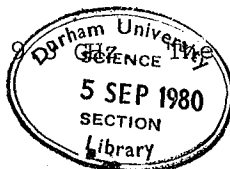
were chosen in order to see the effect of Cr^{3+} and Fe^{3+} ions on the electrical conductivity and dielectric constant behaviour of MgO. The samples have been tabulated in Table 1.1, according to nominal composition. The single crystals were grown by electrofusion from powders by W & C Spicer Ltd., Cheltenham, and all the measurements reported here were made on single crystal material. It was found that, at any particular frequency, the electrical conductivity of Fe or Cr doped magnesium oxide sample was higher than that of pure MgO, although the respective values of dielectric constant ε' were lower than for pure MgO. The variations of conductivity and dielectric constant versus frequency were investigated, and a decrease in ε' with increasing Fe or Cr concentration was also observed.

The measurements of dielectric properties and conductivity were also undertaken at temperatures up to $700^\circ C$ i.e. $\left(\dfrac{10^3}{T} \simeq 1.023 \; K^{-1} \right)$ in the frequency range from 500 Hz to 50 kHz.

The object of this work was to determine the dielectric behaviour of MgO, and in particular to examine the effects of doping with iron and chromium, as part of a systematic study of the effect of transition group dopant ions on the electrical characteristics of MgO. A considerable effort was directed towards finding the most appropriate methods for obtaining precision data since the changes in electrical properties due to doping were expected to be small, at least at the doping levels available. Thus the measurements of dielectric properties and conductivity were carried out using four different techniques, each technique covering a definite frequency range. The basic ideas involved in these techniques differ considerably and for this reason theoretical examinations of each technique were made in order both to assess the experimental errors associated with conventional practice and to develop new techniques which would give greater precision of measurement with dielectrics similar to magnesia. The interpretation of the data

Ref. No.	Nominal Composition
1	MgO (pure)
2	MgO + 310 ppm Fe
3	MgO + 2,300 ppm Fe
4	MgO + 4,300 ppm Fe
5	MgO +12,800 ppm Fe
6	MgO + 800 ppm Cr
7	MgO + 1,300 ppm Cr
8	MgO + 3,600 ppm Cr

TABLE 1.1 :   Nominal Composition of Samples

obtained has been discussed in terms of the hopping model of conductivity and some suggestions made regarding the correlation of conductivity results with structural information derived by different methods.

1.2   HISTORICAL REVIEW

Several determinations of the electrical conductivity of MgO have been published previously by a number of authors (1-23).   Most of these were made on single crystal material but there has been a considerable variation in the techniques of measurement used by different workers.   Thus in attempting to compare previous results it is often found that the purity of the samples was unknown ; that d.c. and a.c. techniques have been utilized, that the electrode materials which were evaporated on the samples were different, that the geometry of the elect-rode systems was not the same and finally that the atmospheres surround-ing the samples involved different gases.

Since it became clear from a brief review that the conduction mechanism is still not well defined, a wider literature survey has been undertaken.   In some early measurements on single crystal MgO, Yamaka and Sawamoto (1) suggested that at room temperature the charge carriers are electrons due to excess magnesium.   Their experiment was performed in oxygen and magnesium vapour ; it was observed that the conductivity increased after heating the sample in magnesium vapour.   They also proposed that this increase in conductivity might be due to surface conduction, since a two terminal measurement was utilized in their experiment.   Later, work by Surplice and Jones(18) showed that the conductivity was due to a motion of n-type electrons at temperatures in the range of $590^{\circ}-870^{\circ}$ C.   This was proved by determining the sign of the thermoelectric power.   Subsequently, Afzal et al (19) proved the idea of conduction by n-type electron by measuring the Seebeck coefficient of MgO ; Mitoff (2) also confirmed that (near room tempera-

ture) the conductivity is electronic rather than ionic. He also found

that introduction of iron in MgO sample considerably increases the

electrical conductivity. By contrast, Schmalzried (4) obtained

experimental evidence for ionic conduction. Later work by Mitoff (3)

showed that the nature of the charge carriers depends on temperature

and also on the impurity content of the crystal. He found that the

conductivity at low temperature is ionic but the nature of conduction

changes to electronic at high temperature (> 1000° C). In his

experiment, Mitoff measured the conductivity of pure MgO single crystal

and MgO doped with lithium. A small change in conductivity was observed.

Shakhtin et al (15) found that the introduction of iron in MgO affected

conductivity, which was increased. They suggested that iron atoms

occupy the position of Mg ions in the lattice and may be in either

divalent (Fe^{2+}) or trivalent (Fe^{3+}) states ; this could increase either

the ionic or electronic conductivity but, since the mobility of ions

is much less than that of electrons, it was deduced that electronic

conductivity predominates over the ionic conductivity. Zirkind and Freeman

(6) pointed out that the nature of electrical conductivity of MgO at

temperatures < 600°C is not known, a fact which probably initiated the

study of electrical conductivity of MgO by Lempicki (7), who also

concluded that it is likely to be electronic rather than ionic.

Davies (9) compared his results with those of previous workers and

concluded that the conduction in pure MgO was purely ionic. His

proposal is the most progressive theory reported recently. According

to him the conduction carriers in MgO are O^{2-} and Mg^{2+}. Pal'guev and Nevimin

(17) is one of the workers on conductivity of MgO who supports the

ionic conduction mechanism within a certain interval of temperature for

MgO.

Mitoff (12) later proposed that the conductivity of MgO is

partially electronic and partially ionic, the latter contribution being

due to the motion of magnesium ions. Choi et al (22) also concluded

that the mechanism of conduction in MgO single crystal is ionic rather

than electronic and, furthermore, reported that the addition of nickel

in MgO increases the electrical conductivity. An alternative model,

suggested by Day (13), is that the conduction process is due to holes

in the valence band, electrons being transferred from the valence band

to localized states above it. Further evidence for conduction by holes

was found by Yamaka and Sawamoto (14), whose results were similar to

those of Day. Finally, it may be noted that Mansfield (16) proposed

an electronic conduction mechanism for MgO single crystal in which the

charge carriers are holes.

Although there is conflicting evidence on the nature of the

mechanisms involved (24), it is generally held that ionic conductivity

predominates in the lower temperature range but that at high tempera-

tures (> 1300° C) the nature of conduction changes and electronic

conductivity predominates (3,11,16). However, the nature of the charge

carriers even in pure magnesium oxide has not been conclusively determined

though it is interesting to note that it has been suggested that there

may be vacancies associated with impurities.

The interpretation of quite a large number of measurements of

conductivity of MgO single crystal are based on ionic and/or electronic

conduction mechanisms. As an alternative approach, in this thesis the

hopping theory of the conduction has been adopted as the basis for

discussion since it has , over the past few years, been shown to be

applicable to a fairly wide range of low mobility materials. Thus an

attempt has been made to interpret the data in terms of Jonscher's

"Universal Law" in which the conductivity is assumed to arise from hopping

processes. The various proposals for the conduction mechanism in MgO

single crystals which have been made within the past thirty years by
various workers have been tabulated in Table 1.2.   This enables one to
have a brief and quick reference to the history of conduction mechanisms
and it is also a reliable illustration of the conflicting ideas on the
nature of the charge carriers. As it is seen most of the earlier theories
assumed that the conductivity was electronic, but the later theories
showed the presence of ionic conduction mechanisms.

Recently the Universal Law of dielectric behaviour has been
developed for materials in which conductivity occurs by hopping process.
The hopping mechanism has been reported by several authors, for example,
on n-type crystalline silicon with various kinds of impurities by Pollak
and Geballe (25). The idea of hopping mechanisms in MgO was suggested
for the first time by Lewis et al (8). They showed that mechanism of
conduction at lower temperatures could be controlled by electrons
hopping between impurities sites in the crystal. According to them, it
is more appropriate to consider localized electronic energy states at
impurities ; and conduction was due to thermally activated electrons
which are jumping from site to site. They also made calculations of
conductivity for pure MgO in terms of a model involving the hopping of
oxygen ions between two sites in the crystal.

The Universal Law has been tested for over sixteen different
materials and the results have been interpreted by Jonscher (26).   All
these indicated that the frequency dependence of the real part of the
conductivity follows

$$\sigma_{ac}(\omega) \propto \omega^n \qquad (1.1)$$

with always n < 1. The Jonscher "Universal Law" (27) can be written
in terms of the real part of the permittivity, ε' and the imaginary

Author Name	Year	Ref No.	Proposed Conduction Mechanism
Lempicki	1953	7	Electronic at low temperature.
Day	1953	13	p-type electronic due to excess of Mg.
Mansfield	1953	16	p-type electronic.
Yamaka & Sawamoto	1955	1	n-type electronic due to excess of Mg.
Yamaka & Sawamoto	1956	14	p-type electronic.
Mitoff	1959	2	electronic.
Schmalzried	1960	4	ionic.
Mitoff	1962	3	high-tem. electronic and low-tem. ionic.
Pal'guev	1962	17	ionic.
Davies	1963	9	ionic (Mg^{2+} and O^{2-}).
Zirkind	1964	6	electronic at low-tem.
Mitoff	1964	12	ionic at low-tem. and electronic at high-tem.
Surplice	1964	18	n-type electronic.
Budnikov	1964	20	n-type electronic and ionic.
Luzgin	1965	21	ionic.
Shakhtin	1967	15	electronics.
Lewis & Wright	1968	8	electron hopping at low-tem.
Lewis & Wright	1970	10	oxygen ion hopping.
Osburn	1971	23	ionic (Mg^{2+}).
Choi	1973	22	ionic.
Afzal	1974	19	n-type electronic.
Wilson	1979	24	ionic.
McMinn & Mauger	1979	11	electronic at high-tem. Ionic at low-tem.

TABLE 1.2 : Proposed conductivity mechanism in MgO.

part of it, ε ", respectively according to the relations,

$$\varepsilon'' (\omega) \propto \omega^{n-1} \tag{1.2}$$

and

$$(\varepsilon' - \varepsilon_\infty) \propto \omega^{n-1} \tag{1.3}$$

where again n <1 and ε_∞ , is the permittivity at very high frequency (limiting permittivity). Generally, it has been found that the magnitude of the conductivity is increased by the addition of impurities.

1.3   CRYSTALLOGRAPHIC ASPECTS

1.3.1 The Magnesium Oxide Structure

Magnesium oxide crystallizes in the sodium chloride-like structure, as do almost a third of the compounds of the type MX, where M denotes a metal ion or atom and X an electronegative element, e.g. oxygen, fluorine, chlorine, etc.   In the case of MgO, M and X mean magnesium and oxygen respectively.   Figure 1.1 provides an illustration of the MgO structure.   The lattice is face-centred cubic with one atom associated with each lattice point, Mg at (0,0,0) and oxygen at (0,0,½). Each of the two types of atom lies upon a face-centred cubic lattice, and each lies at the "largest interstice" of the other's f.c.c. lattice. Each atom being surrounded by six ions of the other type.

The largest interstice occurs at positions in the unit cell with coordinates (½,½,½) and equivalent positions (i.e. 0½0, 00½ and ½00). There are four of these per unit cell, hence one per lattice point ; one largest interstice is illustrated in Figure 1.2. In fact, from Figure 1.2 it is clear that each atom has a coordination number of six, the neighbours being at the vertices of a regular octahedron. It is known that the bonding between the ions is mainly ionic bonding but there is some evidence of covalent behaviour (30).
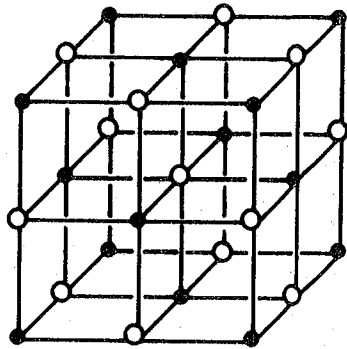
FIG.1.1   THE MAGNESIUM OXIDE LATTICE

• = MAGNESIUM   o = OXYGEN
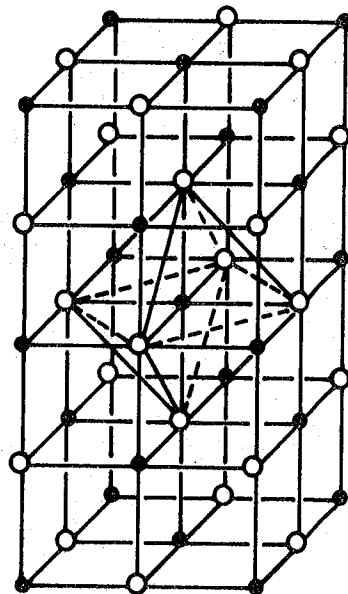
FIG.1.2   A LARGEST INTERSTICE IN
THE   MgO   LATTICE

• = Mg   o = OXYGEN

In this octahedral coordination the ionic radii, according to Kelly and Groves (29), are of 0.65 $\overset{o}{A}$ for the Mg^{2+} and 1.40 $\overset{o}{A}$ for the O^{2-}. The lattice parameter of the MgO, at $21^{o}C$, is given by Wyckoff (30) as a_{o} = 4.2112 $\overset{o}{A}$. Their positions are illustrated in two dimensional representation in Figure 1.3. In single crystals doped at low concentrations, such as the iron or chromium doped specimens used in the present experiment, it is generally assumed that the dopant enters the lattice substitutionally and that the average lattice parameter (or unit cell symmetry) is not changed.

1.3.2 The Crystal Field and Zero Field Splitting

By doping the MgO with iron, the latter is expected to go into the lattice by substitution of the magnesium sites. This assumption is based on the fact that the ferric ion (Fe^{3+}) has an ionic radius of 0.64 $\overset{o}{A}$ (29) which is almost the same as the corresponding ion Mg^{2+}. Although this assumption is fairly reasonable if one adopts the ionic radii as a point of comparison, there still remains to be considered the difference in electric charge between the trivalent doping ion and the divalent magnesium. The ferric ion with its five d electrons ($3d^{5}$) has a symmetrical charge distribution in its ground state but it is a poor fit in the magnesium oxide lattice because of the extra positive charge. Charge compensation in the crystal is affected either by excess oxygen ions (31) or by vacancies distributed at random throughout the crystal.

Considering then that the previous assumption is correct and bearing in mind Figure 1.2, it can be observed that the ferric ion will acquire an octahedral coordination and it is to be submitted to strong internal electric field exerted by the diamagnetic neighbours. In the main, the symmetry of this crystalline field will depend on the local arrangement of the diamagnetic ions rather than on the overall crystal

2.12 Å

4.2112 Å

1.40

O^{2-} ION

0.65
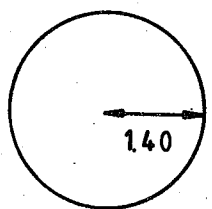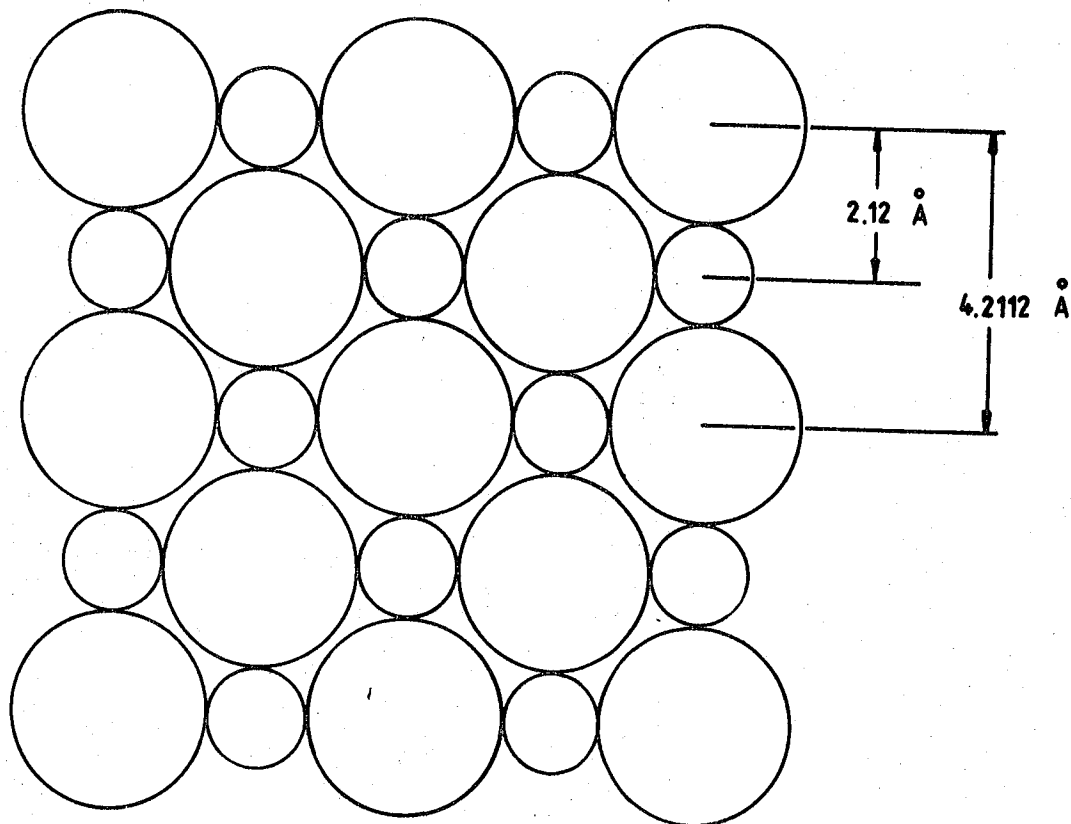
Mg^{2+} ION

FIG.1.3   TWO DIMENSIONAL REPRESENTATION
OF THE MAGNESIUM OXIDE LATTICE.

symmetry ; the strength of the field being dependent on the distribution of the charges, on the amount of the charges of the various ions and on the distance of these charges from the paramagnetic ion. The action of this crystalline field is to shift and split the electronic energy levels. This splitting, in the absence of an external magnetic field, is known as "zero field splitting". The character of the splitting of energy levels of paramagnetic ions by the crystalline field depends to a great extent on the symmetry of this field. This circumstance enabled Bethe (32) to obtain a qualitative solution of the problem with the aid of group theory.

The ion Fe^{3+} has a ground state of $^6S_{5/2}$, and the resultant orbital momentum of the electrons equals zero. Through the spin-orbit interaction a crystalline field of cubic symmetry, as it will approximately result from the octahedral arrangement of the six oxygens surrounding each paramagnetic ion, splits the sixfold degeneracy into a twofold degenerate level and a fourfold degenerate level (32). Van Vleck and Penney (33) have discussed the mechanism by which such a splitting can be effected and have shown that the crystalline cubic field can influence the electron spins only through high order interactions involving spin-orbit coupling with excited states. When the spin-orbit coupling interaction is much less than the crystal field splitting, the wave function of the ground crystal field state will contain admixtures of the next higher state, and as a result of this admixture the g-factor of a transition-metal ion deviates from its free electron value by a term that is proportional to the spin-orbit coupling constant and inversely proportional to the crystal field splitting. For the ferric ion in the magnesium oxide lattice, Low (34) has found the zero field splitting to be $3a = 615 \times 10^{-4}$ cm^{-1} ; this value corresponds to a magnetic field of 658 Gauss (35). Figure 1.4 shows a diagram of the zero field
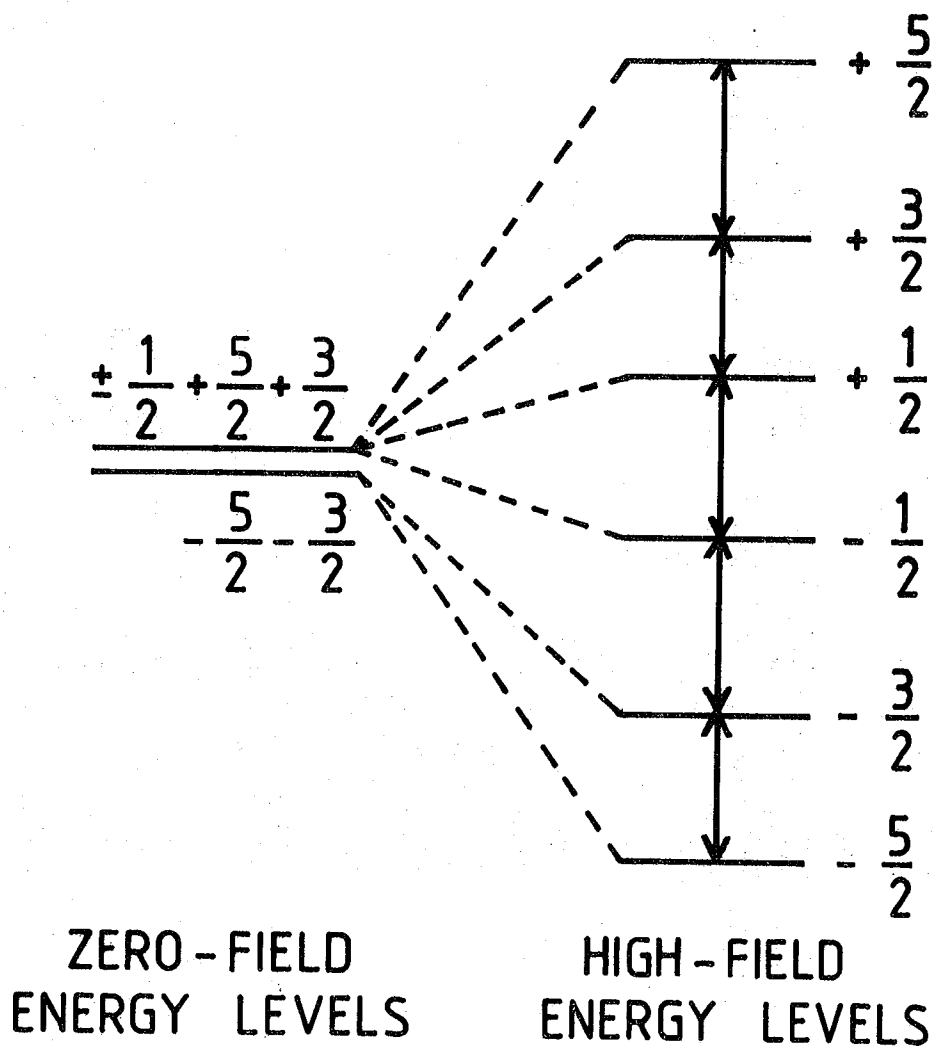
FIG.1.4 ENERGY LEVELS OF THE $^6S_{\frac{5}{2}}$ STATE IN A CUBIC FIELD WITH ZERO FIELD SPLITTING OF $3a = 658$ GAUSS.

splitting of the $^6S_{5/2}$ state in a cubic field.

It will appear in subsequent Chapters that detailed structural information is important for the primary task of enabling an adequate characterisation of each specimen (particularly the doped specimens) to be made. For this purpose extensive electron spin resonance studies of various transition group ions in MgO have been carried out independently in the Department and use of this data has been made to confirm that, at the concentrations used, the iron and chromium did enter the lattice substitutionally at Mg^{2+} sites and that they were present as Fe^{3+} and Cr^{3+} respectively.

1.4   <u>REFERENCES</u>

1.   Yamaka E. and Sawamoto K, 'Electrical Conductivity and Thermo-Electric Motive Force in MgO Single Crystal', Journal of Physical Society of Japan, Vol.10, No.3, pp 176-9, (1955).

2.   Mitoff S.P, 'Electrical Conductivity of Single Crystal of MgO', Journal of Chemical Physics, Vol.31, pp 1261-9, (1959).

3.   Mitoff S.P, 'Electronic and Ionic Conductivity in Single Crystal of MgO', Journal of Chemical Physics, Vol.36, No.5, pp 1383-9,(1962).

4.   Schmalzried H, 'Electrical Conduction in MgO', Journal of Chemical Physics, Vol.33, pp 940,(1960).

5.   Mitoff S.P, 'The Comment on Dr.Schmalzried's Letter', Journal of Chemical Physics, Vol.33, pp 941, (1960).

6.   Zirkind P. and Freeman E.S, 'Effect of Radiation on the Electrical Conductivity of Magnesium Oxide', Journal of Chemical Physics, Vol.41, pp 906-7, (1964).

7.   Lempicki A, 'The Electrical Conductivity of MgO Single Crystal at High Temperatures', Proceedings of the Physical Society, Vol.66B, pp 281-3, (1953).

8.   Lewis T.J. and Wright A.J, 'The Electrical Conductivity of Magnesium Oxide at Low Temperatures', Journal of Physics, Vol.D1, pp 441-7, (1968).

9.   Davies M.O, 'Transport Phenomena in Pure and Doped Magnesium Oxide', Journal of Chemical Physics, Vol.38, No.9, pp 2047-55,(1963).

10.   Lewis T.J. and Wright A.J, 'The Electrical Conductivity of Magnesium Oxide at High Field', Journal of Physics, Vol.D3,pp 1329-39,(1970).

11.   McMinn K.W. and Mauger R.A, 'Third International Conference on Dielectric Materials, Measurements and Applications', IEEE Conf. Public. 177 (1979).

12. Mitoff S.P, 'Bulk Versus Surface Conductivity of MgO Crystal', Journal of Chemical Physics, Vol.41,pp 2561-2,(1964).

13. Day H.R, 'Irradiation-Induced Photoconductivity in Magnesium Oxide', Physical Review, Vol.91, pp 822-7, (1953).

14. Yamaka E. and Sawamoto K, 'Photo-induced Hall Effect in MgO', Physical Review, Vol.101, pp 565-6, (1956).

15. Shakhtin D.M, Levintovich E.V, Pivovar T.L. and Eliseeva G.G, 'Influence of Impurity Oxides on the Electrical Resistance of MgO at High Temperatures', Teplofizika Vysokich Temperature (High Temperatures), Vol.5, Part 3, pp 454-7, (1967).

16. Mansfield R, 'The Electrical Conductivity and Thermoelectric Power of Magnesium Oxide', Proceedings of the Physical Society, Vol.66B, pp 612-4, (1953).

17. Pal'guev, S.F. and Nevimin A.D, 'On the Nature of the Electrical Conductivity of Beryllium, Magnesium, Calcium and Strontium Oxides at High Temperatures', Soviet Physics Solid State, Vol.4, No.4, pp 629-32, (1962).

18. Surplice N.A. and Jones R.P, 'The Thermoelectric Power and Electrical Conductivity of Calcium and Magnesium Oxides', British Journal of Applied Physics, Vol.15, pp 639-42, (1964).

19. Afzal F.A. and Giutronich J.E, 'A Graphite Tube Electronic Furnace Capable of Fast Heating and Cooling, and its Use in Measuring Electrical Properties of Magnesium Oxide Single Crystal', Journal of Physics E, Vol.7, pp 579-82, (1974).

20. Budnikov P.P. and Yanovskii V.K, 'The Electrical Conductivity of Semicrystalline Spectroscopically Pure Magnesium Oxide', Journal of Applied Chemistry of the USSR (Zh.Prikl.Khim), Vol.37, Part 6, pp 1249-57, (1964).

21. Luzgin V.P, Frolov A.G, Vishkarev A.F, Vinogradova L.V, and Rutman D.S, 'The Nature of the Conductivity of MgO and Al_2O_3' Refractories (USSR), Vol.4, pp 202-4, (1965).

22. Choi J.S, Lee H.Y. and Kim K.H, 'Electrical Conductivity of Nickel Oxide-Magnesium Oxide Single Crystals', Journal of Physical Chemistry , Vol.77, pp 2430-3, (1973).

23. Osburn C.M and Vest R.W, 'Electrical Properties of Single Crystals, Bicrystals, and Polycrystals of MgO', Journal of the American Ceramic Society, Vol.54, No.9, pp 428-35, (1971).

24. Wilson I.O, 'Magnesium Oxide as a High Temperature Insulant in Mineral-Insulate Cables', IEE Conference Publication, No.177, Third International Conference on Dielectric Materials, Measurements and Applications, (1979).

25. Pollak M. and Geballe, 'Low Frequency Conductivity due to Hopping Processes in Silicon', Physical Review, Vol.122, No.6, pp 1742-53, (1961).

26. Jonscher A.K, 'The Role of Contacts in Frequency Dependent Conduction in Disordered Solids', Journal of Physics C, Solid State Physics, Vol.6, pp L235, (1973).

27. Jonscher A.K, 'Low-Frequency Dispersion in Carrier-Dominated Dielectric', Philosophical Magazine, B, Vol.38, No.6,pp 587-601,(1978).

28. Mott N.F. and Gurney R.W, 'Electronic Processes in Ionic Crystals', Dover Publications, New York, 1964.

29. Kelly A. and Groves C.W, 'Crystallography and Crystal Defects', Longman Group Ltd, London, (1970).

30. Wyckoff R.W.G, 'Crystal Structure, Vol.I, Interscience Publishers, New York, (1965).

31. Wertz J.E. and Auzins P, 'Crystal Vacancy Evidence from Electron Spin Resonance', Physical Review, Vol.106, pp 484-8, (1957).

32.   Bethe V.H, 'Termaufspaltung in Kristallen', Annalen der Physik, Vol.3, pp 133-208, (1929).

33.   Van Veck, J.H. and Penney W.G, Philosophical Magazine, Vol.17 pp 961, (1934).

34.   Low W, Ann New York, Academy of Sciences, Vol.72, pp 69, (1958).

35.   Low W, Physical Review, Vol.105, pp 792, (1952).

CHAPTER 2

DIELECTRIC THEORY

2.1 DIELECTRIC PROPERTIES OF MATERIAL

There is a complex parameter for any dielectric material which
determines its behaviour in the presence of an electric field. It is a
physical parameter which indicates the usefulness of the dielectric
material for any specific electric field application. This parameter is
usually called the complex dielectric constant or permittivity which is
generally represented by ε^*. It is shown by $\varepsilon^* = \varepsilon_o$ for free space or
vacuum ($\varepsilon_o = \dfrac{10^7}{4\pi C^2} = 8.8542 \times 10^{-12}$ F m^{-1}). The quantity ε^* is
usually used in the form of a normalized complex dielectric constant (ε_r)
or relative permittivity, i.e.

$$\varepsilon_r = \frac{\varepsilon^*}{\varepsilon_o} = \varepsilon' - j\,\varepsilon'' \qquad (2.1)$$

For free space its value is equal to unity. Separating real and imaginary
parts of both sides gives,

$$\varepsilon' = R_e \left\{ \frac{\varepsilon^*}{\varepsilon_o} \right\} \qquad (2.2)$$

and

$$\varepsilon'' = I_m \left\{ \frac{\varepsilon^*}{\varepsilon_o} \right\} \qquad (2.3)$$

ε' is called the real part of the complex dielectric constant, and ε'' is the
imaginary part of the complex dielectric constant or more usually, loss
factor. In these equations, the real part ε', directly represents the
amount of energy which can be stored by the applied electric field in a
dielectric material. Alternatively it can be thought of as a parameter

of the dielectric that determines its ability to form a capacitance
because inserting a slab of dielectric in a capacitor increases the
capacity by a factor of ε'. On the other hand, the imaginary part, ε''
is a direct measure of how much energy is dissipated in the form of heat.
The relative permittivity, then can be written as,

$$\varepsilon_r = \varepsilon' (1 - j \, Tan \, \delta) \qquad (2.4)$$

where

$$Tan \, \delta = \frac{\varepsilon''}{\varepsilon'} \qquad (2.5)$$

Tan δ is proportional to the ratio of the power lost in heat, to the
energy stored per cycle in the dielectric material. It is called the
loss tangent. Therefore, the loss tangent is a useful factor in electronic
engineering and material science for determining the power loss.

The complex relative permittivity and its real (ε') and
imaginary (ε'') components with their associated loss angle are illustrated
vectorially in Figure 2.1. generally for small δ, Tan $\delta \simeq$ sin δ.

The quantities ε' and ε'' are both dimensionless, because it is
assumed that all values are relative to free space ; therefore they
preserve their values irrespective of the selected system of units.

2.2   POLARIZATION

2.2.1 General Description

There are no free charges in an ideal dielectric material.
Since all materials are composed of atoms, therefore they can be assumed
as charge entities in it. These atoms of a dielectric are normally
affected by an applied electric field. The result of this field is a
force which is exerted on each charged particle. Therefore the particles
with positive electric charge are being pushed in the direction of the
field, and those with negative charge oppositely. As a result the

positive and negative charged particles of each atom are displaced from their equilibrium positions in opposite directions. These displacements, however, are sometimes limited, i.e. in most cases to very small fractions of an atomic diameter. From the macroscopic point of view, all efforts may be easily assumed as a displacement of the entire positive charges relative to the negative charges throughout the dielectric. This condition of a dielectric is called polarization. Most authors have shown that the polarization of a dielectric depends on the total electric field in the material, i.e.

$$P = \alpha E \qquad\qquad (2.6)$$

where α is polarizability factor. The polarization is also defined as electric dipole moment per unit volume (36) i.e. it is the sum of n electric dipole moments in a unit volume,

$$P = \sum_{n} P_i \qquad\qquad (2.7)$$

It is obvious that the degree of the polarization depends on the electric field and the properties of the atoms which make the material. In isotropic materials the polarization has the same direction as the electric field causing it. Therefore, polarizability, α, is a scalar quantity. In anisotropic materials polarization has different values in each direction, so α will be a tensor quantity.

The polarization, P and electric displacement, D and electric field E are related to each other (36-38), by

$$D = P + \varepsilon_o E \qquad\qquad (2.8)$$

and

$$D = \varepsilon_o \varepsilon_r E \qquad\qquad (2.9)$$

From Eqns. 2.8 and 2.9, a relation between polarization and complex relative

dielectric constant may be obtained as,

$$P = \varepsilon_o E (\varepsilon_r - 1)$$ (2.10)

From this equation, it is easily deduced that the magnitude of relative permittivity, ε_r, must be greater than unity, otherwise this equation will not have physical significance.

Since there is always the possibility of a phase lag developing between the applied field and the instantaneous polarization, the relative permittivity, ε_r, can be expressed in terms of real and imaginary parts, (Eqn. 2.1).

There are three mechanisms of polarization, namely

1. Electronic Polarization

2. Ionic Polarization

3. Dipole Orientation

These mechanisms will be summarized in the following sections.

2.2.2 Electronic Polarization

It is known that in any dielectric material the positive atomic nucleus is surrounded by a cloud of negative electrons. By applying an external electric field to the material, the electrons are slightly displaced relative to the nucleus and an electric dipole moment is created ; electronic polarization has occurred in the system. It is shown schematically in Fig 2.2. This polarization is established during a very brief interval of time (10^{-15} s) which corresponds to the ultra-violet range of wavelength.

Since this mechanism of polarization occurs in all atoms or ions, it can be observed in all dielectrics irrespective of whether other types of polarization are displayed. This polarization satisfies Maxwell's theory, i.e.

$$\varepsilon = u^2$$ (2.11)

where μ is the refractive index at optical wavelengths.

2.2.3 Ionic Polarization

In this polarization, the positive and negative ions in a partially ionic solid are displaced relatively from their equilibrium positions when an external electric field is applied. This is shown in Fig 2.3. The charge displacement polarizes the ions and produces an induced electric moment. This polarization also arises from the displacement of the nuclei and it is frequency dependent in the infrared region, when the applied frequency approaches that of the molecular vibration. Although only a short time is required for this process of ionic polarization to set in, it is longer than for electronic polarization (about 10^{-13} to 10^{-12} s). In the presence of ionic polarization Maxwell's equation (2.11) does not hold ; in this case $\varepsilon > \mu^2$.

2.2.4 Dipole Orientation

When an external electric field is applied to a slab of dielectric material, atoms with displaced positive and negative charges of equal magnitude (dipole) relative to each other tend to orient themselves in a direction opposite to that of the applied electric field, Fig 2.4. It is known that the electric field is directed from positive to negative charges but the orientation of dipoles in the material is in opposition to it. This, therefore, results in a reduced internal electric field compared with the applied field.

Assuming that all the molecules are oriented with their dipole axes in the direction of the field, a permanent moment will therefore be added to the induced moment. The orientation of the molecules is however opposed by their thermal motion, which varies with temperature. As a result at high temperatures the thermal motion practically prevents the orientation of the molecules and hence the polarization is reduced.

Debye has derived the polarization for polar molecules and
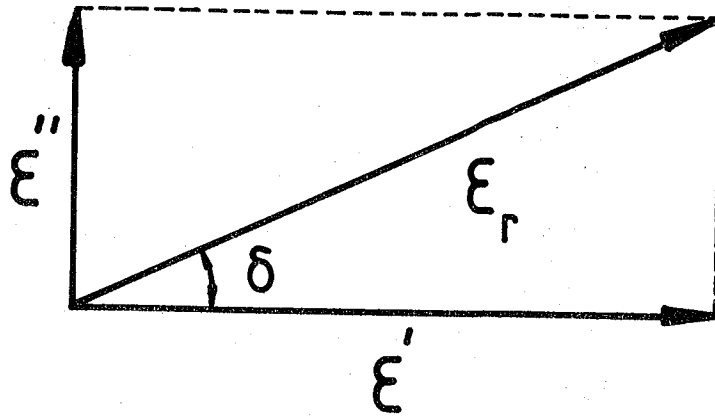
FIG.2.1   COMPONENTS OF RELATIVE DIELECTRIC
CONSTANT.
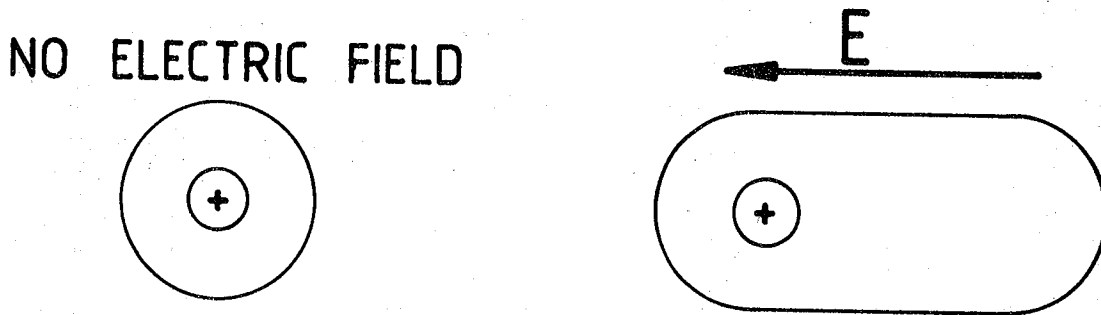
FIG.2.2   ELECTRONIC POLARIZATION.
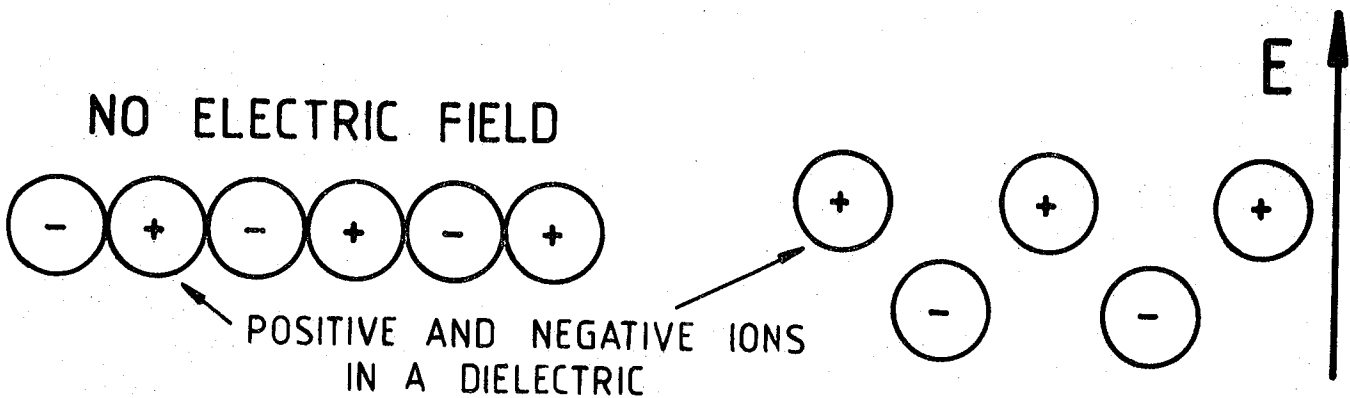
FIG.2.3 IONIC POLARIZATION.

showed that molecules with zero rotational energy contribute to orientation polarizability and that the number of this kind of molecule decreases with increasing temperature. Dipole polarization can appear in pure form only in gases, liquids and amorphous bodies. In crystalline bodies at temperatures below the melting point, the dipoles are frozen and so they can not be oriented and dipole polarization cannot occur in them.

The dipole in the material will rotate through an angle of 180° when the applied electric field changes its direction with the frequency of f. On increasing the frequency the chance of changing dipole direction becomes smaller and it will not be able to be in time.

2.3   DIELECTRIC LOSS ANGLE

If it is assumed that the power is not dissipated at all in the ideal dielectric of the capacitor, the phasor of current would be ahead of the phasor of electric field, E, precisely by 90° and the current would be purely reactive, as is shown in Fig 2.5.

In practice the phase angle, ϕ, is slightly less than 90°, and

$$I_t = I_a + I_r \tag{2.12}$$

where I_t = total current

I_a = active component = $E \omega \varepsilon' C$

I_r = reactive component = $E \omega \varepsilon'' C$

Since the phase angle, ϕ , is very close to 90° in a high quality dielectric capacitor. The angle δ is defined by

$$\delta = 90^{\circ} - \phi \tag{2.13}$$

ELECTRIC DIPOLES

(a)

(b)

E
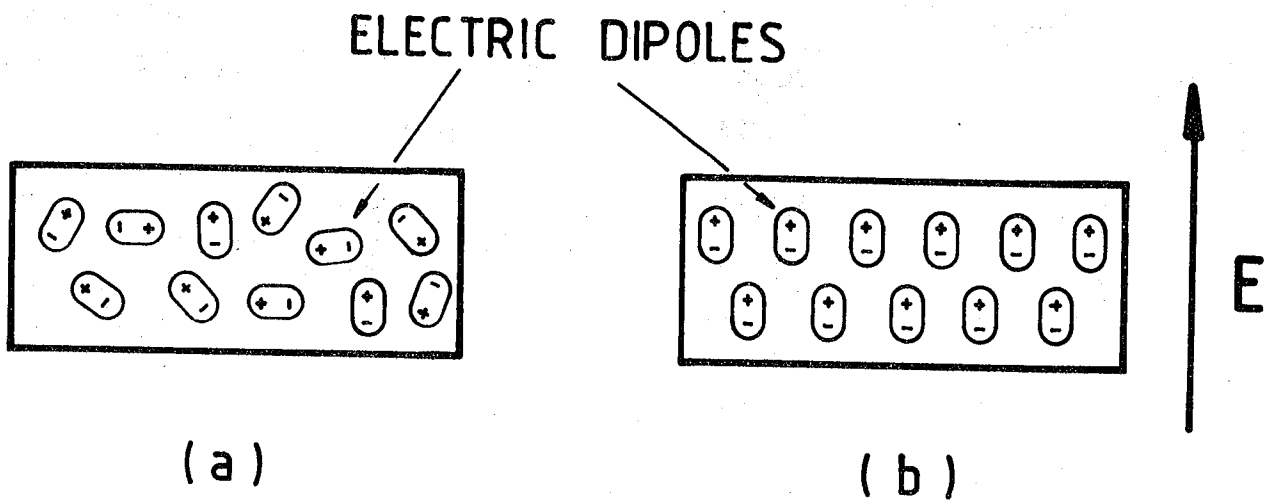
FIG.2.4   DIPOLE ORIENTATION; (a) RANDOM DIPOLES
IN AN UNCHARGED DIELECTRIC.
(b) ORIENTATION POLARIZATION BY AN
ELECTRIC FIELD.

I_a

I_t

δ

I_r

E
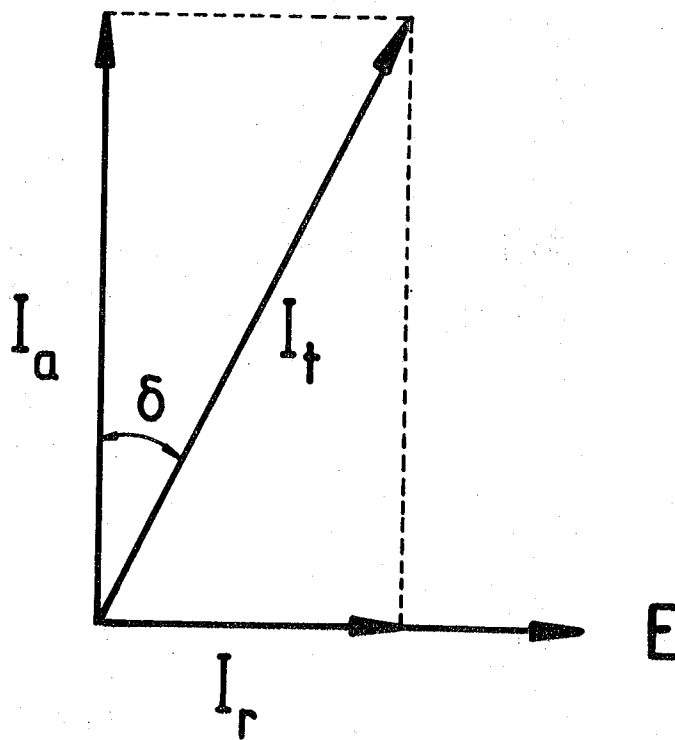
FIG.2.5   VOLTAGE - CURRENT DIAGRAM OF A
DIELECTRIC WITH LOSS.

The angle δ is called the dielectric loss angle ; and

$$\text{Tan } \delta \;=\; \frac{I_r}{I_a} \;=\; \frac{E\left|\omega\varepsilon''\, c\right|}{E\left|\omega\varepsilon'\, c\right|} \;=\; \frac{\varepsilon''}{\varepsilon'} \tag{2.14}$$

This parameter is very important for a dielectric material and it is called the loss tangent (Tanδ). Sometimes the quality factor of a dielectric is specified and this is given by $Q = \dfrac{1}{\text{Tan } \delta}$.

2.4   FREQUENCY DEPENDENCE OF ε' AND ε''

As noted before, the time required for electronic or ionic polarization to be established is very small compared with the period of the applied field.   For this reason there is no reason to expect that any frequency dependence should appear in such dielectrics.   This is not so in the case of the dipole polarization mechanism ; the value of ε' of a polar dielectric begins to drop when the frequency begins to increase.   By removing the applied electric field all the dipoles in the material relax to a new equilibrium position and the polarization decays exponentially.   The relaxation time is defined as the time in which the polarization is reduced to $\dfrac{1}{e}$ times its original value.   Debye states that dielectric relaxation is the lag in dipole orientation behind the applied alternating electric field.   The relaxation time, τ , depends on the various factors such as, the viscosity of the medium, the size of the polar molecules, the frequency and the temperature of the material. If the polar molecules are large, or the viscosity of the medium is high, or the frequency of the applied field is high, the rotary motion of molecules becomes out of step with the field and the polarization will acquire an out-of-phase component.   Thus the displacement current acquires a conductance component in phase with the field which results in a thermal dissipation of energy (Fig 2.5).

The dependence of ε' and ε'' on frequency are shown in Fig 2.6. As the frequency is increased it is reasonable to expect that the total polarization will decrease and hence ε' will decrease. All of the energy applied to the material by the electric field is not used to orient the dipoles, but some is lost to the material by increasing the random thermal motion that exists in every substance. Therefore as ε' decreases, ε'' should increase. This phenomenon is shown in Fig 2.6.

The reduction in ε' in the frequency region near 10^6 Hz is due to dipolar polarization, whereas at regions near 10^{12} and 10^{15} Hz, atomic and electronic polarizations are responsible. As the frequency increases above $f = 10^6$ Hz the contribution of the dipole orientation eventually disappears, and the permittivity levels off at a lower value ε_∞. Where $f > 10^{15}$, i.e. in the visible frequency range, a final limiting value of $\varepsilon' = \mu^2$ (Maxwell's equation) can be reached. At zero frequency (d.c. field), $\varepsilon = \varepsilon_s$, where ε_s is equal to the static value of dielectric constant.

There is a relation between ε_∞, ε_s and frequency which is known as the Debye equation (37,39,40). It can be derived from the relation,

$$\varepsilon^* = \varepsilon_\infty + \frac{\varepsilon_s - \varepsilon_\infty}{1 + j \omega \tau} \tag{2.15}$$

Introducing $\varepsilon^* = \varepsilon' - j\varepsilon''$ and comparing real and imaginary parts yields,

$$\varepsilon'(\omega) = \varepsilon_\infty + \frac{\varepsilon_s - \varepsilon_\infty}{1 + \omega^2 \tau^2} \tag{2.16}$$

and

$$\varepsilon''(\omega) = \frac{(\varepsilon_s - \varepsilon_\infty) \omega \tau}{1 + \omega^2 \tau^2} \tag{2.17}$$

where τ = relaxation time and ε_∞ and ε_s are as defined before. Equations 2.16 and 2.17 are called the Debye equations. Their ratio is
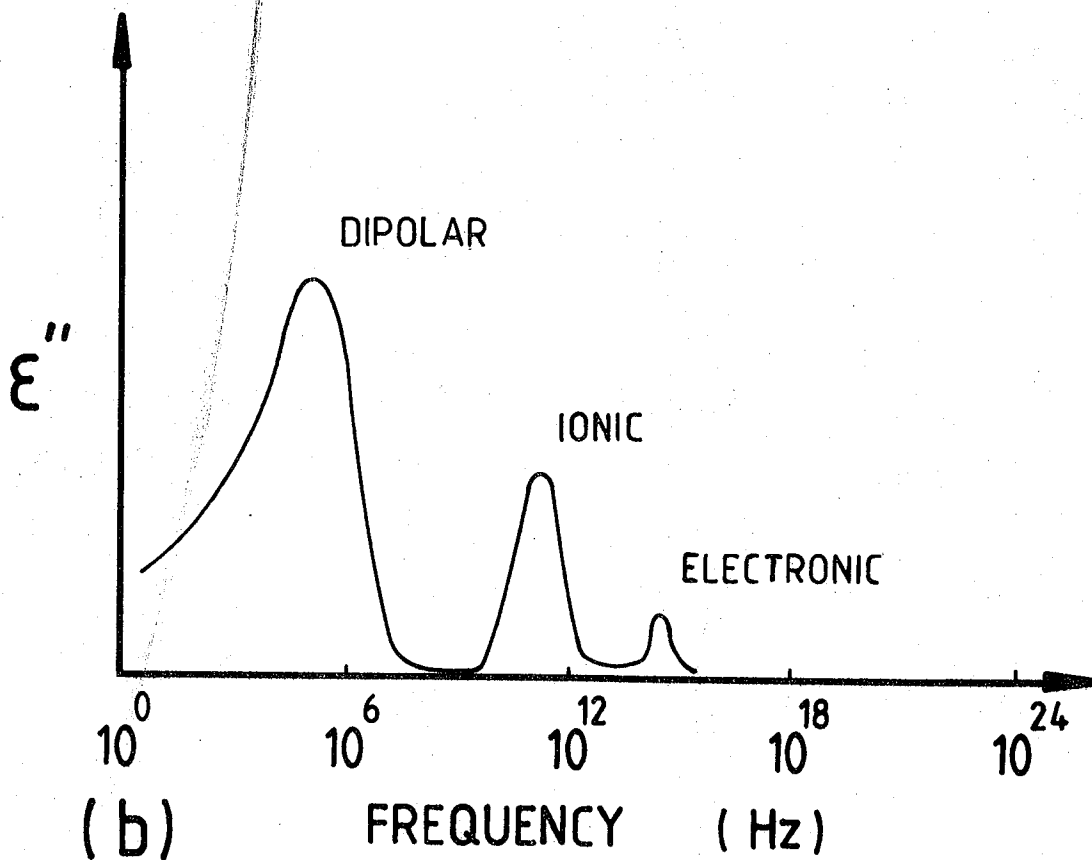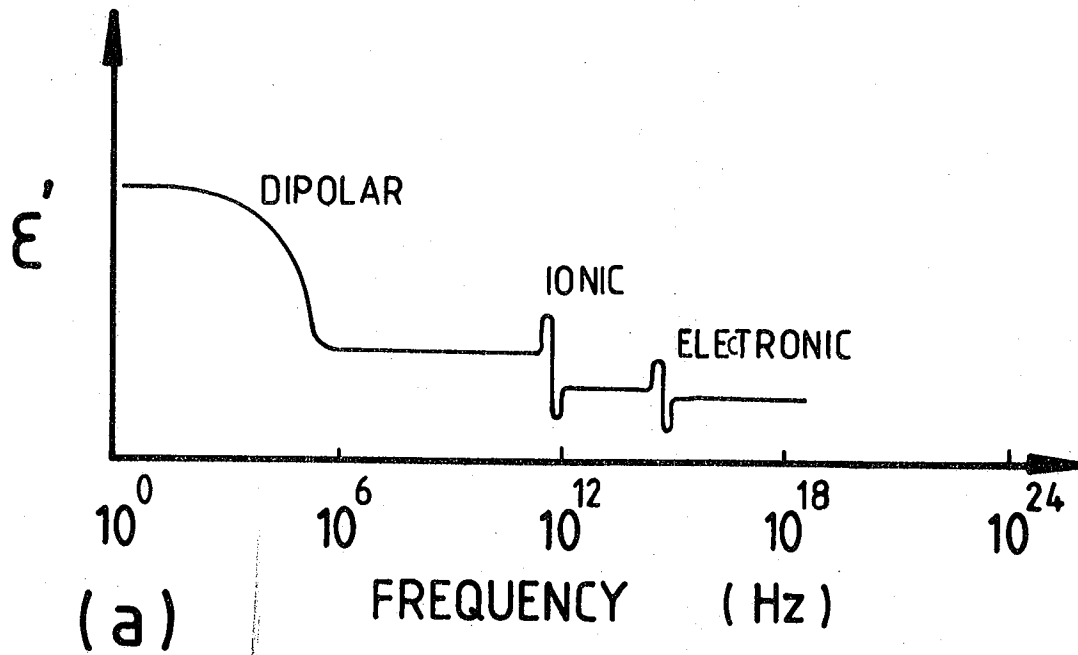
FIG.2.6   FREQUENCY BEHAVIOUR OF (a)
DIELECTRIC CONSTANT AND (b) LOSS FACTOR.

$$\frac{\varepsilon''(\omega)}{\varepsilon'(\omega) - \varepsilon_\infty} = \omega\tau \qquad (2.18)$$

These equations are plotted in Fig 2.7. Eliminating $\omega\tau$ between eqns. 2.16 and 2.17 gives

$$\left[\varepsilon' - \frac{\varepsilon'_s - \varepsilon_\infty}{2}\right]^2 + \varepsilon''^2 = \left[\frac{\varepsilon_s - \varepsilon_\infty}{2}\right]^2 \qquad (2.19)$$

which is the equation of a circle. Since the $\varepsilon'' > o$ a semicircle will be physically meaningful. The Debye semicircle has the advantage of giving a representation of a simple relaxation process when the relative permittivities ε', ε'' are plotted on a complex plane.

The a.c. electrical conductivity can be represented by,

$$\sigma_{ac}(\omega) \propto \frac{\omega^2}{1 + \omega^2\tau^2} \qquad (2.20)$$

this applies only for dipolar processes ; as can be seen at frequencies $f < \frac{1}{\tau}$, σ_{ac} is proportional to ω^2. This result differs from that obtained on the hopping model.

2.5   TEMPERATURE DEPENDENCE OF DIELECTRIC CONSTANT

In solid dielectric materials the nature of the dependence of dielectric constant on temperature may be determined by various factors. In most cases when the temperature increases, the ionic mechanism of polarization increases and hence the magnitude of ε' will be increased. In contrast, the increase of temperature does not affect the electronic polarization. On the other hand the dipole orientation contribution is also directly proportional to the temperature, i.e. the temperature facilitates the rotation of dipoles in an applied electric field. In
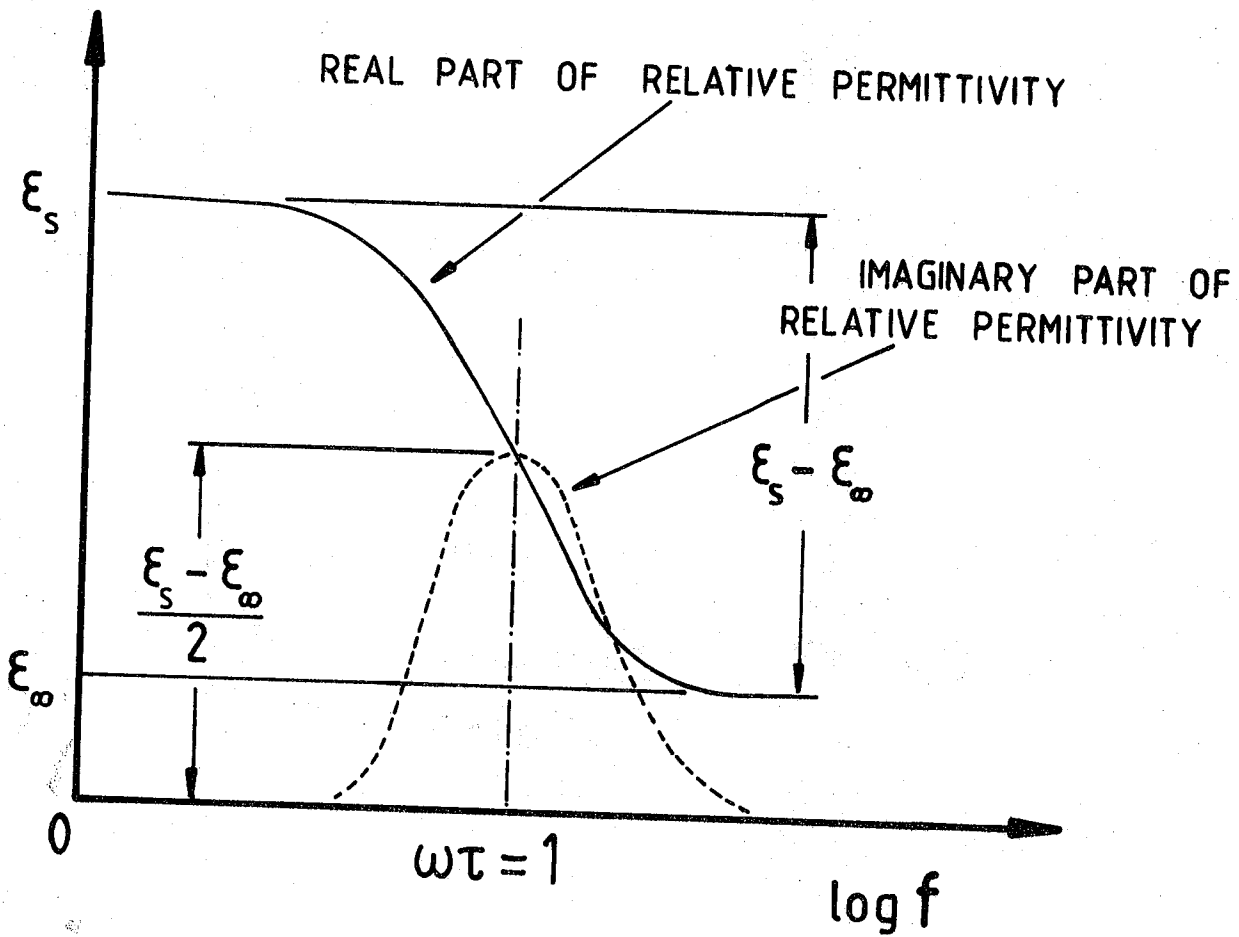
FIG.2.7 THE VARIATION OF ε' AND ε'' WITH FREQUENCY FOR DEBYE RELAXATION.

polar dielectric materials the molecules cannot orient themselves in the low temperature region. In the case of isotropic and cubic dielectrics, the temperature variation of the dielectric constant behaviour depends on three factors. These factors have been studied by Havinga (41). He has attempted to calculate these factors from the Clausius-Mosotti equation, which is given by

$$\frac{\varepsilon'-1}{\varepsilon'+2} = \frac{N\alpha}{3\varepsilon_o} \qquad (2.21)$$

where N = the number of molecules per unit volume

ε_o = permittivity of free space

α = polarizability of molecules

ε' = dielectric constant

The Clausius-Mosotti equation is a relation between a macroscopic property of a dielectric, (.i.e. ε', which can be measured experimentally) and a microscopic property, (i.e. polarizability, α). In eqn. 2.21, N can be replaced by,

$$N = \frac{N_A \rho}{M} \qquad (2.22)$$

where N_A =   Avogadro's number (6.022169 x 10^{23} mol^{-1})

M   =   molecular weight (kg)

ρ =   density (kg m^{-3})

Another version of Clausius-Mosotti equation may be written as (42),

$$\frac{\varepsilon'-1}{\varepsilon'+1} = \left\{\frac{4\pi}{3}\right\} \left\{\frac{\alpha}{V}\right\} \qquad (2.23)$$

where V is equal to the volume of a small sphere of material, and other quantities are as have been defined before. It must be taken that the

volume of the sphere is large relative to the lattice dimensions.

The Clausius-Mosotti equation is applicable to all cubic and isotropic materials and all derivation is based on this assumption. From eqn. 2.21 one can derive the relation

$$\frac{1}{(\varepsilon'-1)(\varepsilon'+2)} \left\{ \frac{\partial\varepsilon'}{\partial T} \right\}_p = A + B + C \tag{2.24}$$

where A, B and C are the factors which have been calculated by Havinga. They are defined as :

A: This factor arises from volume expansion. As a result of expansion the number of polarizable particles per unit volume is reduced (since the number of particles are constant). Therefore by increasing temperature ε' decreases.

B: This factor increases ε' since it relates to the increase of polarizability of the particles when the volume expansion occurs.

C: In a constant volume, this factor arises from the dependence of polarizability of the particles on temperature.

In order to determine A, B, and C some physical quantities must be measured experimentally (41-42). Then these factors can be evaluated from dielectric constant versus temperature data. The calculated magnitudes of A, B and C are invariably for each specific material.

Bosman and Havinga (43) have found that the sum of A and B is always positive and hence, (A + B) contributes in the increasing of ε'. But the factor C is negative for those types of material with $\varepsilon' > 10$ and it is positive for those which have $\varepsilon' < 10$.

According to them, the temperature dependence of a dielectric constant (eqn. 2.24) is always positive for $\varepsilon' < 20$ and it is negative

for $\epsilon' > 20$.

The temperature dependent dielectric constant of magnesium oxide single crystal, $\left|\dfrac{\partial \epsilon'}{\partial T}\right|_p$ has been calculated by Bartels and Smith (42) from their own measurements over the temperature range 15 to 294° K.

All auxiliary data for determination of the factors A, B and C required for calculation of $\left|\dfrac{\partial \epsilon'}{\partial T}\right|_p$ for MgO are given by references listed in (42).

2.6   CONDUCTION MECHANISMS

The phenomenon of electrical conduction shows appreciable variations depending on the nature of the charge carrier in the given material.   It is an electrical property of matter that has an enormous range of values.

It should be noted that both the magnitude of conductivity and the nature of conduction can essentially change according to the temperature and the structure of the material.   It is obvious that when the condition changes, the nature of conduction of a given material may change too.

The type of conductivity can be determined from measurements of transport numbers, which are related to the Hall constant or the thermoelectric coefficient.

Ionic solids at room temperature usually have very low conductivity for the motion of ions through the crystal.

The basic theoretical expression for all mechanisms of conductivity is given (44) as,

$$\sigma = \sum_i z_i e\, n_i\, \mu_i \qquad (2.25)$$

where σ =   conductivity $(\text{ohm}^{-1} \text{ m}^{-1})$

          z_i =   charge of the current carrier (e)

          e =   modulus of the electronic charge $(1.602 \times 10^{-19} \text{ C})$

          n_i =   carrier density (m^{-3})

          μ_i =   mobility $(\text{m}^2 \text{ v}^{-1} \text{ s}^{-1})$

The total conductivity is usually found by summing i for all the various mechanisms. Therefore for any mechanism z, n, μ must be known. Their determination varies according to the class of the mechanism involved. The basic types of conduction are :

1. Electron Conduction : In this conduction the carriers are elementary negatively charged particles, i.e. electrons or positively charged particles, i.e. holes (metallic or semiconductor type n or p).

2. Ionic Conduction : In this conduction the carriers are ions, i.e. the parts of molecules (dielectric). Therefore the flow of the current through the material is accompanied by electrolysis. It takes place by passing ions from one unit cell into another. The ion must overcome a certain energy barrier each time it penetrates and passes a structural element of the solid. The conductivity formula

$$\sigma = \sigma_0 \exp \left\{ \frac{-E_0}{kT} \right\} \tag{2.26}$$

covers all the conduction mechanism which are being considered.

The electronic and ionic conduction mechanisms are divided into four fundamentally different classes as follows

        1. intrinsic ionic

        2. extrinsic ionic

        3. intrinsic electronic

        4. extrinsic electronic

In eqn. 2.25 the magnitude of 'z 'for electrons and holes is unity but for ions it depends on the valence state.

The calculation of carrier density, n, varies from one mechanism to another. In the intrinsic ionic mechanism the carrier density will be equal to the density of ions in the lattice. In the extrinsic ionic mechanism the carrier density may be determined by chemical analysis.

The intrinsic electronic carrier density may be calculated using the standard equations derived from solid state physics. In the case of a dielectric, the material is assumed to be a wide band gap semiconductor. In intrinsic behaviour the number of electrons, n_e, is equal to the number of holes, n_h. Initially, it is assumed that the effective masses of electrons and holes are equal to their rest mass ; then (36) the concentration of electrons or holes may be written as ,

$$n_e = n_h = 2\left[\frac{2\pi M\, kT}{h^2}\right]^{3/2} \exp\left(-\frac{E_g}{2kT}\right) \qquad (2.27)$$

where

n_e = concentration of electrons in the conduction band (m^{-3})

n_h = concentration of holes in the valence band (m^{-3})

M = rest mass of the electron $(9.108 \times 10^{-31}$ kg)

k = Boltzmann's constant $(1.38 \times 10^{-3}$ J $k^{-1})$

T = absolute temperature (k)

h = Planck's constant $(6.625 \times 10^{-34}$ Js)

E_g = energy gap (eV)

It can be simplified as,

$$n_e = n_h = 5 \times 10^{21} \ (T)^{3/2} \exp\left(-\frac{E_g}{2kT}\right) m^{-3} \qquad (2.28)$$

and the conductivity also is given by,

$$\sigma_{in} = \left\{const.\right\} \exp\left[\frac{-(E_c - E_v)}{kT}\right] \qquad (2.29)$$

where σ_{in} = intrinsic conductivity

E_c = energy of conduction band

E_v = energy of valence band

Finally, in the extrinsic electronic mechanism the carrier density depends on the concentration of the isolated energy levels and their states of ionisation. The density of the energy levels is directly related to the concentration of the defect which causes them ; each defect will give rise to an energy level (45). The state of ionisation will depend on the energy level, bandgap separation and temperature.

For measuring electronic mobility it is assumed that the hole and electron mobilities are equal ; the calculation of mobility, μ can be made by measuring of Hall effect in the material. In order to measure ionic mobility, use is made of the Einstein expression (39,46), i.e.

$$\mu = D\frac{Ze}{kT} \qquad (2.30)$$

where D is the diffusion coefficient ($m^2 s^{-1}$) which relates to specific ions, and the other quantities are as defined previously.

In some materials the conductivity takes place with both electrons and ions. The ratio between electron and ion conductivity depends on the temperature and the chemical composition of the material.

2.7   DEFECTS IN CRYSTALS

Defects in the crystal structure may cause isolated energy levels and as mentioned before these isolated levels increase the extrinsic electronic mechanism of conduction.   Therefore, essentially the investigation of defect conduction in crystal structures is required.

Mott and Gurney (47) have suggested that, there are only two ways of sites, 1 - Schottky defect vacancies, or 2 - Frenkel defects interstitial ions.   In the first one it is created by transferring an atom from a lattice site to the surface of the crystal and making a new layer of crystal lattice.   In ionic crystals, it is usually favourable energetically to form roughly equal numbers of positive and negative ion vacancies.   The formation of such pairs of vacancies keeps the crystal electrically neutral.   The number of created vacancies, n is given by,

$$n = N \exp \left\{ - \frac{E}{2kT} \right\} \qquad (2.31)$$

where   N = total number of atoms in unit volume of crystal

E = energy of formation of vacancy

The presence of Schottky defects increases the volume of the crystal.

In the second case (Frenkel defects) in which an atom is transferred from a lattice site to an interstitial position in the lattice, its position is not normally occupied by any other atoms. Therefore, the number of atoms which left their position, n is given by,

$$n = \sqrt{N N'} \exp \left\{ \frac{-E}{2kT} \right\} \qquad (2.32)$$

where   N   =   total number of atoms in unit volume of crystal

         N'   =   total number of possible interstitial position

         E   =   energy required to take an atom from its position

These defects can occur in any part of the crystal ; and are mobile (with different mobility) which causes conductivity in the homogeneous lattice. It is concluded that part of the conductivity is due to motion of these defects in the material, and this represents another type of conduction mechanism.

2.8   IMPURITY CONDUCTION

Impurity conduction in materials has been studied by Mott and Twose(48) and Mott (49). The basic idea is different in that it is assumed that electrons occupy the donor levels and holes also occupy acceptor levels. Mott and Twose pointed out that charge transport can occur by tunnelling from an occupied donor level to an adjacent vacant donor level. Alternatively, charge transport may proceed by excitation of the localized electron over the potential barrier which separates it from an adjacent vacant site. This process can be called impurity conduction.

Impurities have a double effect on the conductivity of crystals. Firstly, they represent a source of highly mobile ions with low activation energy and therefore increase by many times the conductivity of such crystal and secondly they weaken the crystal lattice and facilitate the movement of lattice ions.

2.9   FREQUENCY DEPENDENCE OF THE CONDUCTIVITY

Thermally activated hopping in a high density of localised states has been examined by Mott (50) and Mott and Davis (51). This idea has also been suggested by Pollak (52) and Pollak and Geballe (53). They proposed that the transport of electric charge occurs by electron

hopping between those states which are localized, surrounding acceptor and donor impurities, i.e. the a.c. conductivity of a hopping system has been based on a pair approximation, in which successive hops of a carrier are assumed to be independent of each other. The hopping probability is given by,

$$\frac{\omega^2 \tau}{1 + \omega^2 \tau} \qquad (2.33)$$

where, τ is the mean time which is taken to jump (jumping time).

They also suggested that in order to compensate the impurity (which must be an original feature of impurity conduction) it is necessary that some of the localized states be vacant.

The coulombic potential between states may be altered by thermal energy. However, it can be changed by an applied electric field, which establishes a new equilibrium, and then polarization has occurred. The rate of polarization can be considered as a current in an a.c. measurement. The polarization is related to the hopping time and also to the distance of separation of two sites.

Hopping conduction cannot produce a large amount of conductivity but the introduction of some impurities can increase it significantly and it gives major contribution to the a.c. conductivity at low temperatures. The a.c. conductivity as a function of frequency and temperature when $\frac{\nu_{ph}}{\omega} >> 1$ and $\nu_{ph} = 10^{12}$ Hz can be represented by (51),

$$\sigma(\omega) = \left\{\frac{\pi^4}{12}\right\} e^2 \, kT \, N(E_F)^2 \, \alpha^{-5} \left[Ln \frac{\nu_{ph}}{\omega} \right]^4 \omega \qquad (2.34)$$

where α represents the effective radius of the electronic wavefunction, ν_{ph} represents a characteristic phonon frequency, $N(E_F)$ is the density of states with energy near the Fermi level and the other symbols have their

usual meanings. The main contribution to the conductivity comes from pairs with a spacing between atoms of the order of $\frac{1}{2\alpha}$ (this arises by taking the average over R where R = hopping distance). Since $\sigma(\omega) \sim \omega \left\{ Ln \frac{\nu_{ph}}{\omega} \right\}^4$ holds in eqn. 2.34, over a large frequency range eqn.2.34 may be approximated (54) by the empirical relation,

$$\sigma(\omega) = A \omega^n \tag{2.35}$$

with n = 0.8

Similar equations have been found by other theoreticians, Pollak (55), Austin and Mott (56) Jonscher (57) and others (58-59). In eqn. 2.34 Mott and Davis (51) suggested that,

$$\alpha = \left\{ \frac{2 m^* \Delta E}{\hbar} \right\}^{\frac{1}{2}} \tag{2.36}$$

where m^* = effective mass of the charge carrier

     ΔE = bandwidth of the localized states.

The conductivity can be expressed by the general relation (59) of,

$$\sigma(\omega) = \sigma_{dc} + \sigma(\omega)_{ac} \tag{2.37}$$

where

$$\sigma_{ac}(\omega) \propto \omega^n \tag{2.38}$$

σ_{dc} is frequency independent at low frequency and $\sigma_{dc} \ll \sigma_{ac}$.

If, in hopping conduction hops occur with approximately fixed frequency or the frequency of the applied electric field is very much greater than the hopping frequency, then the conduction will be frequency independent (58).

Pollak and Pike (60) in the study of conductivity of glasses have noticed that the exponent, n, varies with temperature. Also, Moore (58) showed that n is temperature dependent ; at low temperature it is near unity and as the temperature increases it becomes progressively smaller.

The variation in the values of n in eqn. 2.38 are controlled entirely by multiple-hopping processes. Values of n close to unity are obtained when successive hops of the carrier occur with markedly different hopping frequencies, while values of n near zero are obtained either when successive hops occur with approximately the same hopping frequency or when the frequency of the applied field is greater than the hopping frequencies.

The component of the hopping conduction can be easily distinguished from that of ionic and electronic by measuring the frequency dependence of conductivity (61).

2.10   TEMPERATURE DEPENDENCE OF CONDUCTIVITY

It has been noted before that the impurity contributes to the conduction. The experimental results are usually well approximated by the formula,

$$\sigma = \sigma_1 \exp\left\{\frac{-E_1}{kT}\right\} + \sigma_2 \exp\left\{\frac{-E_2}{kT}\right\} \qquad (2.39)$$

where the first term with a high energy, E_1, is related to the lattice ions the second term with lower energy and, E_2, is related to impurity ions. However, the separation of eqn. 2.39 into two terms is reasonable, because,at high temperatures,when the movement of lattice ions is pronounced and small numbers of impurity atoms do not have any appreciable effect on σ, and at low temperatures the number of impurity atoms appreciably exceeds the number of matrix ions even at low impurity contents. It is true to say that at sufficiently high temperatures,σ represents the electrical

conductivity of the lattice and at low temperatures the electrical

conductivity is only due to impurities.

The temperature dependence of the electrical conductivity is

usually represented by eqn. 2.39.   Pollak (52) has pointed out that

the frequency dependence of hopping conductivity becomes weakened at

the higher temperatures and it is proposed that multiple hops can account

for these phenomena.

It is experimentally observed that the more pronounced tempera-

ture dependence is always associated with a weakened frequency dependence

on higher temperatures. An increased temperature dependence and a

decreased frequency dependence always occur together.

2.11   HOPPING MODELS ; THE JONSCHER THEORY

The conduction mechanism in dielectric materials is due to the

electronic and ionic hopping through the solid. Jonscher (62-63) has

shown that the hopping mechanism similarly to electronic and ionic

conduction, has a characteristic of frequency dependence, and therefore,

over the frequency range of interest several mechanisms of polarization

can occur in different kinds of materials.   These polarizations may be

due to permanent or induced dipole or hopping electrons or ions within

the material and they are frequency dependent.

The hopping mechanism was suggested for the first time by

Pollak and Geballe (53). They measured the conductivity of n-type silicon

containing various kinds of impurities and observed that the magnitude of

the measured a.c. conductivity was larger than the measured d.c. conduct-

ivity ; they attributed this to polarization caused by hopping processes.

These polarization mechanisms may be considered fundamentally in terms of

the Debye susceptibility $X(\omega)$, which is due to rotating dipoles or

localized ionic charges and is a function of frequency. The susceptibility

is complex and can be expressed as

$$X(\omega) = \left[X'(\omega) - j X''(\omega) \right] \propto \frac{1}{1 + j\omega\tau} \qquad (2.40)$$

where τ is the relaxation time and is the reciprocal of the natural

hopping frequency in the absence of any external electric field ; (τ

may be temperature dependent) ; ω is the angular frequency ; $X'(\omega)$ and

$X''(\omega)$ are the real and imaginary parts of the Debye susceptibility.

The right-hand side of eqn. 2.40 can be divided into real and

imaginary parts as follows :

$$\left[X'(\omega) - j X''(\omega) \right] \propto \left[\frac{1}{1 + \omega^2\tau^2} - j \frac{\omega\tau}{1 + \omega^2\tau^2} \right] \qquad (2.41)$$

Ideally the imaginary part of the susceptibility, i.e the dielectric

loss is equal to

$$X''(\omega) = \frac{\omega\tau}{1 + \omega^2\tau^2} \qquad (2.42)$$

Examination of eqn. 2.42 shows that there will be a maximum when $\omega\tau = 1$

which corresponds to a peak loss whose width at half-height is equal to

$1/\sqrt{2}$ times the peak height. In real dielectric materials, however,

the majority show much broader peaks. This type of loss can be represented

in empirical form (64-65) by

$$\frac{1}{X''(\omega)} = \left(\frac{\omega}{\omega_1} \right)^{-m} + \left(\frac{\omega}{\omega_2} \right)^{1-n} \qquad (2.43)$$

In this equation ω_1 and ω_2 are dependent on temperature and both

exponents m, and $1-n$, are smaller than unity. It is found that the

behaviour of many dielectric materials in which the polarization is due

to hopping conduction of ions or electrons, the loss in the material, (and consequently the conduction), is described by the second term of eqn.2.43.

The dielectric response of a wide range of materials shows that the observed behaviour departs strongly from the Debye response and it follows a "Universal dielectric response law", in which the dielectric loss follows the empirical law

$$X''(\omega) \propto \omega^{n-1} \qquad (2.44)$$

where the exponent n, lies in the range $0 < n < 1$ with typical values between 0.6 and 0.95. It has been shown that both the Debye and the "Universal Response" may be caused by either dipolar or by hopping charge mechanisms.

The relationship of $X''(\omega)$ with frequency implies that the real part of $X(\omega)$ must have the same frequency dependence, i.e.

$$X'(\omega) \propto \omega^{n-1} \qquad (2.45)$$

There is an important relationship between $X''(\omega)$ and $X'(\omega)$. The ratio of the imaginary to real parts of the susceptibility, $X(\omega)$ is independent of frequency (40) i.e.

$$\frac{X''(\omega)}{X'(\omega)} = \cot\left(\frac{n\pi}{2}\right) \qquad (2.46)$$

This relationship is known as the Kramers-Kronig equation and represents the "Universal Law" of dielectric behaviour. It has a very simple significance, namely that

$$\frac{\text{Energy lost per cycle}}{\text{Energy stored per cycle}} = \text{const} = \cot\left(\frac{n\pi}{2}\right) \qquad (2.47)$$

This behaviour should be compared with the Debye relations which shows that the ratio obtained by dividing the imaginary and real part of Eqn. 2.41 is equal $\omega\tau$. In contrast Eqn. 2.46 has its basis in the non-Debye polarization, and this kind of polarization has been found experimentally to be applicable to all kinds of materials.

The interpretation of the complex dielectric permittivity by considering the "Universal Law" may be expressed by $\varepsilon^*(\omega)$, which is a function of frequency, by writing it in real and imaginary parts :

$$\varepsilon^*(\omega) = \varepsilon'(\omega) - j\ \varepsilon''(\omega) \tag{2.48}$$

$$= \varepsilon_\infty + a(j\ \omega)^{n-1} \tag{2.49}$$

$$= \varepsilon_\infty + a\left[\sin\left\{\frac{n\pi}{2}\right\} - j\cos\left\{\frac{n\pi}{2}\right\}\right]\omega^{n-1} \tag{2.50}$$

where ε_∞ is the limiting permittivity, i.e. the permittivity at high frequency, and $o < n < 1$; the constant (a) determines the strength of the polarization. The characteristic feature of this "non-Debye" or universal relationship is that the ratio of the imaginary to the real part of the dielectric susceptibility is independent of frequency. That is,

$$\frac{\varepsilon''(\omega)}{\varepsilon'(\omega) - \varepsilon_\infty} = \cot\left\{\frac{n\pi}{2}\right\} \tag{2.51}$$

This is in contrast with the Debye dipolar behaviour of Eqn.2.18 where this ratio is equal to $\omega\tau$.

In most materials the conductivity has usually been found to be also a function of frequency and its general form is,(59),

$$\sigma(\omega) = \sigma_o + \sigma_{ac}(\omega) \tag{2.52}$$

where σ_o is the d.c. conductivity and $\sigma_{ac}(\omega)$ is the true a.c. conductivity. The d.c. component σ_o has a high activation energy and experimental evidence shows that the temperature dependence becomes progressively less with increasing frequency, (52). There is no correlation between the values of σ_o and $\sigma_{ac}(\omega)$ for various materials. The a.c. conductivity, $\sigma_{ac}(\omega)$, is also temperature dependent, the dependence again becoming less at high frequencies. Also, there is no evident correlation between the magnitudes of d.c. and a.c. components of conductivity, although $\sigma_{ac}(\omega)$ has a weaker temperature dependence than σ_o.

It has also been mentioned that the conductivity increases at high impurity concentrations (55).

The Eqn. 2.52 can be written in the form of

$$\sigma(\omega) = \sigma_o + \omega \, \varepsilon_o \, \varepsilon''(\omega) \qquad (2.53)$$

where the dispersion obeys the relation

$$\varepsilon''(\omega) \propto \varepsilon'(\omega) \propto \omega^{n-1} \qquad (2.54)$$

and consequently only $\sigma_{ac}(\omega)$ follows the relationship

$$\sigma_{ac}(\omega) \propto \omega^n \qquad (2.55)$$

This dependence of conductivity with frequency is not only found in disordered, glassy and amorphous solids but also in ordered molecular solids in which the carriers involved can be electrons, polarons, protons or ions (66).

The exponent n in Eqn. 2.55 is close to unity (67).

This "Universal Law" was first suggested by Pollak and Geballe. Later, Jonscher (62,65-68) pointed out that, n in fact is not a constant but depends on temperature. At low temperature it approaches unity and as the temperature increases the magnitude of n, decreases and approaches 0.5 or even less. If n is equal to unity, the loss, ε'', will be independent of frequency. This is true in quite a wide range of materials in which the loss is not a function of frequency. Pollak and Pike (60) have also shown that the conductivity of many glasses is due to ionic hopping, and the relation 2.55 is a very general law, not confined to any particular host matrix, type of carrier, or type of disorder. However, in many materials it is not certain whether the observed behaviour should be interpreted by hopping mechanism or dipolar.

The hopping model was introduced for the first time by Conwell and Fritzsche (69-70). According to their model, the transport occurs by electrons, holes or ions, hopping between localized states, which are essentially localized around acceptors or donors at the positions of particular ion cores. Such an electron or ion can hop from its original site to another site with the same energy (52-53,56,63,71). Therefore diffusion of electrons into the crystal is established and this diffusion can be directed by applying an electric field ; all electrons will transport along the positive direction of field gradient. The probability of hopping of electrons or ions is strongly dependent on temperature (52).

At low temperatures the lattice vibration is negligible while at high temperatures the lattice vibration is strong and consequently the hopping probability increases exponentially.

Any of these hoppings must have a distribution of hopping parameters and the most important is the distribution of centres which

may make possible multiple hopping in the material (72). For instance,
one important parameter influencing the hopping mechanism is the
temperature.

If we consider an electron or a hole jumping between two
localised states at a certain rate, the following statement will hold.
By applying a low frequency field, much lower than the jumping rate, the
equilibrium of the states are established much faster than the period
of applied field. So the polarization will be in-phase with the applied
field and there will be no energy loss. Obviously, as the frequency
increases, the chance of keeping the polarization in-phase with the field
decreases and consequently the magnitude of the polarization decreases.
It is clear that this decrease will not be at a faster rate than corres-
ponds to an inverse proportionality with frequency, i.e. proportional
to the rate of change of frequency (52,53,56,73).

2.12   CONCLUSIONS

Examination of possible polarization mechanisms which can take
place in materials and also of the definition of complex dielectric
constant and its relevant electrical properties shows how the components
of the complex dielectric constant, i.e. ε' and ε'' are related to the
polarization mechanisms.

The study of the frequency dependent complex dielectric constant
predicts that according to the polarization mechanism, ε' depends inversely
on frequency but ε'' is directly proportional to it. These are shown in
Fig. 2.6.

Debye has found a relation between ε', ε'' and frequency and
deduced a representation of ε' and ε'' by a complex diagram.

There is little theoretical work on the temperature dependence
of ε' in hopping systems. An interpretation has been given in terms of
thermal expansion and polarizability of the particle in the material.

The classical conduction mechanisms and their corresponding classes have been studied merely to review all possible mechanisms. The basic idea of the hopping conduction mechanism was introduced by Pollak and Geballe, then later Mott and other theoreticians developed this electrical conduction model. In recent years the theory of the "Universal Law" in materials has been considerably developed by Jonscher. He examined this model on many different types of material with various properties. He found that the Universal Law is insensitive to the physical and chemical properties of the dielectric material and to the predominant polarization mechanism which may be dipolar or may be hopping charge carriers, electrons or ions ; this theory can be applicable for any dielectric material.

The review of previous studies of conduction in magnesium oxide showed that its conduction mechanism has not yet been discussed in terms of a hopping model. In this project such an attempt has been made in order to examine the applicability of the Universal Law for pure MgO and also MgO doped with iron or chromium. In order to study the dielectric properties of these crystals over a wide range of frequency, four different techniques were utilized.

2.13   REFERENCES

36.   Kittel C, 'Introduction to Solid State Physics', Wiley & Sons
       Inc., New York, Fourth Edition, London (1971).

37.   Von Hippel R, 'Dielectrics and Waves', John Wiley & Sons Inc.,
       London (1962).

38.   Blakemore J.B, 'Solid State Physics, 2nd Edition, Saunders
       Company, London (1974).

39.   Harrop P.J, 'Dielectrics', Butterworth, London (1972).

40.   Jonscher A.K. 'A New Model of Dielectric Loss in Polymers
       Colloid and Polymer Science', Vol.253, pp 231-50, (1975).

41.   Havinga E.E, 'The Temperature Dependence of Dielectric Constant',
       Journal of Physical Chemistry Solid, Pergamon Press, Vol.18,
       No. 213, pp 253-5 (1961).

42.   Bartels R.A and Smith P.A, 'Pressure and Temperature Dependence
       of the Static Dielecyric Constants of Kcl, Nacl, LiF, and MgO'
       Physical Review, B, Vol.7, No.8, pp 3885-92, (1973).

43.   Bosman A.J. and Havinga E.E, 'Temperature Dependence of Dielectric
       Constant of Cubic Ionic Compounds', Physical Review, Vol.129,
       No. 4, pp1593-1600, (1963).

44.   Samara G.A, ' Pressure and Temperature Dependence of the Ionic
       Conductivities of Cubic and Orthorhombic Lead Fluoride (Pb F_2)
       Journal of the Physical Chemistry of Solids, Vol.40,pp 509-22,(1979).

45.   Kröger F.A   and Vink H.J, Solid State Physics, Vol.3,
       pp 307-435 (1956).

46.   Lidiard A.B, Handbuch der Physik, Vol.20,pp 246-349, (1957).

47.   Mott N.F. and Gurney R.W,'Electronic Processes in Ionic Crystals',
       Second Edition, Oxford, U.K.(1957).

48.   Mott N.F. and Twose W.D, 'The Theory of Impurity Conduction',
       Advance in Physics, Vol.10, pp 107 (1961).

49.   Mott N.F,'Electrons in Disordered Structures', Advance in Physics,
        Vol.16, pp 49 (1967).

50.   Mott N.F,'Metal Insulator Transition', Taylor and Francis,London
        (1974).

51.   Mott N.F. and Davis E.A,'Electronic Processes in Non-Crystalline
        Materials', Clarendon, Oxford (1971).

52.   Pollak M, 'Temperature Dependence of a.c. Hopping Conductivity',
        Physical Review, Vol.138, pp A1822-6 (1965).

53.   Pollak M. and Geballe T.H,'Low Frequency Conductivity due to
        Hopping Processes in Silicon', Physical Review, Vol.122,No.6.
        pp 1742-53 (1961).

54.   Böttger H. and Bryksin V.V,'Hopping Conductivity in Ordered and
        Disordered Solids II', Physica Status Solidi, Vol.78(B),
        pp 403-51(1976).

55.   Pollak M. 'Approximation for the a.c. Impurity Hopping Conduction',
        Physical Review, Vol.133, pp A564-70, (1964).

56.   Austin I.G. and Mott N.F, 'Polarons in Crystalline and Non-
        Crystalline Materials', Advances in Physics, Vol.18, pp 41-102,
        (1969).

57.   Jonscher A.K, 'Frequency-Dependence of Conductivity in Hopping
        Systems', Journal of Non-Crystalline Solids, Vol.8-10,
        pp 293-315, (1972).

58.   Moore E.J,'Numerical Studies of the a.c. Conductivity of Hopping
        Systems': Effects of Space and Energy Disorder', Journal of
        Physics, C, Vol.7, pp 1840-53, (1974).

59.   Ivkin E.B. and Kolomiets B.T, 'High-Frequency Conductivity of
        Arsenic Selenide', Journal of Non-Crystalline Solids, Vol.3,
        pp 41-5 (1970).

60.   Pollak M. and Pike G.E,'d.c. Conductivity of Glasses',
        Physics Review Letter, Vol.28, pp 1449 (1972).

61.   Pollak M, 'Proceedings at International Conference', Physics
        Semiconductors, Exeter, 1962 (Institute of Physics and the
        Physical Society, London),pp 86 (1962).

62.   Jonscher A.K, 'Alternating Current Diagnostics of Poorly
        Conducting Thin Films', Thin Solid Films, Vol.36, pp 1-20 (1976).

63.   Jonscher A.K, 'The Universal Dielectric Response', Nature,
        Vol.267 (1977).

64.   Jonscher A.K, 'Physical Basis of Dielectric Loss', Nature
        Vol. 253, (1975).

65.   Jonscher A.K, 'Dielectric Materials, Measurements and Application',

66.   Jonscher A.K, 'The Role of Contacts in Frequency Dependent
        Conduction in Disordered Solids', Journal of Physics, C,
        Solid State Physics, Vol.6, pp L235 (1973).

67.   Jonscher A.K. and Deori K.L, 'The Dielectric Response of
        $K_x Al_x Ti_{8-x}$ and $K_x Mg_{x/2} Ti_{8-x/2} O_{16}$', Journal of Material
        Science, Vol.14, pp 1308-20, (1979).

68.   Ngai K.L, Jonscher A.K. and White C.T, 'On the Origin of the
        Universal Dielectric Response in Condensed Matter', Nature,
        Vol.277 (1979).

69.   Conwell E.M, 'Impurity Band Conduction in Germanium and Silicon',
        Physical Review, Vol.103, pp 51 (1956).

70.   Fritzsche H, 'Effect of Shear on Impurity Conduction in n-type
        Germanium, Physical Review, Vol.119, pp 1899 (1960).

71.   Adler D, 'Electrical Conductivity in Ceramics and Glass',(1974).

72.   Jonscher A.K, 'Hopping Losses in Polarisable Dielectric Media',
        Nature, Vol.250 (1974).

73.   Golin S, 'Polarization Conductivity in p-type Germanium',
        Physical Review, Vol.132, No.1 pp 178 (1963).

CHAPTER 3

EXPERIMENTAL METHODS

3.1   INTRODUCTION

In order to determine the dielectric properties of solid

materials over a wide range of frequencies, it is necessary to use

different measurement methods. Each method is suitable only for the

appropriate range of frequencies.

At low frequencies (500 Hz-50 kHz) bridge techniques are most

appropriate and suitable for precise measurements of the real component

of dielectric constant and conductivity. It gives direct readings, the

results are repeatable and the accuracy is high.

At high frequencies, i.e. 100 kHz - 30 MHz the measurements

can still be carried out using a standard Q-meter. Above this frequency

range although within the Q-meter capabilities the measurements become

more difficult to carry out and the accuracy of the results is in question.

The procedure of measuring is the same as in bridge technique but with

less precision because of the inconsistency of assembly.

As the frequency is increased further to 500 MHz - 7.5 GHz range,

the standing wave methods become more suitable. It is not an easy

technique, the results are difficult to repeat, the components used must

be precision made and the accuracy of the instruments must be high.

At very high frequency, i.e. microwaves around 9 GHz, due to

short wavelengths involved all the above methods are inappropriate and

cavity resonator method must be used. It gives very accurate results

since there is no need to polish the samples or change its position

within the cavity.

The specimens were grown by electrofusion method from powder

and obtained from W & C Spicer Ltd. They were pure MgO and MgO with iron or chromium concentrations as shown in Table 1.1. The concentrations were determined by X-ray or chemical analysis. The specimens were in the form of thin square plates of differing size for each technique. Making the surfaces of the samples parallel and smooth was a difficult task and it was done by a Logitech mechanical polishing machine which gave the surface flatness to within 0.25 micron.

3.2 BRIDGE TECHNIQUES

3.2.1 Theory

The dielectric properties of the magnesium oxide, MgO, were examined at low frequencies. As Mungall (74) has noted it is conventional to measure the capacitance, C, and the conductance, G, of the sample which is held between a pair of micrometer electrodes, so designed that the stray capacitance is minimized.

In the present experiment the measurements of dielectric constant and the loss tangent (and consequently the a.c. conductivity) were made using a Wayne-Kerr bridge (Type-B224) over the frequency range from 500 Hz to 50 kHz.

Circular gold electrodes of 8 mm diameter were evaporated on the opposite polished surfaces of the specimens to ensure a good electrical contact over a well defined area between the crystal and the electrodes of the dielectric test jig. Gough and Isard (75) have mentioned possible errors due to coated electrodes on the surface of the sample and they found that it is necessary for elimination of any air gaps between the main electrodes and the samples to use gold evaporation. The diameter of gold evaporated area has been chosen in order to allow the sample to project beyond the electrodes, as much as possible ; this projection minimizes the contribution to the conductance due to surface leakage over the edge of the sample (76). However, this projecting crystal

whose extent must be at least twice the specimen thickness, causes an edge capacitance for which a correction must be made. This correction term has been considered by Scott and Curtis (77) later.

3.2.2. Practical Arrangement and Procedures

3.2.2.1 Room Temperature

In the bridge technique, for measurements at room temperature a substitution method is usually employed. The measuring jig as shown in Fig.3.1 was fixed inside a metallic box in order to provide the sample with a high degree of electrical shielding. The balance of the bridge was first obtained without the specimen being present. This removes the effect of any residual capacitance and conductance. Then the specimen was inserted between the electrodes and the bridge rebalanced and the capacitance and conductance of the sample were obtained directly.

The components of the complex dielectric constant (ε') loss tangent, (Tan δ) and conductivity (σ) of the sample were then deduced (78,79) from the equations :

$$\varepsilon' = \frac{C}{C_o} \tag{3.1}$$

$$\text{Tan } \delta = \frac{G}{\omega C} = \frac{\varepsilon''}{\varepsilon'} \tag{3.2}$$

$$\sigma(\omega) = \frac{d}{A} \cdot G \tag{3.3}$$

$$C_o = \varepsilon_o \cdot \frac{A}{d} \tag{3.4}$$
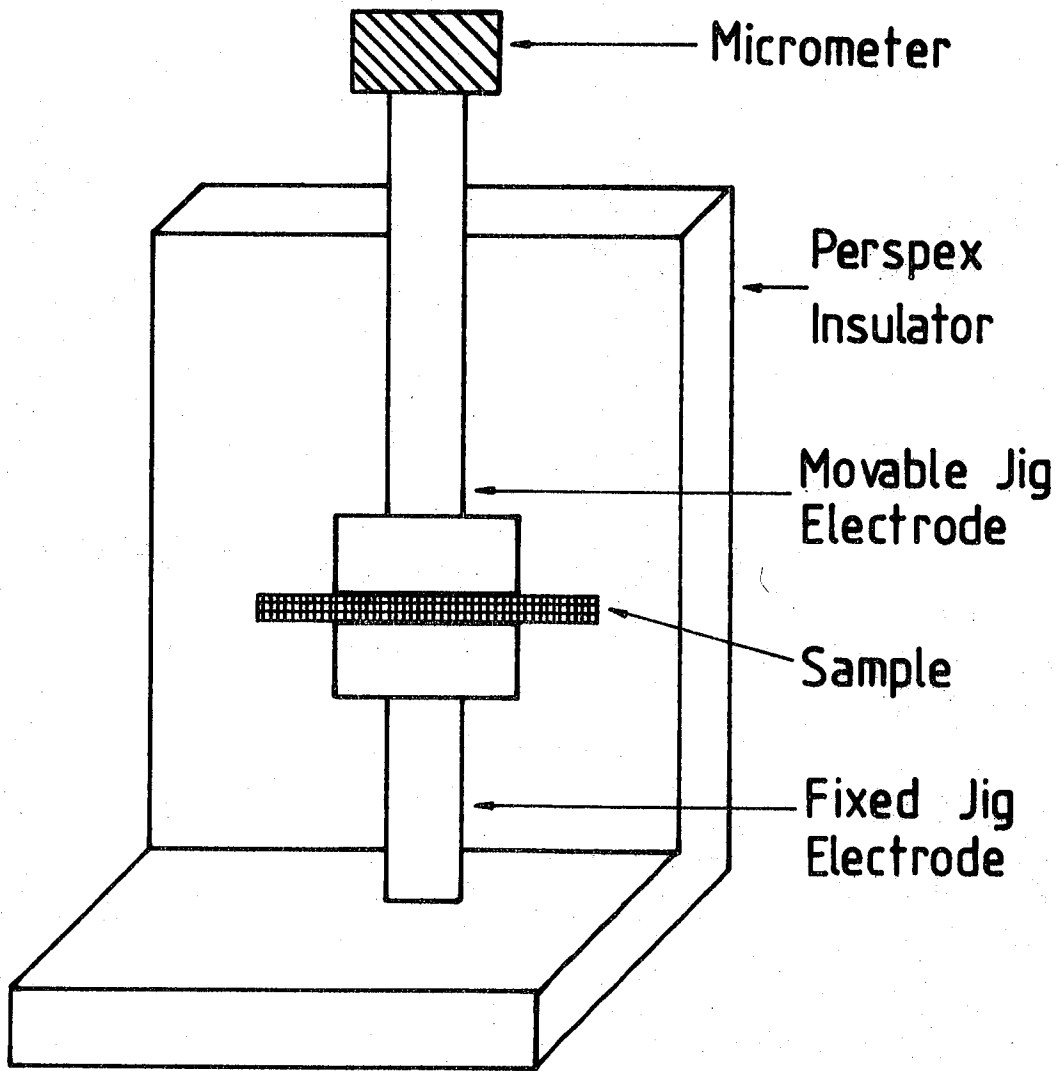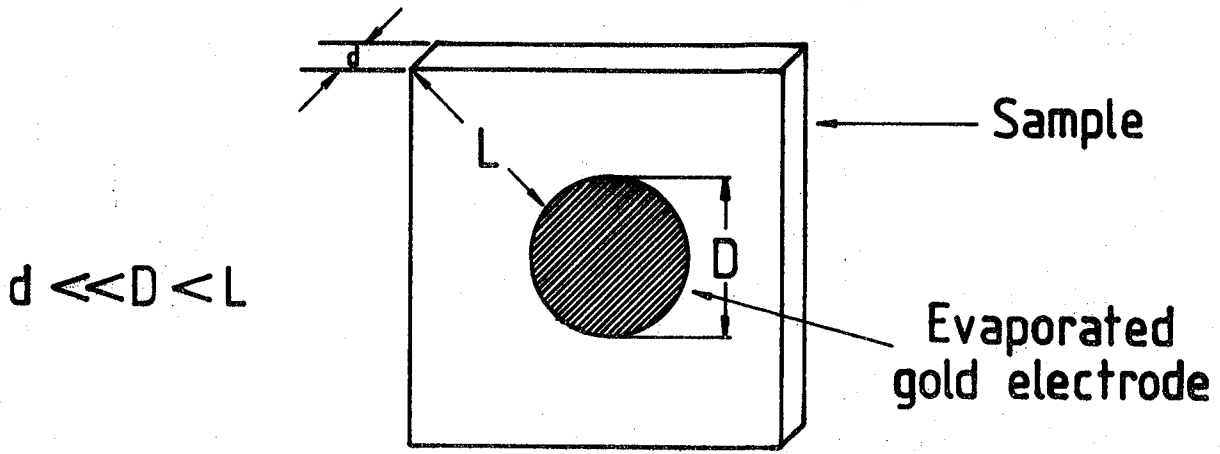
where C = capacitance of sample (pF)

C_o = capacitance of same electrodes with air (pF)

ω = angular frequency (Rad s^{-1})

d = thickness of sample (cm)

A = area of electrodes (cm^2)

ε_o = permittivity of free space = 8.854 x 10^{-14} (F cm^{-1})

d $\ll$ D $<$ L

Sample

Evaporated gold electrode

Micrometer

Perspex Insulator

Movable Jig Electrode

Sample

Fixed Jig Electrode

General form of specimens and dielectric testing jig.

FIG. 3.1

At least three measurements were made on each sample and care
was taken to dry the sample thus eliminating any effect due to moisture.
The frequency generator used was a J3B Gould Advance signal generator
whose stabilized output was applied across the sample and connected to
the bridge.

For convenience the samples were cut in the form of a square
as shown in Fig.3.1 and some extended beyond the circular jig electrodes.
A correction for the edge effects was therefore necessary (80) in which
it was assumed that the thickness of the gold evaporated layer is very
small in comparison to the thickness of the sample. The correction
formula for the edge effects with circular electrodes of the same diameter
due to Scott and Curtis was used (77), i.e.

$$C_e = \frac{1.113\ D}{8\pi} \left\{ Ln\ \frac{8\pi\ D}{d} - 3 \right\} \mu\mu F \qquad (3.5)$$

where D = diameter of each electrode in centimetres.

    d = thickness of the sample (distance between the inner faces of

        the electrodes) in centimetres.

The Eqn. 3.1, which gives the dielectric constant of the sample has now
been modified to

$$\varepsilon' = \frac{C}{C_o + C_e} \qquad (3.6)$$

Since in the capacitance measurement of the sample the stray
capacitance due to the electrodes is included in the measured value,
another correction factor is needed before the true capacitance of the
sample, C, can be determined.

The equivalent circuit of a sample has been discussed by many
authors (39,81) and it is usual to adopt the form illustrated in Fig.3.2a.

In this equivalent circuit the sample is represented by a capacitance, C, shunted by a resistance R which represents the loss in the sample. These quantities represent the true values of capacitance and resistance of the sample and they can be derived from measured quantities ; in general they may vary with temperature and frequency. For a more detailed analysis let C_s be the stray capacitance associated with the electrodes and connecting cables. This capacitance is assumed to be parallel with C as shown in Fig 3.2b.

The inductance has been omitted since the performance is being measured at low frequency and its effect was considered insignificant. It is also assumed that the leakage admittance is eliminated by the use of a correction factor for the edge effects (76).

On this basis the total capacitance, C_t, measured by the bridge when the sample is placed between the electrodes is given by :

$$C_t = C + C_s \qquad (3.7)$$

In the next stage, when the sample is removed from between electrodes, the capacitance of air, C_a, is measured ; it is given by
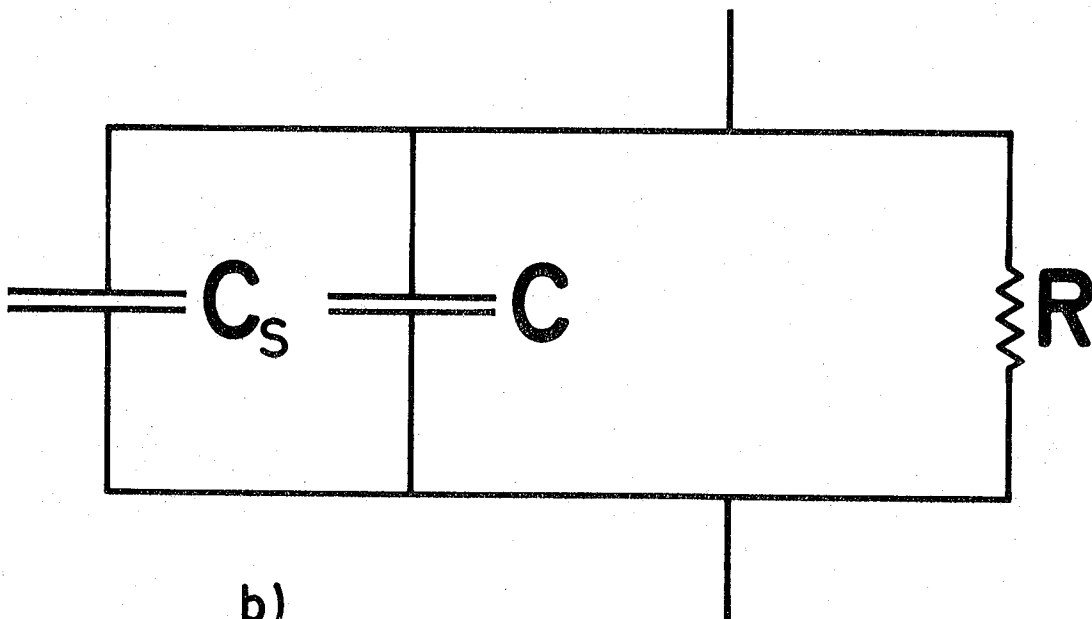
$$C_a = C_o + C_s \qquad (3.8)$$

where C_o is the theoretical capacitance of air. By substitution for C_s from Eqn. 3.8 and Eqn. 3.7, the capacitance of the sample is then given by :

$$C = C_t - C_a + C_o \qquad (3.9)$$

In this equation C_t and C_a are measurable quantities and C_o is found by calculation, so the net capacitance of the sample, i.e. C can be found.
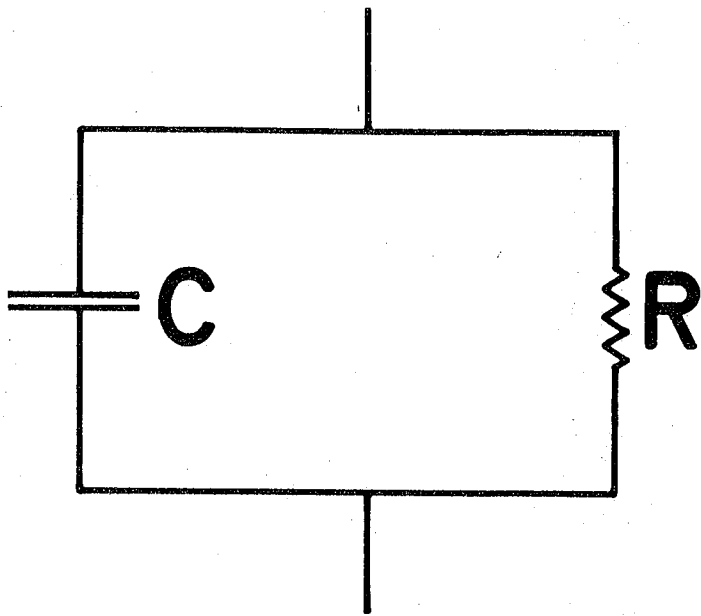
FIG.3.2 EQUIVALENT CIRCUITS OF DIELECTRIC
        SAMPLE.

3.2.2.2 High Temperature

In this measurement a two probe method was employed. The electrodes were made by evaporating initially gold on the surfaces of the sample and then platinum paste was used to keep the connecting wires in place.

The apparatus was arranged as shown in Fig.3.3. It is a cylindrical furnace, equipped with on-off type controlling units in such a way that the temperature of the specimen is kept constant to within $\pm 5^{\circ}$ C.
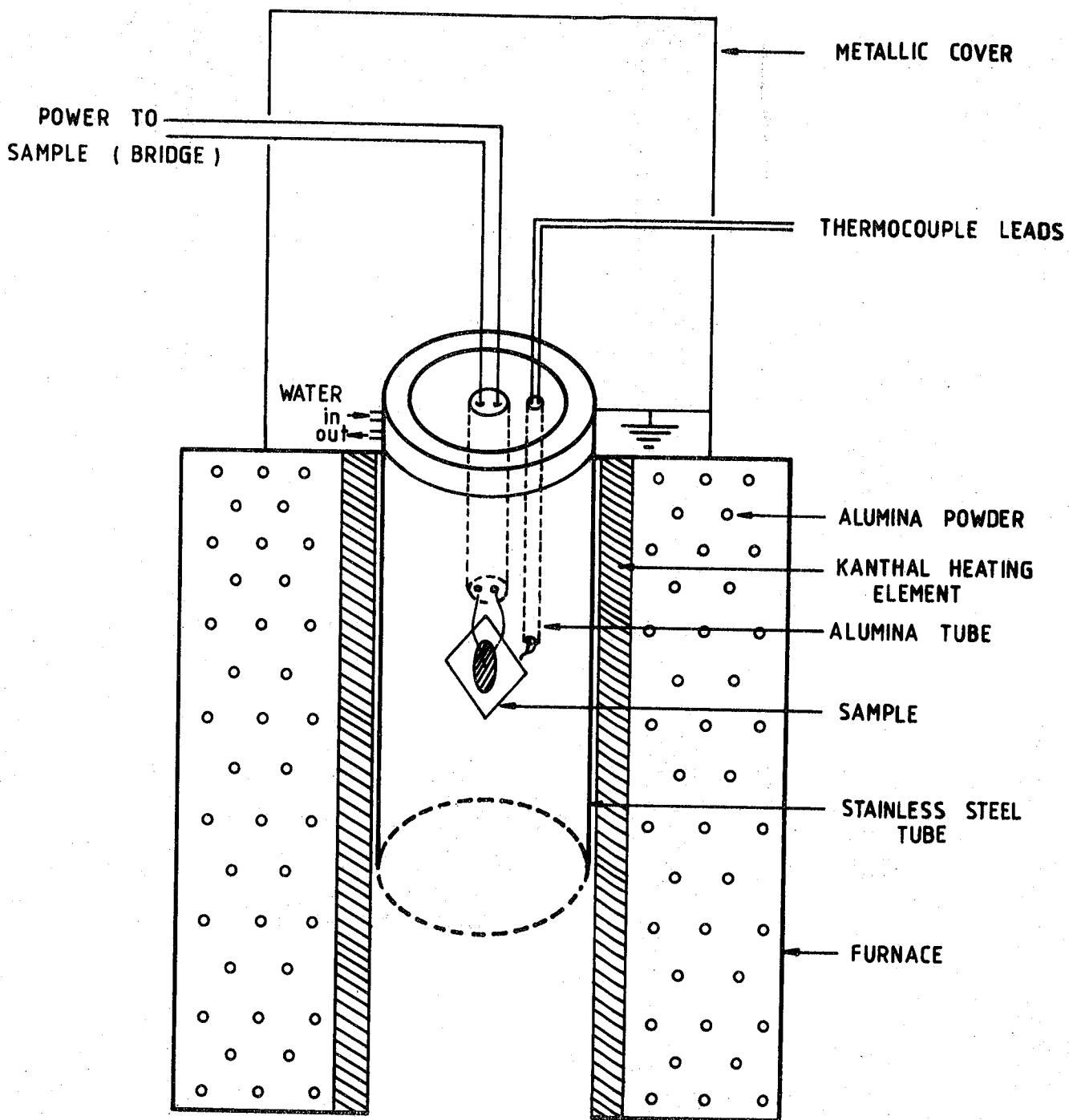
The wires to the specimen were first connected by means of a mechanical pressure and then the whole assembly was fired in a furnace at 300° C to get good mechanical and electrical bonding between electrodes and specimen. The other ends of the wires pass through holes in silica rods and are connected to the bridge.

The temperature of the sample was measured and monitored using two Pt/Pt 13% Rh thermocouple wires passing through holes in a silica rod.

All the measurements were made in air since there is no risk of oxidation up to 700° C. The upper temperature limit was so chosen that the gold electrodes can not diffuse into the specimen.

The specimen was surrounded with a stainless steel tube which was located inside and along the furnace. This tube is used as a shield to protect the samples from all unwanted signals due to thermal noise or electrical and other sources external to the specimen.

The measuring procedure was exactly as mentioned in room temperature case. The measurement of capacitance and conductance of the air gap and the determination of stray capacitance due to leads and electrodes was however not possible.

METALLIC COVER

POWER TO
SAMPLE (BRIDGE)

THERMOCOUPLE LEADS

WATER
in
out

ALUMINA POWDER

KANTHAL HEATING
ELEMENT

ALUMINA TUBE

SAMPLE

STAINLESS STEEL
TUBE

FURNACE

FIG. 3.3   APPARATUS FOR MEASURING a.c.
ELECTRICAL CONDUCTIVITY AND
DIELECTRIC PROPERTIES AT HIGH
TEMPERATURE.

3.3   Q-METER METHOD

3.3.1 Theory

The principle of the Q-meter circuit is based on the series resonant circuit. Its equivalent circuit is shown in Fig. 3.4 and consists of resistor R, inductor L and capacitor C, all in series connected to a variable signal generator. Taking R as the total internal resistance of the circuit and L and C as the total inductance and capacitance we have at resonance $\omega = \omega_r = 2\pi f_r$ and so,

$$f_r = \frac{1}{2\pi \sqrt{LC}} \qquad (3.10)$$

Applying a particular frequency and on inserting the appropriate inductor enables us to resonate the circuit. Then the magnitude of the capacitor C at resonance, corresponding either to when the testing jig is loaded or unloaded with sample is measured. If the testing jig is connected to the circuit with the spacing of the electrodes exactly equal to the thickness of the sample, the air gap capacitance will be C_o and the total capacitance of the circuit, C_T is given by

$$C_T = C_1 + C_o + C_H + C_L \qquad (3.11)$$

where C_1 = the variable capacitor of the Q-meter.

C_H = capacitance of the sample holder (electrodes).

C_L = capacitance of the connecting cables between Q-meter and testing jig.

Since all the above capacitances are constant only the variable capacitor C_1 causes resonance at the chosen frequency.
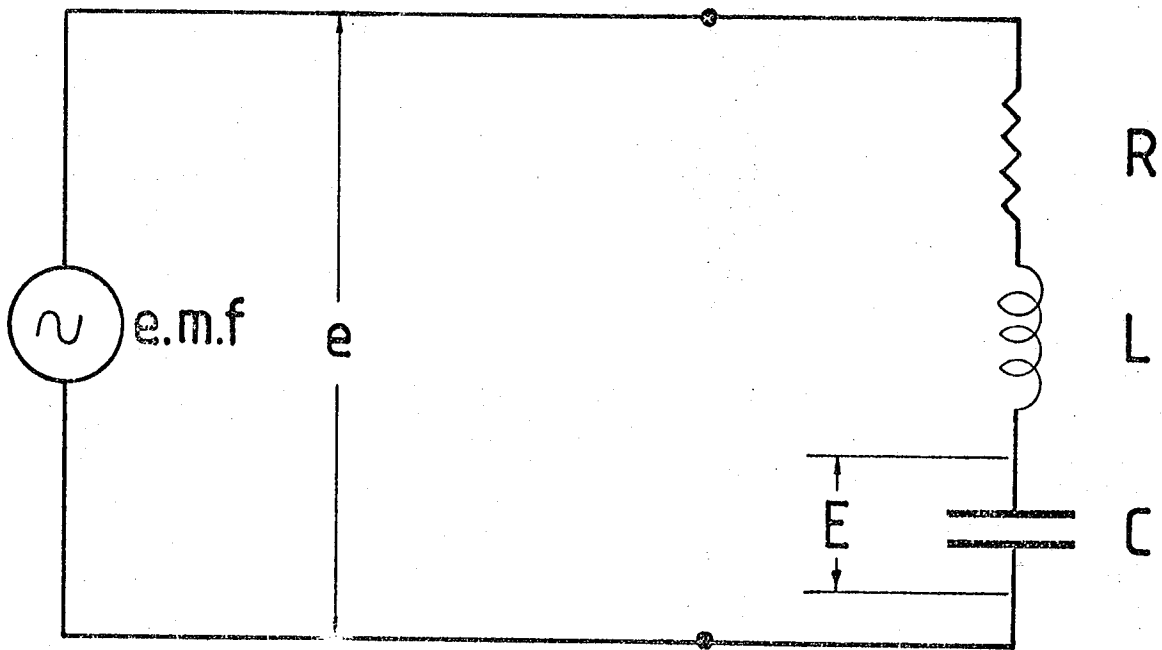
FIG.3.4 EQUIVALENT RESONANT CIRCUIT
OF Q-METER.

By replacing the sample between the electrodes, (the sample having capacitance C_s), C_1 changes to C_2 when resonance occurs. C_T will now be equal to :

$$C_T = C_2 + C_s + C_H + C_L \qquad (3.12)$$

Equating Eqns. 3.11 and 3.12 yields

$$C_1 - C_2 = C_s - C_o \qquad (3.13)$$

The relative permittivity of the sample, neglecting the edge effect, ε' is given by

$$C_s = \varepsilon' C_o \qquad (3.14)$$

where

$$C_o = \varepsilon_o \frac{A}{d}$$

and
$$\varepsilon_o = \text{permittivity of the free space}$$
$$= 8.854 \times 10^{-14} \quad (F\ Cm^{-1})$$
$$A = \text{contact area of electrode with sample } (Cm^2)$$
$$d = \text{thickness of the sample } (Cm)$$

Substitution of Eqns. 3.14 in Eqn. 3.13, gives,

$$C_1 - C_2 = \varepsilon' C_o - C_o \qquad (3.15)$$
$$= C_o (\varepsilon'-1)$$

and then,

$$\varepsilon' = \frac{C_1 - C_2}{C_o} + 1 \qquad (3.16)$$

The loss Tan δ values are given by (82,83)

$$\tan\delta = \frac{Q_1 - Q_2}{Q_1 \cdot Q_2} \cdot \frac{C_1}{C_1 - C_2} = \frac{\varepsilon''}{\varepsilon'} \qquad (3.17)$$

where Q_1 and Q_2 are the Q-value of circuit with the sample out of and in the testing jig respectively.

The effective resistance of the sample at the frequency of the test is given by (82).

$$R = \frac{Q_1 \ Q_2}{Q_1 - Q_2} \cdot \frac{1}{\omega} \cdot \frac{1}{C_1} \qquad (3.18)$$

and finally the real part of conductivity is given by (83).

$$Re \ (\sigma) = \frac{d}{A} \cdot \frac{1}{R} \qquad (3.19)$$

An external e.m.f. with voltage e is injected at the resonant frequency f_r. Since at resonance the reactance components of the circuit are equal, i.e. $X_L = X_C$ (where $X_L = jL\omega$ and $X_C = \frac{-j}{C \omega}$) the total impedance of the circuit is

$$Z = R + j \ (L\omega - \frac{1}{C\omega}) \qquad (3.20)$$

or simplified to Z = R, which is a pure resistive component. The current through the circuit at resonance is equal to $\frac{e}{R}$ is the pure resistive component of the circuit.

The magnification of the circuit is defined as ,

$$Q = \frac{X}{R} \qquad (3.21)$$

where $X = X_L = X_C$ at resonance.

From relation 3.21 it can be seen that the Q of the circuit equals the ratio of the e.m.f. voltage, V_x, across one or other of the reactances at resonance to the applied, constant e.m.f. V_A. Therefore

$$Q = \frac{V_x}{V_A} \tag{3.22}$$

So for the determination of the Q-factor of a resonance circuit a conventional voltmeter may be connected across the circuit capacitor and this can be calibrated directly in terms of Q. This voltmeter is located on the Q-meter and the Q-value of the circuit is read directly from this meter.

3.3.2 Measurements

In this experiment all samples were cut into thin slices by a diamond wheel cutter and then shaped into squares (1 cm x 1 cm). To ensure good electrical contact circular gold electrodes of 8 mm diameter were evaporated on the opposite polished faces. This reduced the contact resistances between electrodes and specimen (84). Since some of the crystal extended beyond the circular gold electrodes the measured capacitance of sample is not exactly the capacitance of that part of the sample which is confined by the electrodes. Therefore, due to fringing effects, an edge correction is required (77). Thus Eqn.3.16 may be modified to

$$\varepsilon' = \frac{C_1 - C_2}{C_o + C_e} + 1 \tag{3.23}$$

where C_e is the edge capacitance, (explained in detail in the low frequency, Bridge method measurements). The edge effect correction arising in the calculation of tan δ was negligible.

The thickness of the samples was 0.3 mm, this is the minimum

thickness which can be easily achieved by the cutting and polishing techniques used. The thickness of the gold evaporation is negligible compared with the thickness of the sample.

The measurements were made in air at room temperature, using a standard Q-meter (Marconi TF 1245) and oscillator (Marconi TF 1246), over the frequency range of 100 KHz - 40 MHz.

The dielectric testing jig (Marconi TJ 155 C/1) was modified using 8mm diameter circular electrodes and was located inside a metallic box to ensure good electrical shielding of the sample.

The Q-meter is set to zero and this must be checked immediately prior to making each measurement. Then the sample is inserted between the jig electrodes. A constant inductor, L is connected across the circuit. Since the applied frequency is constantly changing a variable capacitor, C_2 on the Q-meter enables the resonance condition to be located. This procedure was repeated when the sample was removed from the jig electrodes. This time the variable capacitor is, C_1. In either case the Q-value of the circuit is measured by direct reading of Q, which is indicated on the meter.

The difference in capacity is function of the dielectric constant ε' (Eqn. 3.16) and the change in the magnitude of Q-value is a function of the loss tangent, (Eqn. 3.17 and of conductivity σ (Eqns. 3.18 and 3.19).

Similar measurements were then repeated at different applied frequencies. The data was used to derive the dielectric properties and conductivity from the Eqns. 3.17 - 3.19 and 3.23.

In practice the knowledge of the effective capacitances of C_1 and C_2 is required and it is given by (82) as

$$C_E = C_{ind} \cdot \frac{1}{1 - \omega^2 L C_{ind}} \qquad (3.24)$$

where C_{ind} is equal to the indicated capacitances C_1 and C_2 and L is the constant inductor used in the resonant circuit (C_E = effective capacitance). At high frequencies the value of C_E is significantly different from the indicated value. The value of the effective capacitance C_E may be found from the conversion graphs (82). In general it is sufficient to use the value indicated by the tuning capacitor.

There are two kinds of error in this experiment. First those related to the original calibrations or inherent imperfection of the Q-meter. These errors will give rise to a fixed error in the measurements. The second one arises from errors in taking the reading for each measurement (102). The latter one can be reduced by increasing the number of measurements.

The error in ε' was about 5%, difficulties in precise re-location of the specimen causes some differences in capacitance, which leads to variation of ε'.

The error in Tan δ is somewhat higher than ε' and its estimation is rather difficult, as contributions arise both from errors of capacitance reading and Q-value determination. The estimated error in Tan δ is about 16%. Consequently the error for ε'' is estimated at 19%. The experimental error in measuring conductivity is about 17%.

3.4   COAXIAL LINE TECHNIQUES AT R.F.

3.4.1 Theory

3.4.1.1 General Principle of the Method

The coaxial line technique is very important since it can be applied to the measurements of complex dielectric constant over a wide frequency range at r.f. Measurements were easily obtained using this technique at frequencies between 500 MHz and 7.5 GHz.

In this method a dielectric sample whose electrical properties are to be found is placed between the inner and outer conductors at the

end of a coaxial slotted-line as shown in Fig. 3.5 (a). The permittivity of the sample can then be calculated from the measured reflection co-efficient at any desired frequency.

The technique is fully described by Roberts and Von Hippel (85) also Dakin and Work (86). Other details of this technique can be found in (87) and (88).

Since the absorption of power in the sample is negligible most of the incident power is reflected and causes a standing wave pattern on the line. The measured Voltage Standing Wave Ratio (VSWR) and con-sequently the reflection coefficient and the shift of the first minimum i.e. (phase angle) give the magnitudes of ε' and ε''.

3.4.1.2 Derivations of ε' and ε''

It is assumed that a small shunt capacitance terminates the coaxial transmission line when a sample in a holder is connected as shown in Fig.3.5 (a). The impedance of the line is then measured and the expressions for the ε' and ε'' deduced. This idea originally was suggested by Westphal (89) who also tried to make a suitable sample holder as shown in Fig. 3.6. Initially it is assumed that, $\lambda \gg$ b-a and d $\ll$ b-a (90-92) where,

λ = wavelength of applied frequency (m)

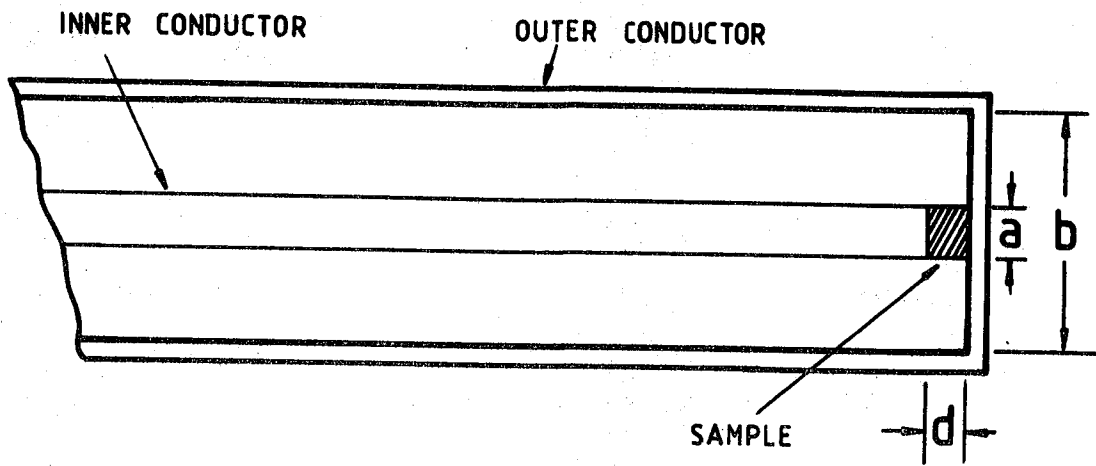The electromagnetic fields are enclosed and propagate along the coaxial line.

The equivalent circuit of the sample impedance is given by a $R(\varepsilon',\varepsilon'')$ and $X_c(\varepsilon',\varepsilon'')$ in series (92) shown in Fig.3.5 (b).

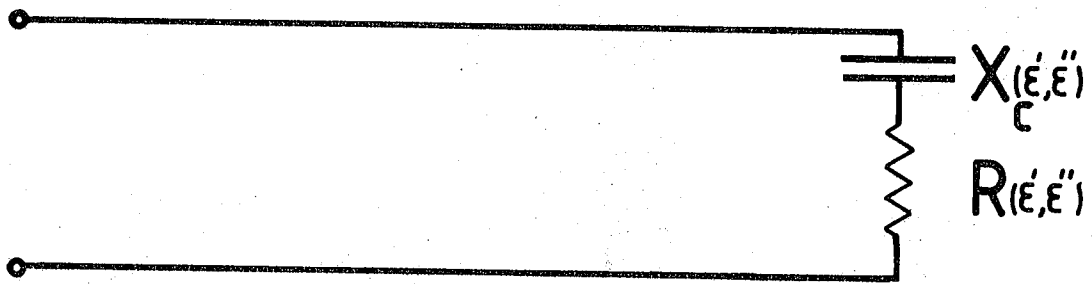The sample impedance is assumed to be given by

$$Z = -\frac{j}{\omega C}$$

where C is the capacitance of the sample, i.e.

$$C = \varepsilon_o \varepsilon^* \frac{A}{d}$$

(a)

(b)

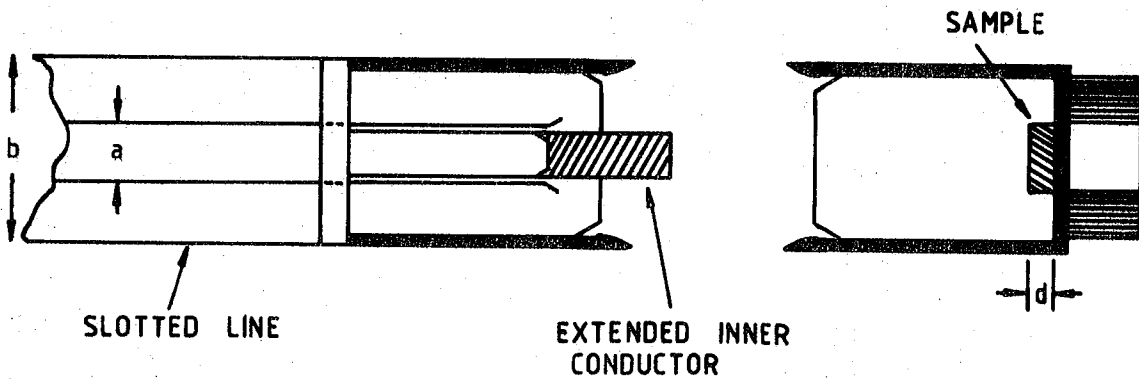FIG. 3.5 (a) COAXIAL LINE WITH SAMPLE.
(b) EQUIVALENT CIRCUIT OF SAMPLE.

FIG. 3.6   SAMPLE HOLDER CONFIGURATION.

and where $\quad \varepsilon_o$ = dielectric constant of free space = 8.854 x 10^{-12} (Fm^{-1})

$\qquad$ A = area of the electrode $\quad$ (m^2)

$\qquad$ d = thickness of the specimen $\quad$ (m)

Since $\varepsilon^* = \varepsilon' - j \varepsilon''$ is the complex dielectric constant of the specimen

the impedance yields real $R(\varepsilon', \varepsilon'')$ and imaginary $X_c(\varepsilon', \varepsilon'')$ components

i.e.

$$R(\varepsilon', \varepsilon'') = \frac{\varepsilon'' \, d}{\omega \, \varepsilon_o \, A(\varepsilon'^2 + \varepsilon''^2)} \qquad (3.25)$$

or

$$X_c(\varepsilon', \varepsilon'') = \frac{\varepsilon' \, d}{\omega \, \varepsilon_o \, A(\varepsilon'^2 + \varepsilon''^2)} \qquad (3.26)$$

From the transmission line theory and assuming that

$$Z = R(\varepsilon', \varepsilon'') - j \, X_c(\varepsilon', \varepsilon'') \qquad (3.27)$$

the real and imaginary parts of the relative permittivity of the sample

can be found in terms of ρ, reflection coefficient and Θ its angle (93-94,

Appendix A) i.e.

$$\varepsilon' = \frac{2 \, |\rho| \quad \sin \Theta}{\omega \, C_o Z_o \, (|\rho|^2 + 2|\rho| \cos \Theta + 1)} \qquad (3.28)$$

and

$$\varepsilon'' = \frac{1 - |\rho|^2}{\omega \, C_o Z_o \, (|\rho|^2 + 2|\rho| \cos \Theta + 1)} \qquad (3.29)$$

where $\quad \omega$ = angular frequency $\qquad\qquad$ (Rad s^{-1})

$\qquad Z_o$ = characteristic impedance (50Ω) $\qquad$ (ohms)

$\qquad C_o$ = capacitance of equivalent capacitor with air:

$$C_o = \varepsilon_o \, \frac{A}{d}$$

As the above equations show ε' and ε'' can now be calculated if $|\rho|$ and θ are known. These can be measured using slotted line technique at the desired frequency.

Iskander (90) has pointed out that the fringing field affects the permittivity measurements. He has shown that the value of ε' is usually larger than the true value, while the value of ε'' is not affected by the fringing. He has also shown that the ε' is larger by a factor of $\frac{B}{A}$ where A is the capacitance of the parallel plates and B is the fringing capacitance. In this experiment the fringing effect was not considered for two reasons. Firstly, the expression for B was not available and secondly it was found that using two different sizes of the sample did not affect appreciably the magnitude of ε'. It was assumed therefore that the effect was within the experimental errors.

3.4.1.3 Standing Wave Ratio

Two waves travelling in opposite directions will interact to produce a standing wave pattern. It is characterised by the stationary points of minimum amplitude along the line called the nodes, and the points of maximum amplitude. The minima and maxima occur alternately along the line and one $\frac{\lambda}{4}$ apart (95). The ratio of the maximum, E_{max} to minimum, E_{min} amplitudes defines the standing wave ratio (SWR), or in the case of voltages the voltage standing wave ratio (VSWR) i.e.

$$S = \frac{E_{max}}{E_{min}} \tag{3.30}$$

It can be shown that (96) VSWR and the reflection coefficient, ρ, are related, thus

$$S = \frac{1 + |\rho|}{1 - |\rho|} \tag{3.31}$$

or

$$|\rho| = \frac{S - 1}{S + 1} \qquad (3.32)$$

where $\qquad \rho = \dfrac{E_r}{E_i} \qquad (3.33)$

in which E_r = reflected wave

$\qquad E_i$ = incident wave

The expression 3.32 can be used to compute the magnitude of

the voltage reflection coefficient from the measurements of the voltage

minima and maxima. By finding the location of the first minimum, x, the

phase angle of ρ may be determined (95) from

$$\theta = 2\beta x - \pi \qquad (3.34)$$

where β is the phase constant given by $\dfrac{2\pi}{\lambda_g}$ and x is the distance.

3.4.2 Experimental

3.4.2.1 Slotted-Line and Probe Assembly

The most important piece of microwave equipment which is used

for measuring VSWR is the slotted line. This is normally used over a

wide range of microwave frequencies. Since the electric field in a

coaxial line is a function of the longitudinal position a probe is mounted

on the line which has a slot along it for sampling the electric field

within the coaxial line. The cross-section of the slotted line is

shown in Fig. 3.7.

As it is illustrated, probe is typically a piece of short

metallic wire which projects into the electric field inside the line.

It is capacitatively coupled to the centre conductor (a). The rf voltage

on the probe is applied to the crystal detector (diode), which produces
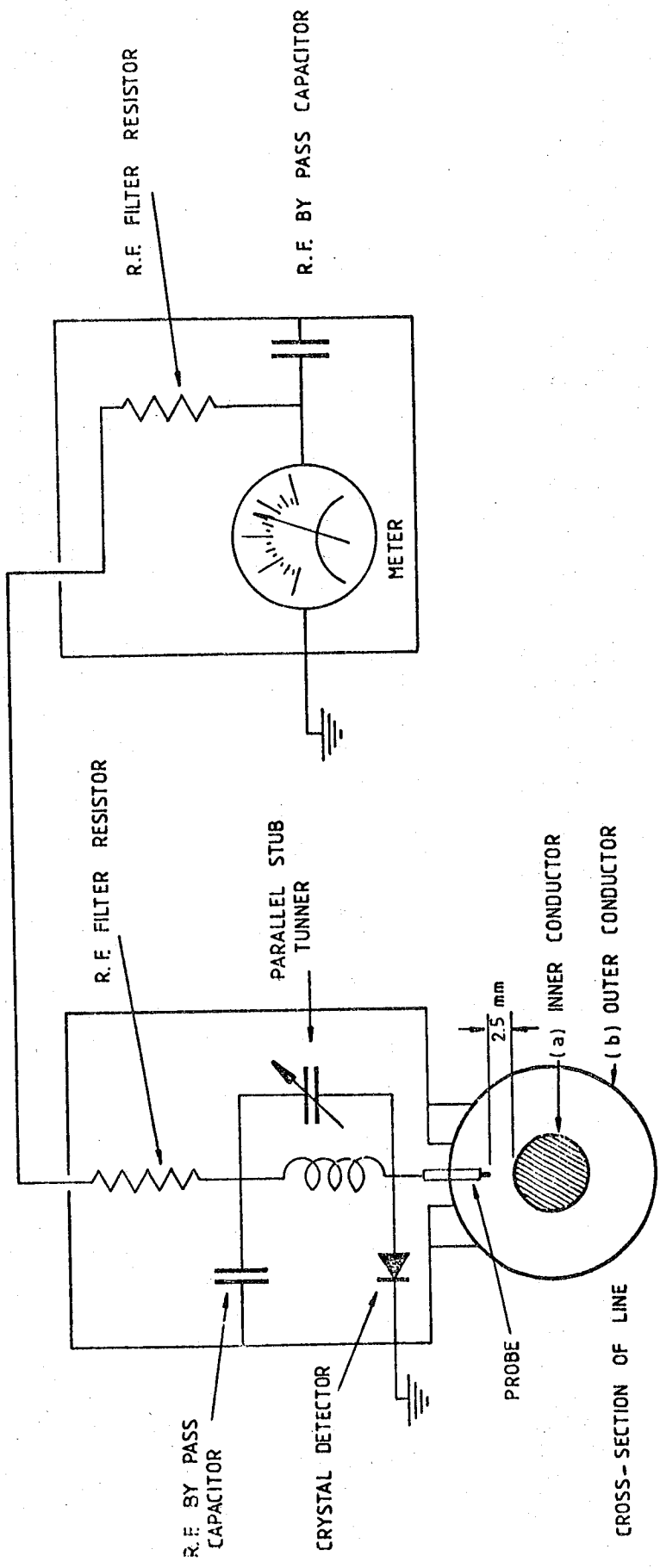
R.F. FILTER RESISTOR

R.F. BY PASS CAPACITOR

R.F. FILTER RESISTOR

PARALLEL STUB TUNNER

R.F. BY PASS CAPACITOR

CRYSTAL DETECTOR

METER

PROBE

2.5 mm

(a) INNER CONDUCTOR

(b) OUTER CONDUCTOR

CROSS-SECTION OF LINE

FIG. 3.7   PRINCIPLE OF SLOTTED LINE.

a direct current output. A meter placed in the circuit will be deflected and will give an indication of the strength of the rf voltage at the probe, which is proportional to the line voltage (Fig.3.7). In order to obtain a sufficient reading on the meter an amplifier is inserted between the probe and the meter. A complete assembly, including probe, carriage, and detector, is often called the Standing Wave Indicator, SWI.

3.4.2.2. Apparatus

The block diagram of the most commonly used standing wave ratio measuring system used in our experiment is illustrated in Fig.3.8.

The lowest carrier frequency in the measurements was 500 MHz modulated with 1 kHz. Another signal generator was used (TF 1060 Marconi) for the frequency range from 750 MHz to 1 GHz. Higher frequency ranges were covered by 1.5-5 GHz and 4-12 GHz signal generator. The frequency values chosen were to give wavelength easy to measure and calculation.

The slotted line used was General Radio (874-LBB) with the frequency range from 300 MHz to 8.5 GHz. The assembly included crystal detector, probe and tuning stub which are shown in Fig. 3.9.

The VSWR measuring instrument which also included the audio amplifier was (V.S.W.R. Amplifier A.K.III).

The sample holder was basically a section of coaxial line in which the sample was placed between the extended inner conductor and the short circuit termination. This is illustrated in Fig.3.6.

3.4.2.3 Setting Up Procedure

The conventional experimental techniques have been used before the measurements were taken. This involved allowing the apparatus initially a warm-up time in order to achieve a stable performance. When the satisfactory conditions have been reached the measurements of VSWR and the distance of the first minimum were noted. A number of measure-
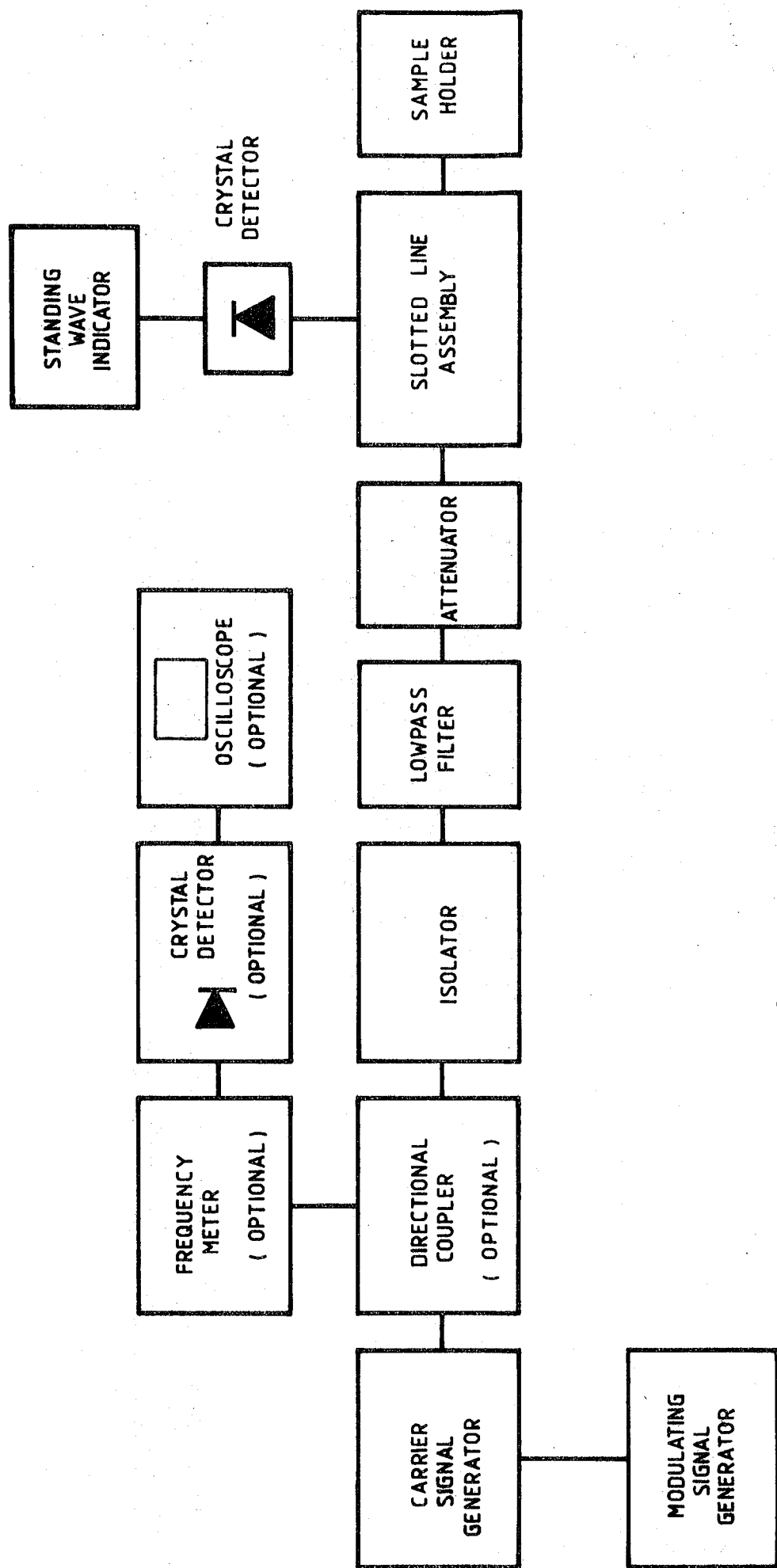
FIG. 3.8   BLOCK DIAGRAM OF APPARATUS;
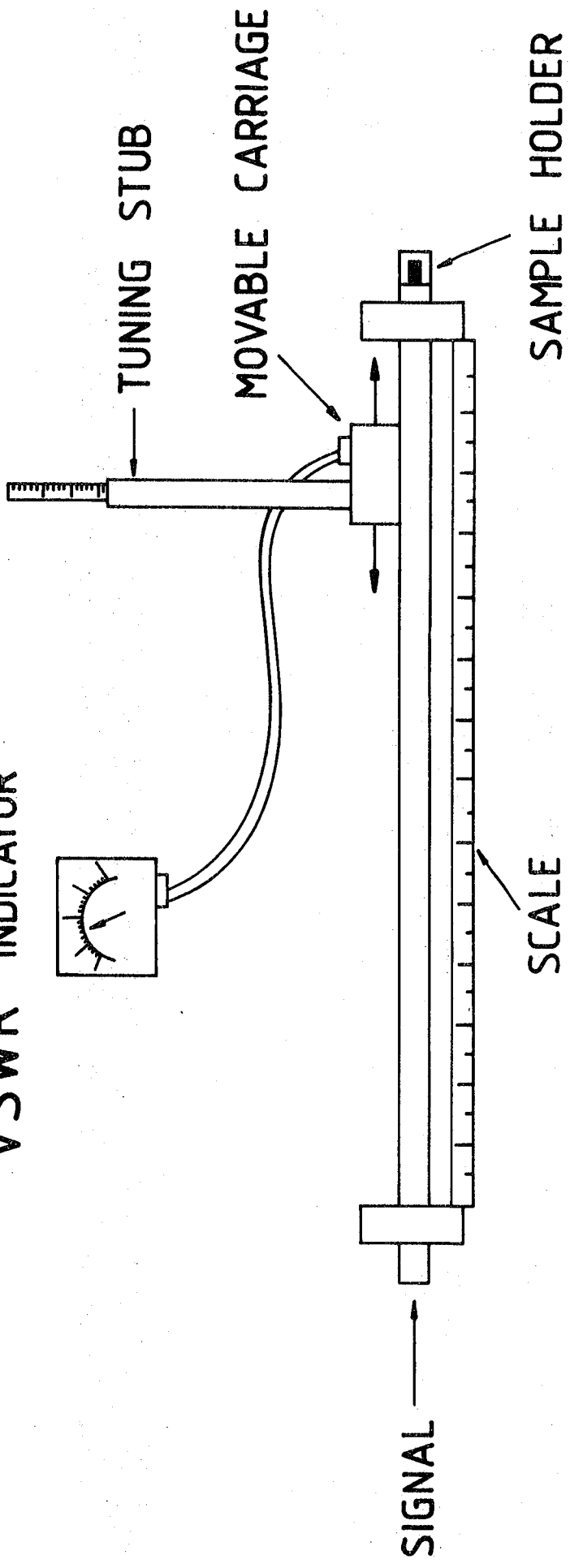r.f. MEASUREMENTS.

FIG. 3.9   SLOTTED LINE AND ITS ASSEMBLIES.

ments were taken and the final result determined by averaging.

The samples were mostly of rectangular shape and as long as the area of the inner conductor was covered actual dimensions did not affect measurements considerably, i.e. fringing effects were negligible. It must be ensured that the sample surfaces are parallel to each other to avoid any stray capacitance effect. In order to obtain the best results it was next necessary to tune the probe and stub assembly on the slotted line. The recommended distance of 2.5 mm from the inner conductor for the probe was set (97) and was found to give the best results (Fig. 3.7). The output from the diode rectifier was adjusted for maximum as indicated on the VSWR instrument using a tuning stub as shown in Fig. 3.9.

Since the carrier was amplitude-modulated the output from the diode detector (envelope detector) was at the frequency of about 1 kHz and was directly proportional to the rf power, provided the detector is operating in the square-law region.

It is important to take care that the stub tuning is done on the required fundamental and not on the harmonics present in the line. This can be ensured by measuring the distance between the two minima which must be equal to $\frac{\lambda}{2}$. The stub was capable of being tuned at anywhere from 275 MHz to 8.5 GHz.

3.4.2.4 VSWR Measurements

There are various methods available for measuring VSWR and which one is suitable will normally depend on the magnitude to be measured. Three basic methods which are very often used are (a) the direct method, which uses the VSWR indicator and amplifier, (b) the attenuator method, which measures the difference in decibels between the minimum and maximum (95,98), i.e. since the (SWR) in decibel is

given by,

$$\text{SWR (dB)} = 20 \text{ Log}_{10} \text{ VSWR} \qquad (3.35)$$

or

$$\text{VSWR} = \text{anti Log}_{10} \frac{\text{dB}}{20} \qquad (3.36)$$

and (c) graphical method used mainly for high values of VSWR. Although the direct method (a) is probably the least troublesome, it is not suitable for VSWR greater than 50, because the accuracy cannot be guaranteed. In addition it was found that the measurement of E_{max} could not be determined with precision, since the amplifier in VSWR instrument was saturating. A direct method of measuring voltage of the standing wave pattern at the minimum is possible using very sensitive electrometer instrument for measurement of d.c. currents down to 10^{-11}, 10^{-12} or even 10^{-13} amperes.

The attenuation method, (b) requires a precision variable atten-uator (91) and since it was not available we could not check the suitability of this method.

It was finally decided that for the magnitude of VSWR involved the graphical method (c) will probably be the most appropriate.

In order, however, to obtain the best results it was necessary to carry out the calibration of the crystal detector (Appendix B), probe and stub assembly. Precise measurements of the field intensity had to be measured on both sides of the minimum from which using slope lines the value of the minimum was determined. Since the detector system is only used for indicating the relative intensity, there was no need to modulate the rf signal generator, and any meter would be suitable. The signal generator was therefore left in C.W. mode of operation and the detected signal was the d.c. component of the crystal detector measured

using a sensitive ammeter or galvanometer. Provided the operation was
in the square-law region one could relate the current measured to the
power input.

The measurements of the standing wave magnitude at each point
were reproduced graphically on paper(Fig.3.10). The ratio of the maxi-
mum to minimum values gives the required VSWR.

Even with this method it was found that large errors are
possible in obtaining E_{min} of the standing wave pattern.

3.5   RESONANT CAVITY METHODS AT MICROWAVE

3.5.1 Theory

3.5.1.1 Cavity Resonator

Various methods of measuring dielectric constant of bulk material
at X-band (9.3 GHz) have been suggested by a number of research workers,
(99-101). One of the most successful is the perturbation technique using
a microwave cavity resonator.

The technique involves inserting a small piece of a dielectric
material inside the resonant cavity. It is placed on the end of a thin
silican rod which is then suspended in the position of maximum electric
field. The resultant shift of the resonant frequency of the cavity gives
the real part of the complex dielectric constant, and the change in the
quality factor, Q, gives the imaginary part.

A cavity resonator is an enclosed space which is capable of
oscillating and storing energy. It is analogous to a low frequency
resonant circuit consisting of an inductance, a capacitance and a loss
resistance. In such a resonant cavity a large number of modes vary
according to the shape of the cavity. The resonant cavity designed was
a 2.23 cm cubic made of copper. In practice a hole in one side of the
cavity is used for coupling the electromagnetic power into it via a
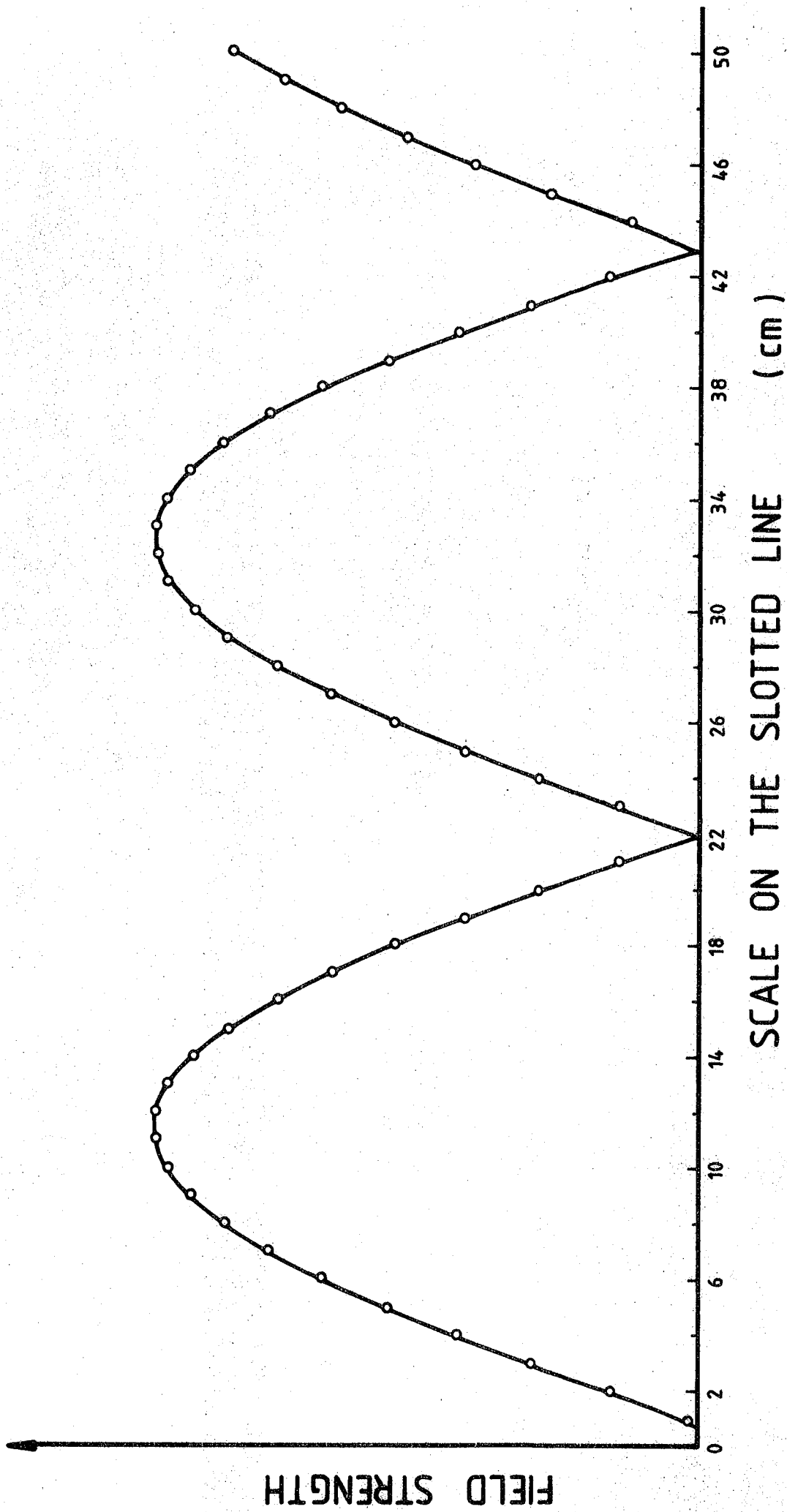length of waveguide. The field patterns are in general denoted by a

FIG. 3.10   STANDING WAVE PATTERN AT 710 MHz; SHORT CIRCUIT.

SCALE ON THE SLOTTED LINE   (cm)

FIELD STRENGTH

particular nomenclature, e.g. $TE_{\ell,m,n}$ or $TM_{\ell,m,n}$. The first means Transverse Electric field and the latter Transverse Magnetic field and subscripts ℓ, m and n indicate half wavelength changes of the field in the three directions x, y and z. The diagram of the resonant cavity with its electric and magnetic field pattern is shown in Fig.3.11. To obtain solution for the electromagnetic fields within a cavity the mathematical treatment is based on Maxwell's field equations with the following assumptions :

1. the cavity is completely surrounded by perfectly conducting walls,

2. the form of the field and the resonant frequency are not affected appreciably by the fact that the walls have a finite conductivity.

The general expression for the fields of a TE_{101} mode in a rectangular cavity are given by Montgomery (99),

$$
\left\{
\begin{aligned}
E_y &= \frac{\sqrt{2}}{2} \sin \frac{\pi x}{a} \sin \frac{\pi z}{c} \\[2ex]
H_x &= \frac{\pi\sqrt{2}}{2a} \sin \frac{\pi x}{a} \cos \frac{\pi z}{c} \\[2ex]
H_z &= \frac{\pi\sqrt{2}}{2a} \cos \frac{\pi x}{a} \sin \frac{\pi z}{c}
\end{aligned}
\right.
\tag{3.37}
$$

The electric field lines of this cavity with TE_{101} mode are seen to have a maximum value at the centre of the xoz-plane (Fig.3.11). The resonant frequency of the cavity is given by (99,103),

$$
f_o = \frac{c}{2} \sqrt{ \left(\frac{\ell}{a}\right)^2 + \left(\frac{m}{b}\right)^2 + \left(\frac{n}{c}\right)^2 }
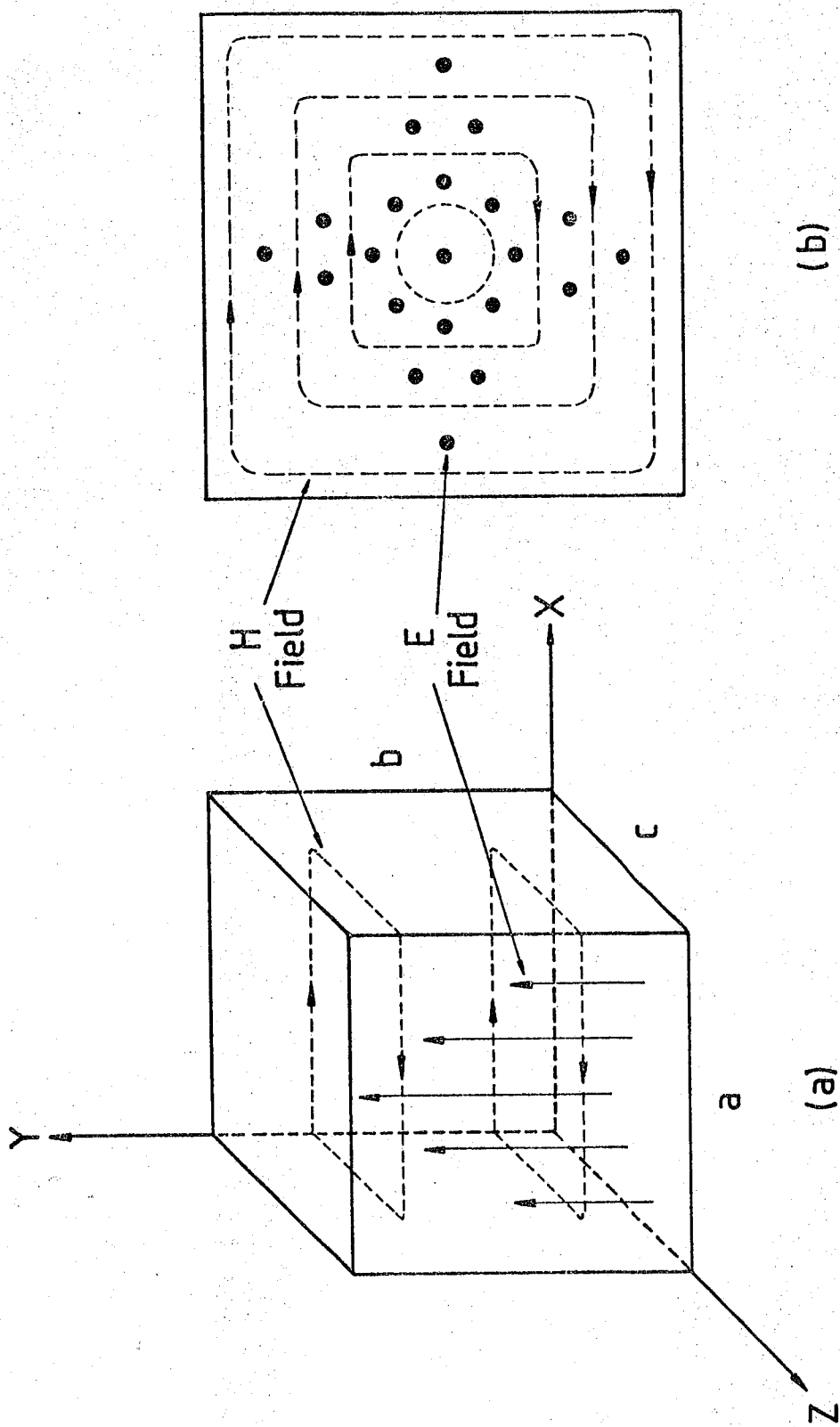\tag{3.38}
$$

FIG. 3.11   a) RESONANT CAVITY, TE$_{101}$ MODE.

b) TOP VIEW OF THE ELECTRIC, E AND MAGNETIC, H
     FIELDS OF THE TE$_{101}$ MODE.

where

C = velocity of electromagnetic wave in free space.

a,b,c = dimensions of cavity

The cavity is characterized by its resonant frequency and the quality factor, Q. It is defined as 2π times the ratio of the energy stored in the cavity to the energy dissipated per cycle (104),i.e.

$$Q = 2\pi \cdot \frac{\text{Energy Stored}}{\text{Energy dissipated per cycle of oscillation}}$$

It may also be approximated to the ratio of the resonant frequency to the bandwidth at the half-power points (at 0.707 of voltage or current maximum) i.e. $\frac{f_o}{\Delta f}$. Q is also proportional to the ratio of the volume to the internal surface area.

Many authors point out (104) that, in order to decrease the losses of the electromagnetic wave inside the cavity the inner surface must be made as smooth as possible. This increases the quality factor, Q, of the cavity. The quality factor for the TE_{101} mode is given by (99,105-106),

$$Q = \left\{ \frac{abc \; \lambda_g}{2\delta} \right\} \frac{\left\{ \frac{1}{a^2} + \frac{1}{c^2} \right\}^{\frac{3}{2}}}{\frac{c}{a^2}(a + 2b) + \frac{a}{c^2}(c + 2b)} \tag{3.39}$$

where δ is the skin depth given by,

$$\delta = \left\{ \frac{\rho}{\pi\mu \; f} \right\}^{\frac{1}{2}} \tag{3.40}$$

and

ρ = resistivity of the metal wall   (ohm m)

μ = permeability of the wall   ($H \; m^{-1}$)

f = frequency of the cavity   (Hz)

3.5.1.2 Coupling

In the theory of the coupling hole it is usually assumed that the radiation may be represented by an equivalent electric and magnetic dipoles located in the hole (103). The electric field is perpendicular and the magnetic field is parallel to the plane of the hole. The physical reprsentation of the hole and the associated fields are shown in Figs. 3.12-14 for the electric field and Figs. 3.15-17 for the magnetic field.

The effect of a small hole on a resonant cavity has been published by Bethe (107). Collin (103) has proposed that if the radius of the hole $r_o < \lambda_o$ then it may be considered as being equivalent to two dipoles, electric and magnetic. The hole with radius r_o and electric field in the plane of hole are shown in Fig.3.18. The magnetic dipole is given by,

$$M = \frac{8}{3} r_o^3 C Y \qquad (3.41)$$

where

C = the amplitude of the incident mode

Y = wave admittance for the TE_{10} mode

The direction of M is shown in Fig. 3.19. The susceptance of the hole is represented by (103),

$$jB = -j \frac{3ab}{8 r_o^3 \beta} \qquad (3.42)$$

whose value will depend on the frequency of the applied signal and the radius of the hole and β is the phase constant. Its magnitude becomes rapidly infinite when the radius of the hole approaches zero as shown in Fig. 3.20. To determine the radius of the coupling hole, two important factors must be considered:
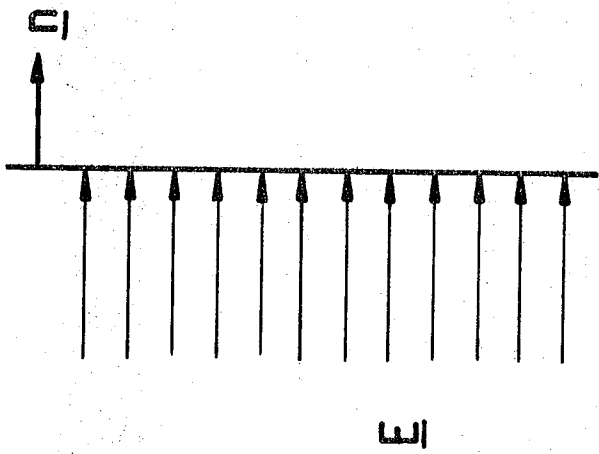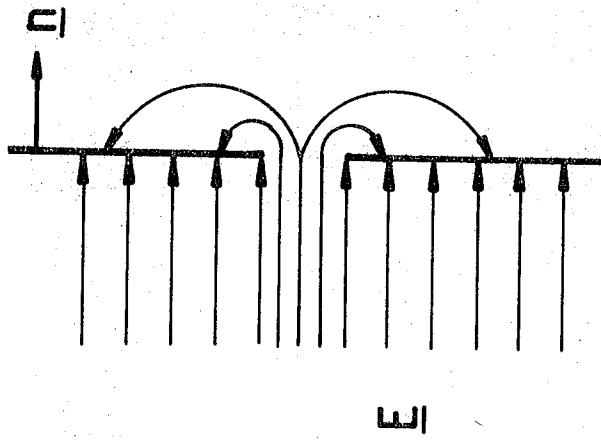
$\underline{n}$

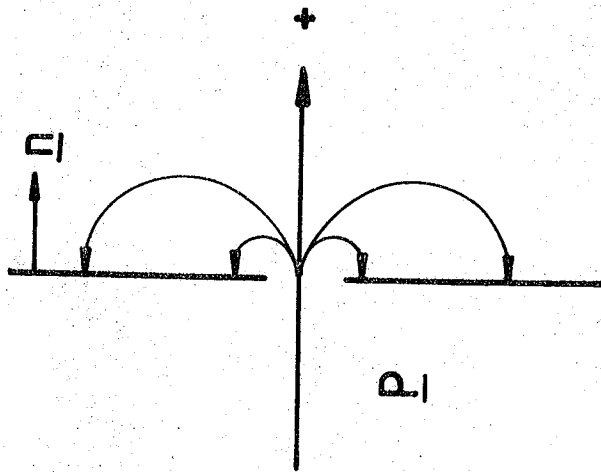$\underline{P}$

FIG.3.14   ELECTRIC DIPOLE.

$\underline{n}$

$\underline{E}$

FIG.3.13

$\underline{n}$

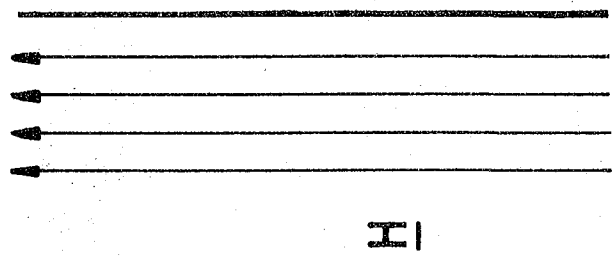$\underline{E}$

FIG.3.12

PHYSICAL REPRESENTATION OF ELECTRIC FIELD.

FIG.3.17

MAGNETIC DIPOLE.

$\underline{P}$

FIG.3.16

$\underline{H}$

FIG.3.15

$\underline{H}$
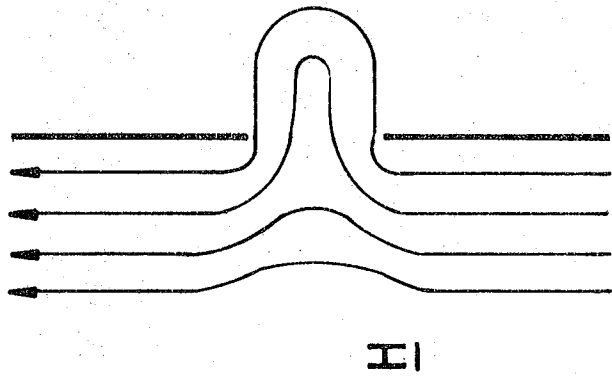
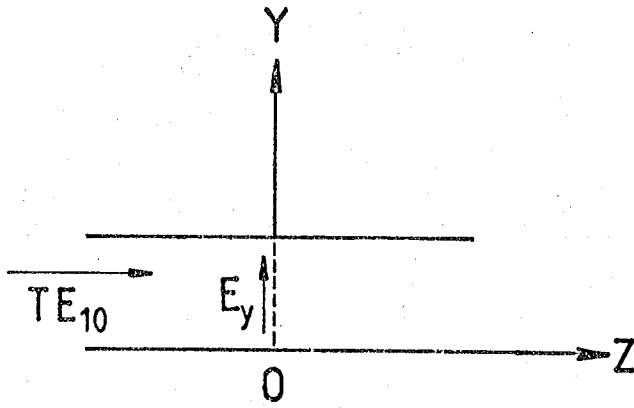PHYSICAL REPRESENTATION OF MAGNETIC
FIELD.

FIG.3.18 b
ELECTRIC FIELD AT THE
COUPLING HOLE.
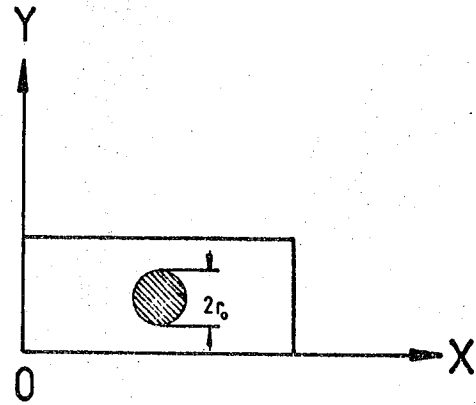
FIG.3.18 a
COUPLING HOLE.

FIG.3.19
MAGNETIC DIPOLE AT THE HOLE.

RADIUS

0   5   10 r_c (mm)

-10

- 30

- 50

- 70

- 90

- 110

- 130

- 150

B

SUSCEPTANCE
(OHM^{-1})

THEORETICAL CURVE,
VARIATION OF COUPLING HOLE
SUSCEPTANCE.
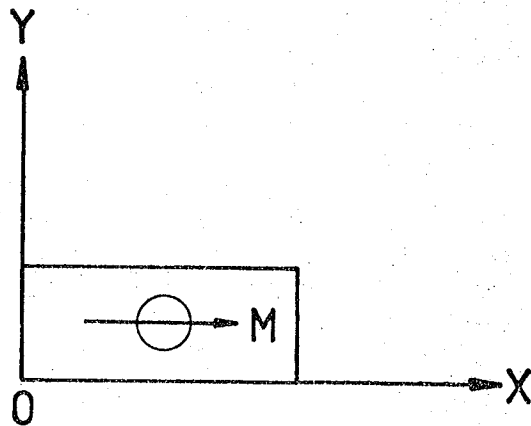
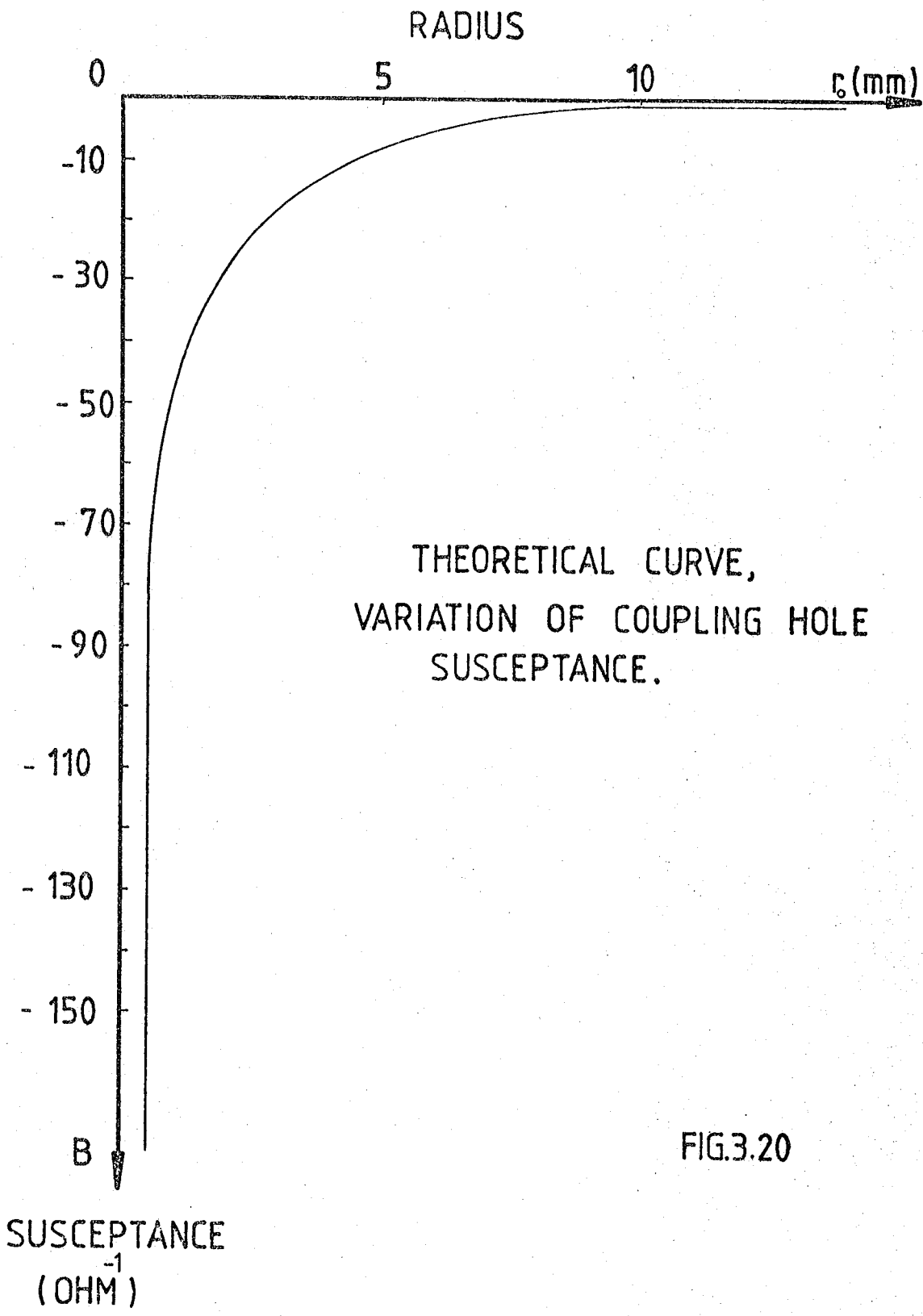FIG.3.20

1. the Q of the cavity should be as high as possible. The increase in the radius of the coupling hole lowers the quality factor Q.

2. on the other hand, the radius of the hole should not be too small since then the magnitude of the susceptance increases too much. (Fig. 3.20).

In this case delivery of power to the resonant cavity encounters difficulties. As a result, the radius is normally found empirically and the best size which is recommended at 9.3 GHz is between 3 and 4 mm.

The inductive susceptance may be represented as discontinuity between the cavity and the waveguide. This discontinuity can be cancelled by employing another discontinuity at another place along the waveguide. This is normally achieved using tuning screws as matching components.

The equivalent circuit of the resonant circuit is shown in Fig. 3.21 (81). From the definition of Q it can be written (100) that,

$$Q = \frac{\omega U}{P} \tag{3.43}$$

where U is the energy stored and P is the power dissipated in the cavity. There are three kinds of Q distinguished (108), (a) Q_u (the unloaded Q) where only loss in the cavity is taken into account, is given by,

$$Q_u = \frac{\omega_o L}{R} \tag{3.44}$$

(b) Q_L (the loaded Q) in which the loss of the cavity and the coupling system (hole) are taken into account, i.e.

$$Q_L = \frac{\omega_o L}{R + Z_o} \tag{3.45}$$

and (c) Q_E (the external Q) where the loss due to an external circuit

is taken into account, i.e.

$$Q_E = \frac{\omega_o L}{Z_o} \qquad (3.46)$$

where by definition $\beta = \dfrac{Z_o}{R}$ is the coupling parameter. On substitution

Eqn. 3.44 in Eqn. 3.45 we obtain,

$$Q_L = \frac{Q_u}{1 + \beta} \qquad (3.47)$$

and

$$Q_E = \frac{Q_u}{\beta} \qquad (3.48)$$

These three types of Q are related to each other via the relation,

$$\frac{1}{Q_L} = \frac{1}{Q_u} + \frac{1}{Q_E} \qquad (3.49)$$

which states that the total loss of energy in the system (cavity and

hole) is equal to the sum of the losses in the cavity and coupling. From

Eqn. 3.48

$$\beta = \frac{Q_u}{Q_E}$$

or since

$$\frac{1}{Q_E} = \frac{Z_o}{\omega_o L} \quad \text{and} \quad \frac{1}{Q_u} = \frac{R}{\omega_o L} \quad \text{therefore} \quad \beta = \frac{Z_o}{R}$$

when $\beta = 1$, $Q_u = Q_E = 2 Q_L$ and consequently, $R = Z_o$. The cavity is

then matched to the waveguide and the coupling is called critical. When

$\beta < 1$, the cavity is undercoupled and when $\beta > 1$ the cavity is over-

coupled. In practice few methods of coupling are used. However, to

obtain a high Q system a round hole should be used as coupling (98).

3.5.1.3 Matching and Perturbation Theory

As it has been pointed out by Bethe and later by Collins, the coupling hole across the waveguide is equivalent to a normalized susceptance and it presents a discontinuity in the waveguide ; as a result mismatch of a condition occurring the energy of the electromagnetic wave cannot go through the hole completely. This effect of mismatch can be cancelled at any particular frequency by introducing another discontinuity else- where in the system, whose reflection coefficient is in antiphase with that of the original mismatch. This can be done by either single or double screw matching sections which may be inserted in the waveguide. These metal screws extend into the guide only a short distance in comparison with the wavelength as shown in Fig. 3.22. Since the electric field E is effectively the same value on either side of the screw, the tuner can be represented by a shunt admittance. Because the line is loss- less, this shunt admittance can be assumed as a pure susceptance as shown in Fig. 3.23.

The tuning screw has a capacitive effect whenever its length $d < \frac{\lambda}{4}$ and it has inductive effect when $d > \frac{\lambda}{4}$.

In practice two screws are often used as shown in Fig. 3.24. Their combination forms a matching unit known as two stub tuner. Their equivalent circuit may be represented as shown in Fig. 3.25. For matching the cavity impedance, the tuners are adjusted in such a way that the normalized input impedance (with respect to Z_0) of the system is unity (109).

The distance of the first screw from the cavity has been given in (105) and its position is very critical. The distance between screws is equal to $\frac{3}{8} \lambda_g$, where λ_g is the guide wavelength.

The normalized susceptance of a single screw is given by (103) and for two screw combination matching units it is usually determined

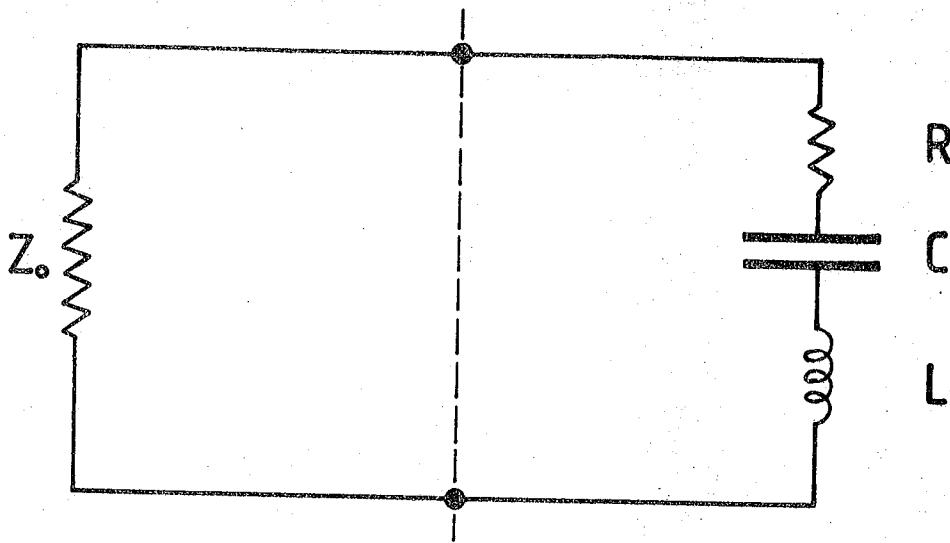FIG.3.21   EQUIVALENT CIRCUIT OF
          RESONANT CAVITY.
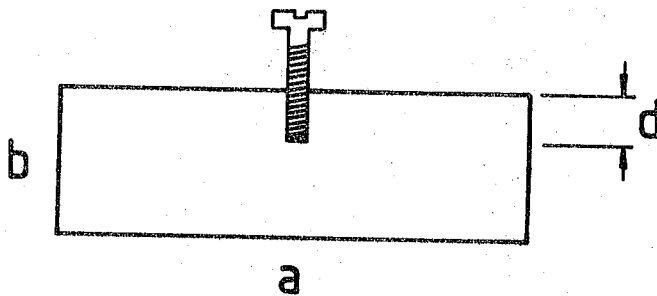
FIG.3.22   MATCHING SCREW
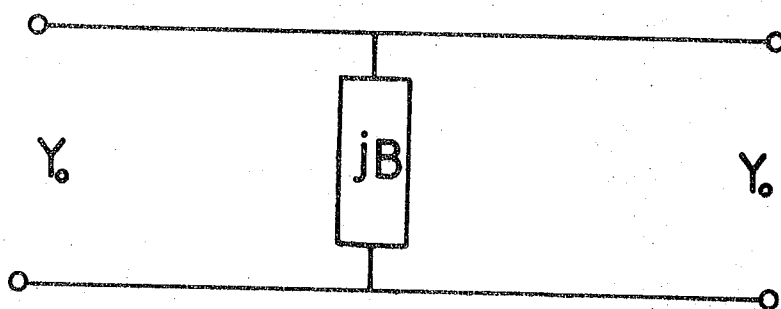
FIG.3.23   MATCHING SCREW AND ITS
          EQUIVALEN CIRCUIT.

QUARTZ ROD

SAMPLE

WAVEGUIDE
16

$\frac{3}{8}\lambda_g$

$\lambda_g/2$

$\lambda_g/2$

MICROWAVE
POWER
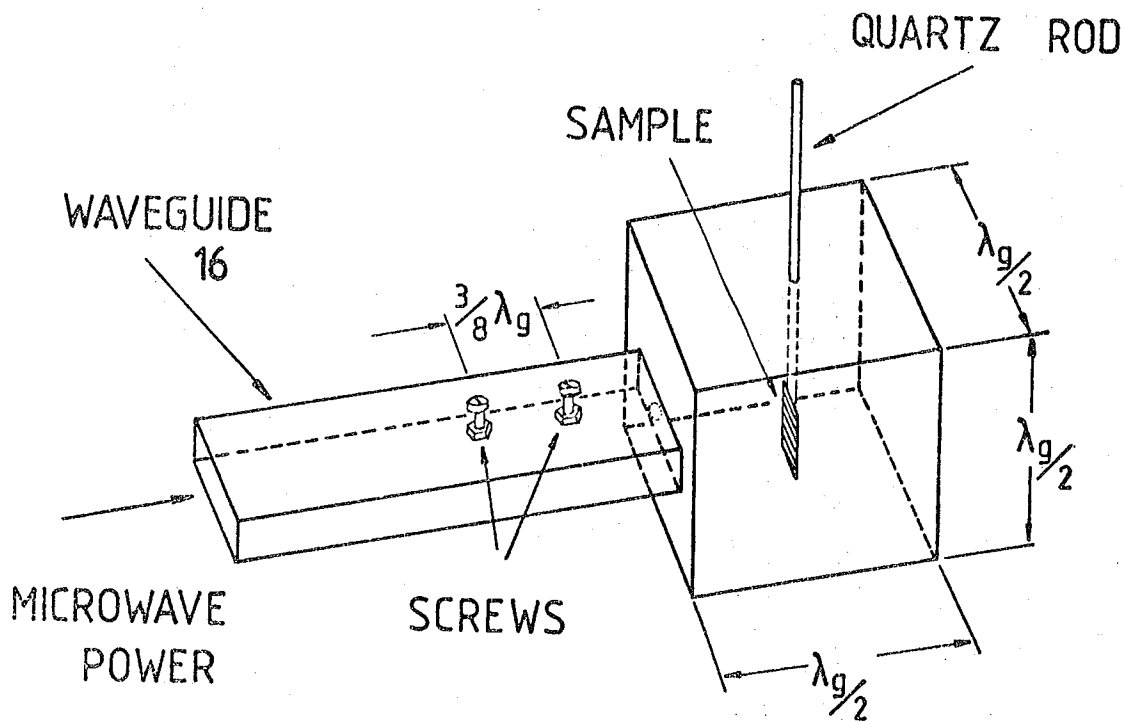
SCREWS

$\lambda_g/2$

FIG.3.24
CAVITY, SAMPLE ARRANGEMENT AND
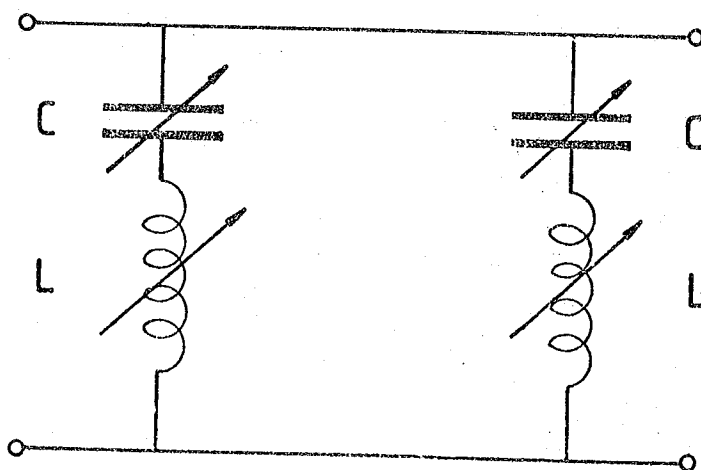MATCHING SCREWS.

C

L

C

L

FIG.3.25
EQUIVALENT CIRCUIT OF SCREWS.

graphically using circle diagram (105).

When a small piece of dielectric material is introduced into a cavity, the quality factor, Q, and the resonant frequency change. The relations between these changes and the properties of the dielectric material which are deduced from the perturbation theory were first proposed by Casimir (110). Then it was further extended and developed by Waldron (111 and 112) and others (100, 113, Appendix C), i.e.

$$\frac{\Delta f}{f_o} = -2 \ (\epsilon'-1) \ \frac{V_s}{V_o} \tag{3.50}$$

and

$$\Delta(\frac{1}{Q}) = 4 \ \epsilon'' \ \frac{V_s}{V_o} \tag{3.51}$$

where V_s = volume of sample

V_o = volume of cavity

The negative sign in Eqn. 3.50 indicates that Δf is negative, i.e. by introducing a sample the frequency of the cavity is lowered (114). If the Q of the unperturbed and perturbed cavity are measured as well as the shift of resonant frequency then the ϵ' and ϵ'' can be determined.

The method is a well known tool, and the only limitations are that the frequency shift should be much less than 1% and that the volume of the material introduced should not alter appreciably the field inside the cavity. It is important to introduce the sample at a point in the cavity where the magnetic field is zero and the electric field is maximum (111).

3.5.2 Experimental

3.5.2.1 Apparatus

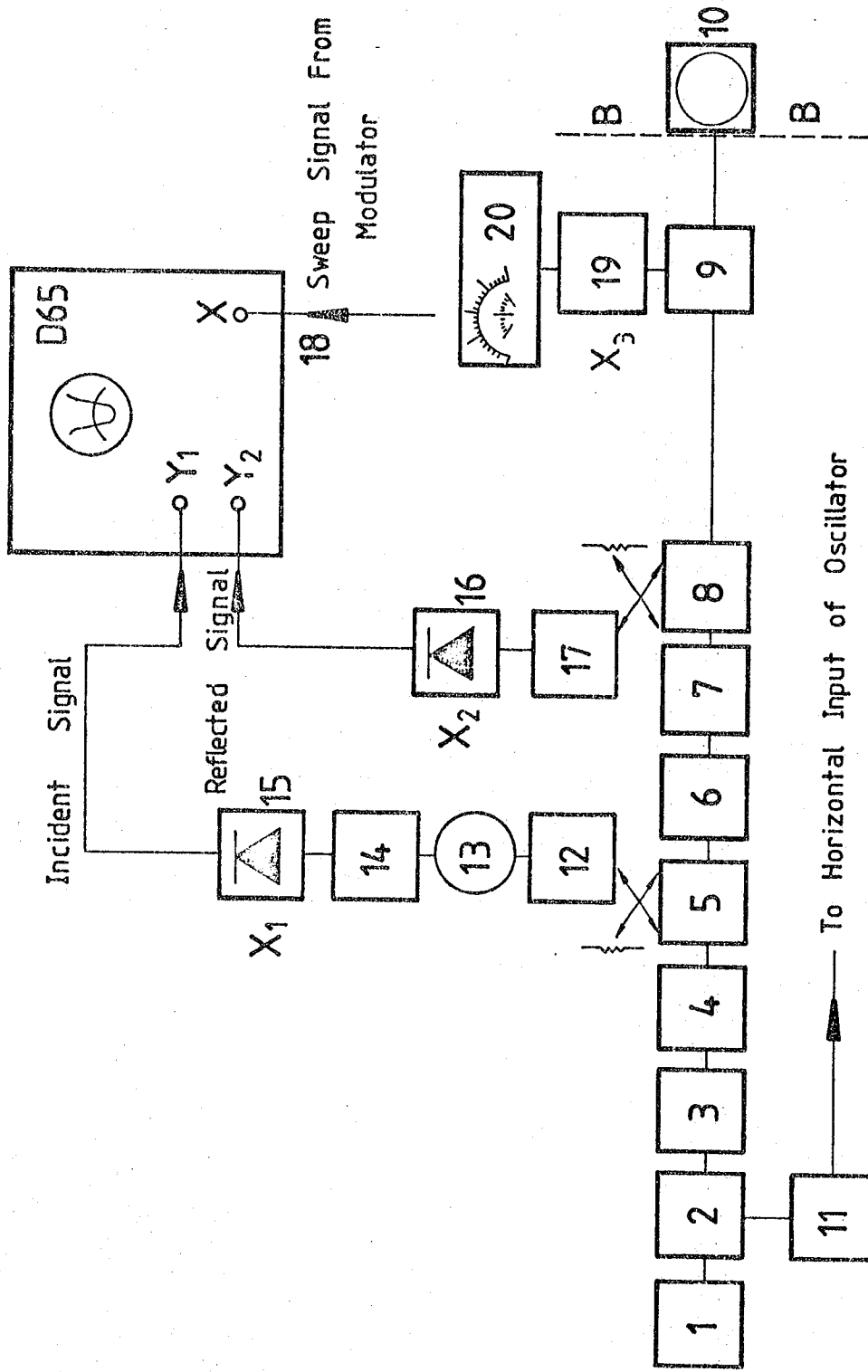The block diagram of the apparatus is shown in Fig. 3.26.

FIG.3.26

BLOCK DIAGRAM OF MICROWAVE APPARATUS.

A reflex klystron was used as the microwave source and the modulation
for producing the frequency sweep was provided by a sawtooth waveform
generator. Two chosen crystal detectors X_1 and X_2 showed an almost
identical response for the required power and frequencies. The set up
consisted of the following equipment :

1. Power Supply

2. Reflex Klystron

3. Isolator I

4. Attenuator I

5. Directional Coupler (incident power)

6. Isolator II

7. Attenuator II

8. Directional Coupler (reflected power)

9. Slotted-line

10. Cavity under test

11. Modulator (Sawtooth waveform generator, RAMP generator)

12. Attenuator III

13. Wavemeter (cavity)

14. Precision attenuator IV

15. ⎫
16. ⎬ Matched pair crystal detector, X_1 and X_2

17. Attenuator V

18. Dual trace osscilloscope (D 65)

19. Crystal detector, X_3

20. V.S.W.R. Indicator

3.5.2.2. Calibration and Matching

Admittance of the combination of coupling hole and cavity is
given by $Y = G - jB$ where R is ($R = \frac{1}{G}$) is the resistance of the cavity
and B is the susceptance of the hole which can be determined with the

aid of graphs (115). It is assumed that the coupling hole does not have any resistance and if it does it is too small to be considered.

The waveguide with admittance $Y_o = \dfrac{1}{Z_o}$ is connected to a termination $Z \neq Z_o$ (Z_o is the characteristic impedance of waveguide). According to the principles of transmission lines the propagated wave, if $Z \neq Z_o$, is partly reflected and the standing wave pattern is created. It is known that the impedance varies in a periodictable manner and repeats its value every half-a-wavelength. It is assumed that the admittance of the guide at B'-B' is G-jB. By means of tuning screws the susceptance of +jB can be introduced at B'-B' which cancels the susceptance of the hole. The resistance of the screws can be ignored. As shown in Fig. 3.27 at the B'-B' the conductance of the cavity is equal to the conductance of the guide, i.e. G_o = G.

The setting up and calibration procedures are as follows :-

(i) With the cavity in test position (B-B plane) the Klystron reflector voltage is adjusted and klystron cavity tuned to the desired mode as indicated by a dip on the oscilloscope (Y_2) display in Fig.3.28. The incident signal without a dip is given by the oscilloscope Y_1 display, Fig. 3.28. The dip is caused by the cavity absorption and placing it on the top of the klystron mode on the Y_2 display ensures that the klystron is operating at the resonant frequency of the cavity.

(ii) For calibration purposes the cavity is disconnected and a short circuit plate is introduced in position B-B.

(iii) Attenuators III, IV and V were set to zero attenuation.

(iv) Attenuator I was adjusted to decrease the incident power to crystal detectors X_1, X_2 and X_3 to ensure that the operating range is within the square law characteristic.

(v) Before applying the outputs of the crystals to the oscilloscope input sockets, the two base lines are first brought into coincidence
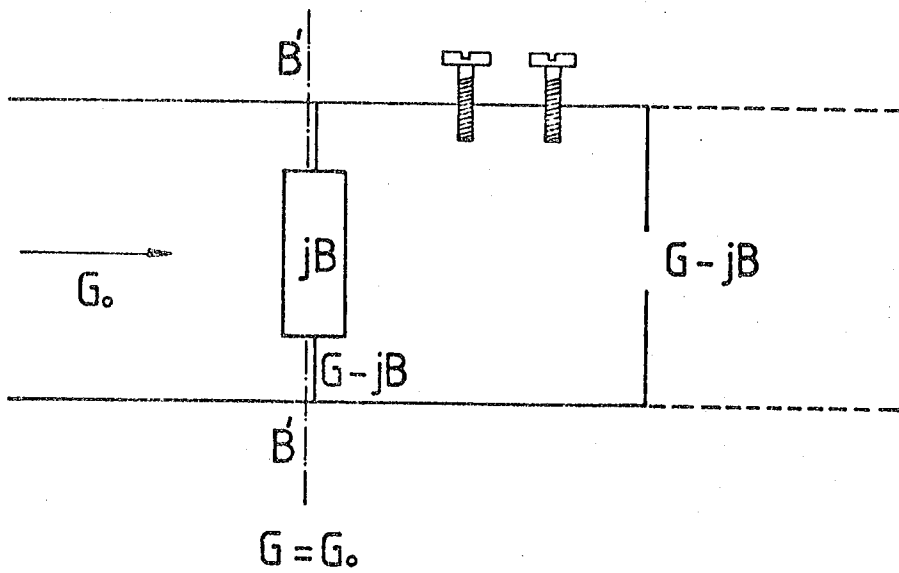
FIG. 3.27

EQUIVALENT CIRCUIT OF CAVITY AND MATCHING
SCREWS ADMITTANCE.

INCIDENT TRACE
OUTPUT OF X_1
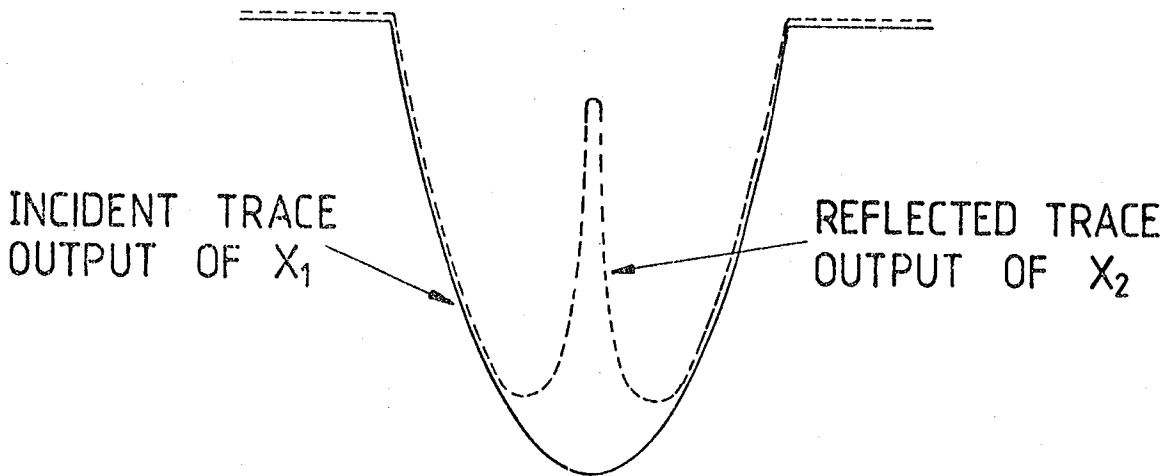
REFLECTED TRACE
OUTPUT OF X_2

FIG. 3.28

KLYSTRON MODE.

by vertical centering control. The output of each crystal was brought

to zero for checking that the base lines are coincident.

(vi) After connecting outputs of X_1 and X_2 to the oscilloscope

inputs, the traces of the crystals should coincide ; if they do not

this can be corrected by attenuator V. Whenever the attenuator I is

varied from (0-15) dB, both outputs should ideally decrease at the same

rate. The discrepancy was determined by the residual attenuation in IV.

The magnitude of this discrepancy was about 1 dB.

After the calibration of the system was carried out the cavity

was replaced back at B-B, and both incident and reflected traces were

then displayed on the screen of the oscilloscope. On the reflected trace

a dip was observed which relates to the resonance of the cavity.

Two methods of tuning the cavity were considered, i.e.

(a) Using the Resonant Curve on the Oscilloscope

When the matching condition is approached the display curve

becomes sharper and the bottom of it reaches up to the base line (114)

as shown in Fig. 3.28. The actual match is indicated by the dip to the

zero power level on the oscilloscope. Obviously this method is fairly

tedious experimentally, because the two screws can have many combinations.

(b) V.S.W.R. Method

When the cavity is matched to the waveguide the VSWR approaches

unity. The values of the VSWR will normally be just above unity. Under

the matched conditions very accurate measurements are required (95).

Special attention should be paid therefore to the instrument measuring the

VSWR. The VSWR of less than 1.05 should be aimed for to obtain a good

match.

3.5.2.3. Measurements

The system was now calibrated and matched and is ready for the

measurement of Q and f_o. At this point it was necessary to ensure that

the incident and reflected traces were coincident as shown in Fig. 3.28.

If there was not an adjustment which had to be made using the calibrated

attenuator IV which also gave the square of the reflection coefficient.

Frequency f_o - By lowering incident power trace the corresponding trace

touches the bottom of the resonant curve (minimum point) of the

reflected power trace as shown in Fig. 3.29.

Then by tuning the wavemeter its resonant dip was brought on

the top of the minimum point and centre frequency (resonant frequency f_o)

was measured as shown in Fig. 3.30.

Quality Factor, Q - By adjusting the precision attenuator IV the three

decibel points were found which determined the half power line on the

resonance curve as shown in Fig. 3.31.

The dip of the wavemeter was brought to the intersection of

the two traces on the right and on the left side of the centre frequency

and two frequencies f_1 and f_2 were then determined as in Fig. 3.32.

The bandwidth $\Delta f = f_1 - f_2$ was calculated and Q determined from

(115).

$$Q = \frac{f_o}{f_1 - f_2} \qquad (3.52)$$

The relationship between loaded and unloaded Q of the cavity is

given by

$$Q_u = (1 + \beta)Q_L \qquad (3.53)$$

where β is the coupling factor.

Coupling Factor, β- For the determination of the coupling factor, β ,

which is the function of the coupling hole dimensions the slotted line

was utilized, Firstly, voltage standing wave ratio, VSWR of the system

was measured precisely, as described in (95). The position of the first

minimum was noted on the slotted line. The probe was then left in that

INCIDENT TRACE
OUTPUT OF X_1

REFLECTED TRACE
OUTPUT OF X_2

FIG.3.29

KLYSTRON MODE.

INCIDENT TRACE
OUTPUT OF X_1

REFLECTED TRACE
OUTPUT OF X_2

FIG.3.30

KLYSTRON MODE.

INCIDENT TRACE
OUTPUT OF X_1

REFLECTED TRACE
OUTPUT OF X_2

FIG.3.31
KLYSTRON MODE.

INCIDENT TRACE
OUTPUT OF X_1

REFLECTED TRACE
OUTPUT OF X_2
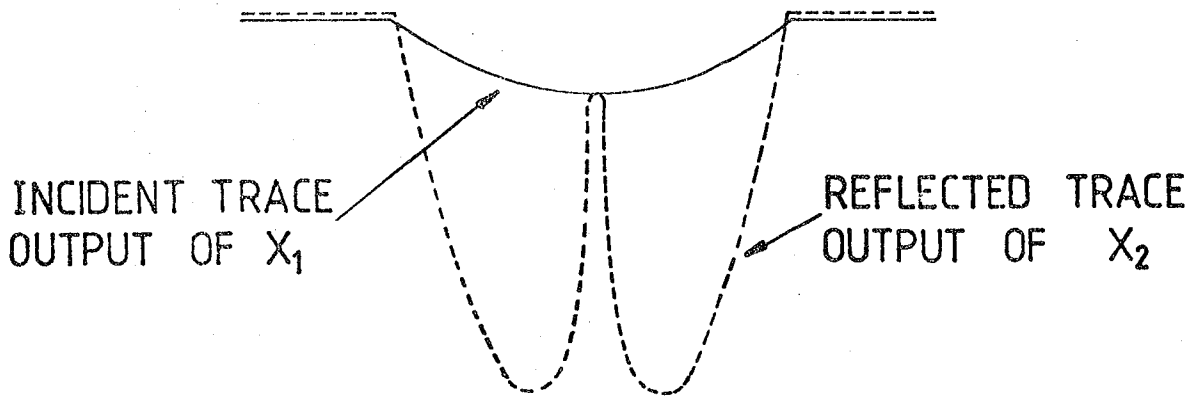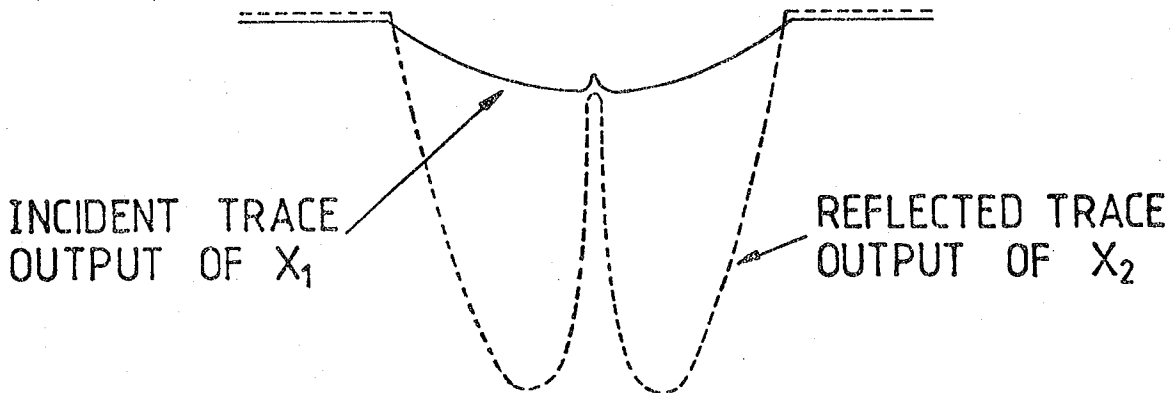
FIG.3.32
KLYSTRON MODE.

position and the resonant frequency of the cavity was changed by the amount of at least five times Δf. Then by moving the probe a little distance the VSWR was measured. If it was near the minimum the cavity was undercoupled and $\beta = \frac{1}{\xi}$ and if it was maximum the cavity was over-coupled and $\beta = \xi$, where $\xi =$ VSWR.

If $\beta = \xi = 1$ the cavity is coupled critically. This was repeated when the cavity was loaded with a dielectric sample. From both measurements the loaded and unloaded Q of the cavity, also its resonant frequency, were determined. The shift in the resonant frequency due to the insertion of the dielectric sample gives the dielectric constant, ε' , according to Eqn. 3.50. 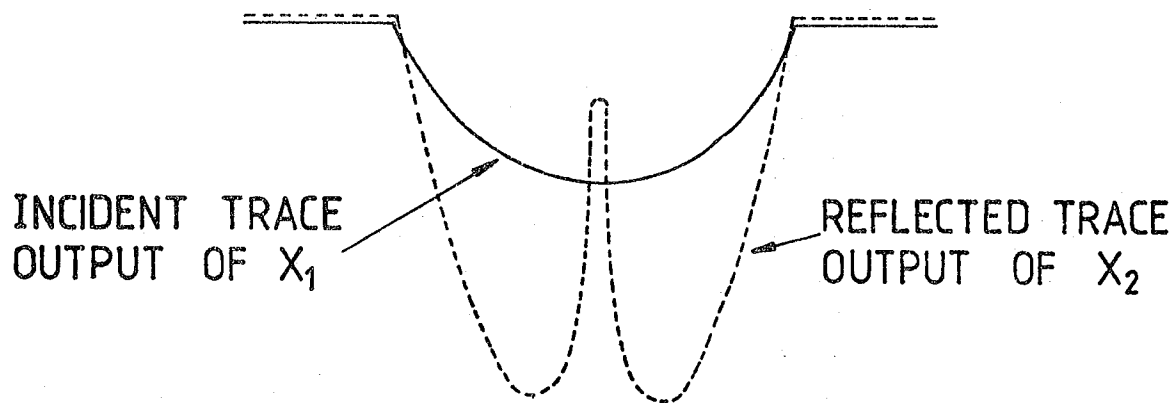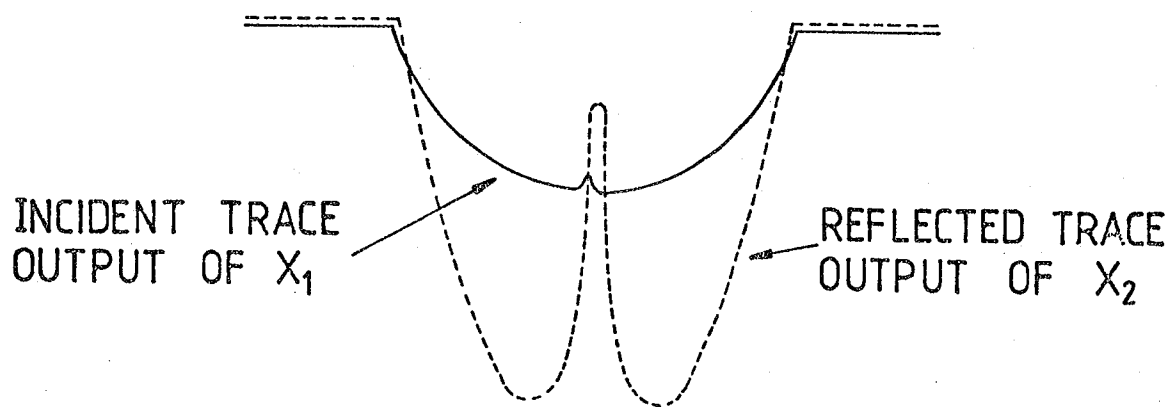The change in the unloaded Q of the cavity due to the insertion of the dielectric sample gives the loss factor, ε'' according to Eqn. 3.51.

3.6   CONCLUSION

As it has already been explained, the dielectric constant of MgO was determined by comparing the capacity of a condenser in air to the capacity with a MgO sample between the plates, using bridge methods or resonant circuit methods at low frequency.

The bridge method has many advantages, it can be used for low and high voltages and currents. The method gives direct readings of the capacitance and conductance. It can also be used at high temperatures since it can be easily connected to the required apparatus.

In contrast with the bridge technique, however, Q-meter has two major difficulties. First, to measure the complex dielectric constant the sample must be taken in and out of the holder for every frequency. This disturbs the system and could create considerable errors. Secondly, as the frequency increases due to inductive effect of the holder and assembly connected to it, the results can be false. Therefore, the measurement range is limited to a narrow band of frequencies. There

are also difficulties in connecting the Q-meter to the high temperature apparatus.

The slotted line technique is very useful for lossy materials. It does not, however, give direct readings of ϵ' and ϵ''. The method of measuring VSWR in this technique was very time consuming and results obtained were unreliable.

The cavity resonator method is able to deal with very low loss materials and its adaptability and accuracy were good. It is a very precise method but it still does not give direct readings of ϵ' and ϵ''. Most important advantages of this method are that the sample which is inserted into the cavity does not require polishing and its dimensions are smaller in comparison to those of samples used in bridge and Q-meter techniques.

It is concluded, therefore, that for low loss materials (e.g. in the case of MgO) the bridge and cavity resonator techniques are possibly the best because of their precision.

A number of errors exist in the slotted line technique. Before any measurements are carried out it is important to establish the sources of these errors and devise methods of minimizing or avoiding them.

The most apparent errors are due to detector characteristic, probe tuning, readings along the line of maxima and minima of the standing wave and signal distortion due to presence of harmonics and frequency modulation.

In the cavity method the errors may be divided into two main groups, i.e. those due to systematic causes and those due to random behaviour.

Systematic errors are those which affect each measurement by the same amount such as the calibration error. Proper design or accurate calibration of components can reduce these errors to a negligible value.

On the other hand random errors as the name implies, are due to random fluctuations of the measured quantities. These can be estimated by means of statistical methods from the results obtained using a large number of measurements (118).

The results obtained using each method will be presented individually and the possible errors and other difficulties encountered will be discussed.

3.7 <u>REFERENCES</u>

74.   Mungall, A. C. and Morris, D, 'Precision Capacitance Conductance

Bridge for Dielectric Measurements at Audio and Low Radio

Frequencies', Review of Scientific Instruments, Vol.34,

pp.839-43 (1963).

75.   Gough, E.R. and Isard, J.O, 'Errors due to Electrode Effects in

Dielectric Measurements on Glass', Proceeding IEE, Vol.116,

pp 471-4 (1969).

76.   Hartshorn, L. and Ward, W.H, 'The Measurement of the Permittivity

and Power Factor of Dielectrics at Frequencies from 10^4 to 10^8

Cycles per Second', Journal of Institution of Electronic Engineers

79, pp 597-609 (1936).

77.   Scott, A.H. and Curtis, H.L, 'Edge Correction in the Determination

of Dielectric Constant', Journal of Research of the National Bureau

of Standards, Vol.22, pp 747 (1939).

78.   Wayne-Kerr Co.Ltd., Handbook No.B224, (1975).

79.   A.S.T.M. (American Society of Testing and Materials) part 29,

D150-65T, 68 (1966).

80.   Lynch, A.C, 'A Method for the Precise Measurement of Permittivity

of Sheet Specimen', Proceeding IEEE, Vol.104B, pp 359-62 (1957).

81.   Chamberlain, J. and Chantry, G.W, 'High Frequency Dielectric

Measurement', Science & Technology Press Ltd. (1972).

82.   The Q-Meter (in the theory and practice), Marconi Instruments

Ltd., England (1961).

83.   Ammar, A.K, Ph.D. Thesis, University of Durham (1976).

84.   Mansfield, R, 'The Electrical Conductivity and Thermoelectric

Power of Magnesium Oxide', Proceeding Physics Society, London,

Vol.B66, pp 612-4 (1953).

85.   Roberts and Von Hippel, R., Journal of Applied Physics, Vol.17,

pp 610-6 (1946).

86.   Dakin, T.W. and Works, C.N, 'Microwave Dielectric Measurements',

        Journal of Applied Physics, Vol.18, No.9, pp 789-96 (1947).

87.   Von Hippel, R, 'Dielectrics and Waves', John Wiley & Sons ICO

        London (1954).

88.   Von Hippel, R, 'Dielectric Materials and Applications', John Wiley

        & Sons ICO, New York (1954).

89.   Westphal, W.B, 'Dielectric Materials and Applications', Ed.New York,

        John Wiley & Sons, (1954).

90.   Iskander, M. and Stuchly, S, 'Fringing Field Effect in the Lumped

        Capacitance Method for Permittivity Measurement', IEEE, Transactions

        on Instrumentation and Measurement, Vol.IM-27, No.1 (1978).

91.   Heston, W.M, Franklin, A.D, Hennelly, E.J. and Smith, C.P,

        'Microwave Absorption and Molecular Structure in Liquids',

        (Frick Chemical Laboratory,Princeton University) Vol.72, (1950).

92.   Green, H.E, 'The Numerical Solution of Some Important Transmission

        Line Problems', IEEE, Transaction on Microwave Theory and Technique,

        Vol. MTT-13, No.5, pp 676-92 (1965).

93.   Iskander, M.F. and Stuchly, S, 'A Time-Domain Technique for Measure-

        ment of the Dielectric Properties of Biological Substances', IEEE

        Transaction on Instrumentation and Measurement, Vol.IM-21, No.4,

        pp 425-9 (1972).

94.   Stuchly, S.S, Rzepecka, M.A. and Iskander, M.F, 'Permittivity

        Measurements at Microwave Frequencies Using Lumped Elements',

        IEEE Transactions on Instrumentation and Measurement, Vol.IM-23,

        No.1, pp 56-62 (1974).

95.   Sucher, M. and Fox, J, 'Handbook of Microwave Measurements',

        3rd Ed. Vol.1, Polytechnique Press, London (1963).

96.   Ginzton, 'Microwave Measurements', New York, McGraw-Hill, (1957).

97.   Type 874-LBB Slotted Line Handbook, General Radio Company,

        Massachusetts, U.S.A. (1966).

98.   Lance, A.L. 'Introduction to Microwave Theory and Measurements',

        McGraw-Hill Book Company, London (1964).

99.   Montgomery, G.G, 'Technique of Microwave Measurement', McGraw-Hill

        Book Company, London, (1947).

100.   Sucher, M. and Fox, J. 'Microwave Measurements', Polytechnic

        Press, Vol.II (1963).

101.   Lakshminarayana, M.R, Partain, L.D. and Cook, W.A,'Simple Micro-

        wave Technique for Independent Measurement of Sample Size and

        Dielectric Constant with Results for a Gunn Oscillator System',

        IEEE, Transaction on Microwave Theory and Techniques, Vol.MTT-27,

        No.7, July, pp 661-5 (1979).

102.   Raddish Bishop, W, Mrs. Buckingham, A, and Hyde, P.J, 'IEE London

        Conference on Dielectric Materials and Applications', University

        of Lancaster, U.K. July 1970, Vol.118, pp 255.

103.   Collin, R.E, 'Foundation for Microwave Engineering', McGraw-Hill

        Book Company, New York, London (1967).

104.   Baden-Fuller A.J, 'Microwave', 1st Ed., Pergamon Press, London,

        New York (1969).

105.   Glazier, E.V.D. and Lamont, H.R.L, 'Transmission and Propagation',

        Vol.5, Wireless World, London (1958).

106.   Harvey, A.F, 'Microwave Engineering', Academic Press, London and

        New York (1963).

107.   Bethe, H.A, 'Theory of Diffraction by Small Holes', The Physical

        Review, 2nd series, Vol.66, Nos. 7 & 8,pp 163-82 (1944).

108.   Malter, L, and Brewer, G.R, 'Microwave Q Measurements in the

        Presence of Series Losses', Journal of Applied Physics, Vol.20,

        (1949).

109.   Ragan, 'Microwave Transmission Circuit', (1960).

110.   Casimir, H.B.G, 'On the Theory of Electromagnetic Waves in

        Resonant Cavities', Philips Research Report, No.6, pp 162-82

        (1951).

111.   Waldron, R.A, 'Perturbation Theory of Resonant Cavities',

        The Institution of Electrical Engineers, No.373E, pp 272-4,

        (1960).

112.   Waldron, R.A, 'The Theory of the Waveguide and Cavities',

        New York, Gorden and Breach Science, (1969).

113.   Spencer, E.G, Le Crew, R.C. and Ault, L.A, 'Note on Cavity

        Perturbation Theory', Journal of Applied Physics, Vol.28, No.1,

        pp 130-2, (1957).

114.   Kabashima, S, and Kawakubo, T, 'A High Frequency Conductivity

        of NiO', Journal of the Physical Society of Japan, Vol.24,

        No.3, pp 493-7, (1968).

115.   Saad, T.S, 'Microwave Engineer's Handbook, Vol.1, Artech House,

        inc. (1971).

116.   Yariv, A, and Clapp, F.D, 'The Review of Scientific Instruments',

        Vol.30, No.8 (1959).

117.   Barlow, H.M. and Cullen, A.L, 'Microwave Measurements', London,

        (1950).

118.   Vigouroux, 'Random and Systematic Error, Colloquium on Analysis

        of Errors in Measurement System', IEE, April (1970).

CHAPTER 4

ROOM TEMPERATURE RESULTS IN THE LOW FREQUENCY RANGE

4.1   BRIDGE TECHNIQUE DATA

The conductivity data was derived directly from the measured conductance and some conductivity - frequency variations are shown in Fig. 4.1.   The values obtained for pure MgO and MgO doped with a low concentration of Fe (310 ppm) were the same, as indicated by the full line.   The addition of larger amounts of iron produces significant changes shown by the characteristics plotted for specimens containing 4,300 ppm and 12,800 ppm Fe respectively.

Comparison suggests that at any particular frequency increasing the concentration of iron increases the conductivity.

The conductivity versus frequency characteristics of a Cr doped MgO specimen is also given in Fig. 4.1.   Adding an almost equivalent concentration of Cr does not increase the conductivity as much as does adding Fe.

All the plots are linear and their slopes were found to be the same.   The data fits the "Universal Law" and comparison with the relation

$$\sigma_{ac}(\omega) \; \propto \; \omega^{n} \tag{4.1}$$

shows that the exponent has the value n = 0.98.   The magnitude of n is the same for all the specimens.

The variation of log $(\epsilon'-\epsilon_{\infty})$ with log ω was also plotted for the same specimens (Fig. 4.2) in deriving this ϵ_{∞} (the limiting value of dielectric constant at high frequencies) was taken to be the value
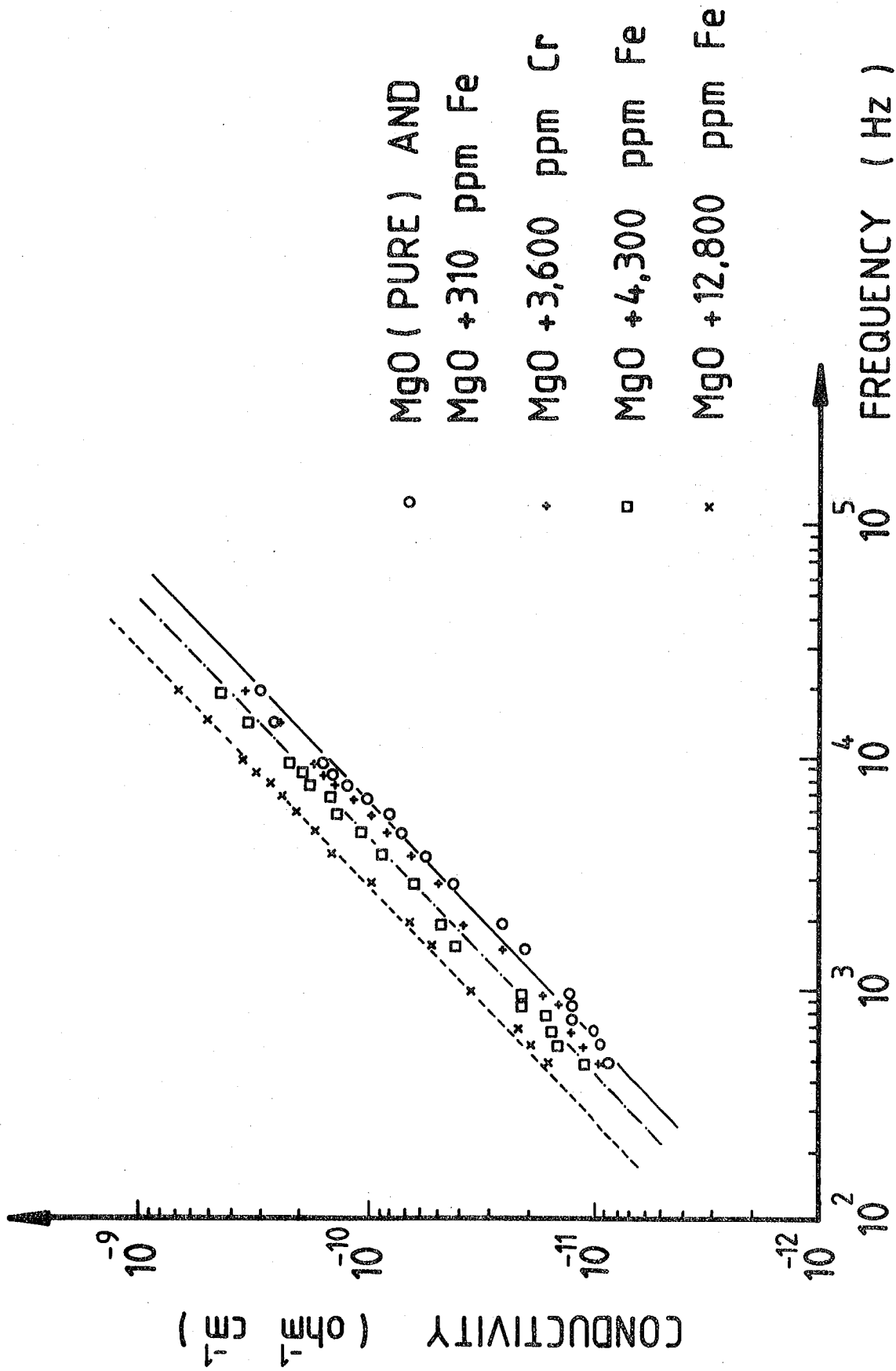
FIG.4.1 CONDUCTIVITY VERSUS FREQUENCY CHARACTERISTICS.

Legend (from the figure):

- ○   MgO (PURE) AND
- +   MgO +310 ppm Fe
- □   MgO +3,600 ppm Cr
- ×   MgO +4,300 ppm Fe
- ×   MgO +12,800 ppm Fe

Y-axis: CONDUCTIVITY (ohm^{-1} cm^{-1}), with values 10^{-9}, 10^{-10}, 10^{-11}, 10^{-12}

X-axis: FREQUENCY (Hz), with values 10^2, 10^3, 10^4, 10^5

● MgO (PURE)

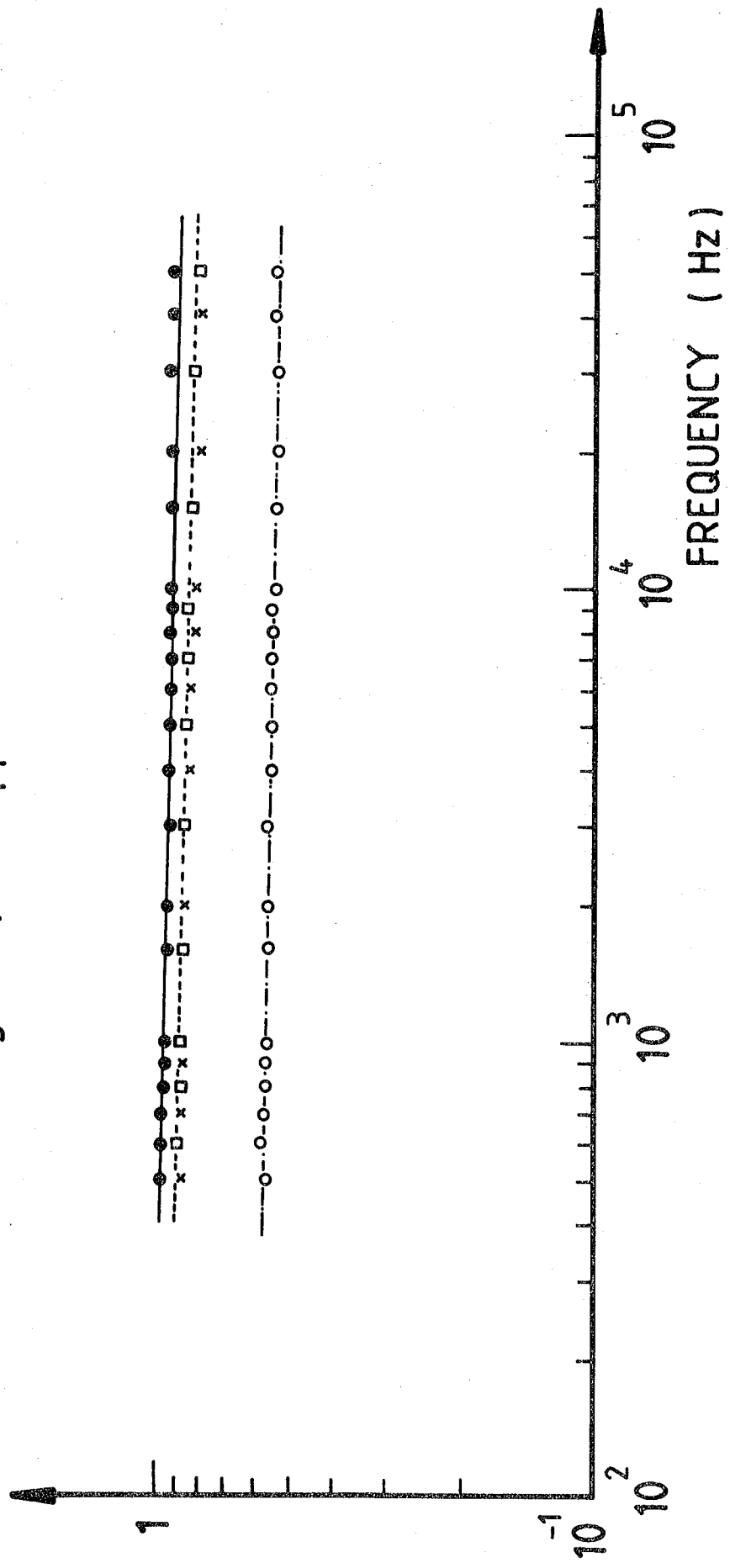□ MgO +3,600 ppm Cr

× MgO +4,300 ppm Fe

○ MgO +12,800 ppm Fe

FIG.4.2   VARIATION OF $\log(\varepsilon' - \varepsilon_\infty)$ WITH $\log \omega$.

obtained in microwave dielectric constant measurements at 9.3 GHz. Once again the plots of this variation for the doped specimens showed that all of them had the same shape of characteristic. All the characteristics are linear with the same slope, and all fit the relation

$$\varepsilon' (\omega) \quad \propto \quad \omega^{(n-1)} \tag{4.2}$$

with n = 0.98. Replotting the data showed that the magnitude of $(\varepsilon' - \varepsilon_\infty)$ at each frequency is inversely proportional to the concentration of Fe.

The variation of ε'' with frequency was also measured and it is shown in Fig.4.3. The plots are linear, following

$$\varepsilon'' (\omega) \quad \propto \quad \omega^{(n-1)} \tag{4.3}$$

with n = 0.98. The loss factor, ε'', at a particular frequency is higher for the heavily doped specimen than for the pure MgO, lower Fe concentrations are located between these values.

In order to clarify the effect of impurity concentration on permittivity and conductivity, plots of ε' versus Fe concentration and also of σ versus concentration are shown in Figures 4.4(a) and 4.4(b) respectively. It is seen that the variations of both ε' and σ are linear over the concentration range examined. There is inverse proportion between ε' and concentration while σ is directly proportional to the concentration of Fe.

4.2 Q-METER METHOD DATA

The dielectric constant and conductivity data of pure Mgo and MgO with different concentrations of Fe and Cr at 1 MHz are summarized in Tables 4.1 and 4.2 in which the values given represent averages of several measurements on each sample. For convenience a reference number has been assigned to each sample. The concentrations of the iron doped samples varied between 310 ppm Fe and 12,800 ppm Fe and for the chromium

Legend:
- MgO (PURE)
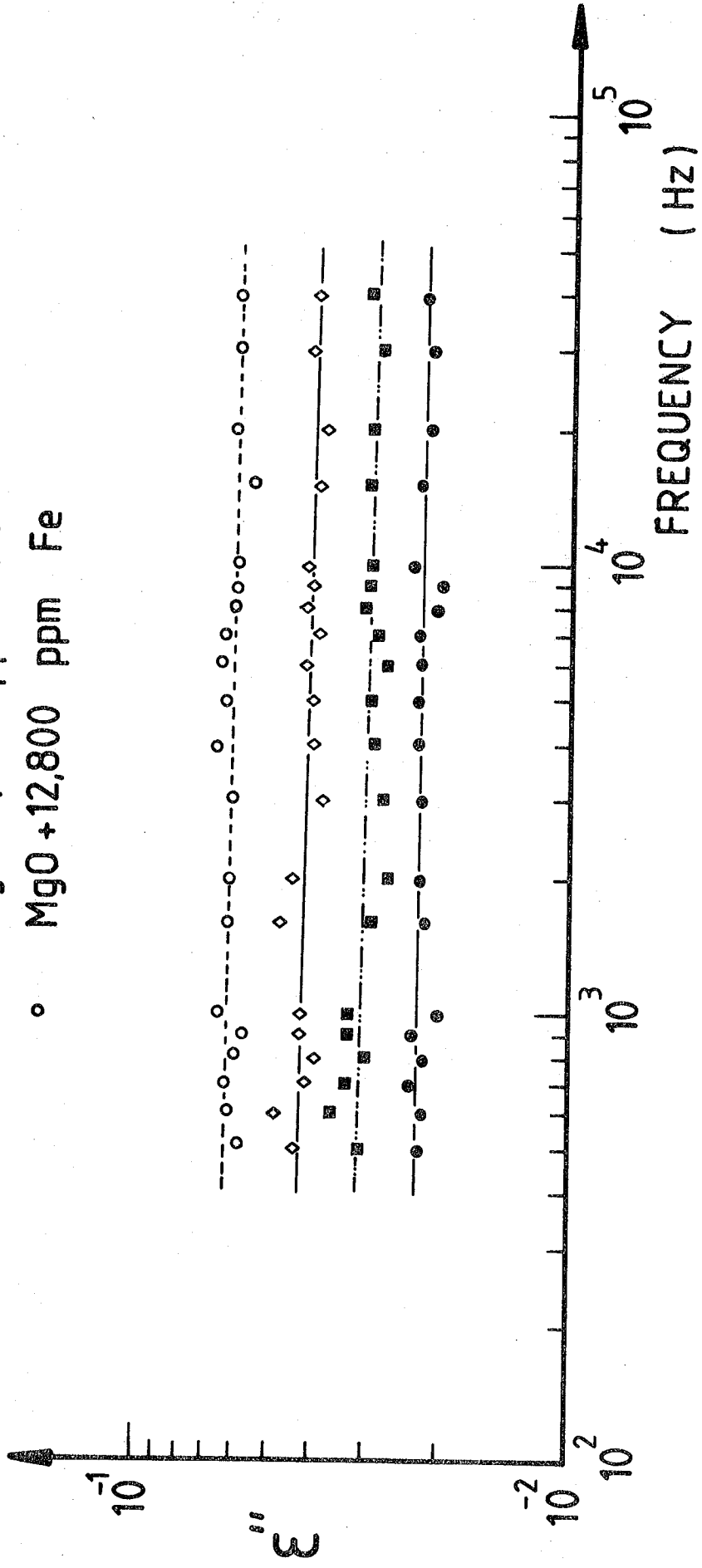- MgO +3,600 ppm Cr
- MgO +4,300 ppm Fe
- MgO +12,800 ppm Fe

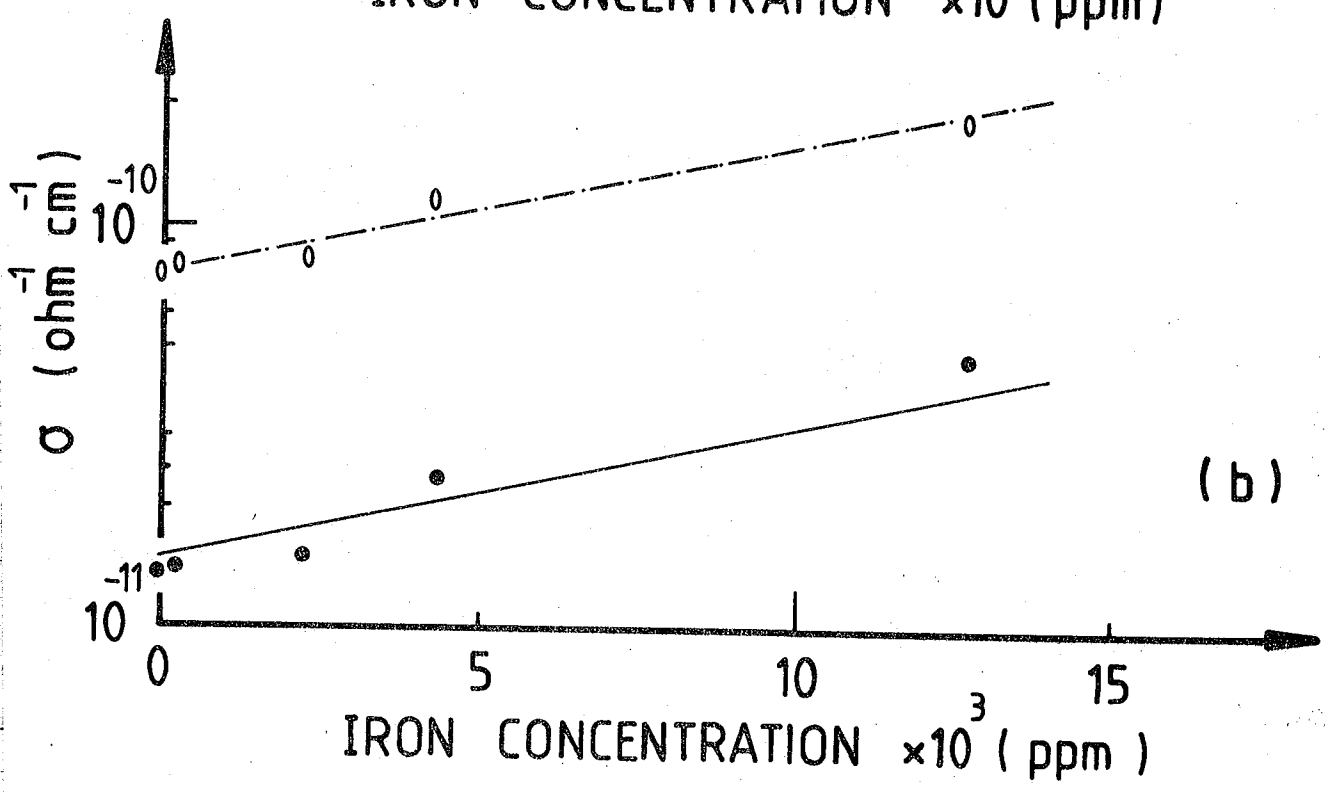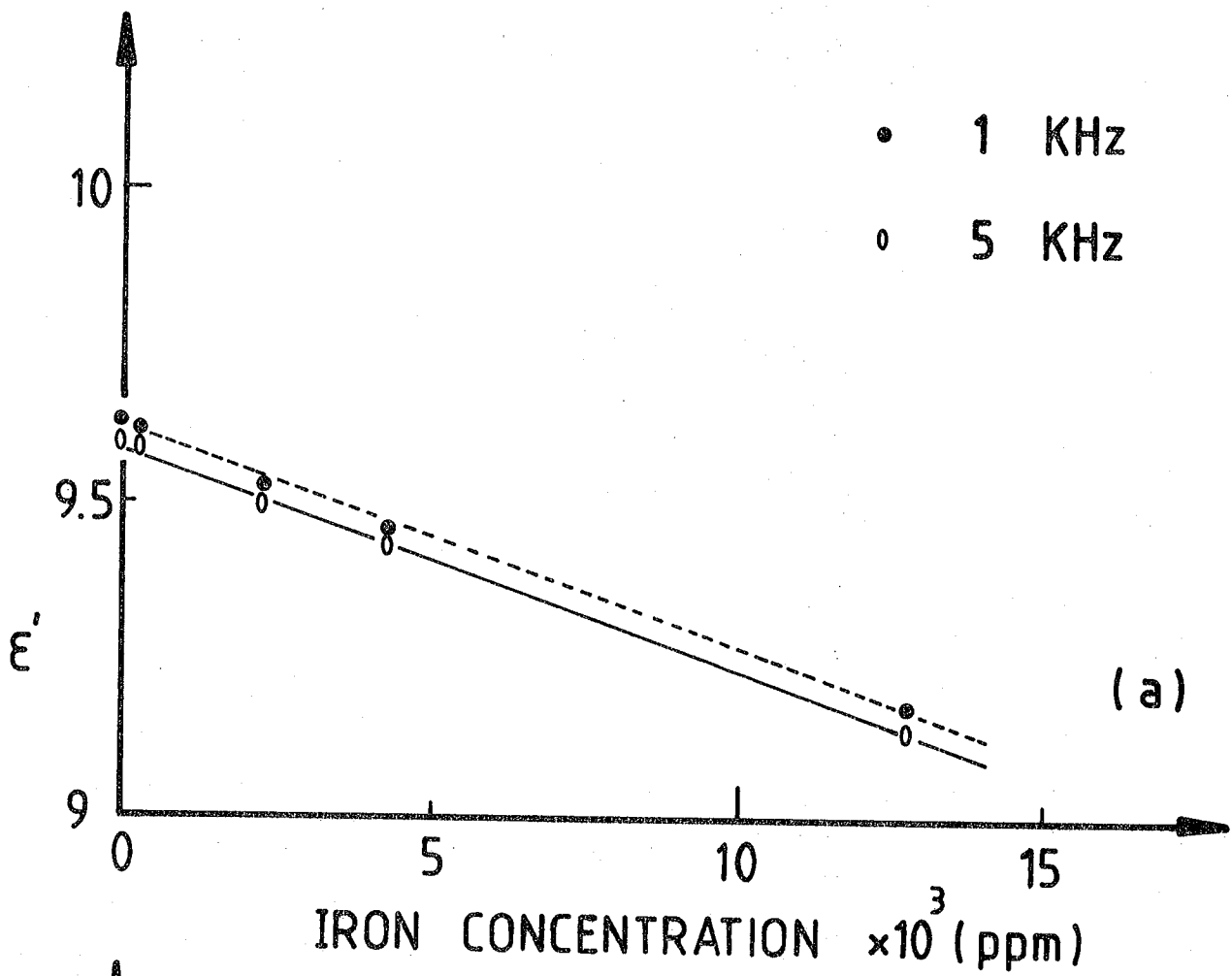FIG. 4.3   VARIATION OF ε'' WITH FREQUENCY.

FIG.4.4   THE DEPENDENCE OF (a) ε' AND (b) σ
ON IRON CONCENTRATION.

Reference No	Nominal Composition	ϵ'	Conductivity, $\sigma \times 10^8$ $(ohm^{-1} \, cm^{-1})$
1	MgO Pure	9.47	1.25
2	MgO + 310 ppm Fe	9.46	1.39
3	MgO + 2,300 ppm Fe	9.37	1.55
4	MgO + 4,300 ppm Fe	9.25	2.3
5	MgO +12,800 ppm Fe	8.81	4.0

TABLE 4.1 :   Dielectric Constant and Conductivity of Pure MgO
          and Iron Doped MgO at 1 MHz.

Reference No	Nominal Composition	ϵ'	Conductivity, $\sigma \times 10^8$ $(ohm^{-1} \, cm^{-1})$
6	MgO + 800 ppm Cr	9.55	1.4
7	MgO + 1,300 ppm Cr	9.44	1.5
8	MgO + 3,600 ppm Cr	9.3	1.85

TABLE 4.2 :   Dielectric Constant and Conductivity of Chromium
          Doped MgO at 1 MHz.

doped samples from 800 ppm Cr to 3,600 ppm Cr. They have been tabulated in order of increasing concentration.

In the present experiment data have been calculated as a mean value of several measurements.

At constant frequency the value of ε' decreases on increasing the concentration of the Fe or Cr. In contrast the a.c. conductivity increases with the concentration of the dopant. The variation of dielectric constant, ε', of pure MgO with frequency is plotted in Fig.4.5. The magnitude of ε' decreases slightly as the applied frequency increases up to 4 MHz ; ε' apparently increases very sharply when the frequency is increased beyond 4 MHz but this is due to inductive effects of the electrodes and jig in the high frequency range, i.e. 10 MHz-40 MHz and maybe misleading. A comparison of the variations of dielectric constant versus frequency for pure MgO and Fe/MgO is given in Fig.4.6. This shows the effect of the dopant (Fe) on the permittivity of the host material over the frequency range of measurements. It can be seen that the magnitude of the dielectric constant of both samples decreases with increasing frequency. At any fixed frequency the ratio of their ' values is constant ; the value of this ratio is about 1.03.

There is not much difference between the dielectric constant of pure MgO and MgO doped with 310 ppm Fe in this frequency range. The data of both samples has been plotted in Fig. 4.7. Over two decades of frequency, their difference does not exceed more than the range of experimental errors. This difference is almost 0.1% whereas the experimental errors are estimated at 3%.

A further comparison between the permittivity of pure MgO and that of specimens having four different concentrations of iron (sample refernences 1-5) made at two distinct frequencies, 200 kHz and 500 kHz, is given in Fig. 4.8. It shows that the magnitude of dielectric constant
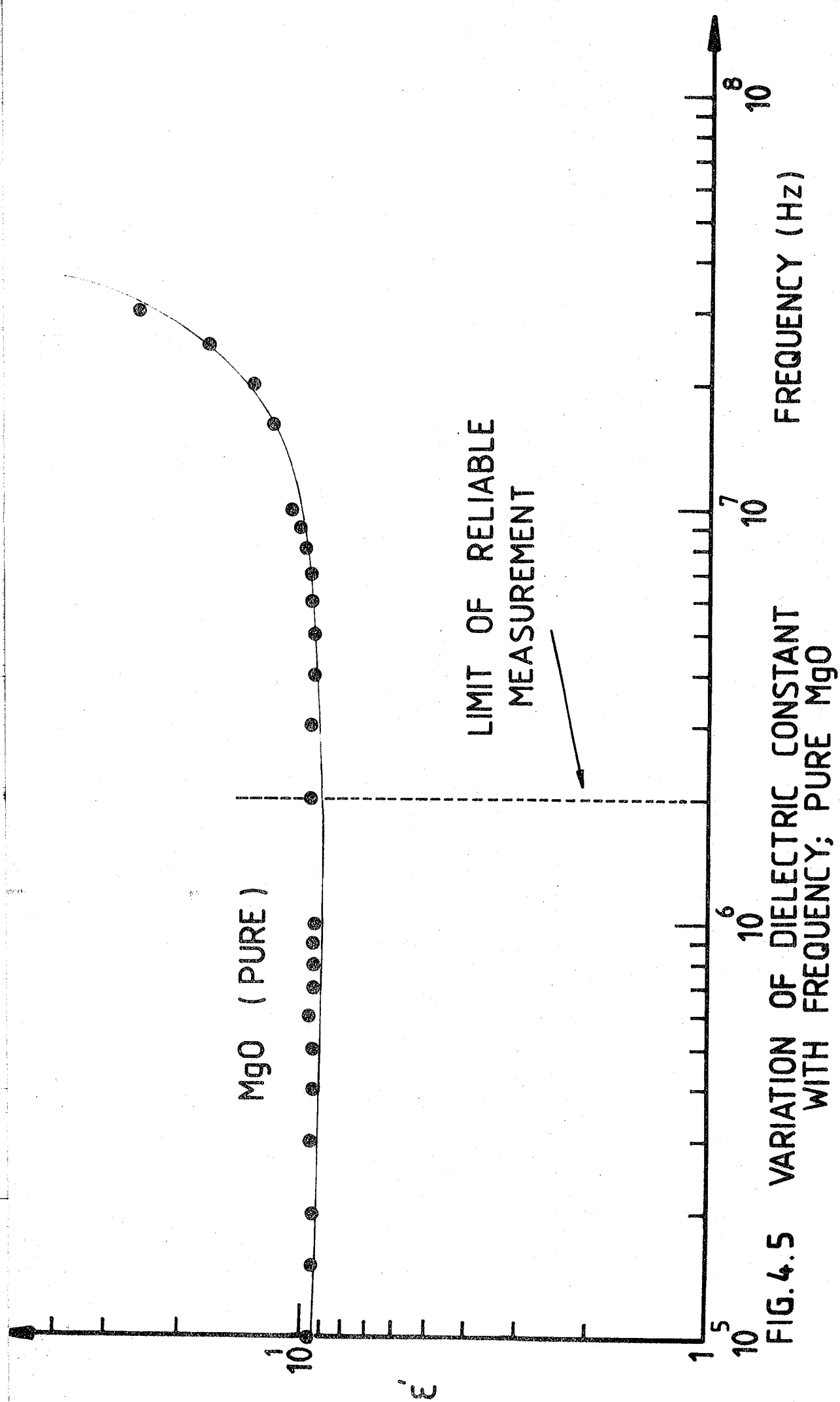
FIG. 4.5   VARIATION OF DIELECTRIC CONSTANT WITH FREQUENCY; PURE MgO

FIG. 4.6   VARIATION OF DIELECTRIC CONSTANT WITH FREQUENCY:

PURE MgO AND MgO +4,300 ppm Fe.

o REF. 1 MgO (PURE)

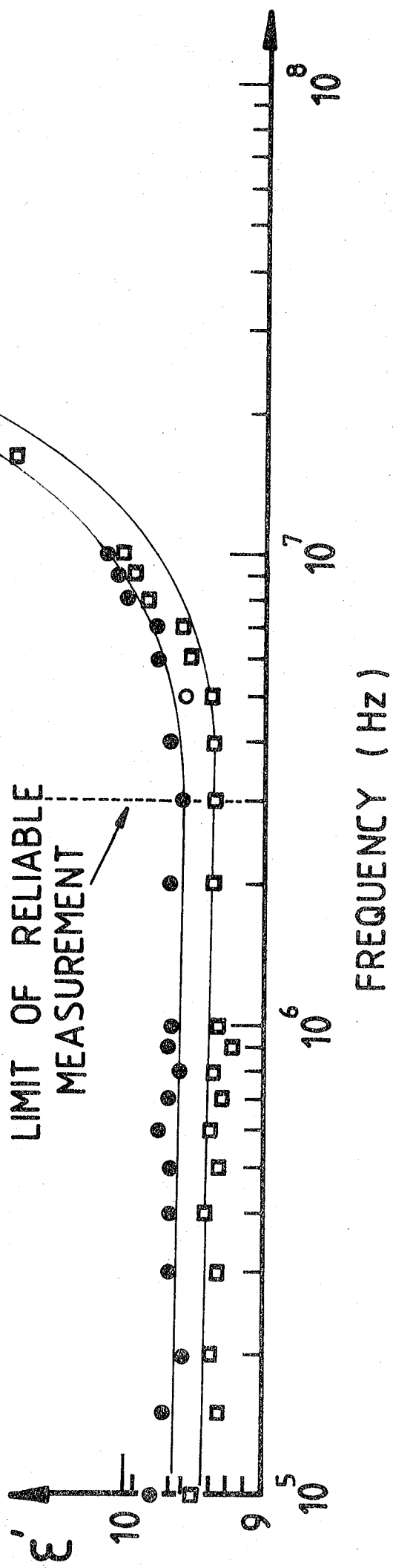x REF. 2 MgO + 310 ppm Fe

LIMIT OF RELIABLE
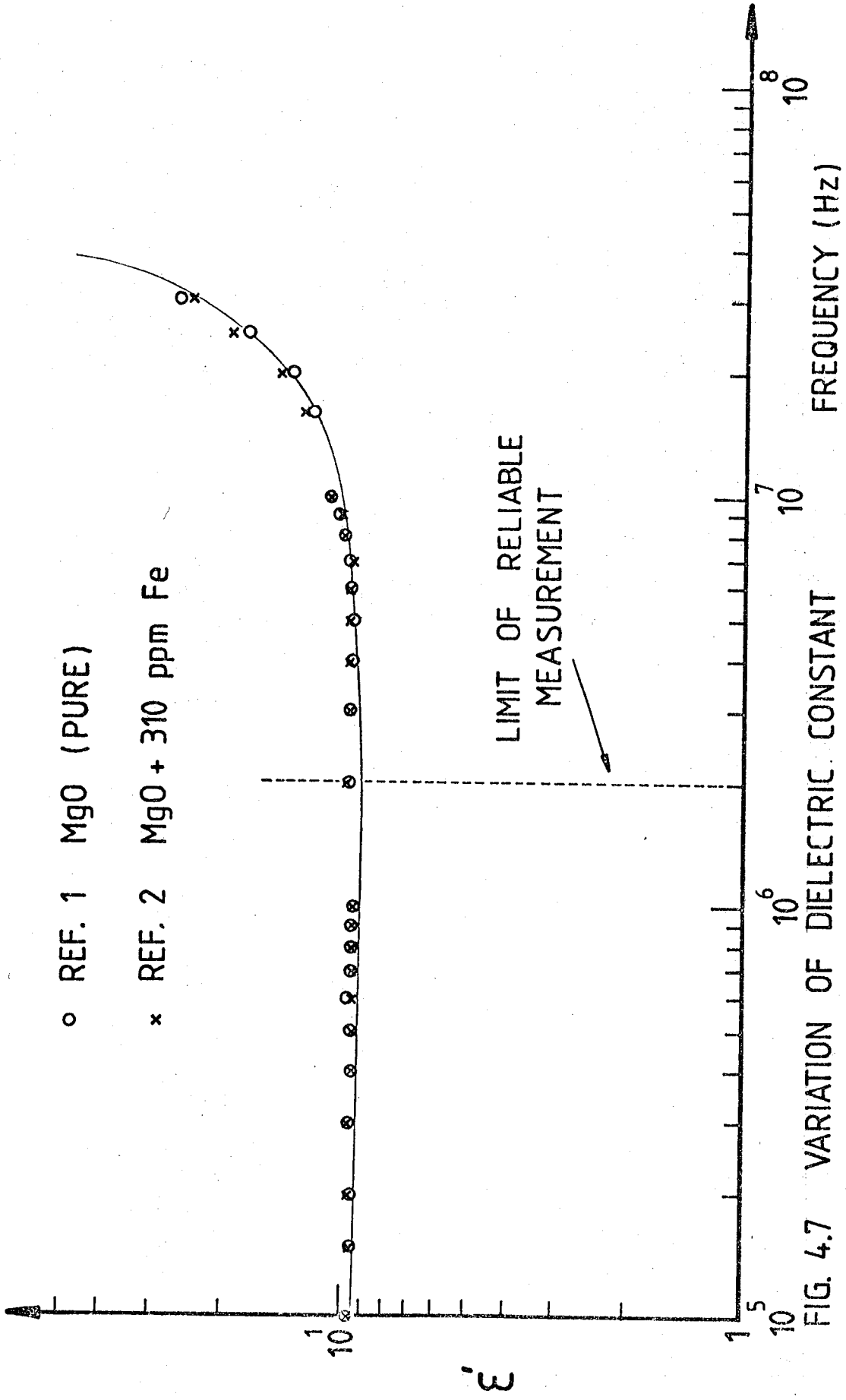MEASUREMENT

FREQUENCY (Hz)

FIG. 4.7 VARIATION OF DIELECTRIC CONSTANT
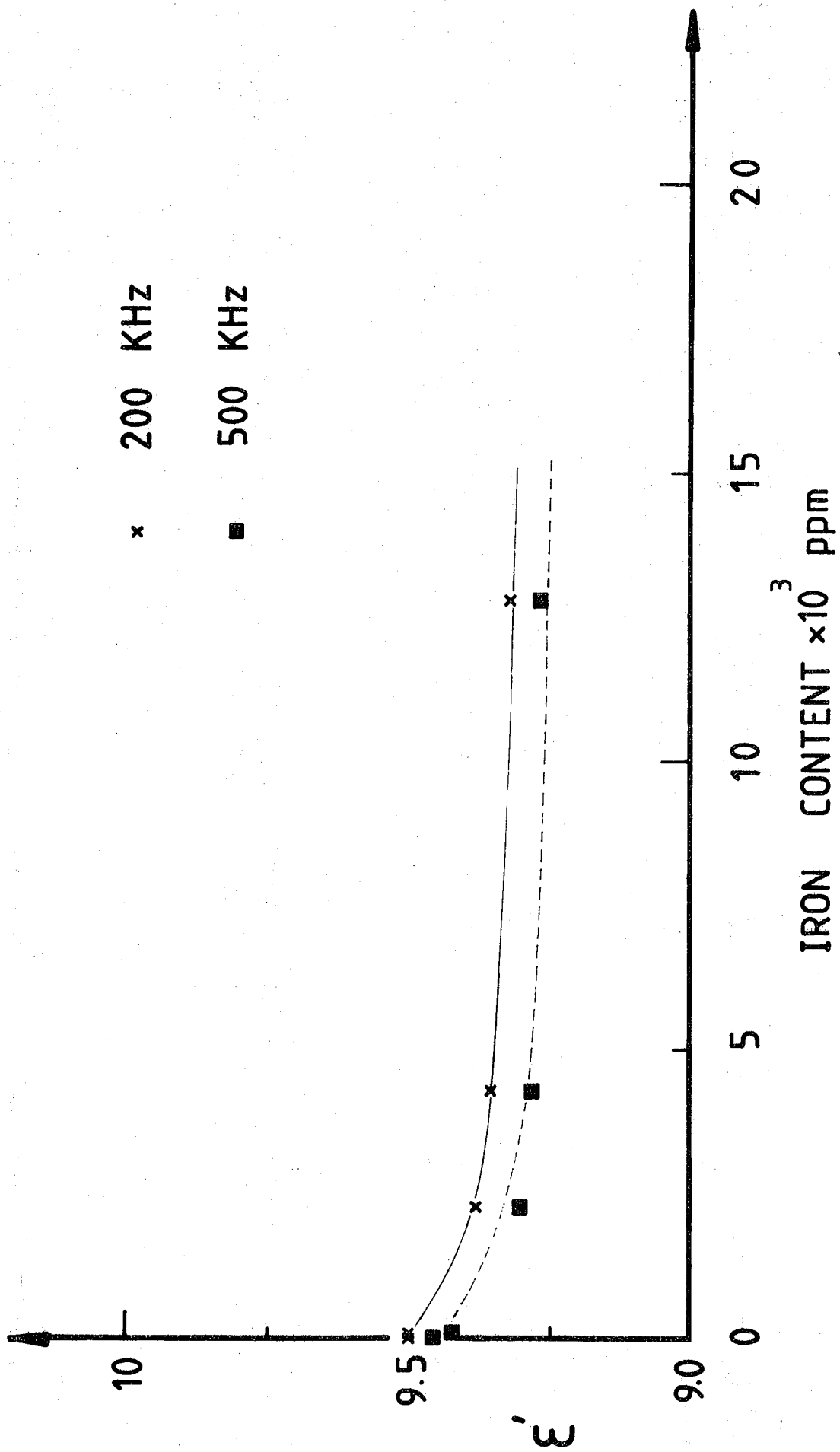WITH FREQUENCY; PURE MgO AND MgO + 310 ppm Fe.

FIG. 4.8 VARIATION OF DIELECTRIC CONSTANT WITH IRON CONCENTRATION.

of Fe/MgO is inversely proportional to the concentration of iron.

In Fig.4.9 the variation of loss factor $\varepsilon''(\omega)$ with frequency for pure MgO has been plotted. This variation can be compared with the loss factor characteristic of heavily doped Fe/MgO which is also shown in this figure. They show a slight decrease up to 1 MHz. The variations have slopes of 0.014 and 0.016 which both fit with the "Universal Law" (Eqn. 4.3) where n is equal to almost 0.985. The a.c. conductivity characteristics of all the samples ($\sigma_{ac}(\omega)$ versus frequency) have been plotted in Fig.4.10. They show similar characteristics and the conductivity ratios ($\sigma(Fe)/\sigma$ Pure) at any particular frequency are constant. The variation of $\sigma_{ac}(\omega)$ just over one decade of frequency is linear and its slope is 0.98, i.e. n = 0.98. All a.c. conductivities agree,(Eqn.4.1).

A comparison of the conductivity of MgO doped with almost the same concentrations of iron and chromium respectively is shown in Fig.4.11.

Finally, log ($\varepsilon'-\varepsilon_\infty$) versus log ω was plotted in Fig 4.12 here ε_∞ is the limiting value of ε', which was taken from data obtained in microwave dielectric constant measurements.

The data for loss tangent, Tan δ, which has been derived directly from measured quantities, is plotted in Fig. 4.13; its variation with frequency is linear.

4.3   DISCUSSION

The Q-meter data in all cases fits the extrapolation of the corresponding bridge data confirming that the same behaviour and mechanisms apply over the whole frequency range from 500 Hz to 30 MHz.

The conductivity of MgO is the sum of the d.c. conductivity and the pure a.c. conductivity and the a.c. conductivity component is the only part which is dependent on frequency. In this experiment extrapolation of Fig.4.1 shows that the d.c. conductivity,σ_o , is very small ($\sim 10^{-14}$ ohm^{-1} cm^{-1}) for all the specimens examined and thus it can be
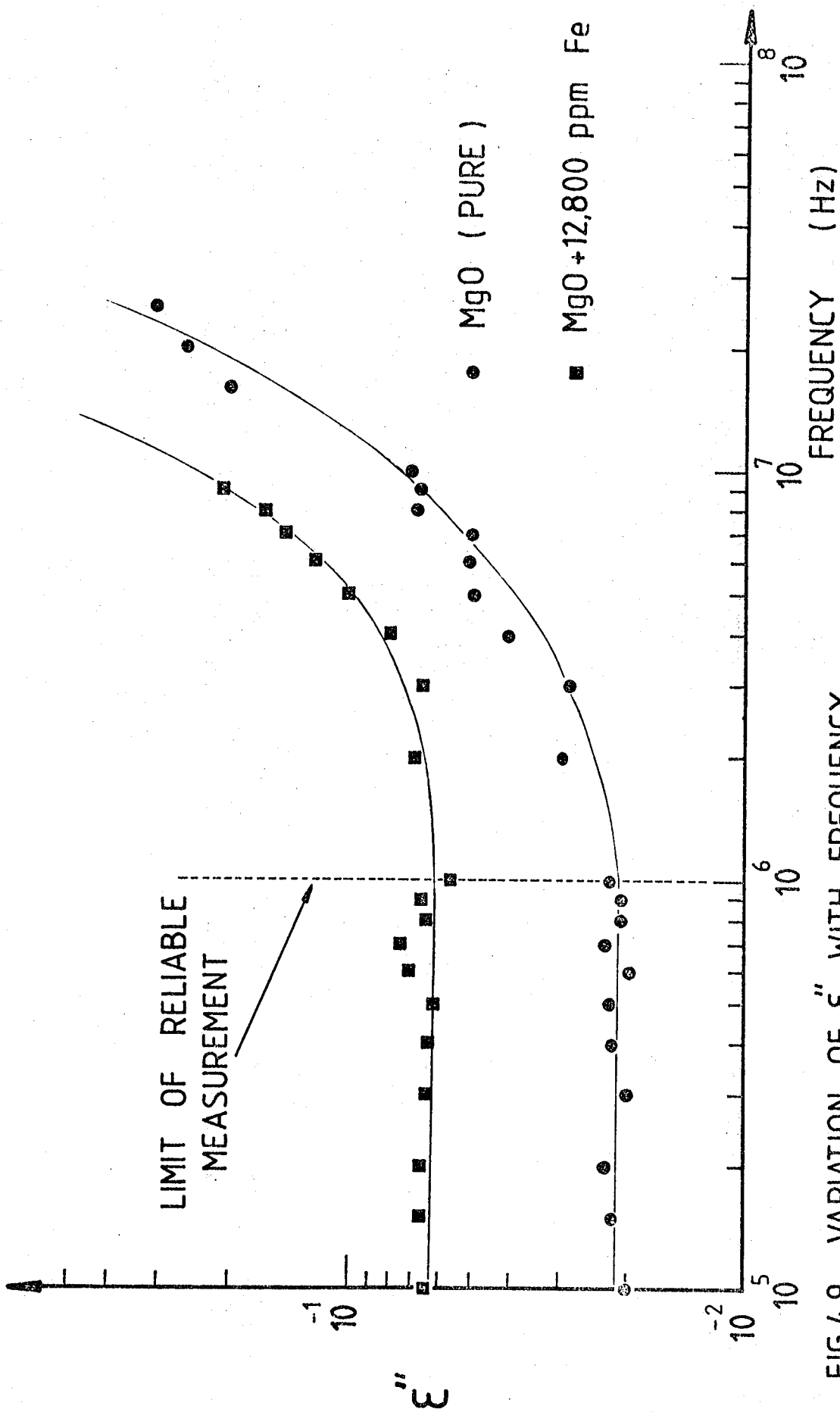
FIG.4.9 VARIATION OF ε'' WITH FREQUENCY.
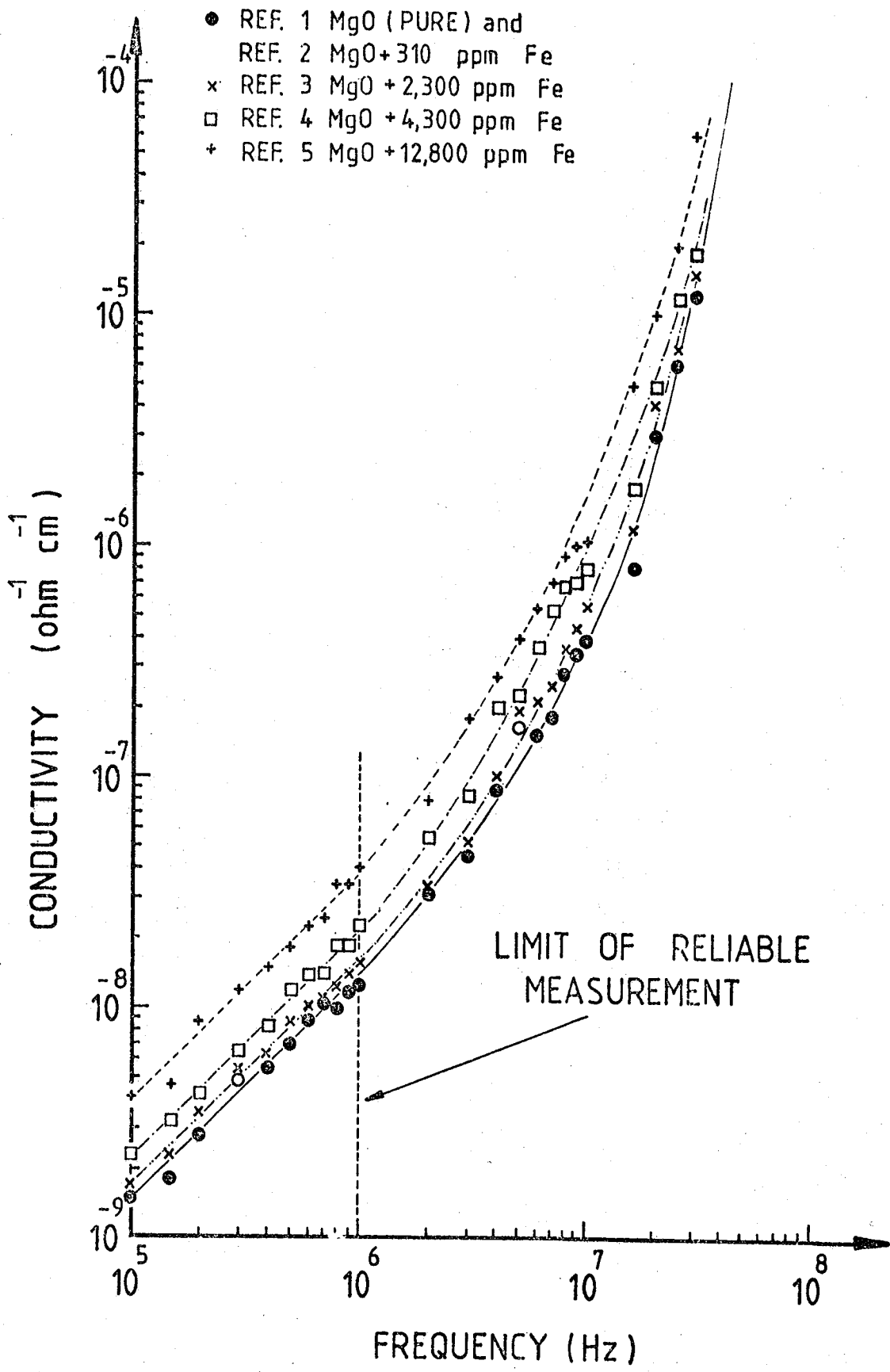
FIG.4.10   VARIATION OF σ VERSUS FREQUENCY; PURE
MgO AND IRON DOPED MgO.
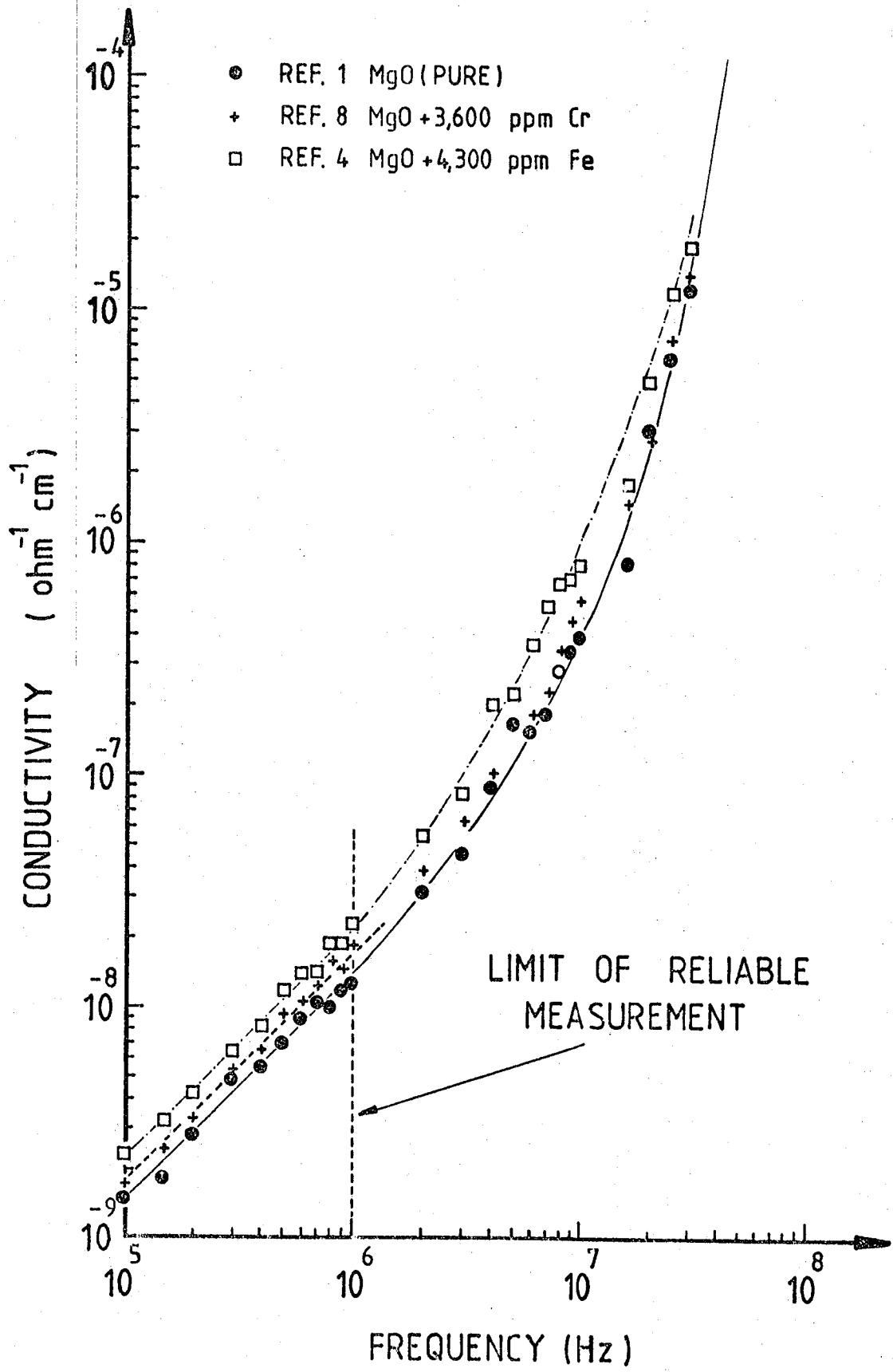
FIG.4.11   VARIATION OF σ WITH FREQUENCY.

▲ REF. 1 MgO (PURE)

LIMIT OF RELIABLE
MEASUREMENT
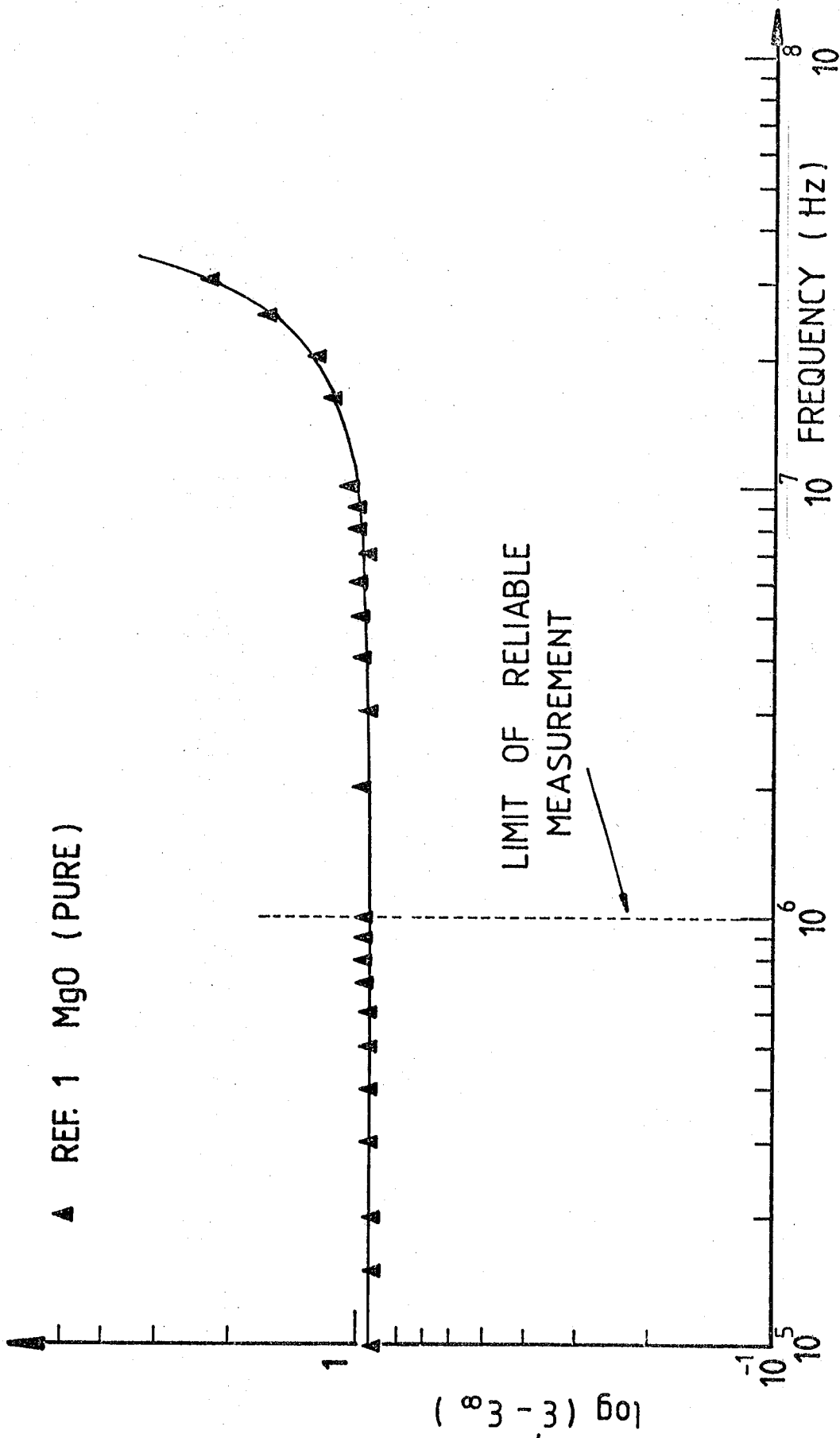
FIG.4.12   VARIATION OF $\log(\varepsilon' - \varepsilon_\infty)$ VERSUS FREQUENCY; MgO (PURE).

$\log(\varepsilon' - \varepsilon_\infty)$

FREQUENCY (Hz)

10^5 10^6 10^7 10^8

10^{-1} 1

FIG.4.13   VARIATION OF Tan δ VERSUS FREQUENCY; MgO (PURE)

neglected. Considering first the data for pure MgO we find that $\sigma_{ac}(\omega)$ follows the relation 4.1 with n = 0.98 over three frequency decades.

As regards the dielectric constant ε', there is a good agreement between the present data on pure MgO (Table 4.3) and that reported by others (Table 4.4).
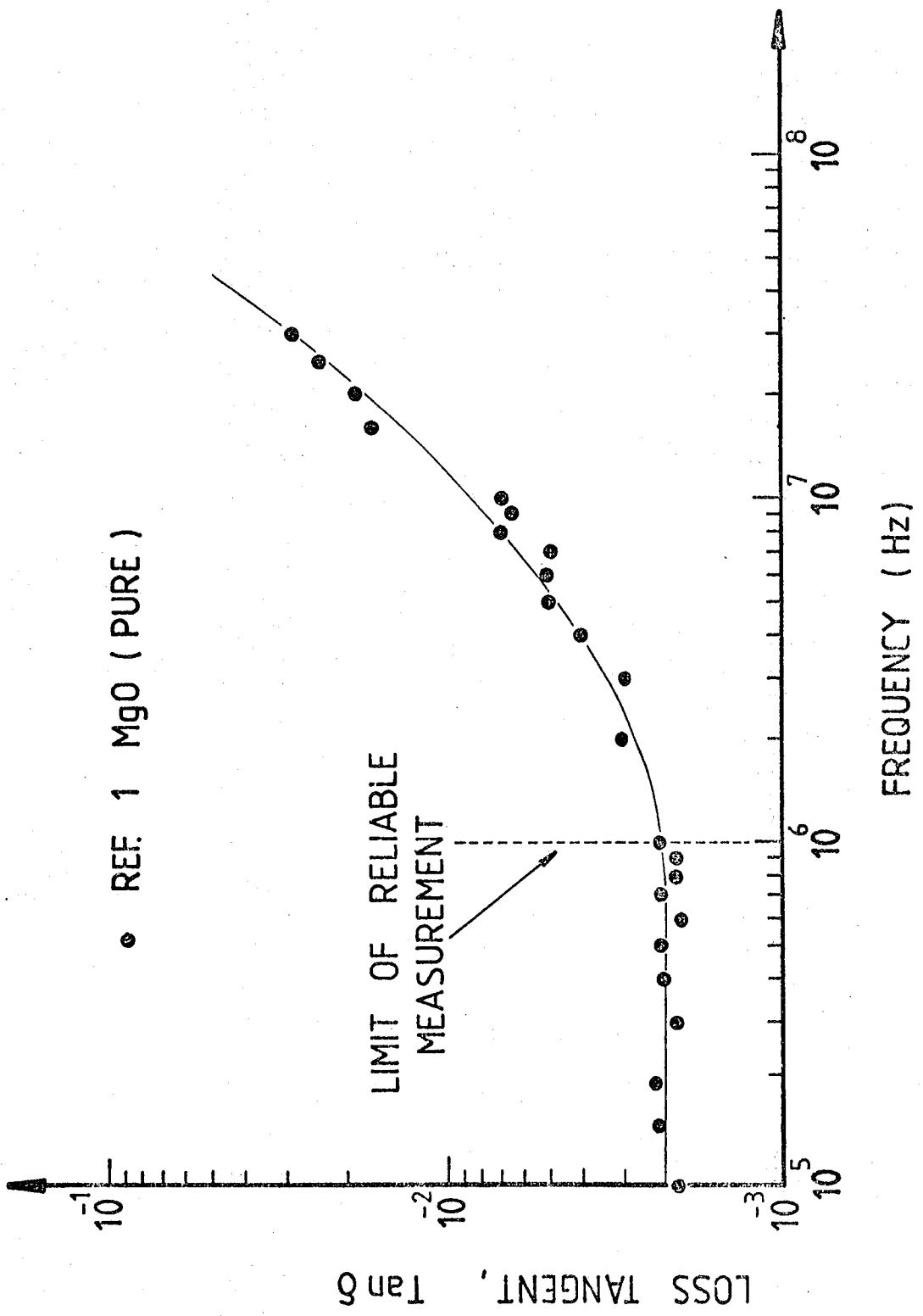
The major conclusions concern the effect of doping. The data for all specimens fits the Jonscher laws, i.e. good agreement was obtained with the relations

$$\sigma_{ac}(\omega) \quad \propto \quad \omega^n \tag{4.4}$$

$$(\varepsilon'-\varepsilon_\infty) \quad \propto \quad \omega^{(n-1)} \tag{4.5}$$

$$\varepsilon''(\omega) \quad \propto \quad \omega^{(n-1)} \tag{4.6}$$

The magnitude of the exponent (n) for all samples being n = 0.98. The three methods for determination of n, as shown in Figures 4.1, 4.2 and 4.3 all give the same magnitude for n, to within experimental error. This value of n is independent of the nature of the dopant and also of dopant concentrations. Since all the specimens yield identical values of (n) (Fig.4.1) it can be concluded that the mechanism of conduction is the same ; only the magnitudes of $\sigma_{ac}(\omega)$ are different and these increase with increasing concentration. Primarily, this suggests that the probability of hopping increases with increasing concentrations of the dopant impurity. This implies that the number of hopping centres increases but that this occurs without a change in hopping mechanism.

It is known from ESR studies (124) that Fe and Cr have entered the magnesium oxide crystal on magnesium sites as Fe^{3+} and Cr^{3+}. Adding Fe ions introduces further vacancies ; since Fe^{3+} is occupying a Mg^{2+}

Specimen Reference	Nominal Composition	ϵ'	$\text{Tan}\delta \times 10^3$	Frequency/Hz
1	MgO Pure	9.62	2.16	1×10^3
2	MgO + 310 ppm Fe	9.62	2.49	1×10^3
3	MgO + 2,300 ppm Fe	9.52	2.87	1×10^3
4	MgO + 4,300 ppm Fe	9.46	3.91	1×10^3
5	MgO +12,800 ppm Fe	9.40	7.47	1×10^3
6	MgO + 800 ppm Cr	9.60	2.44	1×10^3
7	MgO + 1,300 ppm Cr	9.28	3.15	1×10^3
8	MgO + 3,600 ppm Cr	9.43	3.15	1×10^3

TABLE 4.3 : Dielectric Constant for Pure MgO and MgO Doped with Fe anc Cr ; (Present work)

Reported Data		ε'	Tanδ x 10^4	Frequency (Hz)
Yamashita & Kurosawa	(119) MgO	9.8	–	0
Von Hippel	(120) MgO	9.65	<3	$1 \times 10^2 - 1 \times 10^8$
STC	(121) MgO	9.65	<3	$1 \times 10^2 - 1 \times 10^3$
Gourdin & Kingery	(122) MgO	9.86 (Theoretical), 9.65-9.86 (Experimental)	–	–
Mott & Gurney	(47) MgO	9.8	–	0
Mayburney	(123) MgO	9.8	–	0
Lewis & Wright	(10) MgO	9.5	–	0

TABLE 4.4 : Reported Dielectric Constant data for MgO at room temperature.

site in the lattice one extra vacancy per two Fe^{3+} ions is produced in the crystal. Similar vacancy formation will occur with Cr^{3+} ions.

It is of interest to compare the behaviour of Fe and Cr as dopants. For two specimens doped to almost the same concentration but with different impurity ions, (i.e. samples (4) Fe/MgO and (8) Cr/MgO) the conductivities at any particular frequency were different and the conductivity of MgO with Fe doping is higher than with Cr doping. Fe appears to be more effective in changing both, σ and ε' than Cr. This would not be expected on the simple vacancy production model and the reasons for this effect are not yet clear.

4.4   REFERENCES

119.   Yamashita, J. and Kurosawa, 'Formation Energy of Lattice Defect in Simple Oxide Crystal', Journal of the Physical Society of Japan, Vol.9, No.6 (1954).

120.   Von Hippel, 'Tables of Dielectric Materials', Vol.IV, Masst.Inst. Technol. Research Lab., Insulation Technical Report.

121.   Reference data for Radio Engineers, Standard Telephone & Cable Ltd. (STC).

122.   Gourdin, W.H. and Kingery, W.D, 'The Defect Structure of MgO Containing Trivalent Cation Solutes : Shell Model Calculations', Journal of Material Science, Vol.4 (1979).

123.   Mayburg, S, 'Effect of Pressure on the Low Frequency Dielectric Constant of Ionic Crystals', Physical Review, Vol.79, pp 375-89 (1950).

124.   Thorp, J. S, Vasques, R.A, Adcock, C, and Hutton, W, 'Electron Spin Resonance Linewidths of Fe^{3+} in Magnesium Oxide', Journal of Material Science, Vol.11, pp 89-95 (1976).

CHAPTER 5

ROOM TEMPERATURE RESULTS AT R.F. AND MICROWAVE FREQUENCIES

5.1   R.F.RANGE

5.1.1 General

The dielectric constant, ε' and the loss factor, ε'' of all

samples have been calculated directly using Eqns. 3.28 and 3.29

respectively and their conductivity obtained using ε''.

In order to determine the magnitude of reflection coefficient,

$|\rho|$, and the distance of the first minimum, the VSWR pattern for pure

MgO was plotted as shown in Fig. 5.1 at the frequency 710 MHz. To

illustrate the shift caused by the introduction of the sample that plot

of Fig.3.10 (short circuit) was superimposed in Fig.5.1. As can be seen

the shape of the pattern for pure MgO has not changed as there is very

little power dissipation in the single MgO crystals, i.e. $\sigma \to o$.

To see the effect of dopant impurities on the magnitude of the

reflection coefficient, ρ, and the shift of the first minimum the VSWR

pattern for MgO doped with iron (12,900 ppm Fe) was plotted in Fig.5.2

at the frequency of 710 MHz. As it is seen the readings at the minimum

points are higher than for the pure MgO case in Fig.5.1.

5.1.2 Complex Dielectric Constant

The variation of ε' with frequency for pure MgO has been plotted

in Fig.5.3. The frequencies were chosen so as to cover adequately the

region between the X-band and the frequencies using Q-meter technique

i.e. O.5 GHz- 7.5 GHz. It can be seen that ε' decreases with frequency

linearly and it is difficult to determine the slope of the line precisely

because of the variations. By extrapolating to low and medium frequencies

the line has gi$\overset{v}{}$en the slope of O.02. Determination of the slope of this

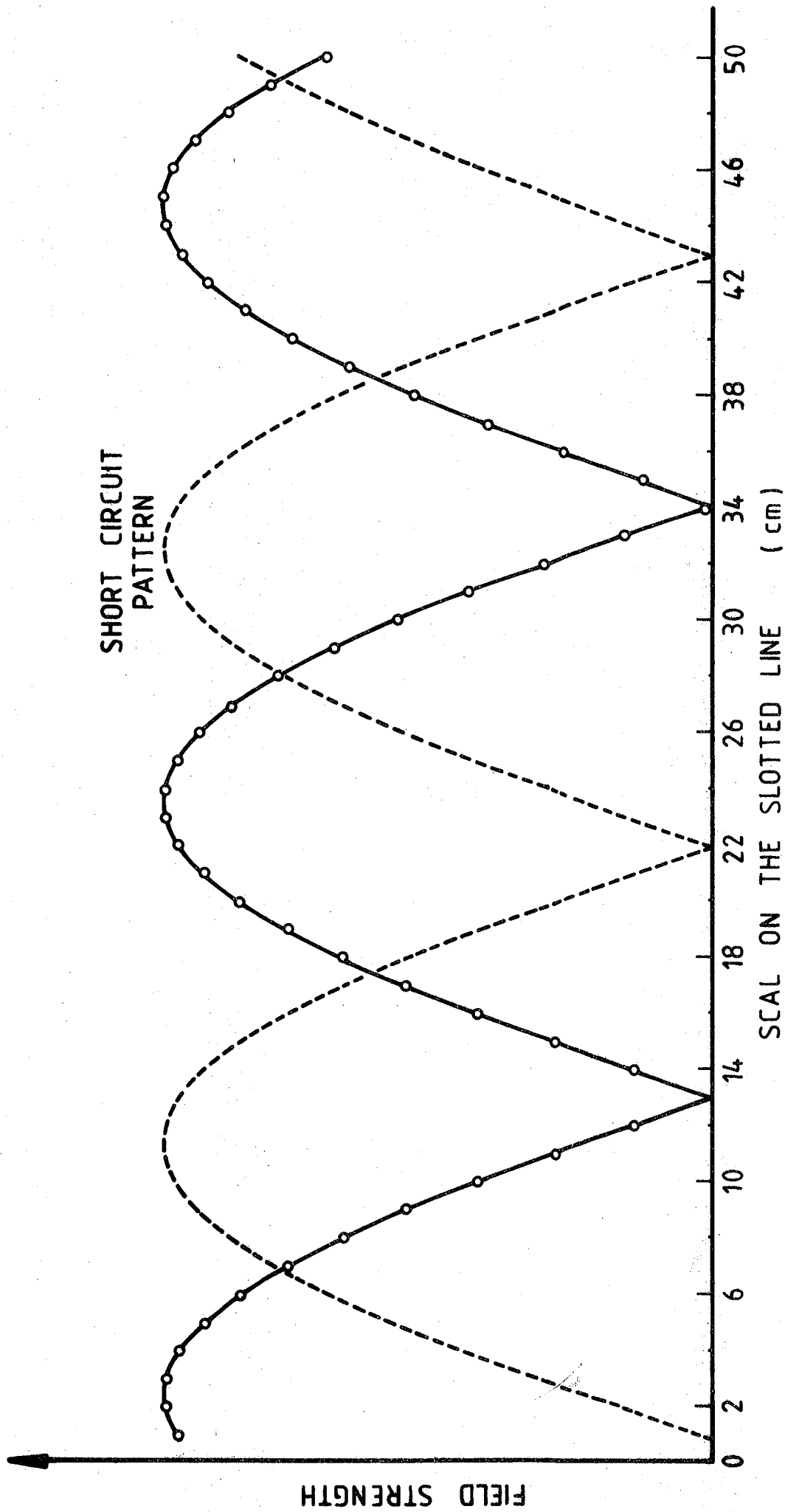SHORT CIRCUIT
PATTERN

SCAL ON THE SLOTTED LINE   (cm)

FIELD STRENGTH

FIG.5.1   STANDING WAVE PATTERN AT 710 MHz; MgO (PURE)
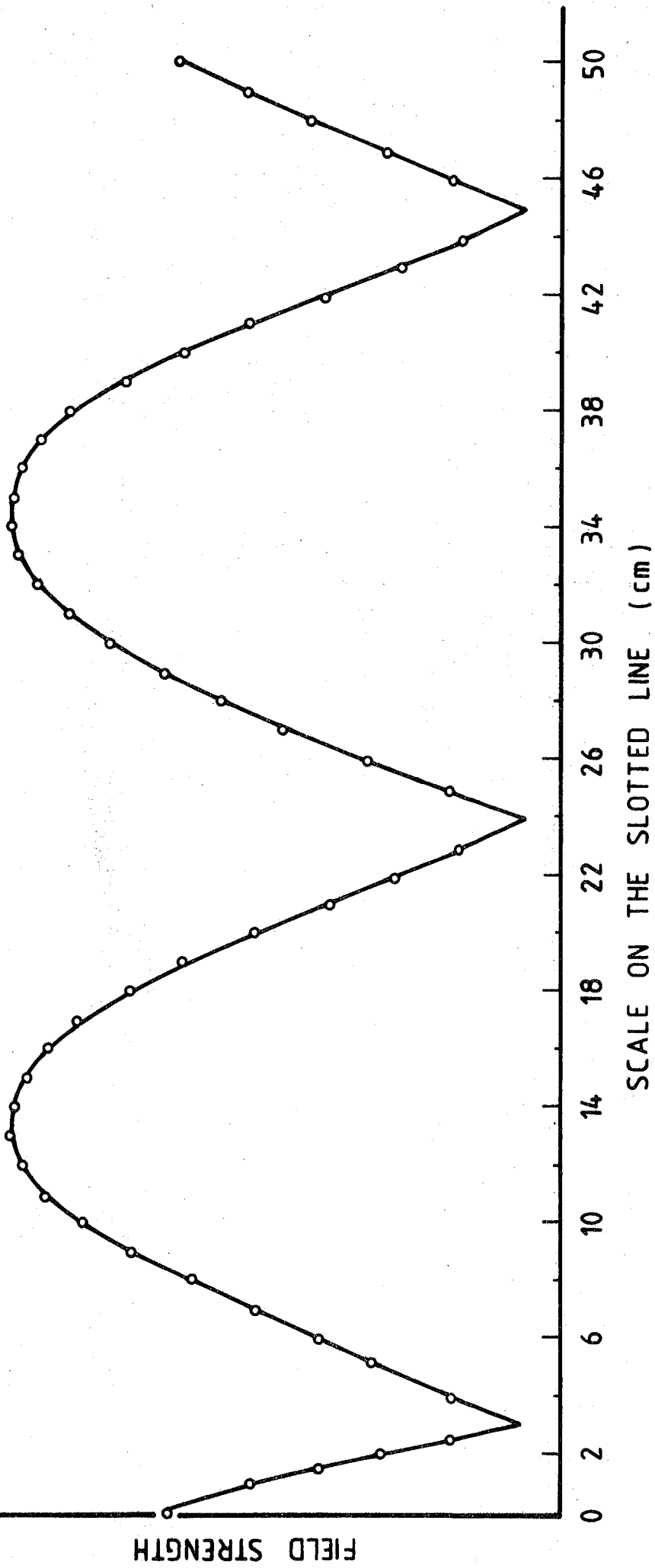
FIG.5.2   STANDING   WAVE   PATTERN   AT   710   MHz;   MgO + 12,800   ppm   Fe.
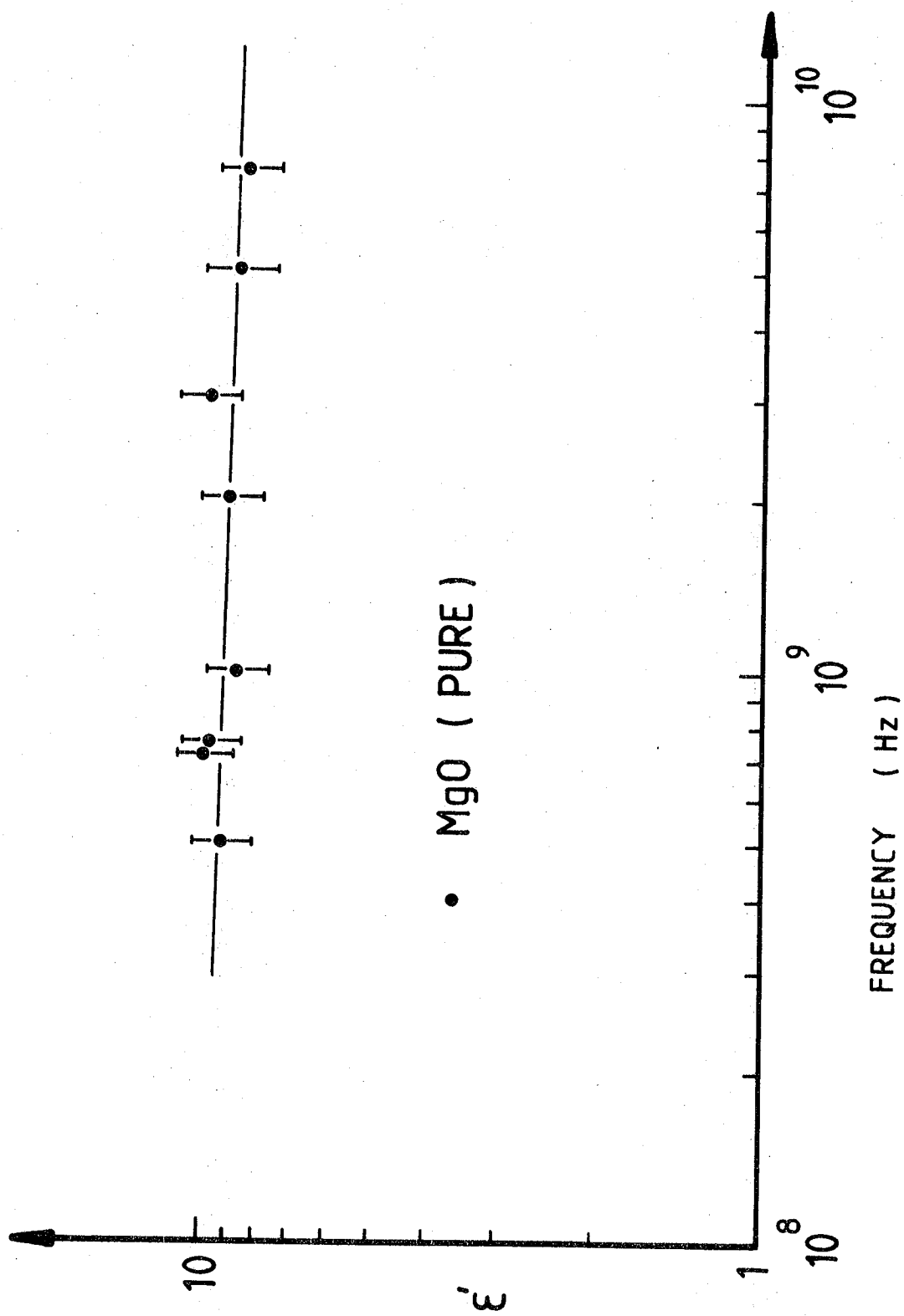
ε'

• MgO (PURE)

FREQUENCY (Hz)

FIG.5.3 VARIATION OF ε' WITH FREQUENCY; MgO (PURE)

variation by itself is quite difficult, since any arbitrary line with various slopes can be considered. This is because of the variation in results at the measured frequencies.

The plots for the doped samples showed the same characteristics except for a constant shift. This is shown in Fig. 5.4. At any particular frequency the value of ε' is inversely proportional to the concentration of Fe in the samples. It is obvious from Fig. 5.4 that the doped samples with medium concentrations lie between high and low concentrations as expected, i.e. between pure MgO and heavily doped MgO with Fe. However, the separation of results is difficult at any frequency as they lie within the experimental errors.

In Fig. 5.5 the plot of ε' versus concentration of Fe was plotted. This not only clarifies the effect of dopant impurities in dielectric properties of MgO but also shows the effect of frequency on ε'. The magnitude of ε' at lower concentrations increases exponentially. As the concentration increases ε' gradually decreases and finally becomes linear. Still, however, being inversely proportional to the level of concentration of Fe. The magnitude of ε' for each sample is determined at three different frequencies and shows the decrease with frequency.

In Fig. 5.6 the variation of ε'' with frequency for pure MgO and heavily doped MgO are shown. The loss factor variations were obtained using Eqn. 3.29. Because of the inaccuracy in the measurement of the reflection coefficient, ρ, about 45% error in the results is expected. The uncertainty in the measurement of ρ will be discussed later.

The variation of ε'' is linear. The mean value is higher in comparison with the lower frequency data. However, the effect of Fe concentration may be deduced from these plots and concluded that ε'' is directly proportional to the concentrations of the dopant impurities.
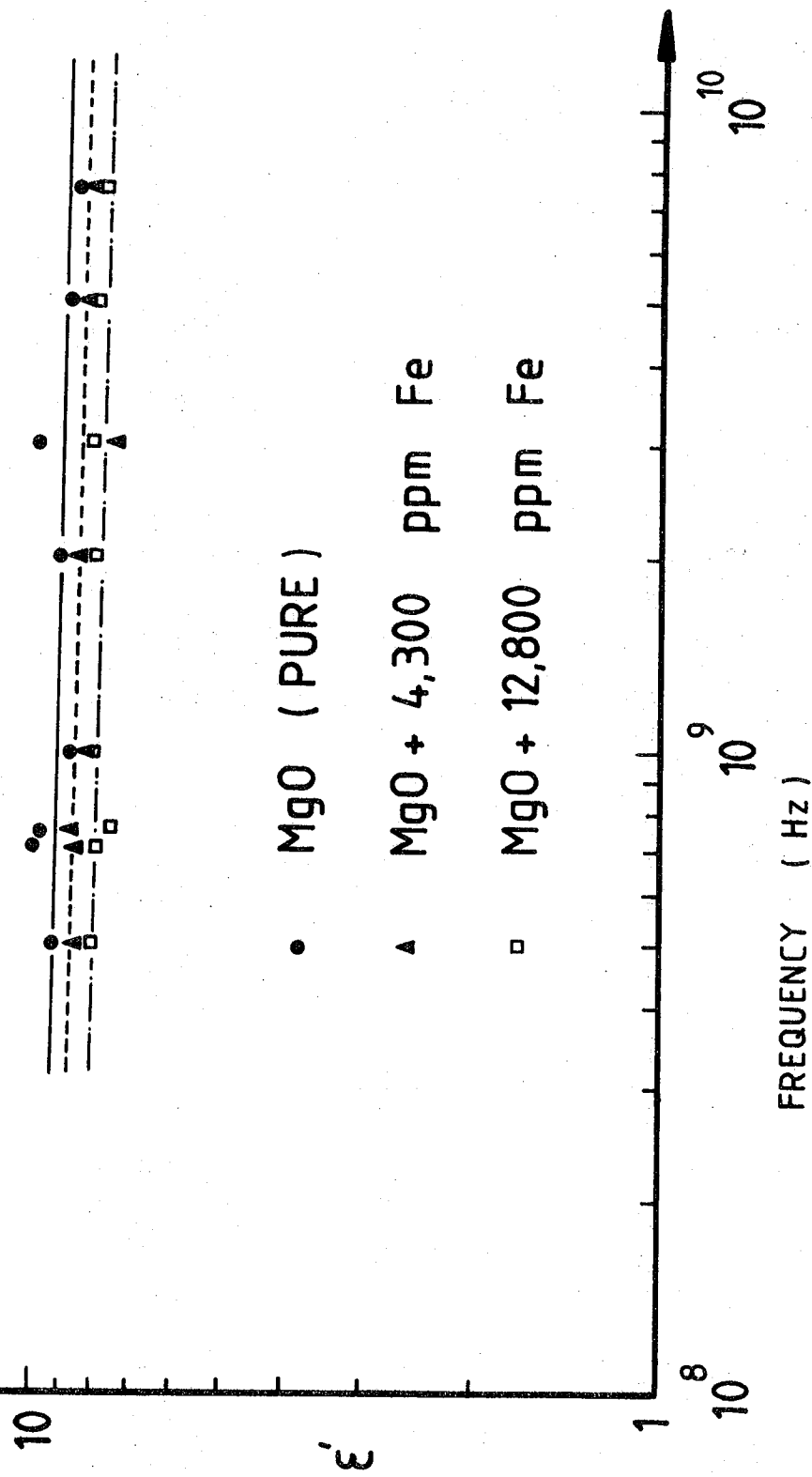
FIG. 5.4   VARIATION OF ε´ WITH FREQUENCY; MgO (PURE),
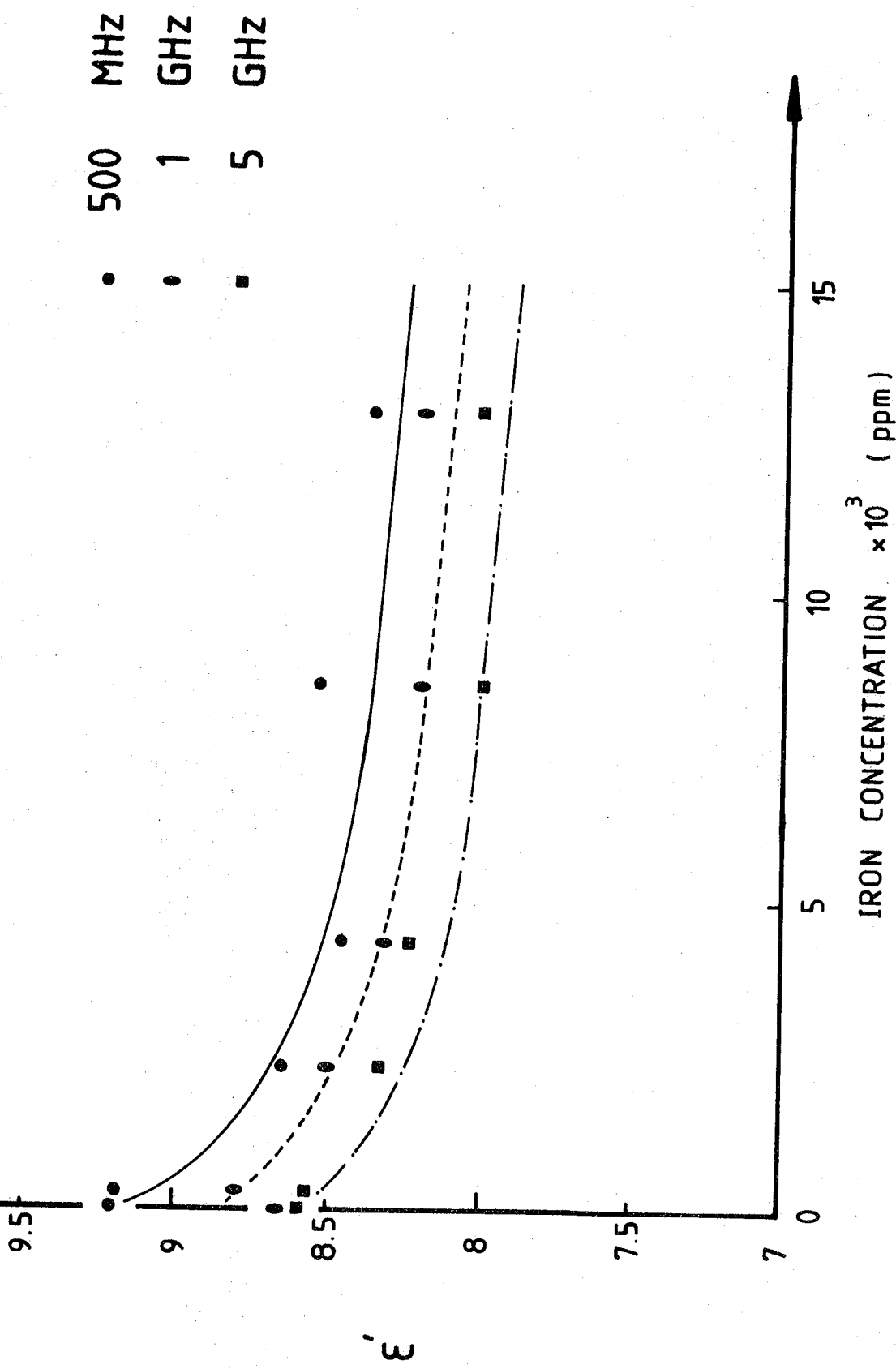MgO + 4,300 ppm Fe , MgO + 12,800 ppm Fe

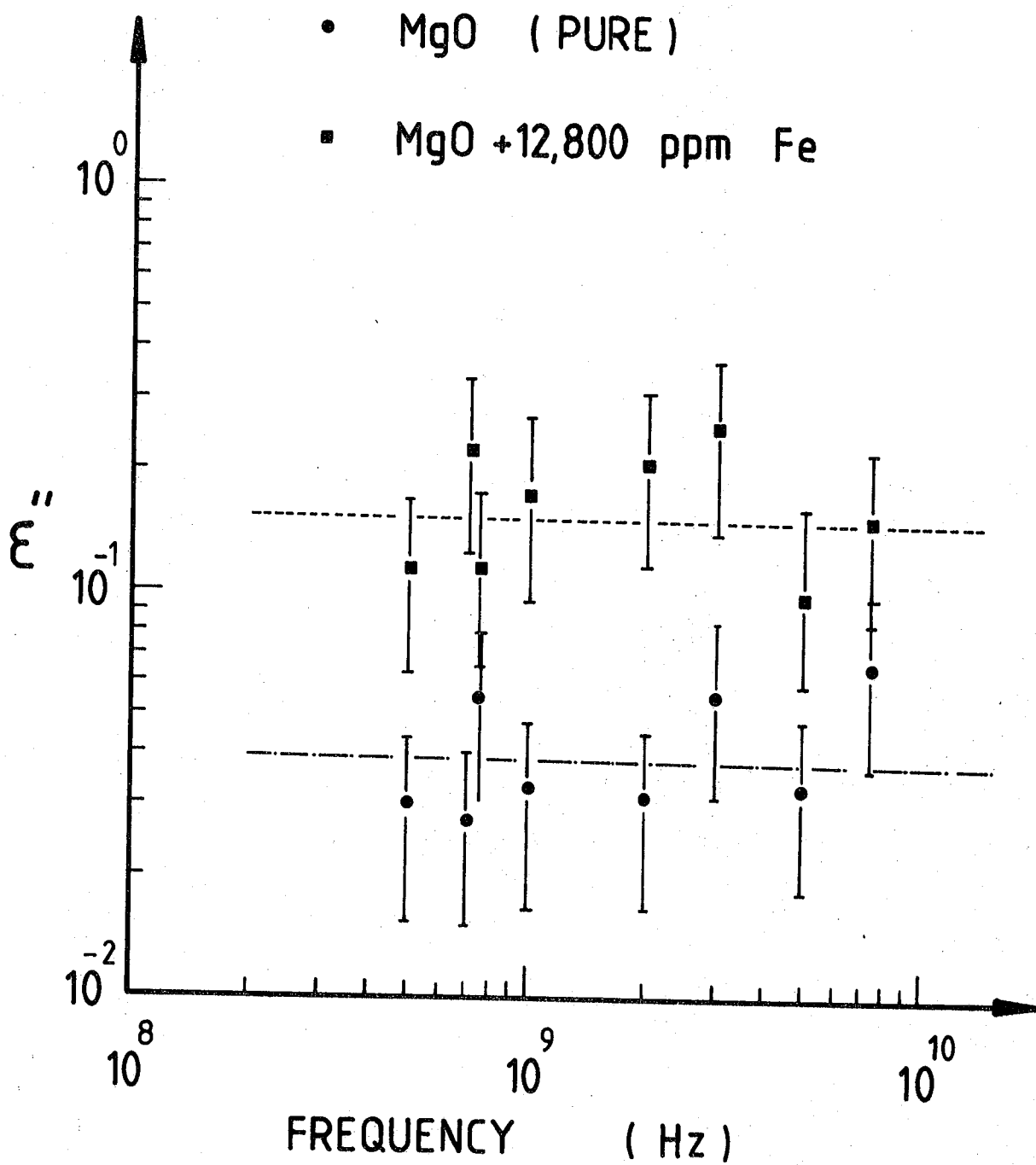FIG.5.5   VARIATION OF ε′ VERSUS Fe CONCENTRATION.

FIG.5.6   VARIATION OF ε'' WITH FREQUENCY ; MgO(PURE) AND MgO +12,800 ppm Fe.

The a.c. conductivity, $\sigma_{ac}(\omega)$ was calculated from the measured loss factor. It was found that the value of the conductivity in this frequency range, in comparison to the medium frequencies conductivity, is higher. This is due to the 45% error in the measurement of the reflection coefficient.

In order to see the effect of other concentrations of the dopant impurities, σ versus concentrations of Fe was plotted in Fig. 5.7 which shows linear behaviour and direct proportionality to the Fe concentration. The plots also show the increase of conductivity with frequency.

The comparison between Fe and Cr doped MgO was made and the results at most frequencies showed that the conductivity for Fe/MgO was higher than for Cr/MgO.

5.1.3 The Relationship between the ρ and Fe Concentration

It is interesting to see how the reflection coefficient, ρ varies for different concentrations of Fe in MgO crystals. The reflection coefficient was measured for various concentrations as shown in Table 5.1. The measurement was performed at 7.5 GHz. The plot of ρ versus the percentage of Fe concentration is shown in Fig. 5.8 and it shows that it is inversely proportional to the magnitude of Fe in single MgO crystals. It is seen that the slope is constant up to about 0.7% of Fe concentration and then it rises exponentially. For pure MgO the value of ρ is 0.97 and differs very little from ρ at short circuit ($\rho = 1$). It can be assumed with very little error that they are equal to each other. In Fig. 5.9 the theoretical plot of VSWR versus reflection coefficient is shown. Examining the result in plot Fig. 5.9 and comparing with the result in Fig. 5.8, may be concluded that there are difficulties in measuring VSWR> 65. Therefore our measurements for short circuit, pure MgO and low concentration of Fe or Cr are not very reliable. This error
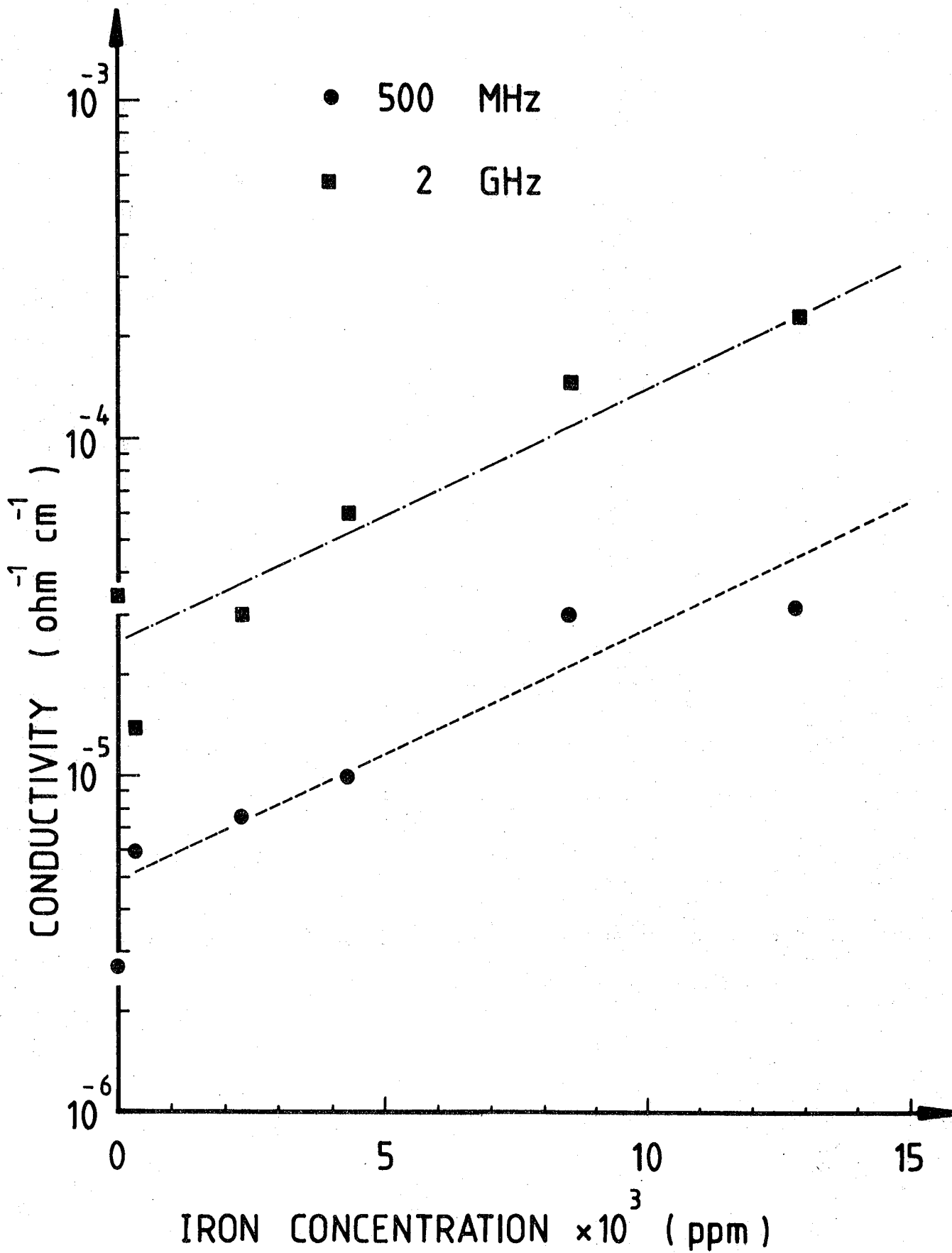
FIG.5.7   CONDUCTIVITY VARIATION WITH Fe
CONCENTRATION.

Nominal Composition of Sample	VSWR, S	$\dfrac{\Delta S}{S}$	ρ	$\dfrac{\Delta\rho}{\rho}$	ΔS
MgO (pure)	65.7	0.5076	0.97	0.010	33.33
MgO + 310 ppm Fe	24	0.3404	0.92	0.0196	8.17
MgO + 2,300 ppm Fe	9.2	0.1173	0.804	0.0187	1.08
MgO + 8,500 ppm Fe	8.7	0.1172	0.7938	0.0198	1.02
MgO + 12,800 ppm Fe	7.2	0.0972	0.7551	0.0192	0.6969

TABLE 5.1 :   Effect of Fe concentrations on S (VSWR) and ρ ;

at frequency of 7.5 GHz.

FIG.5.8   VARIATION OF ρ. VERSUS PERCENTAGE OF Fe AT 7.5 GHz.

FIG.5.9   VARIATION OF VSWR WITH ρ
NEAR UNITY.

directly affects the loss factor of the sample, ε'', i.e.

$$\sigma = \omega \, \varepsilon_o \, \varepsilon'' \qquad\qquad (5.1)$$

Substitution of ε'' from Eqn. 3.29 in 5.1 yields,

$$\sigma = \frac{1 - \rho^2}{\dfrac{A}{d} Z_o \, (\rho^2 + 2\rho \, \cos\theta + 1)} \qquad\qquad (5.2)$$

Apparently it is frequency independent but it is known,

$$|\rho| = \frac{S-1}{S+1}$$
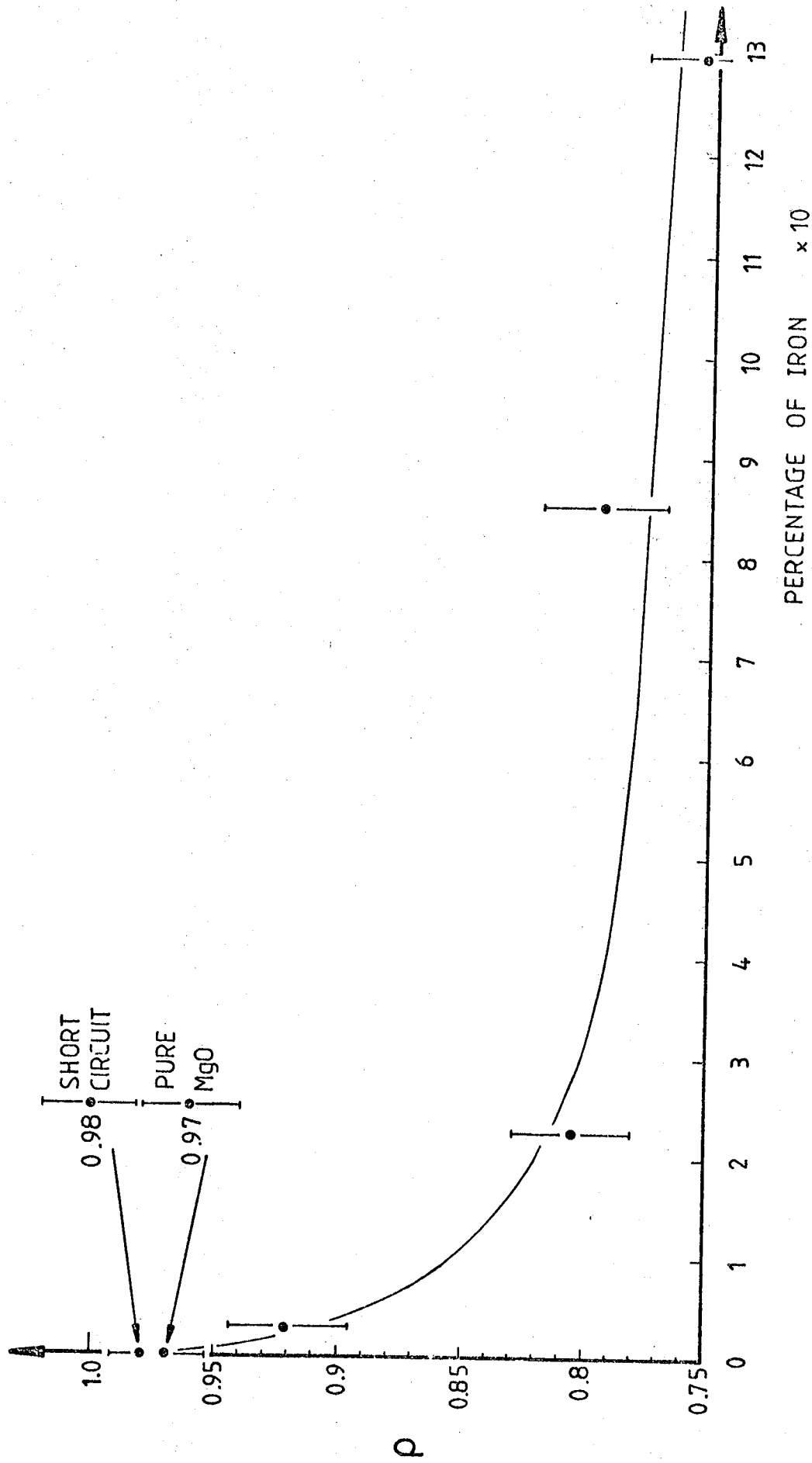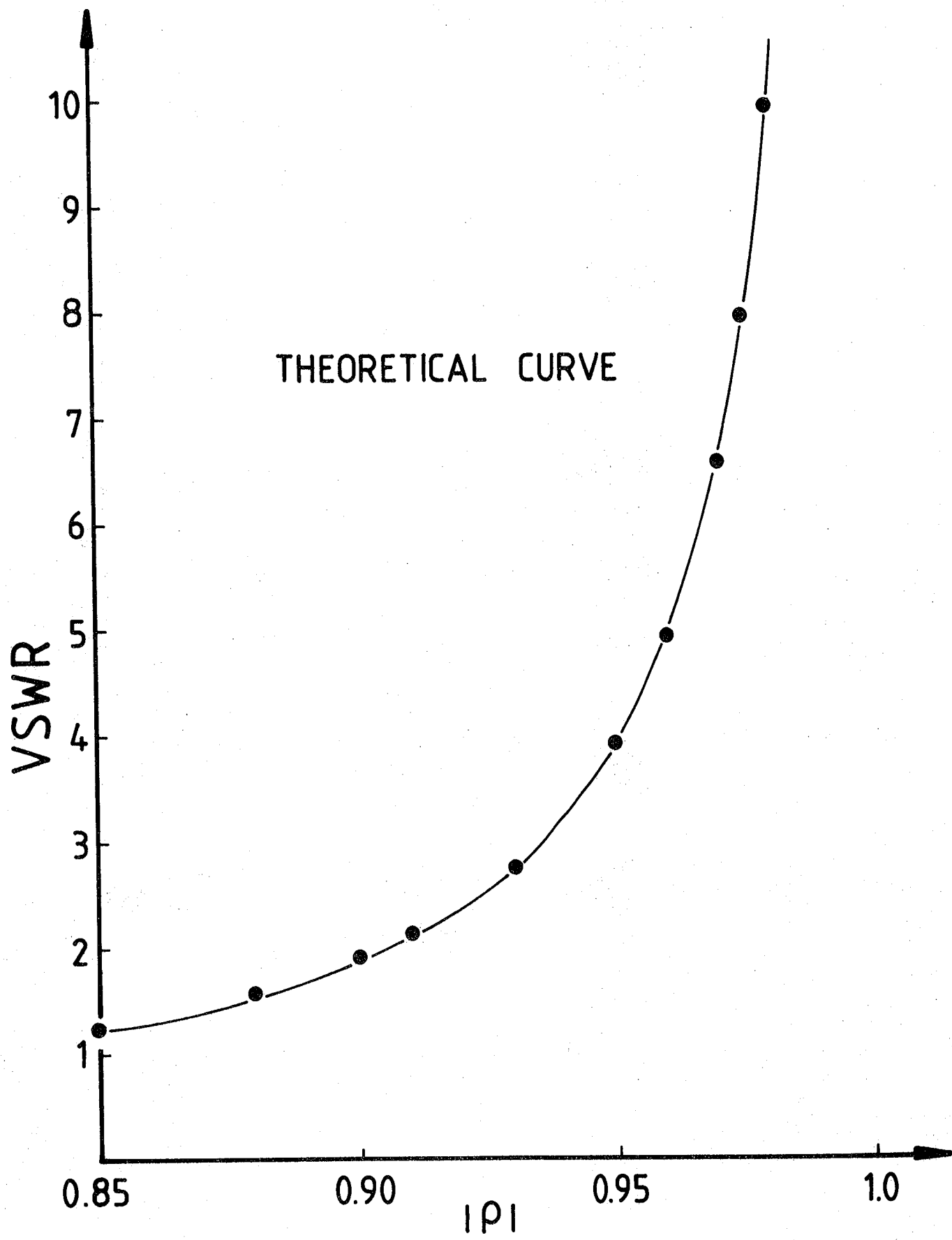
or

$$= \frac{Z_R - Z_o}{Z_R + Z_o} \qquad\qquad (5.3)$$

where Z_R = impedance of load which terminates the line. Z_R is frequency dependent, therefore, ρ will also be frequency dependent and consequently σ from Eqn. 5.2. According to Eqn. 5.2 conductivity of each crystal is related to its reflection coefficient. Accurate measurements of σ depend on the accuracy of ρ. The conductivity is also related to the position of the first minimum which gives the phase angle of the reflection coefficient, θ. The location of the first minimum point for any VSWR can be measured precisely, thus minimizing the errors.

Obviously, the experimental error in locating the voltage minimum point for high VSWR is less than for low VSWR (125), because in the former case the minimum is sharper and more defined (126).

Ishii and Hsu (125) have shown that the magnitude of relative error on voltage reflection coefficient is not related to the magnitude of VSWR in a range between 2 and 24. Their proposal has been checked

in our experiment and as it is seen in Table 5.1 that $\frac{\Delta\rho}{\rho}$ values are almost constant for VSWR <24 and decreases with the increase of VSWR.

On the other hand the error in VSWR, $\frac{\Delta S}{S}$ decreases with the increase of VSWR as shown in Table 5.1. It is also clear that for small VSWR values such as MgO + 12,800 ppm Fe, the relative error is less than the relative error of pure MgO.

5.1.4 Error in Slotted Line Technique

5.1.4.1 Detector characteristics

A large degree of error can result from the change in the detector characteristic at higher r.f. levels. The probe which is connected to the diode detector picks up the electric field in the line at various levels. The change in level to be handled by the detector, can therefore be very large as the probe moves between the maximum and minimum of the standing wave pattern. In order to make sure that the readings are meaningful, it is important that the diode law is the same at these levels. Any deviation from that will introduce errors. It is important to keep the levels within a certain constant point on the diode characteristic and it is usual to work in the square law region. This means that the rectified output current is proportional to the square of r.f. power. In the higher regions the characteristic becomes linear.

The departure from the square-law may be checked using an ammeter in series with the diode for different power levels and this was done in order to minimize this error (127). The procedure is explained in Appendix B.

5.1.4.2 Measurements of Reflection Coefficients

By examining Eqn. 3.31 it can be deduced that the value of the VSWR is very sensitive to small changes in the magnitude of reflection coefficient when it is close to unity (89). This can be seen in Fig. 5.9. When the line is low-loss and the short circuit reference is used the reflection is very near to unity and liable to large errors.

The reflection coefficient of a short circuited line was measured at 7.5 GHz the magnitude of reflection coefficient for the short circuit condition was $\rho = 0.9799$. This showed that the figure was questionable and the error possibly occurs in the method of measurement. However, the measurements of VSWR and determination of ρ for pure MgO and MgO doped with different concentration with Fe, were still valid on the relative basis.

5.1.4.3 Harmonics and Frequency Modulation

The output from any signal generator especially at higher frequencies will always be distorted and consequently contain harmonics. In addition there will also be difficulties in the measurements and introduce errors in the rectifier diode current and detection. The difficulties may arise in establishing the minimum and maximum at the fundamental frequency in the presence of the other harmonics. This can be overcome by continuously checking the distance between two minima which must be a half of wavelength ($\frac{\lambda}{2}$) at the fundamental frequency. Harmonics can be usually reduced to negligible value by using low-pass filters as shown in Fig.3.8.

Frequency modulation is usually produced when the generator is amplitude modulation. The effect of this on the applied signal can introduce large errors for high VSWR because of the distortion in the standing wave pattern. Square wave modulation may be used to minimize the frequency modulation (86).

5.1.4.4 Probe Penetration Error

When measuring a high VSWR it is sometimes necessary to increase the probe coupling to obtain a reading at the voltage minimum. This increase in coupling may result in a deformation of the pattern at the voltage maximum and hence introduce some error. This may be one of the major sources of error in standing wave measurements (127). An excessive coupling to the line may also cause a shift in the position of maxima and

minima because of the capacitive effect between the probe and the slotted line. All these errors can result in the measured VSWR to be lower than it actually is (95).

In order to minimize the errors due to excessive coupling a high sensitivity crystal detector should normally be used and the probe penetration should not be more than 5 to 10% of the internal cross-section of the line (97). For the best performance it is obvious that the probe coupling should be as small as possible.

5.2   MICROWAVE REGION

The dielectric constant, ε', loss factor, ε'' and a.c. conductivity, $\sigma_{ac}(\omega)$ obtained for the pure MgO and MgO doped with different concentrations of Fe or Cr at X-band (9.3 GHz) are summarized in Table 5.2. The values given represent average values of several measurements carried out on pure and doped MgO with different concentrations. The magnitude of ε' decreases as the concentration of iron or chromium increases. But the magnitudes of ε'' and $\sigma(\omega)$ are directly proportional to the concentration of Fe or Cr in the crystal.

It was found that the loss measurements (consequently conductivity) were more difficult to carry out than the measurements of the dielectric constant. Because ε'' is related to the change of Q values of the cavity (Eqn. 3.51) and determination of Q requires great accuracy.

In this experiment the unloaded Q (Q_u) was found to be about 9000 in comparison to the calculated value of 11400. This difference can be accounted for by the losses in the cavity wall surfaces.

The theoretical resonant frequency, f_o in particular TE_{101} mode, was calculated and it was 9.5 GHz ; however in practice due to losses inside the cavity and also other imperfections, this frequency dropped to 9.398 GHz.

Nominal Composition	ε'	$\varepsilon'' \times 10^2$	$\sigma \times 10^4$ (ohm^{-1} cm^{-1})
MgO (pure)	8.67	1.98	1.02
MgO + 310 ppm Fe	8.58	1.84	0.96
MgO + 2,300 ppm Fe	8.40	3.03	1.56
MgO + 4,300 ppm Fe	8.31	4.25	2.21
MgO + 8,500 ppm Fe	8.05	6.74	3.47
MgO + 12,800 ppm Fe	7.78	7.36	3.79
MgO + 800 ppm Cr	8.55	2.32	1.20
MgO + 1,300 ppm Cr	8.45	2.62	1.36
MgO + 3,600 ppm Cr	8.36	3.88	2.01
MgO + 6,200 ppm Cr	8.10	4.83	2.50
MgO + 9,500 ppm Cr	7.89	6.47	3.35

TABLE 5.2 : Complex Dielectric Properties of pure MgO and MgO doped with Fe and Cr ; At 9.3 GHz.

By inserting a sample into the cavity, the electric field inside the sample is affected by the shape of the sample (101). In this experiment it was placed vertically on a thin silican rod which was suspended inside the cavity. The width of the sample must not be wider than the diameter of the rod as the electric field will not then be uniform in the sample. This was checked by putting the sample in vertical and horizontal positions. The magnitude of ε' in horizontal position was less than that in the vertical position. The sample should be placed in a uniform and strong electric field region which in the TE_{101} mode is at the centre of the cavity and of the same strength from top to bottom.

The resonant frequency versus insertion length of the silicon rod was plotted in Fig. 5.10. This relation was plotted again when the samples have been placed on the end of the silicon rod (Fig. 5.11). Both plots showed linear relationship and the shift in frequency for particular position was the same, i.e. both variations have the same slope and they are parallel to each other. As a result the sample can be put anywhere between these two plates, i.e. top and bottom plates of the cavity. At the same time Q of the cavity versus the length of the rod insertion length was plotted in Fig.5.12. The cavity has maximum Q when the rod is at 11.5mm from the top plate. The samples were put at that point and the difference of two Q's was calculated. These experiments were necessary because the high accuracy of the perturbation formula would only be realised if the specimen shape is suitably chosen and if the specimen is suitably placed in the cavity.

For the lowloss materials and since the losses in the samples are small, the change in Q is low, however, this produces a large change in ε'' (Eqn. 3.51).

Different sizes of samples have been tested. Samples of small volume presented some difficulties. Variations of $\frac{\Delta f}{f_o}$ versus volume of
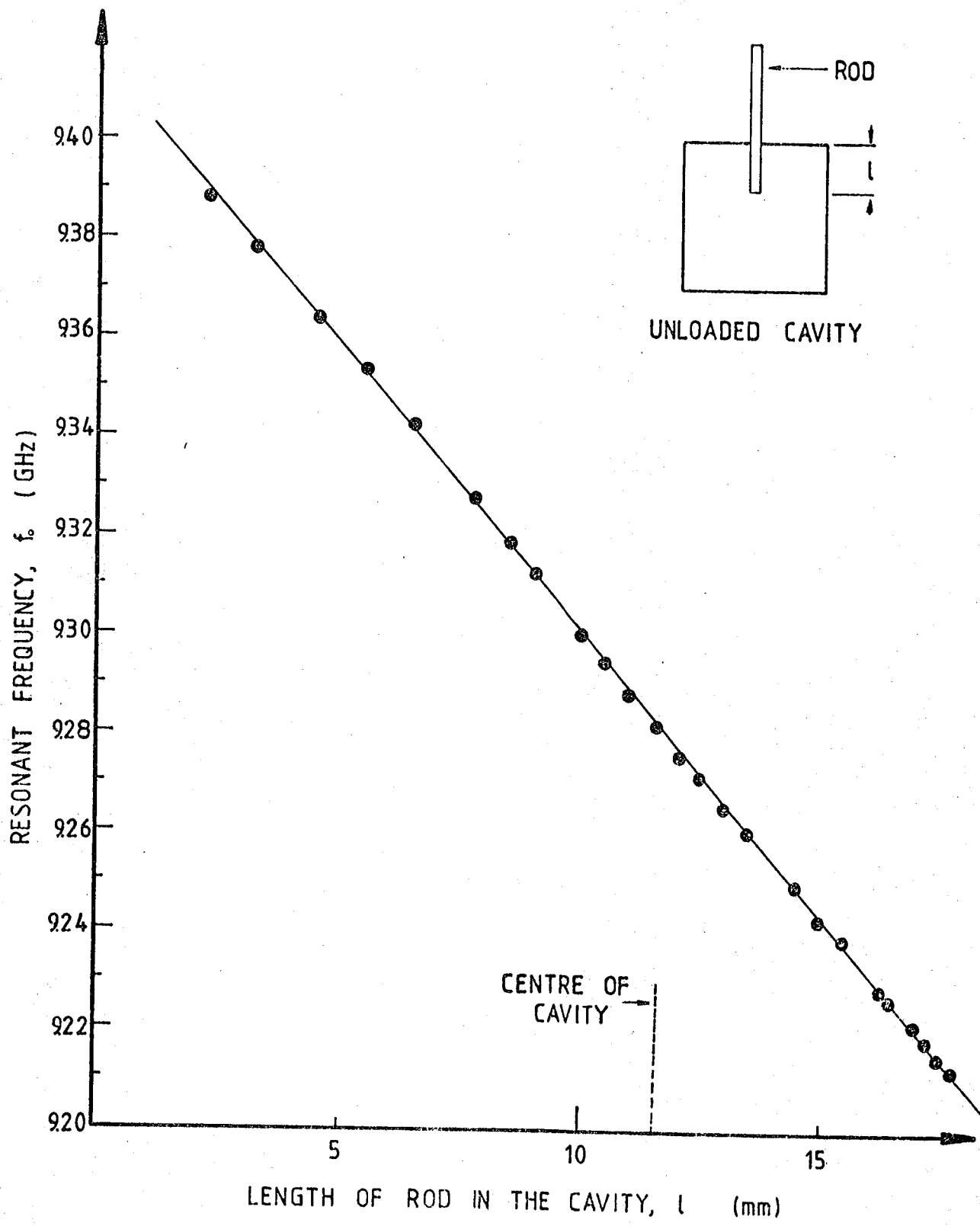
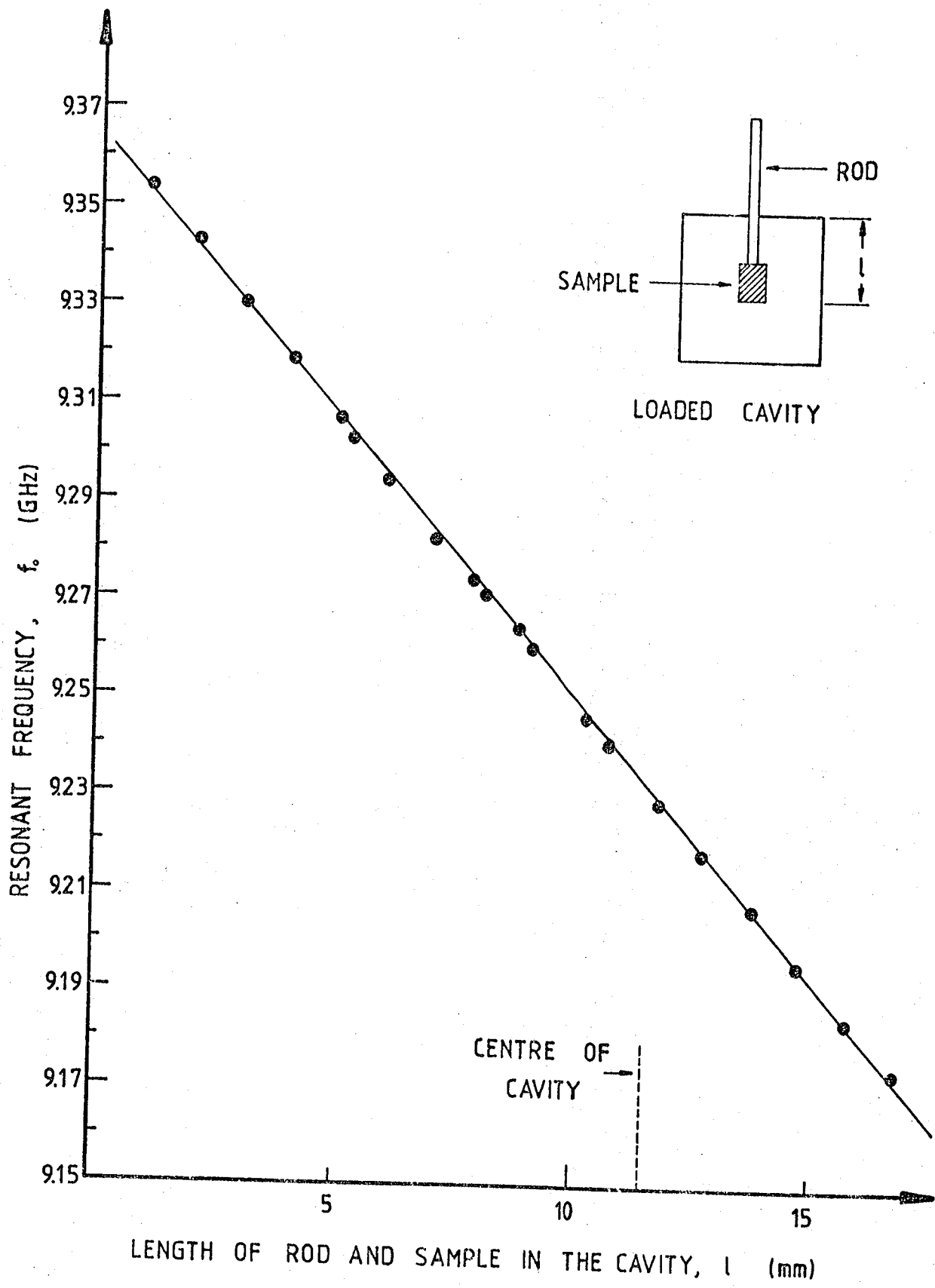FIG.5.10   VARIATION OF f_0 DUE TO INSERTION OF ROD.

FIG.5.11   VARIATION OF f_0 DUE TO INSERTION OF SAMPLE PLUS ROD.
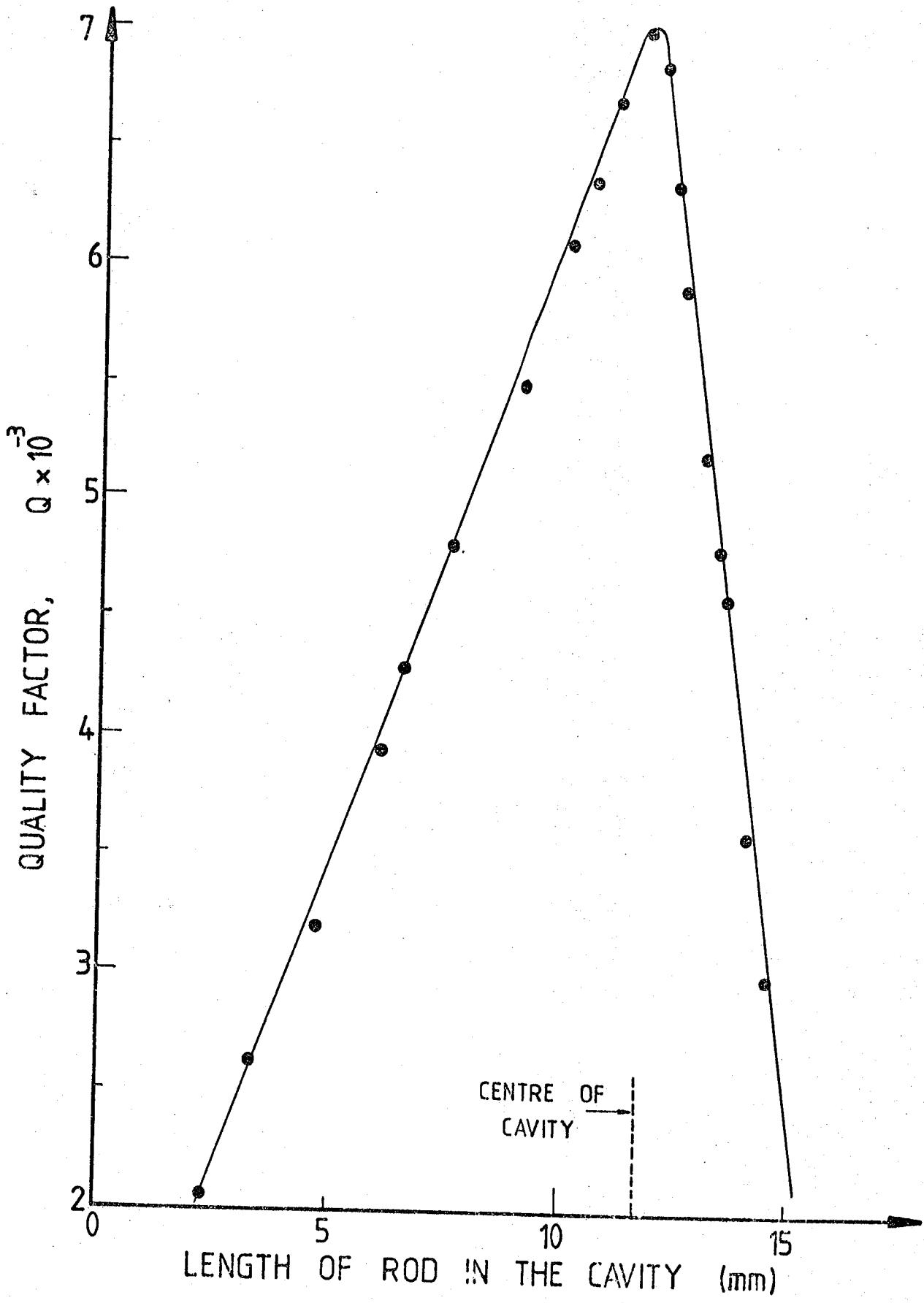
FIG.5.12   Q - FACTOR VARIATION

the samples are plotted in Fig. 5.13. The value of ε' for the ratio

of $\frac{\Delta f}{f_o} \simeq 0.005$ was obtained for the volume of about 4 mm^3.

5.3   DISCUSSION

In order to investigate the reliability of the slotted line

technique, measurements were carried out for each sample several times.

The final result was deduced by averaging the spread. As a result

of this procedure it was found that the following conclusions may be

drawn.

(1) The magnitude of dielectric constant, ε' is dependent more

on the distance of the first minimum (x) than the loss factor, ε''.

Very small changes in x, give large changes in ε'. For accuracy the

distance x, was measured using a micrometer.

(2) The sample holder was a part of the extended inner con-

ductor as shown in Fig. 3.6 whose diameter was varied. It showed that

as the diameter of the inner conductor increases the ε' and ε'' both

decrease. The magnitude of VSWR was found to be inversely proportional

to the diameter of the sample holder. The diameter of 3.18mm was used to

obtain the value of ε' and ε''. The error of measuring the diameter was

estimated to be about 1.5%.

(3) The effect of thickness of the sample, d, has been tested

on the magnitudes of ε' and ε'' and it was found that it did not affect

the result to any extent. The error in measuring the thickness of d

was in the order of 1.5%.

(4) The most critical measurement using the slotted line tech-

nique was that of the reflection coefficient, ρ, because its magnitude for

the samples used will normally be close to unity. It was discussed in

section 5.1.3 that very small changes in $|\rho|$ will produce large changes

in the magnitude of ε'' hence the measurement of reflection coefficient

is of great importance.

Because of the losses in the slotted line and imperfect connectors the measured $|\rho|$ is lower and therefore the magnitude of ε'' will always be higher than its true value. There is no way of correcting this error except by using more sensitive instruments.

(5) Evaporation of gold on the polished surfaces of samples increases the magnitude of ε' and σ by about 1.2% and 20% respectively. This was deduced from the increase of VSWR of MgO doped with 6,200 ppm Cr as shown in Fig. 5.14. Therefore, to avoid this increase of σ, all samples were measured without introducing gold.

The variation of magnitude of ε' with frequency for pure MgO in the slotted line technique changes linearly and it is in good agreement with Jonscher's Universal Law, i.e.

$$\varepsilon'(\omega) \quad \propto \quad \omega^{n-1} \tag{5.4}$$

where in general $0<n<1$ and it was found to be 0.98. It is seen that the experimental results obtained from two methods lie on a same line.

The behaviour of a very heavily and medium doped specimen showed that they have similar characteristics (Fig. 5.4). However, heavily doped samples showed lower ε' than the lightly doped ones for the same frequency. From Table 5.2 it was also found that this effect was present and ε' is decreasing by increasing concentration of Fe or Cr.

From Fig. 5.6, it is concluded that the loss factor, ε'' for the doped sample is higher than in the case of pure MgO. The plots show that they also fit the "Universal Law", i.e.

$$\varepsilon''(\omega) \quad \propto \quad \omega^{n-1} \tag{5.5}$$

The data of a.c. conductivity of pure MgO and heavily doped MgO versus frequency showed that both change linearly with the slope of
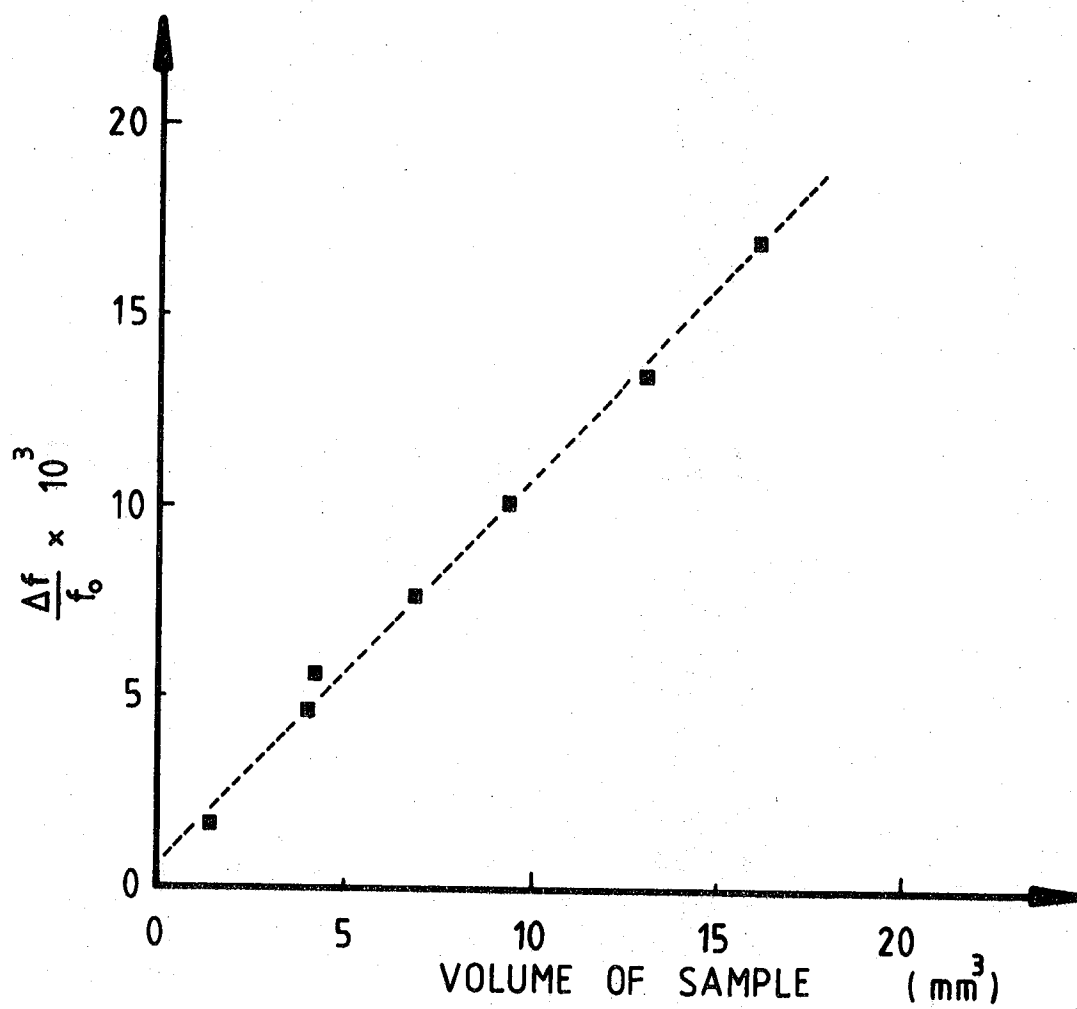
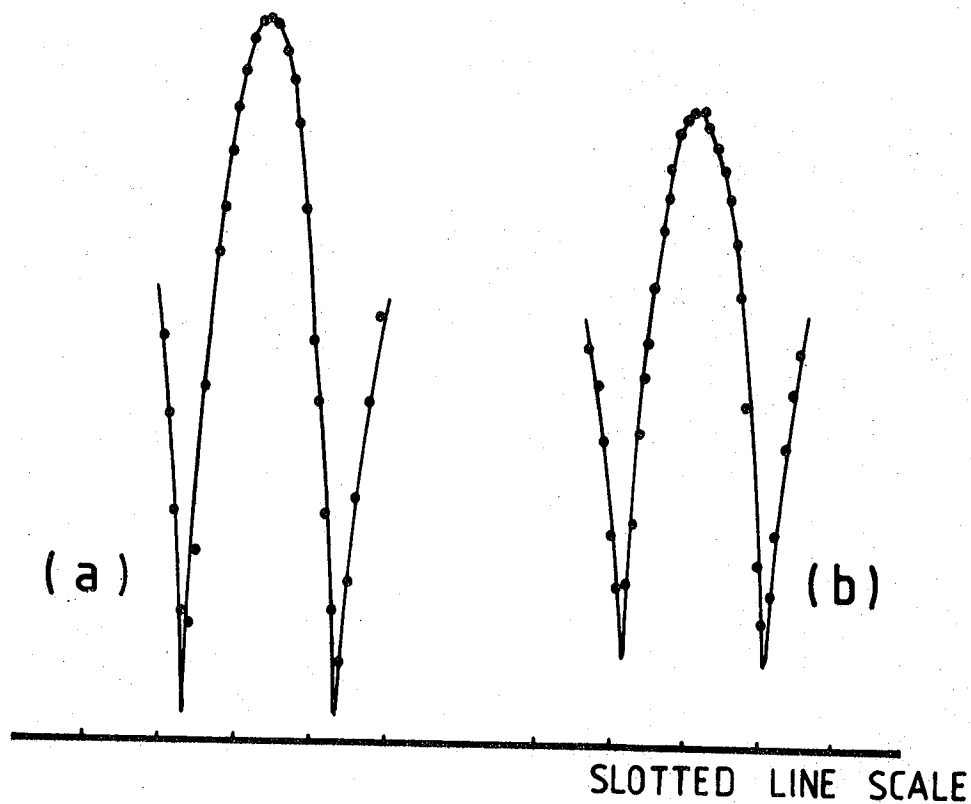FIG.5.13   VARIATION OF $\dfrac{\Delta f}{f_o}$ WITH VOLUME OF SAMPLE.

FIG.5.14   VSWR PATTERN FOR MgO +6,200 ppm Cr;
(a) WITH GOLD. (b) WITHOUT GOLD.

n = 0.98. The results agree well with the "Universal Law", i.e.

$$\sigma_{ac}(\omega) \quad \propto \quad \omega^n \tag{5.6}$$

The perturbation technique used here is suitable for measuring the dielectric properties of high loss materials. The principle of the method is based on the perturbation theory and consequently some assumptions are made, i.e.

(1) The basic assumption is that the change of field is small on the introduction of the sample (110). The sample must therefore be as small as possible.

(2) The homogeneity of the specimen should be maintained since this gives error in ε'.

(3) An assumption has been made that the shape of the sample is such that the electric field inside is equal to the electric field outside it.

(4) Ideally $\frac{\Delta f}{f_o}$ must be less than 0.01 in the Eqn. 3.50 to prevent large errors in the calculations.

To meet the requirement (4) above is difficult since in practice $\frac{\Delta f}{f_o}$ equalled about 0.5. If it is less than 0.05, it presents difficulties in measurement and if it is greater than 0.05, it violates perturbation theory.

In the measurements of Q and the resonant frequency, f_o, the main sources of error were essentially in the determination of the 3dB bandwidth, i.e.

(a) due to the inaccuracy of the attenuators (systematic

(b) due to the wavemeter (110) calibration and fluctuations (systematic and random error). The reasons for the error in the wavemeter readings may be in turn attributed to, (i) instability of the
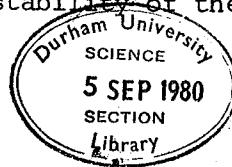
microwave source, and (ii) the error in the calibration of the wavemeter itself.

(c) the effect of the crystal detector in measuring the VSWR because of the difference in the detector characteristic at minimum and maximum readings. Its characteristic may be checked (Appendix B) and it was assumed to have square law characteristic.

(d) due to the small mismatch obtained using coupling screws.

In the slotted-line technique in order to achieve accurate results, the slotted-line and associated apparatus should satisfy the following requirements :

1. A good quality slotted-line must be used.

2. The connections must be firm and rigid.

3. Determinations must use connectors which are dimensionally and electrically identical to the slotted-line.

4. The sample holder must be so designed that it does not affect the characteristic of slotted-line, i.e. it must be tested and calibrated without sample.

5. The characteristic of the detector must be calibrated.

6. The geometrical dimensions of the sample should ideally be smaller than the wavelength used.

7. The detector and the probe should be well screened against stray fields.

8. The sample should preferably have parallel and well polished surfaces. Also the surfaces of the sample holder should be smooth.

9. Finally, it must be ensured that signal source is stable in amplitude and frequency ; also has low harmonic content.

The slotted-line method is particularly suitable for lossy dielectric material (96), because it produces a lower $|\rho|$. Measurements of reflection coefficient when it is close to unity are difficult

and unreliable. The technique gives direct information about the magnitudes of ϵ' and ϵ'' and their behaviour with frequency.

It is possible to measure higher VSWR within the square-law region of the diode. The method will be entirely suitable for the determination of the dielectric constant of material. The low values of detector current at the minima of the standing wave pattern may be measured using an electrometer instrument which for this project was not available. In this case the power standing wave ratio will be obtained from which VSWR can be calculated and hence the reflection coefficient.

In order to overcome the unreliability of slotted line tech - nique in measuring dielectric properties of low loss materials due to existing high VSWR, another method has been suggested. The method is called "Comparison Method" and is explained in detail (Appendix D).

Due to lack of time it has not been developed although some initial tests were undertaken which proved satisfactory and reliable. This is left for the future work in the instrumentation and measurement of complex dielectric constants.

5.4   REFERENCES

125.   Ishii, T.K.and Hsu, K.W. 'Dependencey of Error of Reflection

        Coefficient Measurement on VSWR Magnitude', IEEE, Transaction

        on Instrumentation and Measurement, pp 98 (March, 1973).

126.   Tischer, F.J, 'Mikrowellen-Mesztechnik', Berlin, Springer (1958).

127.   Barlow, H.M. and Cullen, A.L, 'Microwave Measurements',

        Constable and Company Ltd., London (1950).

CHAPTER 6

DISCUSSION OF ROOM TEMPERATURE DATA

6.1   RELATIVE ADVANTAGES OF THE MEASUREMENT TECHNIQUES

Generally speaking the advantages of each method over the others

cannot be easily distinguished since each technique is the most suitable

for a particular frequency range and they differ from each other in

important essentials. For a brief comparison of the methods used in

the present project, some of their specifications are presented in

Table 6.1 ; this enables comments to be made on the sensitivity and

accuracy of each method. It is important to realise that the advantage

of each technique varies according to the type of material under investi-

gation, therefore the conclusions on their reliabilities are limited by

the dielectric behaviour of the material examined in the frequency range

used.

For both pure MgO and doped MgO, the bridge method was found

very suitable and reliable for low frequency measurements. Some

corrections for edge effects were needed in the calculation of ϵ' and

ϵ''. It is very sensitive to small changes in the magnitude of conduct-

ance and capacitance for the sample under test. Therefore, it can be

used to determine the effect of very small percentages of dopant

impurities on the magnitude of conductivity or dielectric constant

(assuming that specimens of suitable area and thickness are available).

In the Q-meter method, by contrast, great accuracy is required

in placing the sample in its previous position between the electrodes

since (due to measuring procedure) the sample must be taken out of the

jig and then replaced. Its accuracy is not as high as that of the

bridge, but still it was found to be a very reliable technique for

	Determination of ε' and ε''	Principle of Method	Applied Frequency in This Project	Ambient Temperature
Bridge Technique	Direct reading	Bridge	500 Hz – 30 kHz	Room Temperature & High Temperature
Q-meter Method	Direct reading	Resonant Circuit	100 kHz – 30 MHz	Room Temperature
Slotted-line (coaxial line)	Indirectly Obtained	Change of Impedance	500 MHz – 7.5 GHz	Room Temperature
Cavity Resonator	Indirectly Obtained	Resonant Circuit	9.3 GHz	Room Temperature High Temperature

TABLE 6.1 : Comparative Specifications of the Techniques

MgO single crystals. The operational frequency range is shorter than that for the bridge. It was observed that on increasing the frequency the inductive effect of the assembly and other circuit elements becomes significant and under these conditions it does not give true values of capacitance or Q of the circuit. This effect usually manifests itself at about 4 MHz and data of over this limit cannot be regarded as acceptable.

The greatest advantage of the coaxial line is that, it covers quite a wide range at high frequencies (r.f. range). In practice, however, some difficulties were encountered due to the characteristics of the MgO samples. For instance the method of measuring VSWR of the standing wave created on the line due to the insertion of a sample was found to be very critical and time consuming. Because pure MgO is inherently a low loss material, the VSWR on the line was consequently very high. Other methods for VSWR measurement were tried but proved either impossible or unreliable. The present technique is not suitable for low loss material but it will give reasonable data for high loss materials which is its conventional area of application. This technique does not give direct readings of ε' and ε''. The method can be developed however, and some suggestions and calculations for derivation of ε' and ε'' were made and are given in Appendix D. Due to the lack of time it was not possible to use these developments in this project.

Finally, the cavity resonator (perturbation) method has been found to be a very appropriate technique for measuring the dielectric properties of low loss materials such as MgO. It gives the highest accuracy when measuring dielectric constant but some difficulties were encountered in the determination of the loss factor. In general this method is often simple, convenient and reasonably accurate, especially for low values of ε' and moderate losses ; even for low loss material

it still gives reasonable data although it does not give direct readings
of ε' and ε''. It is known that ε'' is related to the change in Q
between the unloaded cavity and the cavity loaded with the sample. In
practice due to low loss sample (MgO) this change was small and great
care is needed to make a reliable determination of this change. In this
method the effect of variation of room temperature has been also investi-
gated ; data obtained at different times and slightly different tempera-
tures were compared and gave 0.5% error in ε' and 1% in the conductivity
for a change of temperature of between 3-5° C.

In all the techniques the 3% uncertainty in the results may be
caused mostly by errors in the sample thickness measurements and by the
non-uniformity of the sample thickness or the surface of the electrodes.
It is concluded that more precision is required in measuring the thick-
ness of the samples and controlling their geometry.

It was felt that the results obtained using the bridge and
Q-meter are more accurate than those obtained using the slotted-line
technique ; and more reliable results could be obtained only up to 4 MHz
in the latter method. Unquestionably, the most precise results were
obtained at microwave frequencies where the 0.6% error was caused by
Klystron-frequency and cavity dimension fluctuations (due to ambient
temperature). This method has been proved to be accurate and convenient
at 9.3 GHz and could in principle fairly be extended to longer wavelengths
(e.g. 3 GHz), where the cavity dimensions are increased, to give an over-
lap with the slotted-line.

The error in the measurement of dielectric constant with the
bridge method was estimated as $\pm$ 3% and for conductivity $\pm$ 4%. Edge
effect corrections were about 8% in the ε' and 10% in the conductivity.
In the Q-meter method error in ε' was increased to $\pm$ 5% for dielectric
constant and $\pm$ 17% for conductivity. The edge effect correction has

the same value as in the bridge method. The accuracy of the present
slotted-line technique is $\pm$ 12% for the dielectric constant and $\pm$ 45%
for conductivity. The errors in the cavity resonator method were esti-
mated at about 1 to 2% on the dielectric constant but higher ($\sim$ 5%)
in the conductivity. As Bussey (128) pointed out for those materials
which have $\varepsilon' = 2$ to 10 the error in the cavity method is increased by
increasing the frequency.

It may be concluded that the comparison has been worthwile,
especially because it gives a good indication of the actual limits of
accuracy of each technique and of the respective suitabilities of the
methods for the study of materials with particular characteristics.

6.2 COMPARISON WITH JONSCHER'S THEORY

The complex dielectric constant behaviour of pure magnesium
oxide and MgO doped with iron or chromium have been investigated over
a very wide range of frequencies at room temperature. Consideration of
the effect of frequency on the magnitude of conductivity and of dielectric
constant was the original object of this work. Therefore, the frequency
dependence of $\sigma_{ac}(\omega)$ has been investigated and the conductivity versus
frequency variation was plotted in Fig.6.1, for pure MgO. This illustrates
the combination of the individual sets of results obtained in the differ-
ent ranges of frequency. As can be seen, the data obtained from the
bridge and Q-meter lie on a good straight line which, when extrapolated,
includes the microwave results ; its slope was measured as 0.984 $\pm$ 0.02,
i.e. the linear frequency dependence of $\sigma_{ac}(\omega)$ was observed in the whole
frequency region (f $\leqslant$ 9.3 x 10^9 Hz). This variation agrees with the
Jonscher "Universal Law"

$$\sigma_{ac}(\omega) \propto \omega^n \qquad\qquad (6.1)$$

with n = 0.984 $\pm$ 0.02. Data from slotted-line shows that the apparent
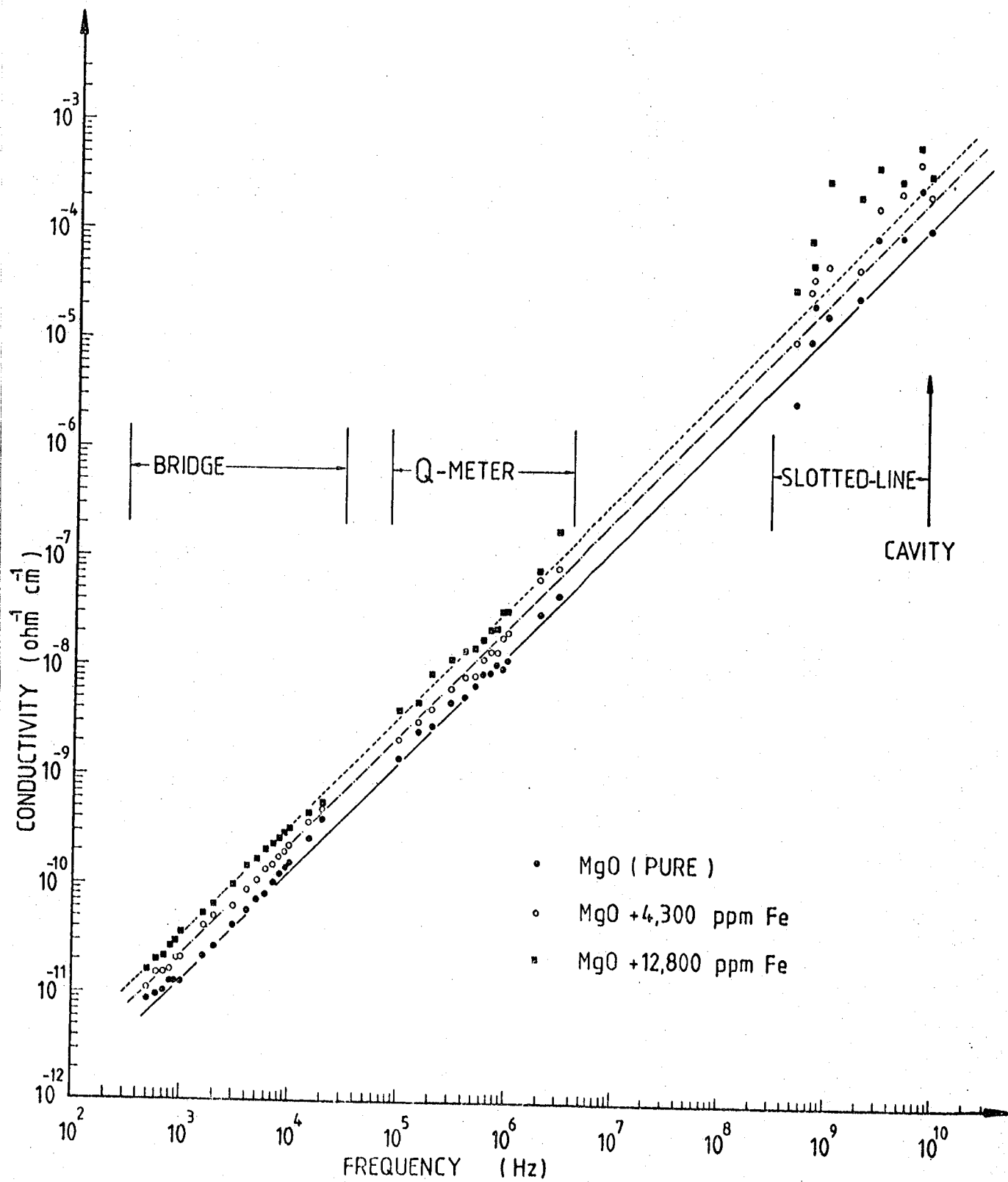
FIG.6.1   VARIATION OF σ VERSUS FREQUENCY; PURE MgO , MgO +4,300 ppm Fe
AND MgO +12,800 ppm Fe

conductivity observed was a factor of two times higher than the conductivity obtained from the other regions. This is due to a systematic error and its origin was explained in Chapter 5.

The effect of doping impurities (especially iron) has been fully examined. A dependence following $\sigma \propto \omega^n$ with the same magnitude of n was also observed in magnesium oxide doped with different concentrations of Fe ; this data is also given in Fig.6.1. It can be compared with the result of pure MgO and hence it is concluded that the iron dopant considerably increases the conductivity of the sample. The reason for this effect was discussed in Chapter 4 where it was suggested that the iron impurities play an important role in the conduction mechanism in that their introduction into the sample produces extra vacancies which contribute to the conduction by providing additional hopping sites.

Since the slope of the line is the same for all samples it can therefore be concluded that over all the frequency range conduction is basically due to the same type of mechanism.

In order to see the effect of chromium in the conductivity, its variation with frequency was plotted in Fig. 6.2. It showed similar characteristics to Fe/MgO. Comparison between two samples doped with different impurities but to almost the same doping level can be made by noting the conductivity of MgO + 4,300 ppm Fe in Fig.6.2. The variation for both samples parallel to each other but at any particular frequency the conductivity of the Fe doped sample is higher than the Cr doped specimen.

In Fig.6.3 the data of dielectric constant ε' was plotted for pure MgO, a highly doped Fe/MgO sample and a Cr/MgO sample over the whole frequency range of 500 Hz-9.3 GHz. The data lies on parallel straight lines and fits the "Universal Law"
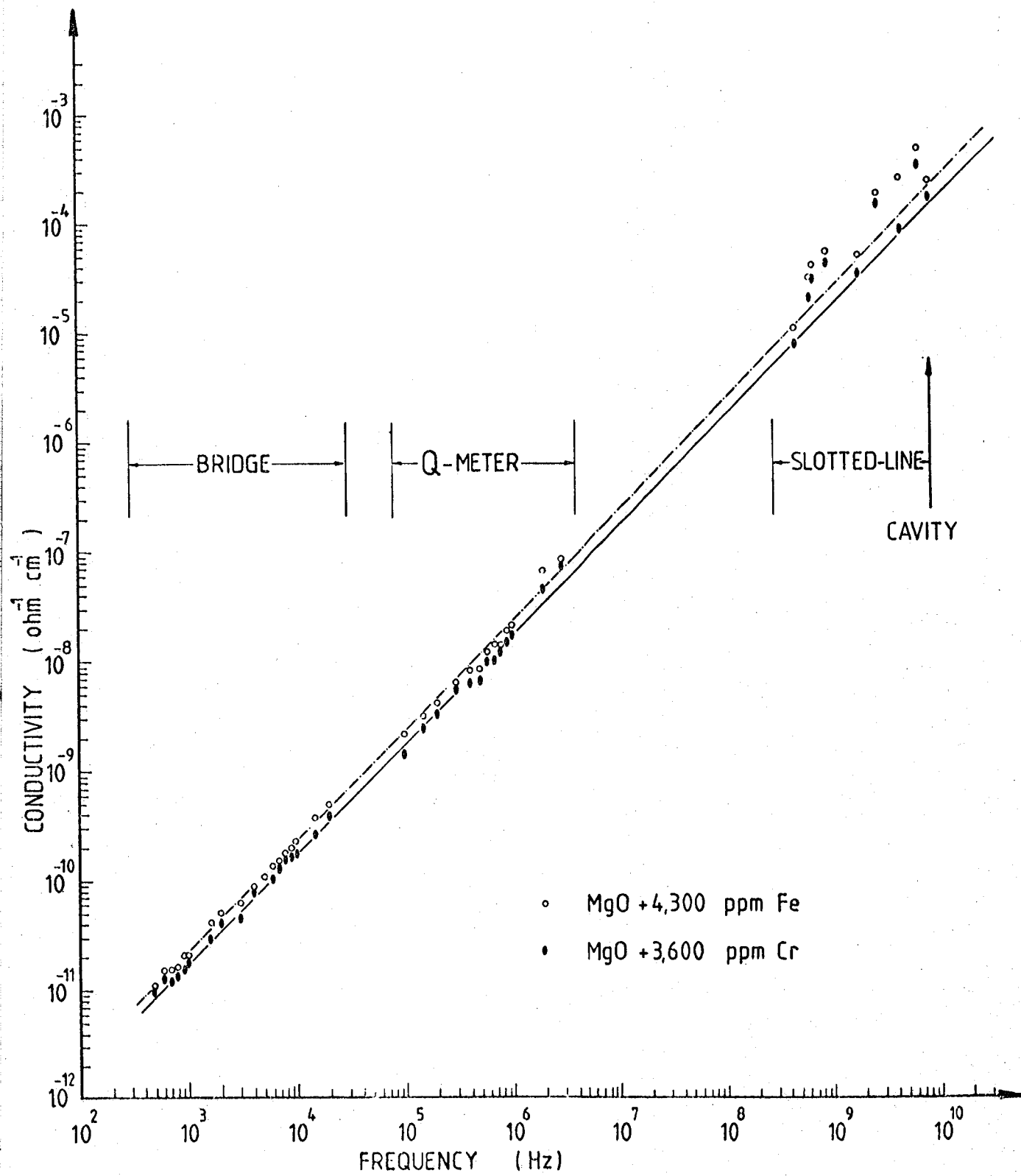
$$\varepsilon'(\omega) \propto \omega^{n-1}$$

(6.2)

FIG.6.2 VARIATION OF σ VERSUS FREQUENCY; MgO +4,300 ppm Fe AND
MgO +3,600 ppm Cr
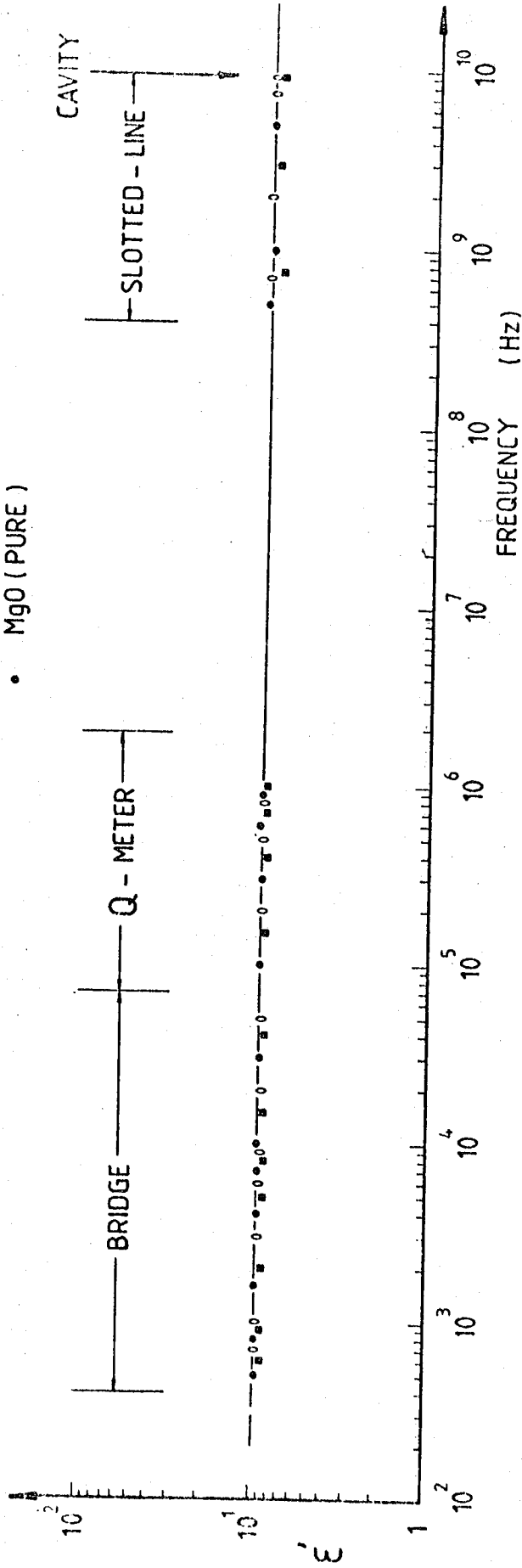
FIG.6.3 VARIATION OF ε' WITH FREQUENCY: MgO (PURE)
MgO+3,600 ppm Cr

with n = 0.985 ± 0.02 supporting the idea that the same hopping mechanism applies over the whole range of frequencies. Comparison of the variation of ε' with frequency for the heavily doped Fe/MgO shows that at all frequencies its dielectric constant is lower than that of the pure MgO ; the values for the Cr/MgO specimen were indistinguishable from those of the pure MgO.

The variation of loss factor, ε'' of pure MgO and heavily doped Fe/MgO were plotted in Fig.6.4 (a) and both exhibit similar characteristics. The microwave data also lies on the extrapolated low frequency. The slotted line results have a considerable error and are displaced (as already noted) from the extrapolation ; however, they still keep the same relative differences as they have at low frequency. The variations are linear with slope 0.985 and agree very well with the "Universal Law"

$$\varepsilon''(\omega) \propto \omega^{n-1} \qquad (6.3)$$

Further comparison of Cr and Fe doped samples is given by their loss factor behaviour, plotted in Fig.6.4 (b), which shows characteristics similar to their conductivity plots.

Finally, the loss tangent for pure MgO was plotted in Fig.6.5 and it also showed linear changes over all the frequency range.

The important information to be obtained from Fig.6.4(a) and Fig. 6.4(b) is the dependence of the dielectric loss on the composition of the samples ; it is clear that the dependence is much stronger in Fe series than in the Cr.

The real and imaginary parts of complex dielectric constant are related to each other through the Kramers-Kronig relations,

$$\frac{\varepsilon''(\omega)}{\varepsilon'(\omega) - \varepsilon_\infty} = \cot\left\{\frac{n\pi}{2}\right\} = constant \qquad (6.4)$$
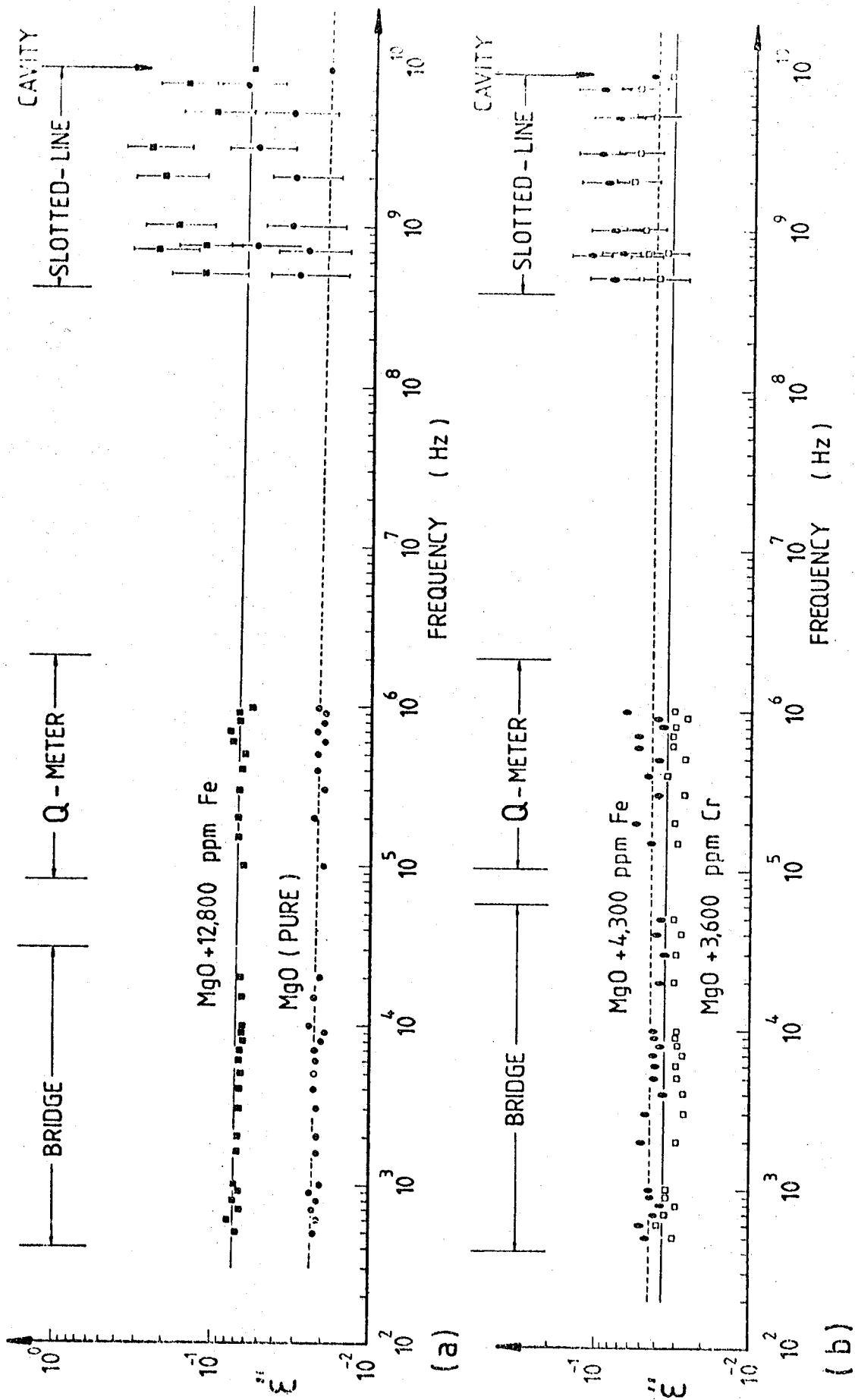
FIG.6.4 VARIATION OF ε'' WITH FREQUENCY, (a) MgO(PURE) AND MgO+12,800 ppm Fe
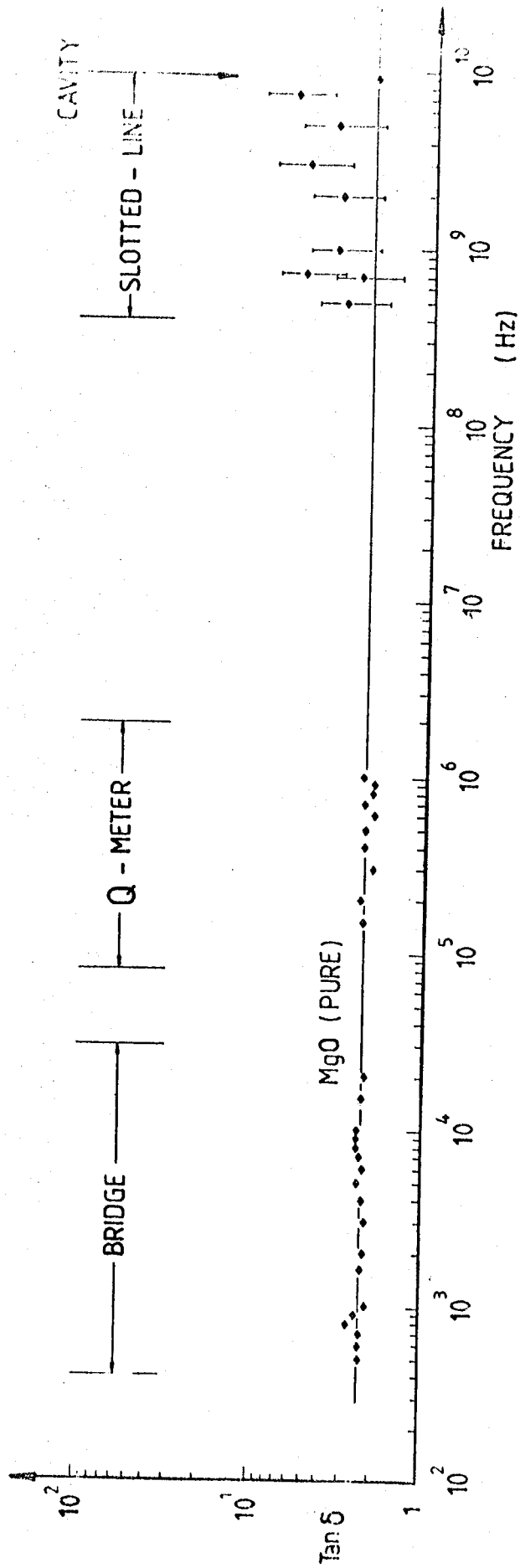(b) MgO+4,300 ppm Fe AND MgO+3,600 ppm Cr

FIG.6.5 VARIATION OF Tan δ WITH FREQUENCY; PURE MgO

This ratio has been calculated from the experimental data at a number of points in the frequency range from 500 Hz to 9.3 GHz and some data for two samples is tabulated at particular frequencies in Table 6.2. According to Jonscher and Deori (67), this ratio is smaller than unity for n >0.5 and becomes larger than unity for n< 0.5.

In deriving ratio values the directly measured microwave estimate was used for ε_∞ .   For both specimens the ratio is about 0.07 and is constant up to 1 MHz ; inserting the value of n as n = 0.98 gives $\cot\left\{\frac{n\pi}{2}\right\}$ = 0.03.   Thus, there appears to be fair agreement with equation 6.4 (up to 1 MHz) and further,the ratio is smaller than unity as expected.

At high frequencies (500 MHz and 1 GHz) the ratio values are much larger than $\cot\left\{\frac{n\pi}{2}\right\}$; this may be due to the growing invalidity of taking the microwave value for ε_∞ at frequencies approaching a few GHz and it is probable that the limiting (optical) value for ε_∞ should be used instead.

All the evidence is consistent with the suggestion that the charge carriers involved in the conduction mechanism move by single hops, the carrier being either electrons or holes.   However, in this work no attempts have been made to determine the nature of charge carriers.   Regarding previous work on the nature of charge carriers (Chapter 1, Section 1.2, and Table 1.2) the distinction between ionic and electronic carriers is still not defined and there is conflicting evidence among those who work on this material.

The observed frequency dependence of conductivity can be best described by a thermally activated hopping model. The relative increase of the a.c. conductivity suggests that localized states, generated by impurities or structural defects, may contribute to the conduction mechanism ; carriers hop between localized states randomly distributed

$$\frac{\varepsilon''(\omega)}{\varepsilon'(\omega) - \varepsilon_\infty}$$

Frequency Nominal Composition	500 Hz	1 kHz	5 kHz	10 kHz	100 kHz	200 kHz	500 kHz	1 MHz		500 MHz	1 GHz
MgO (pure)	0.07	0.07	0.065	0.065	0.077	0.082	0.077	0.077		0.618	0.618
MgO + 12,800 ppm Fe	0.064	0.064	0.064	0.07	0.067	0.067	0.066	0.066		0.106	0.105

TABLE 6.2 : Illustration of Kramers-Kronig Relation

throughout the crystal.

According to the predictions of the pair model the conductivity in the low-frequency region is given by Eqn. 6.1 and hopping occurs exclusively between pairs of impurities. Pollak and Geballe [53] have shown that if hopping takes place between a random distribution of localized states then $\sigma(\omega) \propto \omega^n$ where $0.5 < n < 1$ the lower value of n occurs for multiple hops while the higher value occurs for single hops.

According to Pollak [129] single hops predominate at low temperature while at higher temperatures multiple hops occur frequently. This frequency dependence of conductivity becomes weaker at higher temperatures [129] and this will be discussed in the next Chapter. All the predictions of the theory for randomly distributed hopping states are satisfied for MgO and doped MgO at room temperature.

It has been suggested [2,15,20] that iron increases the conductivity of MgO. Ions of Fe^{3+} in the MgO lattice increase the electron and singly ionized Mg vacancy concentrations, and at the same time decrease the hole concentration. The level of vacancy concentration and hence the conductivity appears to be dominated by variable valence iron impurities [11].

It is concluded from the present discussion that the entire interpretation of the interesting and varied dielectric response of pure and doped MgO can be placed within the framework of the "Universal Law" of dielectric response.

6.3 REFERENCES

128.   Bussey, H.E, 'Measurement of RF Properties of Materials -

A Survey', Proceedings of the IEEE, Vol.55, No.6, pp 1046-53,

(1967).

129.   Pollak, M, 'Temperature Dependence of a.c. hopping conductivity',

Physical Review, Vol.138, pp A.1822, (1965).

CHAPTER 7

HIGH TEMPERATURE RESULTS IN THE LOW FREQUENCY RANGE

7.1   RESULTS

The determination of the real and imaginary components of complex

dielectric constant, ε' and ε'' and the conductivity $\sigma_{ac}(\omega)$ at high

temperatures from room temperature to 700° C was carried out, as previously

using the capacitance and conductance of each sample.

7.1.1 Conductivity-Temperature Characteristics

The variation of a.c. conductivity, $\sigma_{ac}(\omega)$ with temperature

were plotted $(Log_{10}\sigma \quad V \quad T^{-1})$ in Fig.7.1 at different frequencies for

heavily iron-doped magnesium oxide. Similar characteristic plots were

obtained for pure MgO and MgO doped with iron and chromium impurities.

It can be seen first that in the lower temperature region (< 550° C)

the conductivity is strongly frequency dependent, while at higher

temperatures (> 550° C) it has the same magnitude at all frequencies.

Secondly, there are three different regions which can be distinguished

by the bends in the characteristic outside of which the experimental

points follow straight lines.   The first region starts from room temp-

erature and extends to about 100°C.   The second begins about 100° C

and continues to 550° C and finally the third is from 550° C to 700° C.

At a constant frequency the slope of the experimental line is different

in each region indicating that the conduction mechanism is changing its

nature.   The activation energies for three regions (derived from the

slopes of the lines) were 0.08 eV, 0.29 eV and 1.90 eV, respectively.

At any particular temperature below 700° C the magnitude of the conduct-

ivity is almost directly proportional to the applied frequency ; this

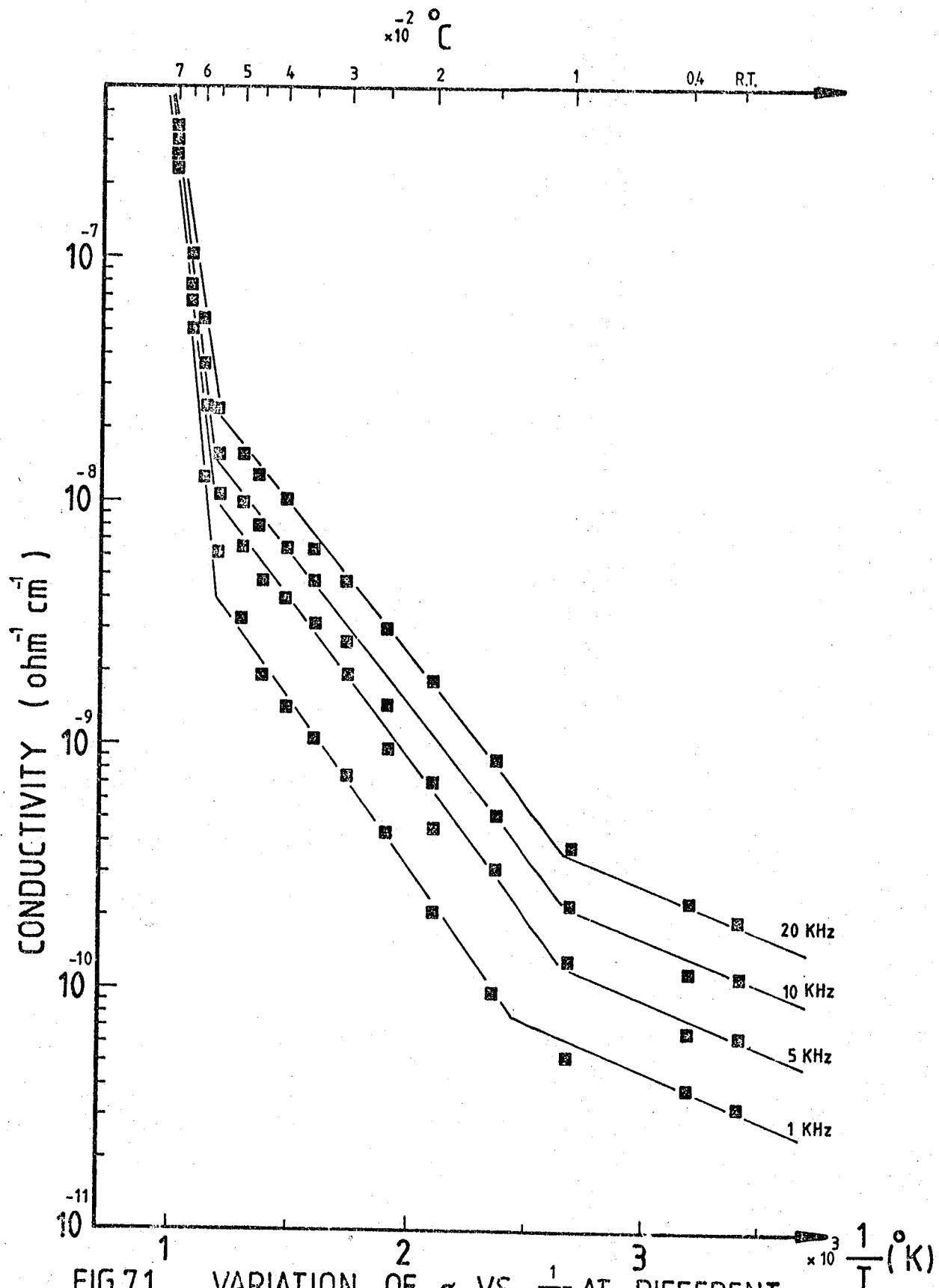proportionality vanishes above 700° C and $\sigma_{ac}(\omega)$ becomes frequency

FIG.7.1 VARIATION OF σ VS $\frac{1}{T}$ AT DIFFERENT
FREQUENCIES; MgO + 12,800 ppm Fe

independent.

In Fig. 7.2 the $Log_{10}\sigma$ versus T^{-1} plots are shown for pure MgO and MgO doped with iron or chromium with different concentrations at a constant frequency (1 kHz). The three regions mentioned above appear for all the samples at almost the same temperature and the individual characteristics are very similar. An important result of this is that, 'at any temperature the magnitude of $\sigma_{ac}(\omega)$ is directly proportional the concentration of the dopant impurities'. Also, the ratio of

$\dfrac{\sigma_{Fe/MgO}}{\sigma_{pure/MgO}}$ is the same in each region. Heavily Fe-doped magnesium

oxide has the highest value of conductivity and the data for medium doping levels lies between that of pure and heavily-doped MgO.

Comparison of those samples doped to the same level but with different dopant ions (e.g. MgO + 4,300 ppm Fe and MgO + 3,600 ppm Cr) showed that althogh the characteristics were similar the magnitude of conductivity for Cr-doped MgO is lower than for Fe-doped at temperatures below 550° C.

7.1.2 Conductivity-Frequency Characteristics

The variation of a.c. conductivity, $\sigma_{ac}(\omega)$, with frequency at different temperatures for pure MgO is illustrated in Fig.7.3. Below about 550°C all the data lies on a family of almost straight lines whose slopes gradually decrease with increasing temperature. The change in the slopes was from n = 0.85 to n = 0.84 in the first region (room-temperature - 150°C) and from n = 0.84 to n = 0.69 in the second range (150°C-550°C). At the highest temperature there appear to be departures from linearity which become progressively more pronounced as the temperature increases. Thus at 700°C for example $\sigma_{ac}(\omega)$ appears to be almost constant over the frequency range 500 Hz to 10 kHz after which $\sigma_{ac}(\omega) \propto \omega^{n}$ with an n value of 0.5.
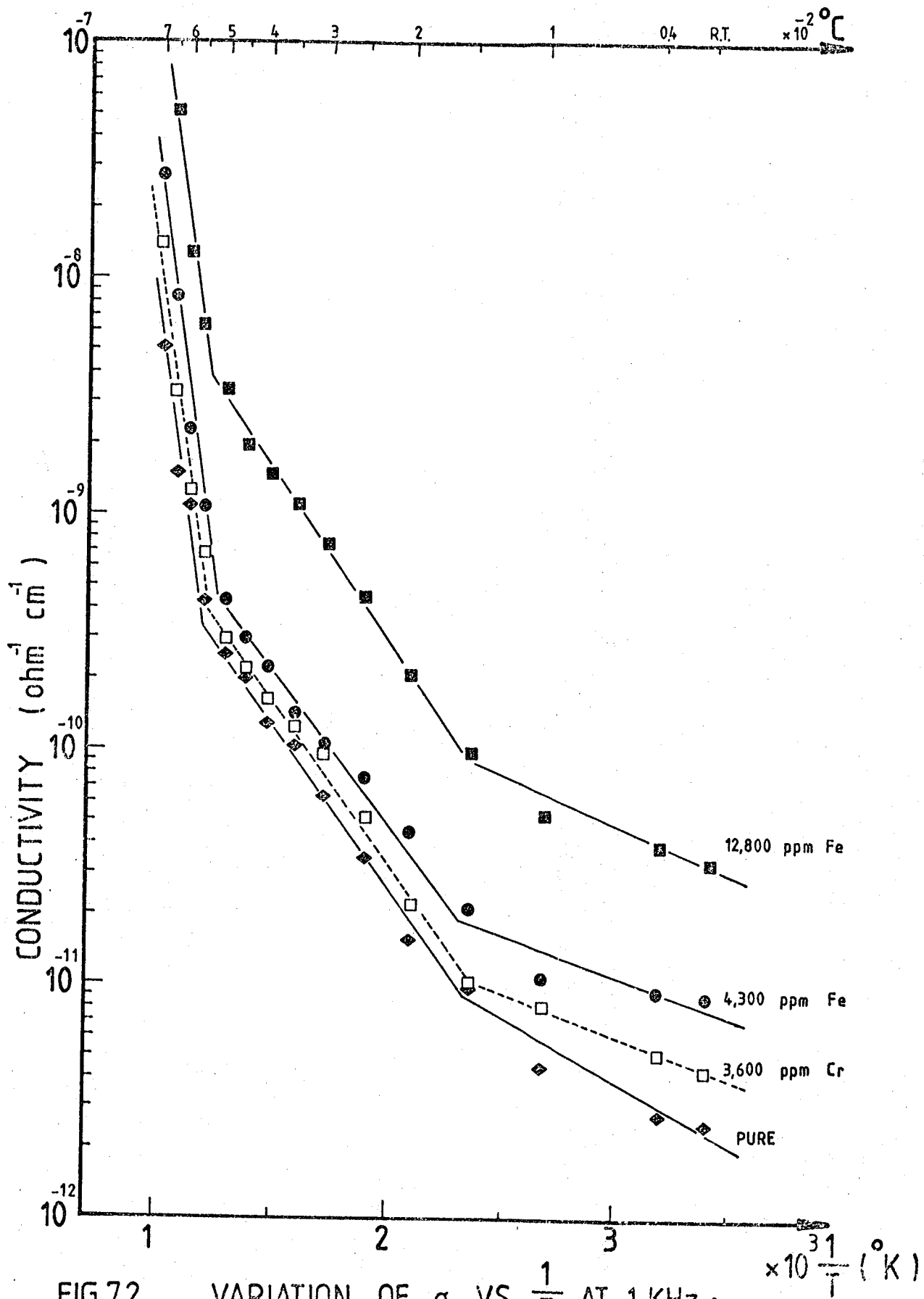
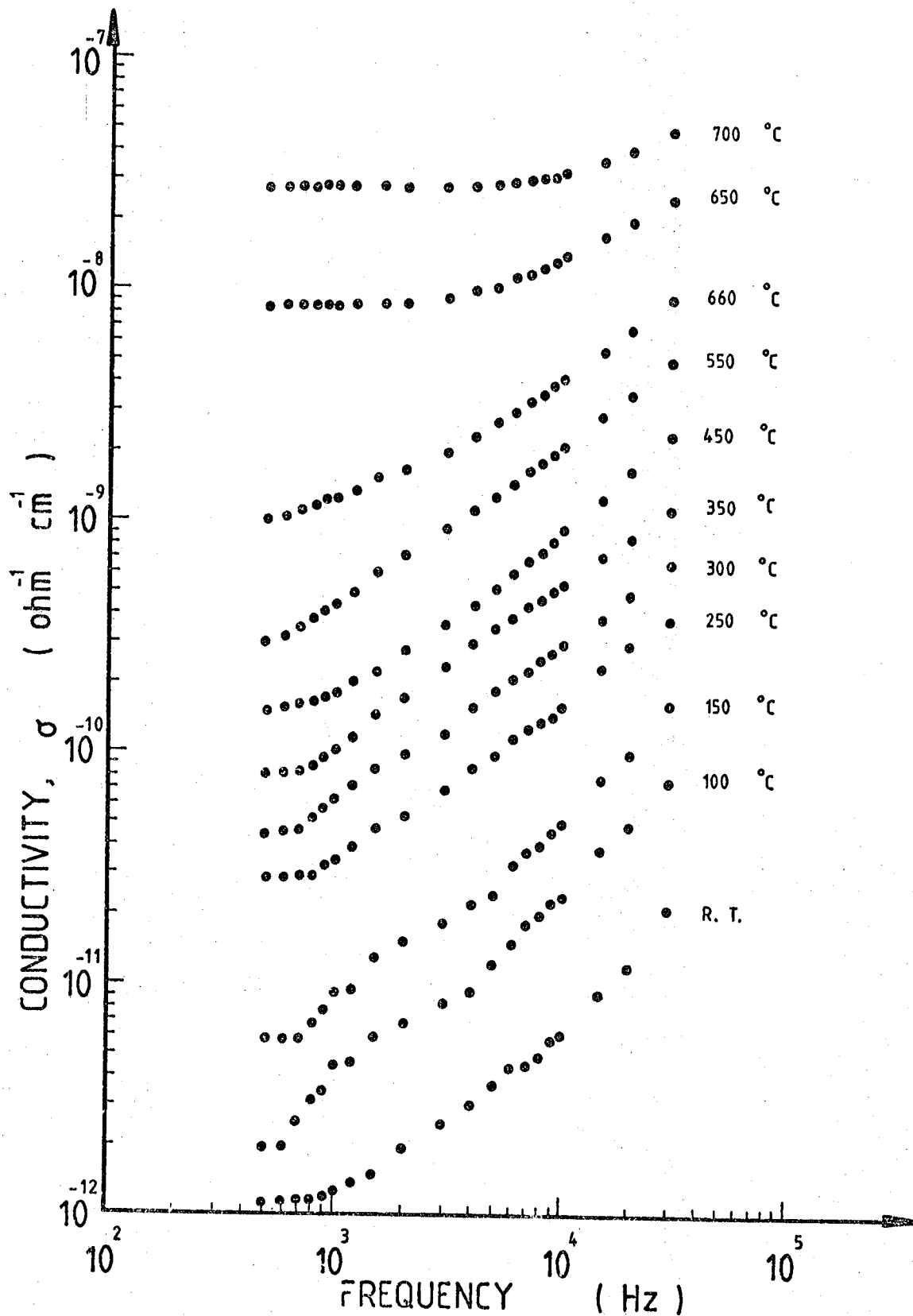FIG.7.2   VARIATION OF σ VS $\frac{1}{T}$ AT 1 KHz ;
PURE AND DOPED MgO

FIG.7.3   VARIATION OF σ VERSUS FREQUENCY
AT DIFFERENT TEMPERATURES ;
MgO   (PURE)

The variation of $\sigma_{ac}(\omega)$ versus frequency for MgO doped with 4,300 ppm Fe, 12,800 ppm Fe and 3,600 ppm Cr at different temperatures are given in Figs.7.4, 7.5 and 7.6, respectively. They showed similar characteristics to pure MgO (Fig.7.3) except that there is no evidence for flat regions in the higher temperature data. Comparing plots of Figs.7.3 and 7.5 shows that the magnitude of the conductivity was considerably increased in the heavily Fe-doped MgO crystal. This effect has already been pointed out at room temperature but is now also found to be true at high temperatures. At corresponding temperatures all the plots relating to the medium concentration (4,300 ppm Fe) lie between these extremes. Comparison of Figs.7.4 and 7.6 also shows in conclusion that the effect of Fe ions in increasing $\sigma_{ac}(\omega)$ is larger than of Cr and is still valid at high temperatures.

In order to clarify the effect of the different impurity levels on the conductivity of MgO, the ratio of $\dfrac{\sigma_{Fe/MgO}}{\sigma_{pure/MgO}}$ for different concentrations of Fe was calculated from Figs. 7.3-7.6 at different temperatures for various frequencies. These ratios are tabulated in Table 7.1 which also includes the ratios of $\dfrac{\sigma_{Cr/MgO}}{\sigma_{pure/MgO}}$ for the Cr-doped samples

7.1.3 Dielectric Constant (ε') Frequency Characteristics

The effect of temperature on the magnitude of ε' for pure MgO is shown in Fig.7.7. The individual plots were linear but their slopes increase as the temperature increases.

The corresponding data for MgO doped with 12,800 ppm Fe has been plotted in Fig.7.8. It showed similar characteristics to pure MgO and the data is in good agreement with the relation $\varepsilon'(\omega) \propto \omega^{(n-1)}$ with Cr/MgO (Fig.7.9) the same general pattern was found but here, at any frequency, the dielectric constant is lower than the corresponding value in Fe/MgO.
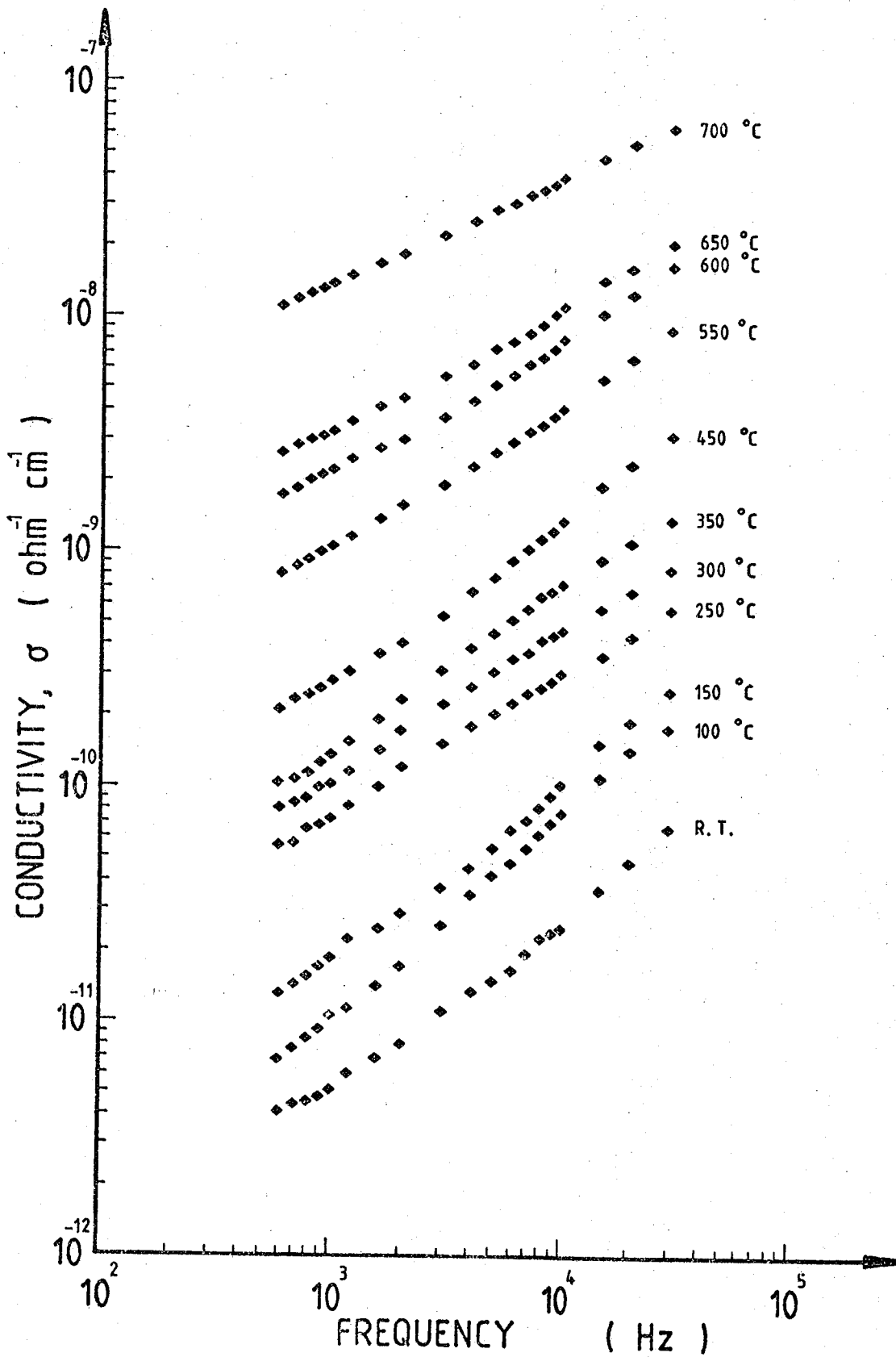
FIG. 7.4   VARIATION OF σ VERSUS FREQUENCY
        AT DIFFERENT TEMPERATURES ;
            MgO + 4.300   ppm   Fe

FIG.7.5 VARIATION OF σ VERSUS FREQUENCY
AT DIFFERENT TEMPERATURES ;
MgO + 12,800 ppm Fe

FIG.7.6   VARIATION OF σ VERSUS FREQUENCY
      AT DIFFERENT TEMPERATURES ;
            MgO + 3,600   ppm Cr

f (kHz) \ T (°C)	Iron $\sigma_{Fe(12,800)}/\sigma_{pure\ MgO}$			Iron $\sigma_{Fe(4,300)}/\sigma_{pure\ MgO}$			Chromium $\sigma_{Cr(3,600)}/\sigma_{pure\ MgO}$		
	R.T.	300	550	R.T.	300	550	R.T.	300	550
1	21.6	12.0	10.4	5.0	1.6	2.4	2.1	1.6	1.5
5	18.2	10.7	8.5	4.2	1.7	2.1	3.1	1.5	1.2
10	18.9	9.2	7.6	5.0	1.6	2.0	4.0	1.5	1.2

TABLE 7.1: Conductivity ratios of doped MgO to pure MgO at different frequencies.

FIG.7.7   VARIATION OF ε' VERSUS FREQUENCY AT DIFFERENT
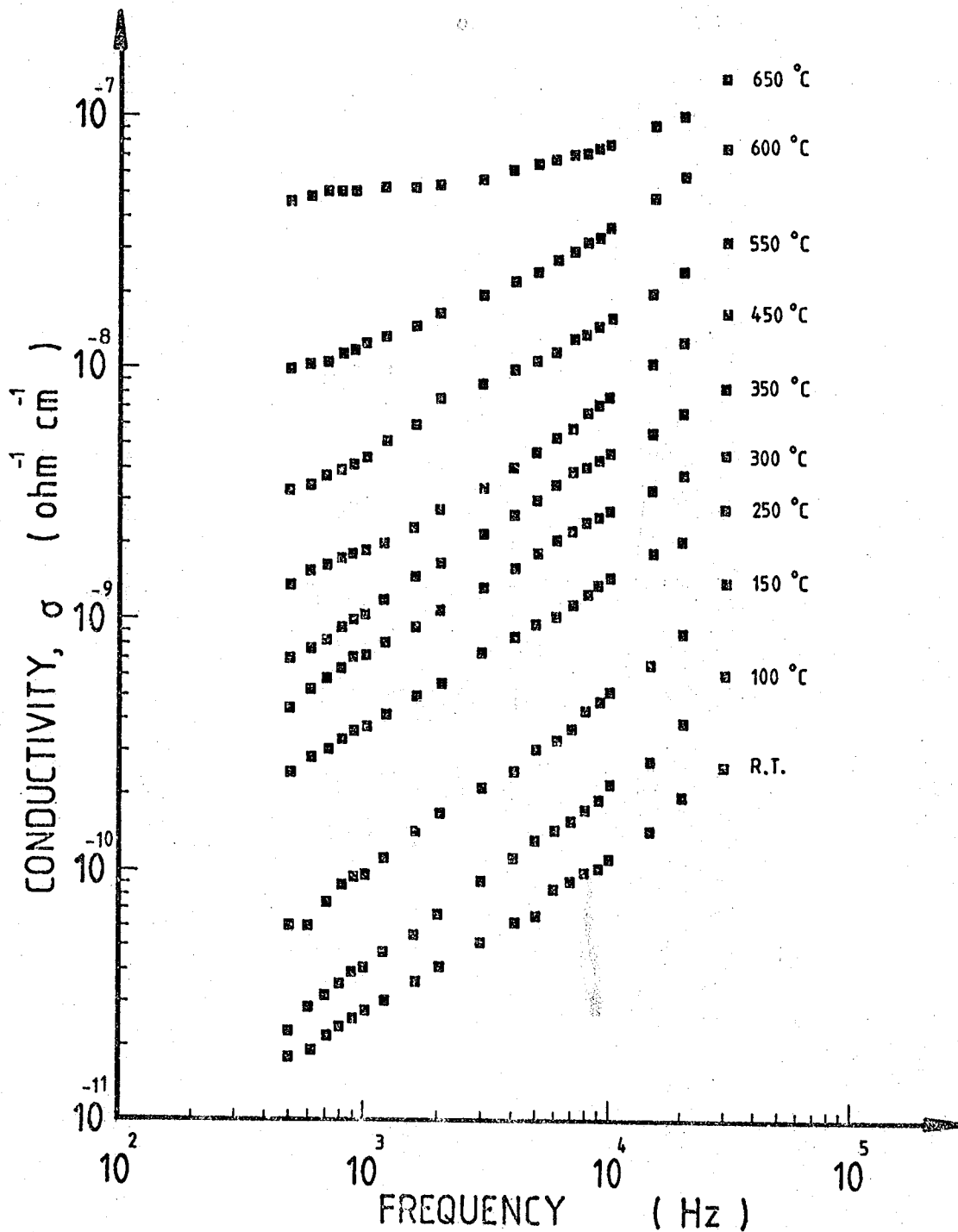TEMPERATURES ; MgO (PURE)

FIG.7.8   VARIATION OF ε' VERSUS FREQUENCY AT DIFFEREN

TEMPERATURES; MgO + 12,800 ppm Fe

FIG.7.9   VARIATION OF ε' VERSUS FREQUENCY AT DIFFERENT
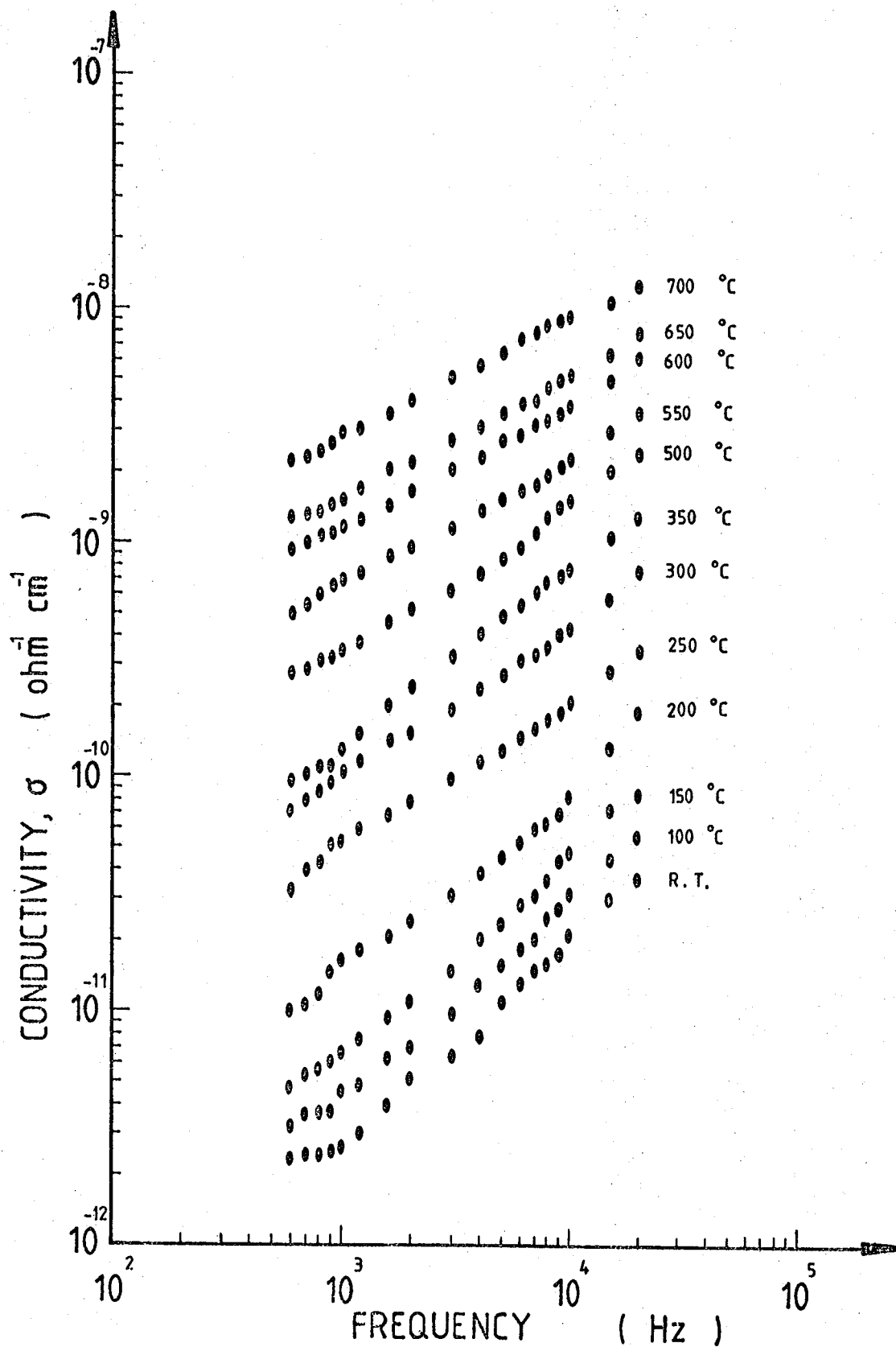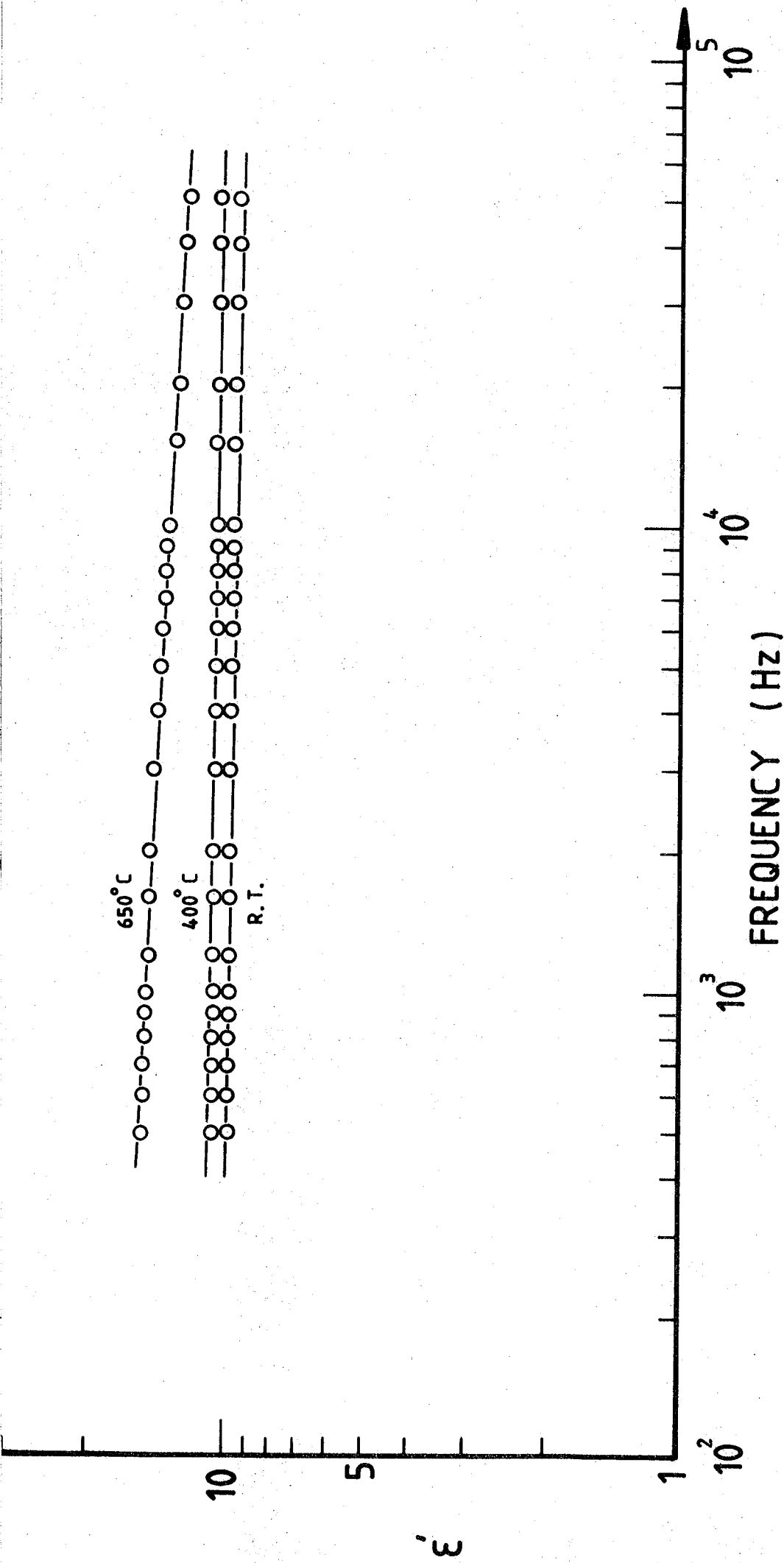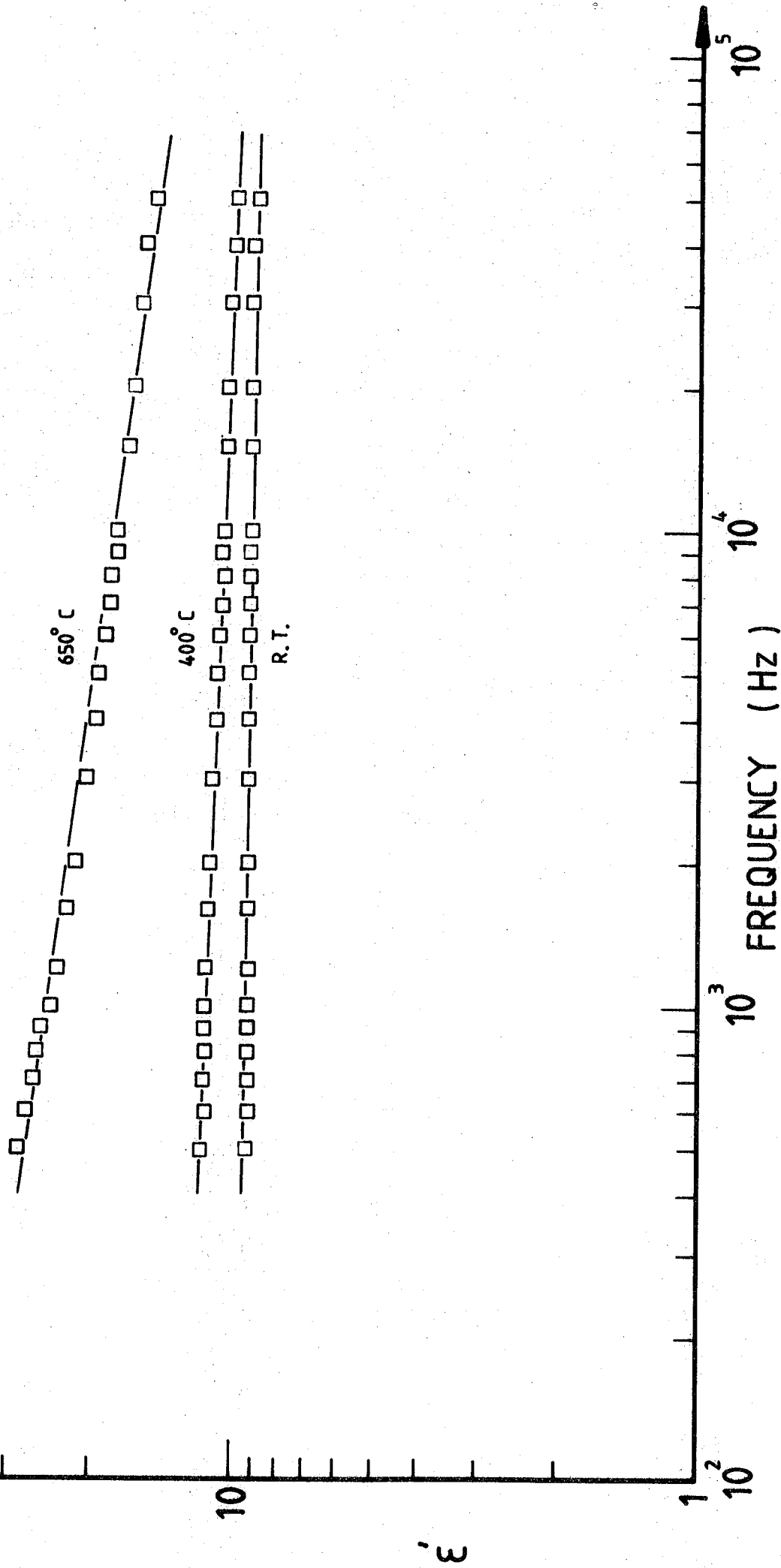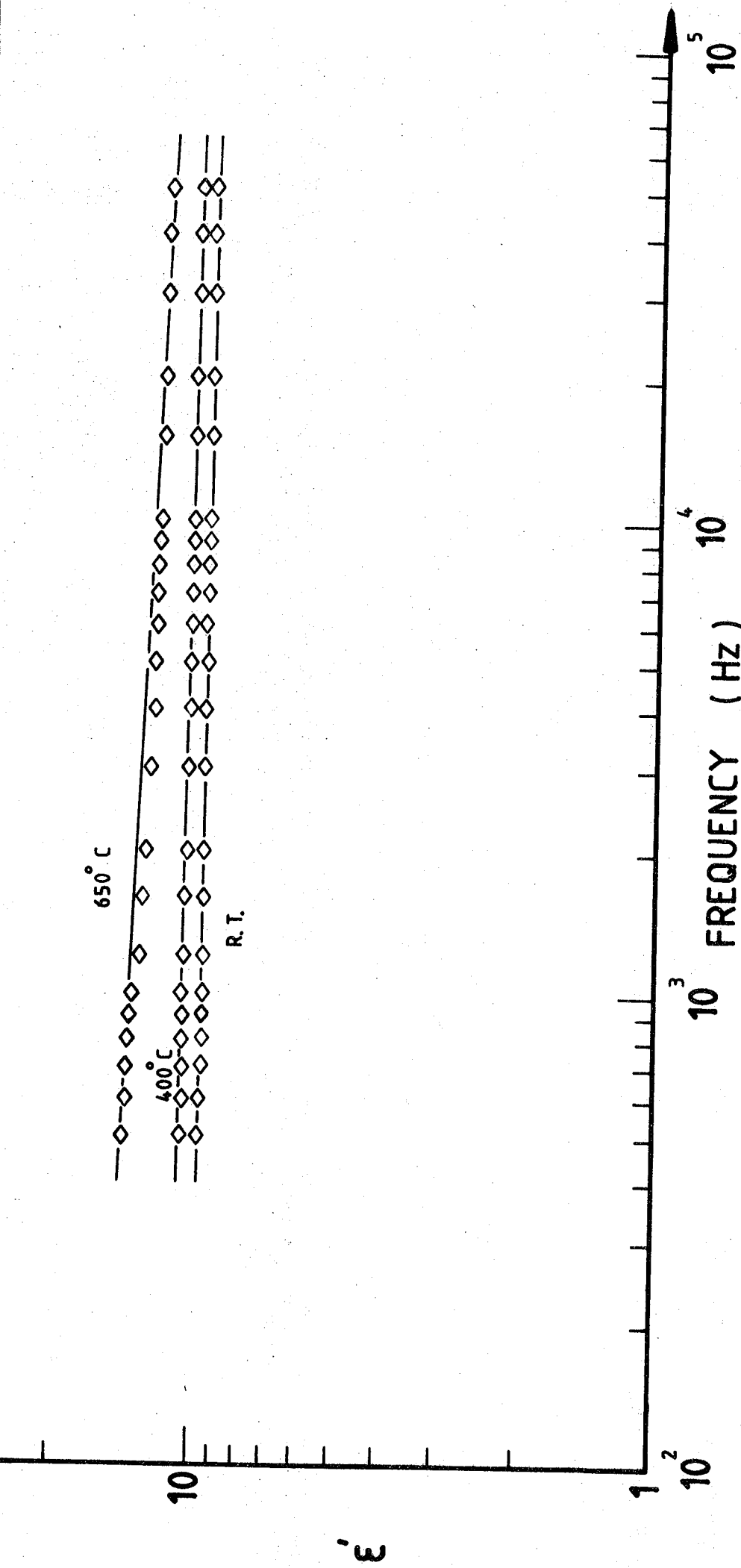TEMPERATURES; MgO + 3,600 ppm Cr

Fig.7.10 shows the behaviour of dielectric constant, ε' , as a function of temperature at 1 kHz frequency for pure MgO and iron-doped MgO samples. The plots of dielectric constant for pure MgO increase linearly up to about 250°C and then continue to increase very much more rapidly. The data for medium iron doped sample also showed the same characteristic. The magnitude of ε' for doped samples at some temperatures is less and at some higher temperature range is higher than the magnitude of ε' for pure MgO. The ratio of $\dfrac{\varepsilon'_{pure/MgO}}{\varepsilon'_{Fe(4300\ ppm)/MgO}}$ is getting near to 1 as the temperature increases to 700°C and finally it approaches unity at about 500°C while in the temperature range 500°C-700°C the magnitude of ε' related to MgO + 4,300 ppm Fe sample is greater than for pure MgO. This effect has been observed for heavily Fe-doped (12,800 ppm Fe) sample while the ratio of $\dfrac{\varepsilon'_{pure/MgO}}{\varepsilon'_{Fe(12,800\ ppm)/MgO}}$ reaches unity at about 250°C. It can be concluded that the dopant impurity has a great effect on the dielectric constant of MgO crystal especially at higher temperatures.

The variation of dielectric constant of pure MgO with temperature has been illustrated in Fig.7.11 over the frequency range of measurements. All the data lies on a family of straight lines.

7.2 DISCUSSION

The changes in magnitude of dielectric constant, $\Delta \varepsilon'$, with temperature (at any frequency) have been compared with Havinga's proposal, which was fully explained in Section 2.5. The values of the expression

$$\frac{1}{(\varepsilon'- 1)\ (\varepsilon' + 2)} \left\{ \frac{\partial \varepsilon'}{\partial T} \right\}_p = A + B + C \qquad (7.1)$$

were deduced at different frequencies for pure MgO from Fig.7.11 and then tabulated in Table 7.2. For comparison some workers reported temperature dependences for pure MgO and are given in Table 7.3. In the temperature
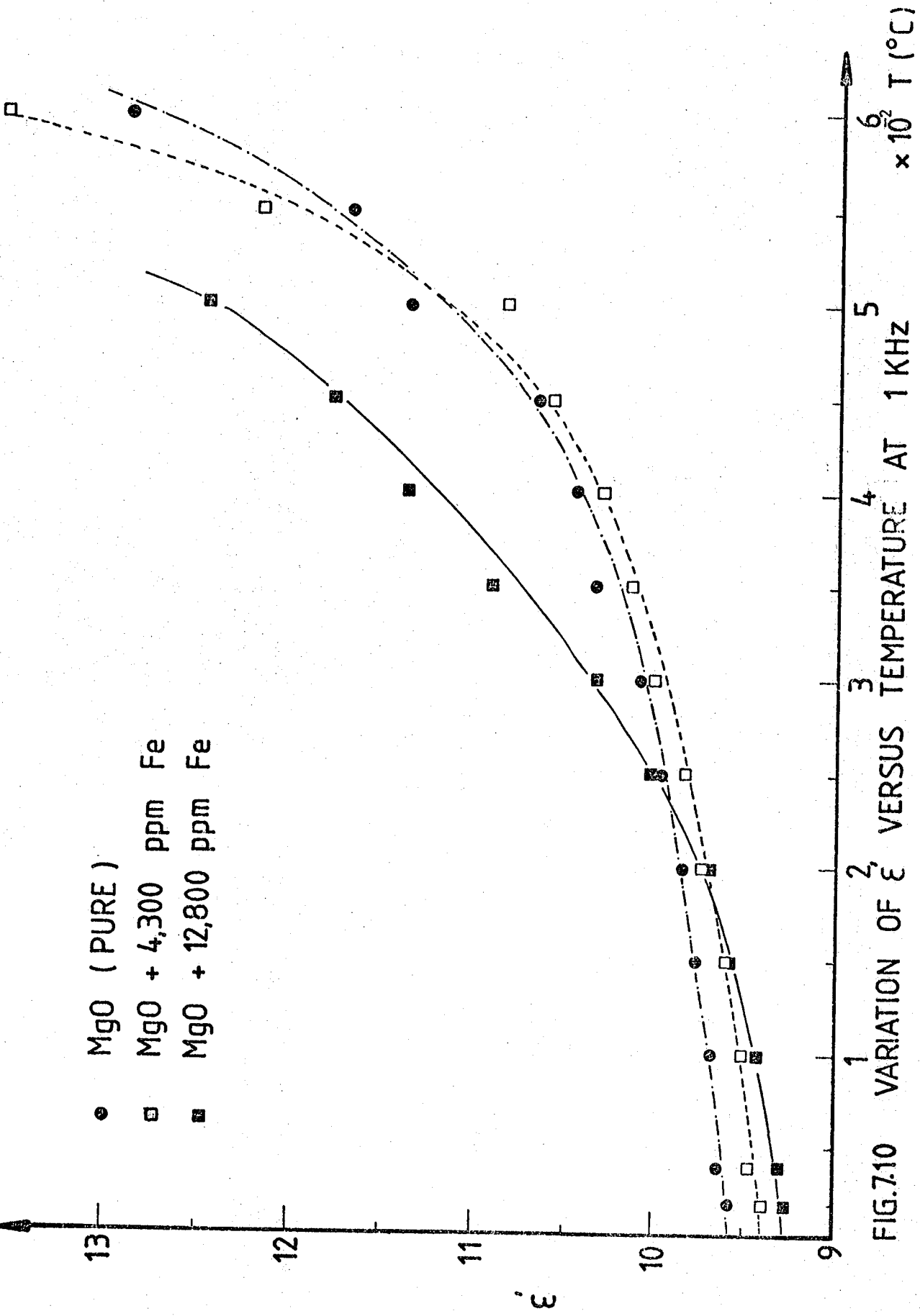
FIG.7.10 VARIATION OF ε' VERSUS TEMPERATURE AT 1 KHz

Legend:
- MgO (PURE)
- MgO + 4,300 ppm Fe
- MgO + 12,800 ppm Fe

$\times 10^2$ T (°C)
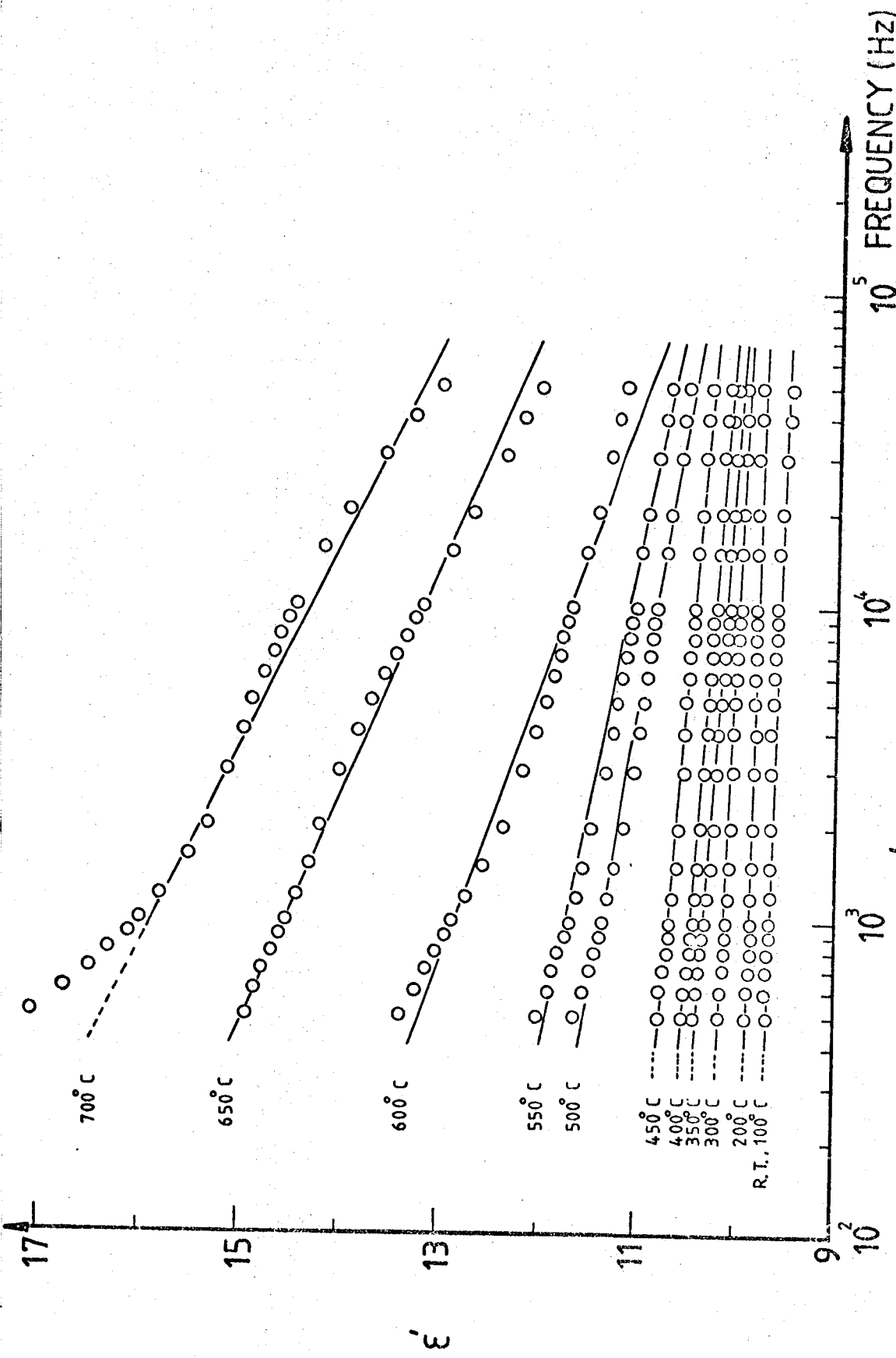
FIG.7.11   VARIATION OF ε' VERSUS FREQUENCY AT DIFFERENT
TEMPERATURES ; MgO (PURE)

Nominal Composition	Frequency (kHz)	Temperature range (°C)	ε' at R.T.	$\dfrac{10^5}{(\epsilon'+2)(\epsilon'-1)} \left\{ \dfrac{\partial \epsilon'}{\partial T} \right\}$
MgO (pure)	1	R.T. – 200	9.64	1.02 ± 0.24
MgO (pure)	1	R.T. – 300	9.64	1.59 ± 0.28
MgO (pure)	1	R.T. – 400	9.64	2.04 ± 0.19
MgO (pure)	5	R.T. – 200	9.62	1.03 ± 0.23
MgO (pure)	5	R.T. – 300	9.62	1.45 ± 0.29
MgO (pure)	5	R.T. – 400	9.62	2.45 ± 0.3
MgO (pure)	10	R.T. – 200	9.6	1.03 ± 0.27
MgO (pure)	10	R.T. – 300	9.6	1.42 ± 0.21
MgO (pure)	10	R.T. – 400	9.6	1.66 ± 0.25
MgO (pure)	20	R.T. – 200	9.54	1.22 ± 0.27
MgO (pure)	20	R.T. – 300	9.54	1.54 ± 0.31
MgO (pure)	20	R.T. – 400	9.54	1.75 ± 0.19

TABLE 7.2: Temperature dependence of ε' ; MgO (pure)

Nominal Composition	Frequency (kHz)	Temperature range ($^{\circ}$C)	ε' at R.T.	$\dfrac{10^5}{(\varepsilon'+2)(\varepsilon'-1)}\left\{\dfrac{\partial \varepsilon'}{\partial T}\right\}$	Refs.
MgO (pure)	250	R.T. - 150	9.8	1.05	(43)
MgO (pure)	Low frequency	-223 - R.T.	9.958	0.915	(42)
MgO (pure)	Low frequency	> R.T.	9.8	1.76	(130)

TABLE 7.3 : Reported Data for Temperature Dependence of ε' ; MgO (pure)

range $16°C - 200°C$ the present values agree at all frequencies with the value obtained by others (43) and are rather higher than that which has been given in (42). Examination at higher temperatures showed that the value of (A + B + C) increased and consequently did not agree with the previously reported data. Comparison of values (A + B + C) obtained in the room temperature to $300°C$ range (Table 7.2) here with the data given in literature reference (130) shows that the values are about 20% lower, while at higher temperatures (room temperature- $400°C$) the high frequency data (10 kHz and 20 kHz) agrees fairly well.

The temperature dependence of ε' for Fe or Cr-doped MgO at different frequencies is given in Table 7.4. The values of (A + B + C) were deduced from experimental data and it was found that they are dependent on the concentration of dopant impurities ; this effect is most marked in Fe-doped samples. All samples behave similarly and the values of (A + B + C) are positive hence supporting the Bosman and Havinga (43) proposal ; there is a slight reduction in (A + B + C) as the frequency increases. The values of (A + B + C) for Cr-doped samples seem to be independent of the Cr concentration and they agree with the literature (42-43) for pure MgO as shown in Table 7.3.

The Havinga formula for (A + B + C) is not specifically based on the assumption of hopping conduction and it is therefore of interest to see how the same experimental data fits the predictions of the Jonscher theory. In this comparison the first difficulty arises because there appears to be no specific formula quoted in the literature for the temperature dependence of n. The general prediction is that n should fall as the temperature increases but, at present, the theory is not available to estimate the magnitudes of change to be expected.

Here these magnitudes have been obtained from experimental observations in two ways viz : from $\varepsilon'-\omega$ measurements and from $\sigma_{ac}-\omega$

Nominal Composition	Frequency (kHz)	Temperature range (°C)	ε' at R.T.	$\dfrac{10^5}{(\varepsilon'+2)(\varepsilon'-1)}\left\{\dfrac{\partial\varepsilon'}{\partial T}\right\}$
MgO + 4,300 ppm Fe	1	R.T. – 200	9.46	1.54 ± 0.18
	5		9.42	1.49 ± 0.20
	10		9.42	1.46 ± 0.26
MgO + 12,800 ppm Fe	1	R.T. – 200	9.27	2.85 ± 0.19
	5		9.25	2.25 ± 0.27
	10		9.24	2.18 ± 0.23
MgO + 3,600 ppm Cr	1	R.T. – 200	9.555	1.22 ± 0.19
	5		9.55	1.11 ± 0.26
	10		9.55	0.98 ± 0.27

TABLE 7.4: Temperature Dependence of ε' ; Doped MgO

characteristics both kinds of data being obtained at temperatures from $16^{\circ}C$ to about $700^{\circ}C$.

It has been found from Figs. 7.7 - 7.9 that the slope of the variation of ε' with frequency increases slightly with increasing temperature, i.e. n is getting lower in the relation $\varepsilon'(\omega) \propto \omega^{n-1}$. In order to see the effect of temperature on the magnitude of the exponent n more easily these values for different samples have been tabulated in Table 7.5 at various frequencies. From this Table, it is concluded that : firstly, at any constant temperature, the magnitude of exponent (n) is almost the same for all the samples ; secondly, n decreases as the temperature increases ; thirdly that the decrease in n for a given temperature rise is somewhat greater for higher doping concentrations. Overall, this data thus suggests that n is weakly temperature dependent, its magnitude decreasing only by about 5% for a $600^{\circ}C$ rise in temperature.

A conflicting estimate is obtained from the conductivity data. The values of n have been also deduced from Figs. 7.3 - 7.6 for pure and doped MgO samples at the various temperatures and these are tabulated in Table 7.6. Excluding the high concentration Fe/MgO specimen, it is again found that the n value at any constant temperature is nearly the same. As the temperature increases the magnitude of n decreases for each sample but this table indicates that n is strongly temperature dependent ; chaning by about 30% for a $600^{\circ}C$ temperature rise and showing some tendency for even more rapid variation above $600^{\circ}C$. The reasons for this discrepancy are not clear ; in so far as the Jonscher theory is applicable one would expect both methods of derivation to yield the same result (the precision room temperature bridge data given in Chapter 4 do agree with this condition). The most likely explanation seems to be that, as Fig.7.1 indicates, the three conduction regimes imply the onset, at

n values

Nominal Composition \ Temperatures °C	Room	400	550	650
MgO (pure)	0.982	0.977	0.968	0.952
MgO + 4,300 ppm Fe	0.98	0.972	0.959	0.91
MgO + 12,800 ppm Fe	0.979	0.968	0.927	0.885
MgO + 3,600 ppm Cr	0.98	0.975	0.97	0.95

TABLE 7.5 : Variation of n with temperature derived from (ϵ' vs f) plots

n values

Nominal Composition \ Temperatures °C	Room	100	200	300	400	500	600	700
MgO (pure)	0.85	0.85	0.84	0.67	0.76	0.75	0.69	0.5
MgO + 4,300 ppm Fe	0.84	0.84	0.81	0.73	0.73	0.59	0.54	0.46
MgO + 12,800 ppm Fe	0.78	0.78	0.74	0.67	0.66	0.59	0.55	0.48
MgO + 3,600 ppm Cr	0.87	0.87	0.78	0.72	0.71	0.66	0.53	0.50

TABLE 7.6 : Variation of (n) with temperature derived from (σ vs f) plots.

successively higher temperatures, of different types of contribution
to conduction ; such additional contributions might invalidate the
direct applicable of the "Universal Law" equations to high temperature
conductivity-frequency plots. If this is so the ε'-f variations may be
more reliable.

7.3   <u>REFERENCES</u>

130.   Krishnan, R.S, Progress in Crystal Physics (Central Art Press,

Chetput Madras ; India), Vol.1, pp 193 (1958).

CHAPTER 8

SUMMARY AND FUTURE WORK

The relevant conclusions on each part of the project have been made at the end of the appropriate Chapters.

Consideration of the work as a whole leads to several summary conclusions which are given in this chapter. The main points concern the suitability of techniques for dielectric measurements on low loss materials. detailed interpretation of some of the effects of doping, and suggestions for future work.

As regards techniques, the main area where uncertainties remain is in the accuracy of measurement in the slotted line method. This method has so many potential advantages - not least in the wide frequency coverage, that its use would be very desirable. Adequate accuracy could probably be obtained using the existing coaxial arrangement if the VSWR maximum were recorded by the present manner but the minimum (where magnitudes are more sensitive to small changes in ε' and ε'') were measured with an electrometer sensitive to at least 10^{-12} A ; this would give a possible improvement but would need very careful experimentation. A more fruitful approach seems to be to undertake a rigorous analysis of the equivalent circuit, attempting to add known amounts of capacitance so as to reduce the effective VSWR to be measured to smaller values ; this reduction is amenable to theoretical and experimental testing and offers the best long term solution. An independent requirement arising from the extension of the range of measurements to r.f. and microwave frequencies is the need for accurate values of ε_∞ ; here optical methods could be used and although reference tables give some data for nominally pure materials there is little information on the effects of impurities.

Turning next to the experimental data the most reliable, and possibly most important of this relates to the room temperature measurements and the effects of doping. It was shown that the addition of either Fe or Cr increased the conductivity above that of pure MgO ; to explain this result it was postulated that, as both ions are trivalent, their introduction into the lattice would give rise to extra vacancies which in turn would increase the number of hopping sites and hence lead to the observed increase in conductivity (without requiring change in the type of charge carrier, taken to be electrons). On this basis only, one would expect an increase in conductivity (for trivalent ions) to be independent of the nature of the particular ion and further, that doping with divalent ions should produce no change. Both of these predictions are open to experimental testing, for example with Ni/MgO and Co/MgO both of which can be obtained in single crystal form. There is of course no specific restriction on the lattice and calcium oxide ; CaO, might form a useful alternative host which can be doped with a variety of ions. Work along these lines is desirable in order to widen the basis for discussion of the following point of interest.

Comparison of the data for Fe/MgO and Cr/MgO, doped at similar levels, shows that the conductivity is increased substantially more in the case of Fe than Cr. This is not expected on the model outlined above which must therefore be regarded as incomplete. It is interesting to note that in hopping theory two factors are important, the number of hopping sites (considered in the above model) and the hopping frequency. An increase in the latter would also lead to an extra contribution to the conductivity and several authors have tended to equate the hopping frequency to the frequency of exchange interaction between the impurity centres involved (36). Following these ideas one is lead to examine the

possibility of exchange interaction between the Fe^{3+} and Cr^{3+} respectively

in the Fe/MgO and Cr/MgO crystals since the exchange energy, expressed

as frequency, might therefore be taken as equivalent to the hopping

frequency. Here data from completely different types of experiment,

i.e. magnetic measurements, is required and some results obtained from

electron spin resonance studies may be quoted. In summary, these have

shown that in both Fe/MgO and Cr/MgO (131) exchange narrowing of the

Fe^{3+} and Cr^{3+} esr lines is pronounced (at the level of concentration used

in the dielectric measurements), and that the exchange energy J is, in

both cases, proportional to the concentration. The relevant results

are shown in Fig.8.1 which also gives the quantitative values of J. It

is noticeable that, at equivalent concentrations, $J_{Fe} > J_{Cr}$ and that

there seems to be some correlation with the conductivity data in two

respects

(a) for a particular ion both J and σ increase with concentration.

(b) at a given concentration $J_{Fe} > J_{Cr}$ in accordance with the

observation that $\sigma_{Fe} > \sigma_{Cr}$.

These preliminary observations suggest that a contribution to

conductivity arising from exchange may be a feature of some doped

materials and the trends seem to be sufficiently established to warrant

much closer examination.

131.   Thorp, J.S. and Hossain, M.D,'Exchange Energies of Iron Group

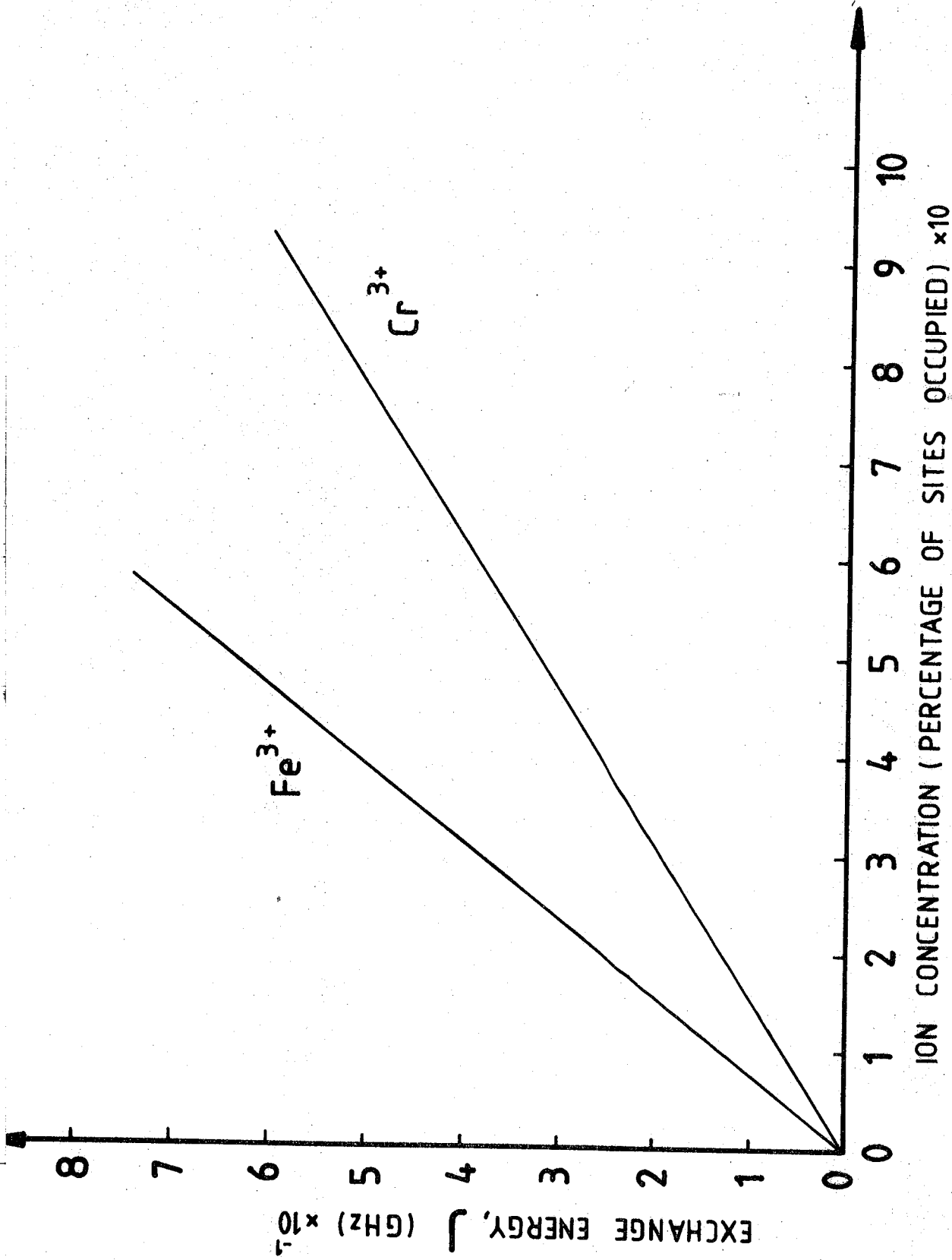Ions in Single Crystal MgO', Journal of Materials Science,

(to be published).

FIG.8.1   VARIATION OF J WITH CONCENTRATION IN Fe/MgO AND Cr/MgO.

APPENDICES

APPENDIX A   DERIVATIONS OF ε' AND ε''

In the derivation, the specimen is assumed to be an impedance, which terminates the end of a coaxial line as shown in Fig.3.5. This assumption is not absolutely correct because of small fringing effects which are, however, ignored. In this case the impedance can be written as :

$$Z = - \frac{j}{\omega C} \tag{AP.1}$$

where C, is complex, because the dielectric constant of the sample is complex. It is assumed that there is no series resistance with this capacitance.

Now, $C = \varepsilon_o \varepsilon^* \frac{A}{d}$ and $\varepsilon^* = \varepsilon' - j \varepsilon''$ which finally gives,

$$Z = R - jX = - \frac{jd}{\omega \varepsilon_o \varepsilon^* A} \tag{AP.2}$$

or

$$= - \frac{jd}{\omega \varepsilon_o A(\varepsilon' - j \varepsilon'')} \tag{AP.3}$$

and

$$R - jX = \frac{\varepsilon'' d}{\omega \varepsilon_o A(\varepsilon'^2 + \varepsilon''^2)} - j \frac{\varepsilon' d}{\omega \varepsilon_o A(\varepsilon'^2 + \varepsilon''^2)} \tag{AP.4}$$

where

ε_o = permittivity of free space = 8.854×10^{-12} (F m^{-1})

ε' = real component of the complex permittivity (dielectric constant)

ε'' = imaginary component of the complex permittivity (loss factor)

A = area of inner conductor which contacts the sample (m^2)

d = thickness of the sample (m)

ω = angular frequency (rad s^{-1})

Equating real and imaginary parts of Eqn. (AP.4) leads to

$$R(\varepsilon', \varepsilon'') = \frac{\varepsilon'' d}{\omega \varepsilon_o A(\varepsilon'^2 + \varepsilon''^2)} \qquad (AP.5)$$

$$X(\varepsilon', \varepsilon'') = \frac{\varepsilon' d}{\omega \varepsilon_o A(\varepsilon'^2 + \varepsilon''^2)} \qquad (AP.6)$$

from which ε' and ε'' can be determined, i.e.

$$\varepsilon' = \frac{Xd}{\omega \varepsilon_o A(R^2 + X^2)} \qquad (AP.7)$$

$$\varepsilon'' = \frac{Rd}{\omega \varepsilon_o A(R^2 + X^2)} \qquad (AP.8)$$

From transmission line theory, the reflection coefficient of the line which is terminated with an arbitrary impedance Z_L, at the plane of the Z_L, is given by

$$|\rho| e^{j\theta} = \frac{Z_L - Z_o}{Z_L + Z_o} \qquad (AP.9)$$

where Z_o = characteristic impedance of the line (ohms)

$|\rho|$ = magnitude of the reflection coefficient

θ = phase angle of the reflection coefficient

The Eqn. (AP.9) may also be written in an expanded form as,

$$|\rho| (\cos\Theta + j\sin\Theta) = \frac{R - Z_o + jX}{R + Z_o + jX} \qquad (AP10)$$

from which

$$|\rho| \cos\Theta = \frac{R^2 - Z_o^2 + X^2}{(R + Z_o)^2 + X^2} \qquad (AP.11)$$

$$|\rho| \sin\Theta = \frac{2 Z_o X}{(R + Z_o)^2 + X^2} \qquad (AP.12)$$

After some manipulation the resistance, R and reactance, X can be found,
i.e.

$$R = \frac{Z_o (1 - |\rho|^2)}{1 + |\rho|^2 - 2|\rho| \cos\Theta} \qquad (AP.13)$$

$$X = \frac{2|\rho| Z_o \sin\Theta}{1 + |\rho|^2 - 2|\rho| \cos\Theta} \qquad (AP.14)$$

Substituting Eqns. (AP.13) and (AP.14) in Eqns. (AP.7) and (AP.8) gives
finally the magnitudes of ε' and ε'', i.e.

$$\varepsilon' = \frac{2 |\rho| \sin\Theta}{\omega C_o Z_o (|\rho|^2 + 2 |\rho|\cos\Theta + 1)} \qquad (AP.15)$$

and

$$\varepsilon'' = \frac{1 - |\rho|^2}{\omega C_o Z_o (|\rho|^2 + 2 |\rho|\cos\Theta + 1)} \qquad (AP.16)$$

APPENDIX B CALIBRATION OF CRYSTAL DETECTOR

In order to measure the characteristic of the crystal detector

two different methods were used :

1. In the first method the slotted-line was terminated by a short

circuit. The signal oscillator was set to an arbitrary frequency, e.g.

710 MHz. The carriage (probe) was moved to any maximum position as

indicated on the VSWR meter., then the tuning stub was adjusted to give

maximum output from the crystal detector.

Next, the distance between two minima was determined and hence

the $\frac{\lambda}{2}$ (95). The exact positions of the minima were found by using two

identical points on either side of nodes and halving the distance. A

calibration plot was then obtained by recording the micro-ammeter readings,

at suitable intervals between the nodes. For each point the electric

field strength, E, was calculated (127) using,

$$E \quad = \quad \sin\theta \qquad\qquad\qquad (AP.17)$$

where

$$\theta \quad = \quad \frac{2\pi d}{\lambda}$$

and

d = distance of each point from reference plane (cm)

λ = wavelength of applied frequency (cm)

Variations of E versus rectified current, I, were then plotted

in Fig. APP.1. As it shows at lower electric field the current increases

exponentially, and then becomes linear at higher electric fields. In

order to determine the exponent of $I \propto E^n$, $\text{Log}_{10}E$ versus $\text{Log}_{10}I$, was

plotted in Fig.APP.2. The slope measured represented the crystal law

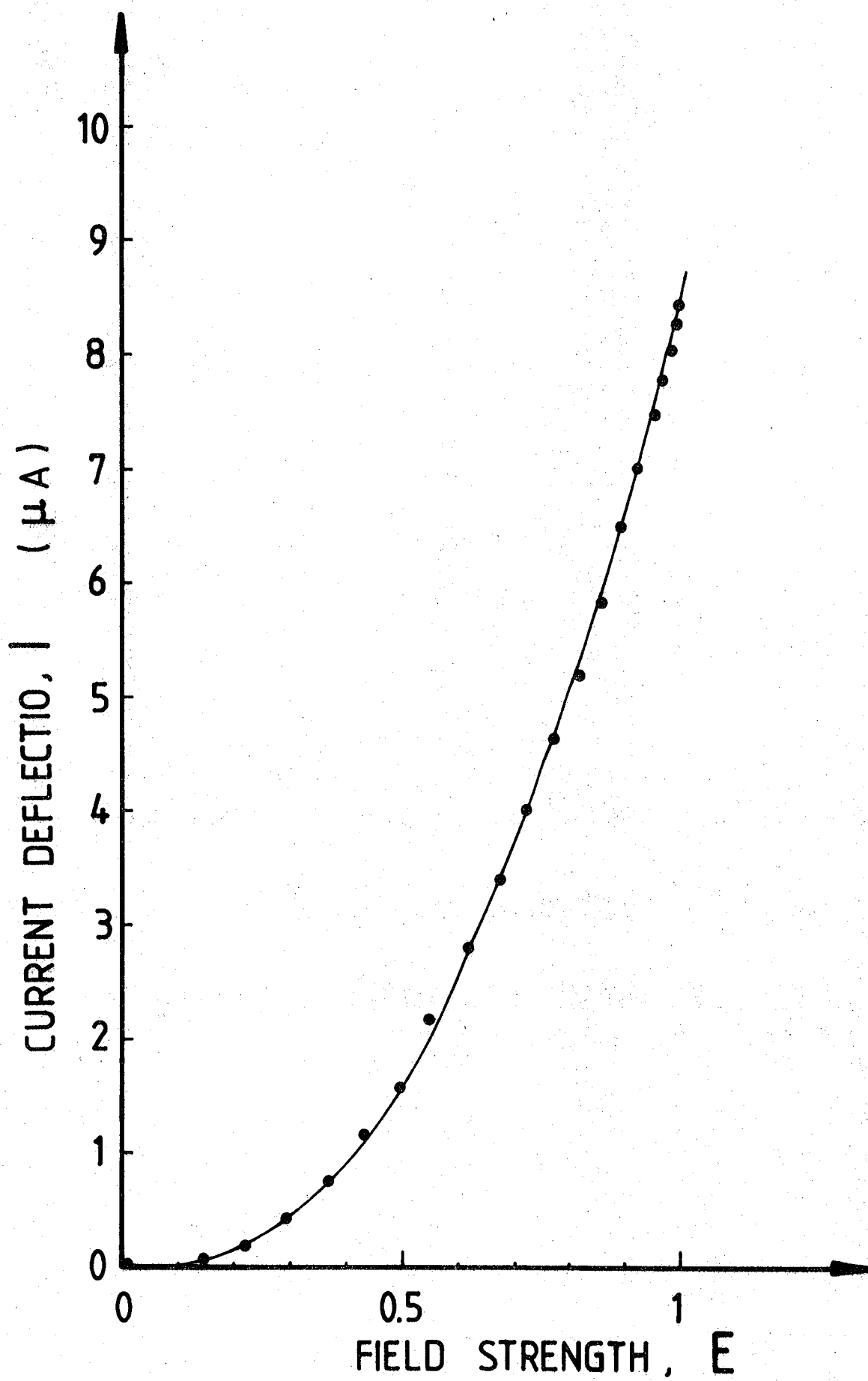and it was found that n = 2.3, i.e. an approximately square-law

FIG. APP. 1   CALIBRATION GRAPH OF CRYSTAL
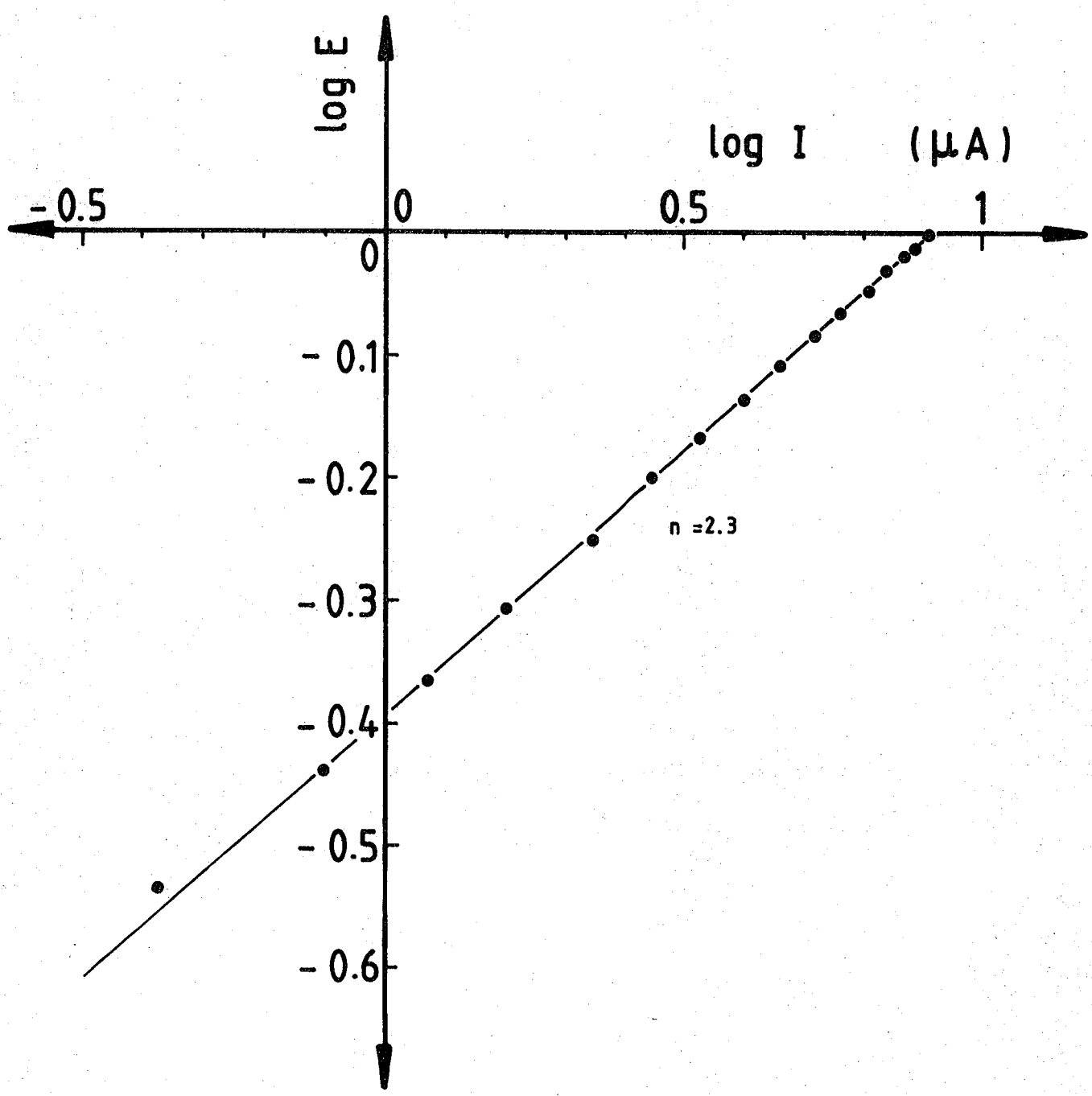DETECTOR AT 710 MHz; METHOD I

FIG. APP. 2   DETERMINATION OF CRYSTAL LAW
            AT 710 MHz; METHOD I

characteristic.

2.   In the second method the carriage and probe were placed in one

position on the slotted-line which gave suitable reading and the input

level was varied. The changes in the input level were plotted against

the measured current as shown in Fig.APP.3.   It was found that the

plot was similar to the one in Fig.APP.1 with a slightly different slope

as shown in Fig.APP.4, i.e. n = 1.94. This has proved the square-law

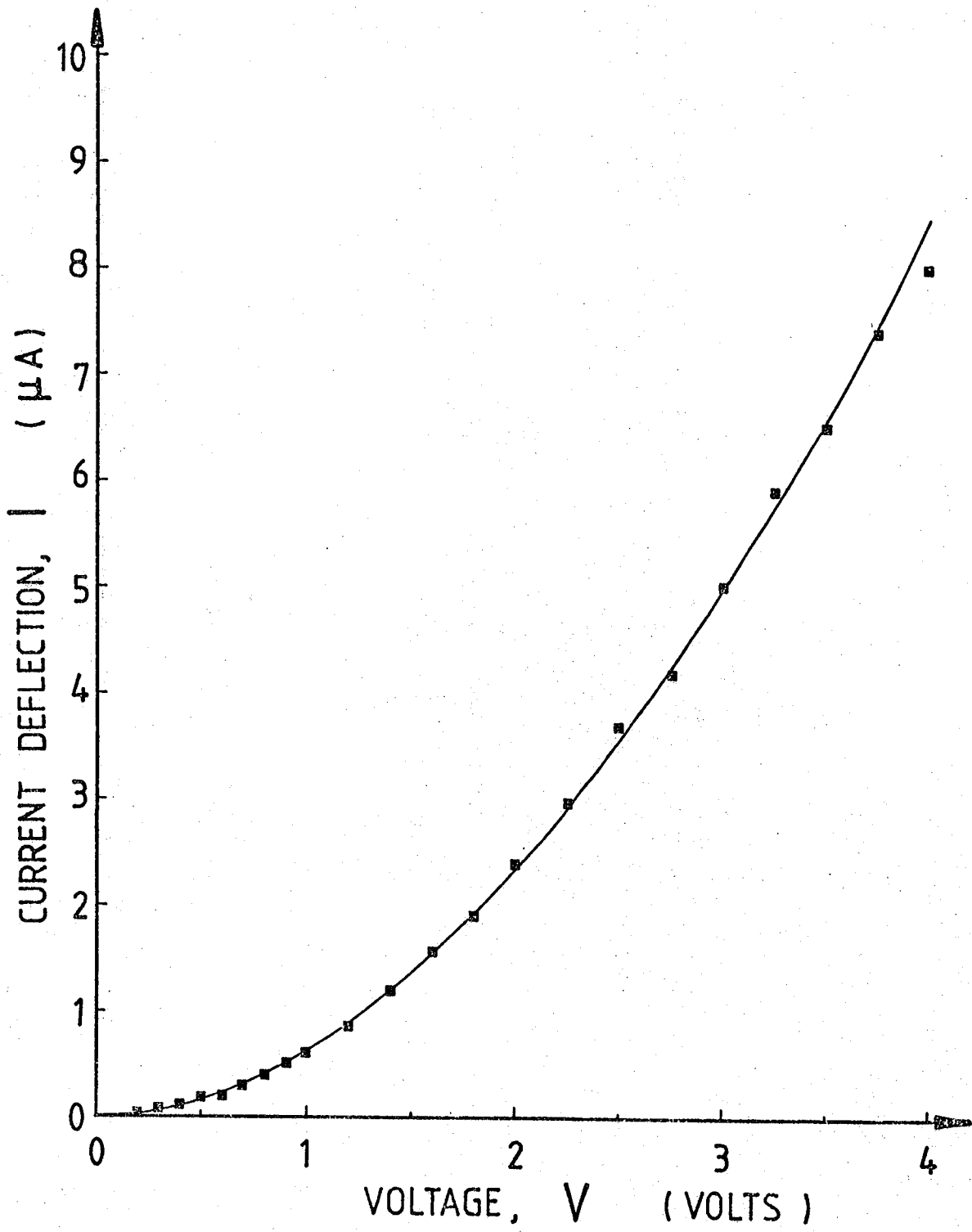behaviour of the crystal.

FIG. APP.3 CALIBRATION GRAPH OF CRYSTAL
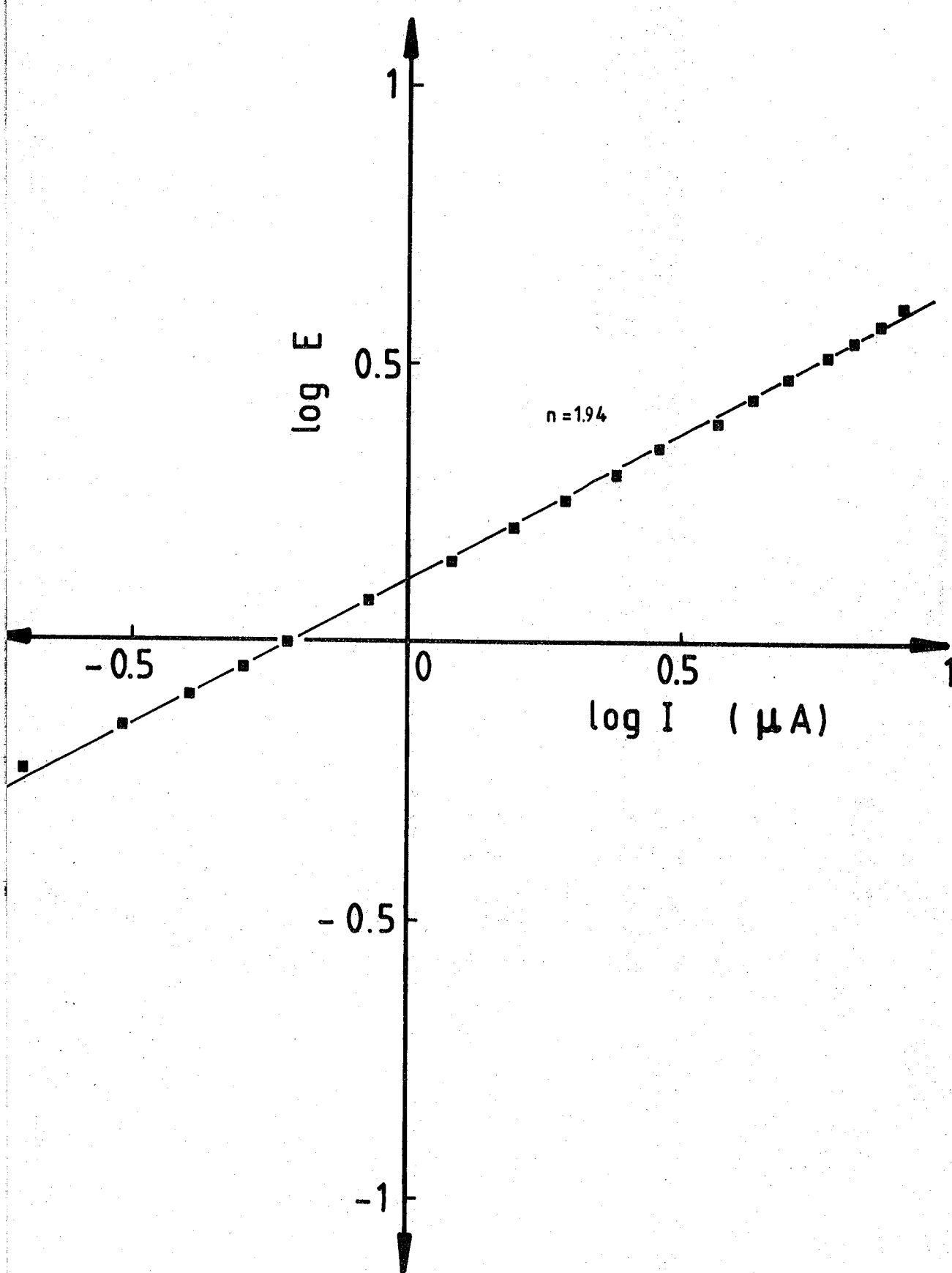DETECTOR AT 710 MHz; METHOD II

FIG.APP.4 DETERMINATION OF CRYSTAL
LAW AT 710 MHz; METHOD II

APPENDIX C   PERTURBATION THEORY

In an empty cavity the electric and magnetic fields are given by :

$$
\left\{
\begin{array}{l}
\bar{E} = \bar{E}_o \; e^{j\omega t} \\[3em]
\bar{H} = \bar{H}_o \; e^{j\omega t}
\end{array}
\right.
\qquad\qquad (AP.18)
$$

where $\bar{E}_o$ and $\bar{H}_o$ are function of positions. After introducing a small dielectric sample into the cavity, the fields and the resonant frequency are modified, thus

$$
\left\{
\begin{array}{l}
\bar{E}' = (\bar{E}_o + \bar{E}_1) \; e^{j(\omega+\delta\omega)t} \\[3em]
\bar{H}' = (\bar{H}_o + \bar{H}_1) \; e^{j(\omega+\delta\omega)t}
\end{array}
\right.
\qquad\qquad (AP.19)
$$

The Eqns. AP.18 and AP.19 are now substituted into the Maxwell's equations

$$
\text{curl } \bar{E} = - \frac{\partial \bar{B}}{\partial t}
\qquad\qquad (AP.20)
$$

which yields

$$
\text{curl } \bar{E}_o = - \frac{\partial \bar{B}_o}{\partial t} = - j\omega \bar{B}_o
$$

and

$$
\text{curl } (\bar{E}_o + \bar{E}_1) = - j(\omega + \delta\omega) \, (\bar{B}_o + \bar{B}_1)
$$

subtracting we get

$$
\text{curl } \bar{E}_1 = -j \left\{ \omega \bar{B}_1 + \delta\omega(\bar{B}_o + \bar{B}_1) \right\}
\qquad\qquad (AP.21)
$$

similarly from

$$\text{curl } \bar{H} = \frac{\partial \bar{D}}{\partial t} \tag{AP.22}$$

we get

$$\text{curl } \bar{H}_1 = j \left\{ \omega \bar{D}_1 + \delta\omega(\bar{D}_o + \bar{D}_1) \right\} \tag{AP.23}$$

Assuming that $\delta\omega\bar{D}_1$ and $\delta\omega\bar{B}_1$ are very small, using Eqns. AP.18, AP.21 and AP.23, it is obtained finally,

$$\bar{E}_o \cdot \text{curl } \bar{H}_1 + \bar{H}_o \cdot \text{curl } \bar{E}_1 = j\omega (\bar{E}_o \cdot \bar{D}_1 - \bar{H}_o \cdot \bar{B}_1) + j\delta\omega \left\{ (\bar{E}_o \cdot \bar{D}_o - \right.$$

$$\left. \bar{H}_o \cdot \bar{B}_o) + (\bar{E}_o \cdot \bar{D}_1 - \bar{H}_o \cdot \bar{B}_1) \right\} \tag{AP.24}$$

inside the sample

$$\bar{D}_1 = \varepsilon_o \left\{ \varepsilon_r (\bar{E}_o + \bar{E}_1) - \bar{E}_o \right\} \tag{AP.25}$$

using the vector identity,

$$\text{div} \left\{ (\bar{H}_o \times \bar{E}_1) + (\bar{E}_o \times \bar{H}_1) \right\} \equiv \bar{E}_1 \cdot \text{curl } \bar{H}_o - \bar{H}_o \cdot \text{curl } \bar{E}_1 +$$

$$\bar{H}_1 \cdot \text{curl } \bar{E}_o - \bar{E}_o \cdot \text{curl } \bar{H}_1 \tag{AP.26}$$

which, by virtue of Eqns. AP.20 and AP.22, may be written

$$\bar{H}_o \cdot \text{curl } \bar{E}_1 + \bar{E}_o \cdot \text{curl } \bar{H}_1 = j\omega (\bar{E}_1 \cdot \bar{D}_o - \bar{H}_1 \cdot \bar{B}_o) -$$

$$\text{div} \left\{ (\bar{H}_o \times \bar{E}_1) + (\bar{E}_o \times \bar{H}_1) \right\} \tag{AP.27}$$

Substituting Eqns. AP.27 into the left-hand side of Eqn. AP.24 gives,

$$j\omega\ (\bar{E}_1 \cdot \bar{D}_o - \bar{H}_1 \cdot \bar{B}_o) - \text{div} \left\{ (\bar{H}_o \times \bar{E}_1) + (\bar{E}_o \times \bar{H}_1) \right\} =$$

$$j\omega\ (\bar{E}_o \cdot \bar{D}_1 - \bar{H}_o \cdot \bar{B}_1) + j\delta\omega \left\{ (\bar{E}_o \cdot \bar{D}_o - \bar{H}_o \cdot \bar{B}_o) + (\bar{E}_o \cdot \bar{D}_1 - \bar{H}_o \cdot \bar{B}_1) \right\} \quad \text{(AP.28)}$$

Let v_o be the volume of the cavity and v_s the volume of the sample, then $(v_o - v_s)$ is the part of the cavity not occupied by the sample. Integrating Eqn. AP.28 over the volume v_o gives,

$$j\omega \int_{v_o} (\bar{E}_1 \cdot \bar{D}_o - \bar{H}_1 \cdot \bar{B}_o)\ d v - \int_{v_o} \text{div} \left[(\bar{H}_o \times \bar{E}_1) + (\bar{E}_o \times \bar{H}_1) \right] dv$$

$$= j\omega \int_{v_o} (\bar{E}_o \cdot \bar{D}_1 - \bar{H}_o \cdot B_1)\ d v + j\delta\omega \int_{v_o} \left[\bar{E}_o \cdot \bar{D}_o - \bar{H}_o \cdot \bar{B}_o) \right.$$

$$\left. + (\bar{E}_o \cdot \bar{D}_1 - \bar{H}_o \cdot \bar{B}_1) \right] dv \quad \text{(AP.29)}$$

For the divergence integral we have, by Green's theorem,

$$\int_{v_o} \text{div}\ (\bar{H}_o \times \bar{E}_1 + \bar{E}_o \times \bar{H}_1)\ dv = \int_{s_o} (\bar{H}_o \times \bar{E}_1 + \bar{E}_o \times \bar{H}_1) \cdot nds$$

where s_o is the surface of the cavity and n is the unit vector normal to the element ds of surface s_o. The cavity walls may be regarded as perfectly conducting, therefore $\bar{H}_o \times \bar{E}_1$ and $\bar{E}_o \times \bar{H}_1$ are tangential to the walls and their scalar product with n is zero. Thus the divergence integral vanishes. Since $\delta\omega$ is much smaller than ω, we can neglect $\bar{D}_1$

and $\bar{B}_1$ in the second integral on the right-hand side of Eqn. AP.29, i.e.

$$j\omega \int_{v_s} (\bar{E}_1 \cdot \bar{D}_0 - \bar{H}_0 \cdot \bar{B}_0) \, dv = j\omega \int_{v_s} (\bar{E}_0 \cdot \bar{D}_1 - \bar{H}_0 \cdot \bar{B}_1) \, dv +$$

$$j\delta\omega \int_{v_s} (\bar{E}_0 \cdot \bar{D}_0 - \bar{H}_0 \cdot \bar{B}_0) \, dv \qquad\qquad (AP.30)$$

$\bar{D}_1$ and $\bar{B}_1$ are small compared with $\bar{D}_0$ and $\bar{B}_0$, and therefore, from Eqn. AP.30

$$\frac{\delta\omega}{\omega} = \frac{\displaystyle\int_{v_s} \left\{ (\bar{E}_1 \cdot \bar{D}_0 - \bar{E}_0 \cdot \bar{D}_1) - (\bar{H}_1 \cdot \bar{B}_0 - \bar{H}_0 \cdot \bar{B}_1) \right\} \, dv}{\displaystyle\int_{v_0} (\bar{E}_0 \cdot \bar{D}_0 - \bar{H}_0 \cdot \bar{B}_0) \, dv} \qquad (AP.31)$$

On substitution of

$$\bar{D}_0 = \epsilon_0 \bar{E}_0, \quad \bar{D}_1 = \epsilon_r \bar{E}_1, \quad \bar{B}_0 = \mu_0 \bar{H}_0 \quad \text{and}$$

$$\bar{B}_1 = \mu_r \bar{H}_1 \quad \text{in eqn. AP.31 we get,}$$

$$\frac{\delta\omega}{\omega} = \frac{(\mu - \mu_0) \displaystyle\int_{v_s} \bar{H}_0 \bar{H}_1 \, dv - (\epsilon - \epsilon_0) \displaystyle\int_{v_s} \bar{E}_0 \bar{E}_1 \, dv}{2 \epsilon_0 \displaystyle\int_{v_0} |E_0|^2 \, dv} \qquad (AP.32)$$

Since in the denominator of Eqn. AP.31 $\bar{H}_0 \cdot \bar{H}_0 = - |H_0|^2$ the change of sign will occur. Also the maximum energies stored in the cavity in

the electric field and magnetic field are always equal, i.e.

$$\int_{V_o} \varepsilon |E_o|^2 \, dv = \int_{V_o} \mu |H_o|^2 \, dv$$

and since $\mu = \mu_o$ (sample is assumed non magnetic) and $\varepsilon = \varepsilon_r \varepsilon_o$ we obtain :

$$\frac{\delta \omega}{\omega} = - (\varepsilon_r - 1) \frac{\int_{V_s} \bar{E}_o \bar{E}_1 \, dv}{\int_{V_o} |\bar{E}_o|^2 \, dv} \tag{AP.33}$$

It is assumed that the field around the sample is uniform and then $\bar{E}_1$ is found from the knowledge of the sample geometry and $\bar{E}_o$. The magnitude of $\bar{E}_1$ in the sample as Sucher and Fox (100) point out in detail, depends on the shape of the sample. For the sample in the shape of a rod, located in the centre of the cavity where the electric field is maximum and parallel to the surface of the sample $|\bar{E}_1| = |\bar{E}_o|$ (98,100,104,132-133) and the electric field is continuous over the boundary.

Eqn. AP.33 is used for the calculation of $\frac{\delta \omega}{\omega}$. The complex angular ω associated with a dissipative system can be written as

$$\omega = \omega_r + j \, \omega_i \tag{AP.34}$$

where ω_r is the real and ω_i is the imaginary part of complex angular frequency. And $\omega_i \ll \omega_r$

Considering the expression

$$\frac{\delta \omega}{\omega} = \frac{\omega_1 - \omega_2}{\omega_1} \tag{AP.35}$$

where ω_1 is the unloaded angular resonant frequency and ω_2 is the resonant frequency of loaded cavity. Both ω_1 and ω_2 are complex. We assume that the change of resonant frequency of cavity, i.e. $\omega_1 - \omega_2$ is small, therefore, real parts of ω_1 and ω_2 are almost equal, $\omega_{r1} \simeq \omega_{r2}$. Expanding Eqn.AP.35 and considering all approximations, we get

$$\frac{\delta\omega}{\omega} = \frac{\left\{\omega_{r1} - \omega_{r2}\right\} + j\left\{\omega_{i1} - \omega_{i2}\right\}}{\omega_{r1} + j\omega_{i1}} \tag{AP.36}$$

$$= \frac{\left\{\omega_{r1} - \omega_{r2}\right\} + j\left\{\omega_{i1} - \omega_{i2}\right\}}{\omega_{r1}\left\{1 + j\dfrac{\omega_{i1}}{\omega_{r1}}\right\}}$$

$$= \frac{\left\{\omega_{r1} - \omega_{r2}\right\} + j\left\{\omega_{i1} - \omega_{i2}\right\}}{\omega_{r1}\left\{1 - j^2\dfrac{\omega_{i1}^2}{\omega_{r1}^2}\right\}}\left\{1 - j\,\dfrac{\omega_{i1}}{\omega_{r1}}\right\} \tag{AP.37}$$

Since $\left\{\dfrac{\omega_{i1}}{\omega_{r1}}\right\}^2$ <<1 it can be neglected from denominator of Eqn. AP.37

therefore

$$\frac{\delta\omega}{\omega} = \frac{\left\{\omega_{r1} - \omega_{r2}\right\} + j\left\{\omega_{i1} - \omega_{i2}\right\}}{\omega_{r1}}\left\{1 - j\,\dfrac{\omega_{i1}}{\omega_{r1}}\right\} \tag{AP.38}$$

Separating real and imaginary parts yield,

$$\frac{\delta\omega}{\omega} = \left[\frac{\omega_{r1} - \omega_{r2}}{\omega_{r1}} + j\left\{\frac{\omega_{i1}}{\omega_{r1}} - \frac{\omega_{i2}}{\omega_{r1}}\right\}\right]\left\{1 - j\,\frac{\omega_{i1}}{\omega_{r1}}\right\} \tag{AP.39}$$

Sucher and Fox (100) have represented the amount of Q_L,

$$Q_L = \frac{\omega_r}{2\omega_i} \qquad \text{(AP.40)}$$

substituting Eqn. AP.40 in Eqn. AP.39,

$$\frac{\delta\omega}{\omega} \simeq \left[\frac{f_1 - f_2}{f_1} + j\left\{\frac{1}{2Q_{L1}} - \frac{1}{2Q_{L2}}\right\}\right]\left\{1 - j\frac{1}{2Q_{L1}}\right\} \qquad \text{(AP.41)}$$

Since $\frac{1}{2Q_{L1}}$ can be neglected compared with unity

$$\frac{\delta\omega}{\omega} \simeq \frac{f_1 - f_2}{f_1} + \frac{j}{2}\left\{\frac{1}{Q_{L1}} - \frac{1}{Q_{L2}}\right\} \qquad \text{(AP.42)}$$

or

$$\frac{\delta\omega}{\omega} \simeq \frac{\Delta f}{f_1} + \frac{j}{2}\left\{\frac{1}{Q_{L1}} - \frac{1}{Q_{L2}}\right\} \qquad \text{(AP.43)}$$

where Q_{L1} and Q_{L2} are the loaded and unloaded quality of the cavity. On substituting of Eqn. AP.43 in Eqn. AP.33, yields,

$$\frac{\Delta f}{f_o} + \frac{j}{2}\left\{\frac{1}{Q_{L1}} - \frac{1}{Q_{L2}}\right\} = \frac{-(\epsilon_r - 1)\displaystyle\int_{v_s} \bar{E}_o \bar{E}_1 \, dv}{2\displaystyle\int |\bar{E}_o|^2 \, dv} \qquad \text{(AP.44)}$$

Since $\epsilon_r = \epsilon' - j\epsilon''$ Eqn. AP.44 on integration can be reduced to,

$$\frac{\Delta f}{f_o} = -2(\epsilon' - 1)\frac{v_s}{v_o} \qquad \text{(AP.45)}$$

and

$$\Delta\left(\frac{1}{Q}\right) = 4\epsilon''\frac{v_s}{v_o} \qquad \text{(AP.46)}$$

APPENDIX D   COMPARISON METHOD

In earlier descriptions of the slotted-line technique, we have talked and discussed in detail about the uncertainties in measuring ε' and ε'' of a solid material. All possible errors which might occur were explained in section 5.1.4, and suggestions were made in order to get more accurate results and avoid the above mentioned errors.

The major difficulty was measuring high VSWR and consequently $|\rho|$. Other difficulties can be overcome by modifications on the slotted line or using more accurate and sophisticated instruments. The problem of measuring high VSWR still remained and therefore, attempts have been made to reduce its magnitude. This was done using a different method which may be called "Comparison Method".

In this technique ideally the transmission-line (slotted-line) is assumed to be terminated with a resistor equal to the characteristic impedance of the line, Z_0, and a crystal whose dielectric properties are going to be determined is mounted in a sample holder. The equivalent circuit may be represented with a resistance Z_0 and a capacitance in series as in Fig.APP.5. The total impedance of the sample, Z_s associated with Z_0 can be written as

$$Z_s = Z_0 + j\, X_s \qquad\qquad (AP.47)$$

where X_s is the reactance component of crystal equal to $\left\{ -\dfrac{1}{C_s \omega} \right\}$
then,

$$Z_s = Z_0 - \dfrac{j}{C_s \omega} \qquad\qquad (AP.48)$$

Substituting capacitance of the sample, $C_s = \varepsilon_0 (\varepsilon' - j\, \varepsilon'')\, \dfrac{A}{d}$ in Eqn.AP.48

results in

$$Z_s = Z_o - \frac{jd}{\varepsilon_o(\varepsilon'-j\varepsilon'')\frac{A}{d}\omega}$$

(AP.49)

$$= Z_o - \frac{jd(\varepsilon'+j\varepsilon'')}{\varepsilon_o A\omega(\varepsilon'^2+\varepsilon''^2)}$$

where

    d = thickness of the specimen (cm)

    A = area of inner conductor (cm^2)

    ω = angular frequency   (rad s^{-1})

Separating real and imaginary terms on the left-hand side in Eqn. AP.(49) gives

$$Z_s = Z_o + \frac{\varepsilon''d}{\varepsilon_o A\omega(\varepsilon'^2+\varepsilon''^2)} - \frac{j\varepsilon'd}{\varepsilon_o A\omega(\varepsilon'^2+\varepsilon''^2)}$$

(AP.50)

It can be seen that the X_s contains two terms ; first resistive term which involves ε'' (loss factor) and second, capacitance term which involves ε'.

Now, removing crystal the equivalent circuit is as in Fig.APP.6 The total impedance of the air gap and Z_o can be given as

$$Z_a = Z_o + jX_a$$

(AP.51)

with $X_a = - \frac{1}{C_a\omega}$ reactance of air gap. Putting capacitance value of the air gap, C_a,

$$C_a = \varepsilon_o \frac{A}{d}$$

(AP.52)

and Eqn. AP.51 results in

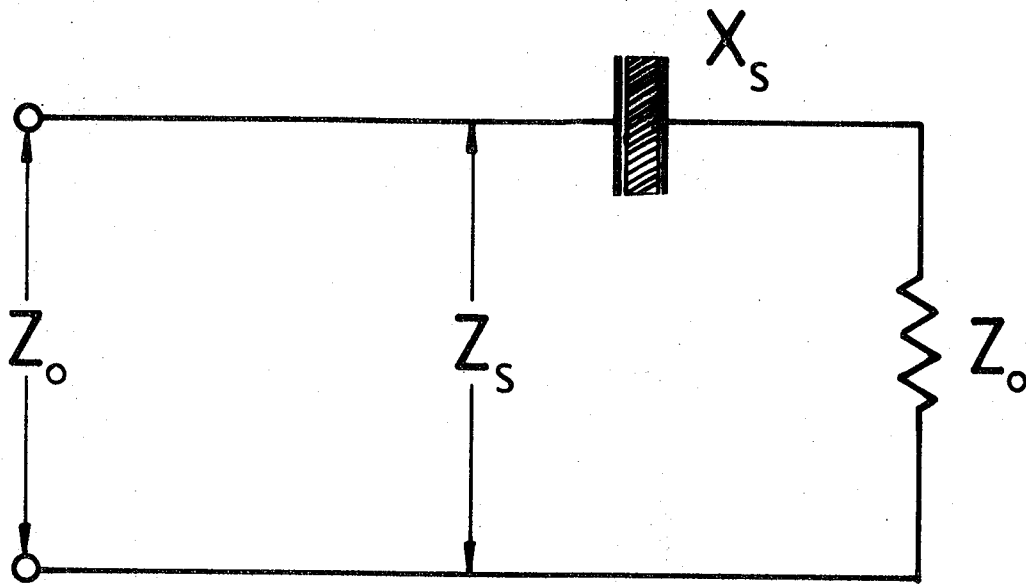$$Z_a = Z_o - \frac{jd}{\varepsilon_o \omega A}$$

(AP.53)

FIG.APP.5   EQUIVALENT CIRCUIT OF
TERMINATION AND SAMPLE.
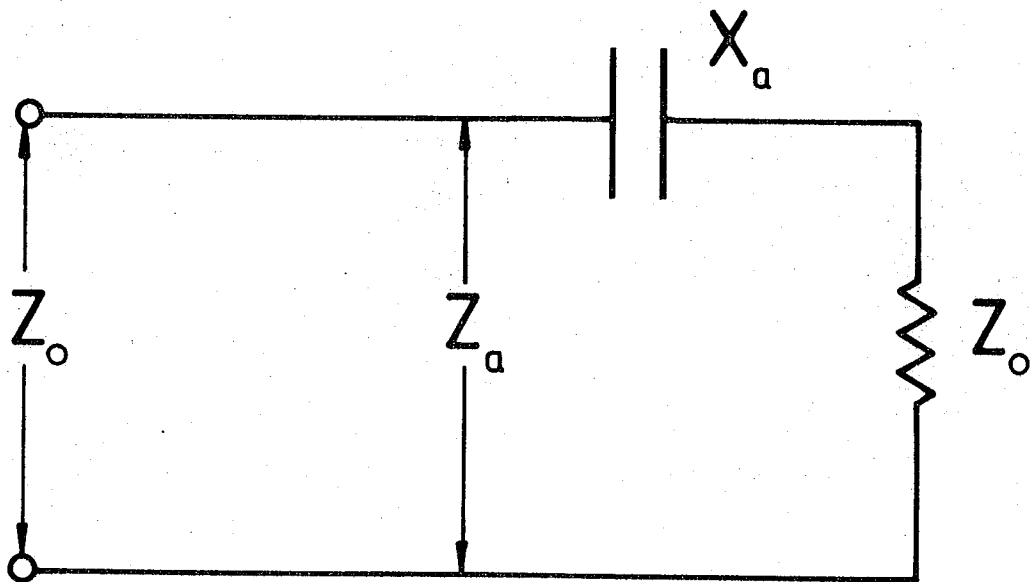

FIG.APP.6   EQUIVALENT CIRCUIT OF
TERMINÂTION AND AIR GAP.

As expected Z_a has resistive component (Z_o) and reactive component due to air gap which has no resistive component, i.e. there is no energy loss in the air gap.

In general the reflection coefficient, $|\rho|$ of any arbitrary impedance, Z_L, terminating the transmission-line is given by,

$$|\rho| \; e^{j\theta} = \frac{Z_L - Z_o}{Z_L + Z_o} \qquad \text{(AP.54)}$$

where, $|\rho|$ is the magnitude of reflection coefficient and θ is equal to its phase angle. Therefore the reflection coefficient for an air gap is given by,

$$|\rho|_a \; e^{j\theta_a} = \frac{-jd}{2Z_o \omega \varepsilon_o A - jd} \qquad \text{(AP.55)}$$

and similarly the reflection coefficient for a crystal is given by,

$$|\rho_s| \; e^{j\theta_s} = \frac{(\varepsilon'' - j\varepsilon')d}{2Z_o \varepsilon_o A\omega(\varepsilon'^2 + \varepsilon''^2) + (\varepsilon'' - j\varepsilon')d} \qquad \text{(AP.56)}$$

The Eqns. AP.55 and AP.56 can be simplified as follows :

$$|\rho_a| \; e^{j\theta_a} = \frac{-j}{\dfrac{2Z_o \omega \varepsilon_o A}{d} - j} \qquad \text{(AP.57)}$$

and

$$|\rho_s| \; e^{j\theta_s} = \frac{1}{\dfrac{2Z_o \omega \varepsilon_o A}{d}(\varepsilon'' + j\varepsilon') + 1} \qquad \text{(AP.58)}$$

assuming $\dfrac{Z_o \omega \varepsilon_o A}{d} = a$ they become

$$|\rho_a|\, e^{j\Theta_a} = \frac{-j}{2a-j} \qquad\qquad (AP.59)$$

and

$$|\rho_s|\, e^{j\Theta_s} = \frac{1}{2a(\varepsilon''+j\varepsilon') + 1} \qquad\qquad (AP.60)$$

dividing AP.59 by AP.60 gives,

$$\frac{|\rho_a|}{|\rho_s|}\, e^{j(\Theta_a-\Theta_s)} = \frac{(2a\varepsilon''+1) + j\, 2a\varepsilon'}{2a - j}\ (-j) \qquad (AP.61)$$

or

$$\frac{|\rho_a|}{|\rho_s|}\, e^{j(\Theta_a-\Theta_s)} = \frac{\left[(2a\varepsilon''+1)^2+(2a\varepsilon')^2\right]^{\frac{1}{2}}}{\left[(2a)^2 + 1\right]^{\frac{1}{2}}}\ e^{\,j\left\{\tan^{-1}\frac{2a\varepsilon'}{2a\varepsilon''+1} - \frac{\pi}{2} +\tan^{-1}\frac{1}{2a}\right\}}$$

$$(AP.62)$$

From Eqn.AP.62 we deduce $\dfrac{|\rho_a|}{|\rho_s|}$ and $(\Theta_a-\Theta_s)$ as,

$$\left\{\frac{|\rho_a|}{|\rho_s|}\right\}^2 = \frac{(2a\,\varepsilon''+1)^2+(2a\,\varepsilon')^2}{(2a)^2 + 1} \qquad\qquad (AP.63)$$

and

$$\Theta_a-\Theta_s = \tan^{-1}\frac{2a\varepsilon'}{2a\varepsilon''+1} - \frac{\pi}{2} + \tan^{-1}\frac{1}{2a} \qquad (AP.64)$$

Solving these two equations in terms of (a) and constants, the
magnitudes of ε' and ε'' are found, i.e.

$$\varepsilon' = \frac{\left\{\frac{|\rho_a|}{|\rho_s|}\right\}(4a^2+1)^{\frac{1}{2}}\left[\tan(\Theta_a-\Theta_s+\frac{\pi}{2}-\tan^{-1}\frac{1}{2a})\right]}{2a\left\{1+\left[\tan(\Theta_a-\Theta_s+\frac{\pi}{2}-\tan^{-1}\frac{1}{2a})\right]^2\right\}^{\frac{1}{2}}} \qquad \text{(AP.65)}$$

and

$$\varepsilon'' = \frac{\left\{\frac{|\rho_a|}{|\rho_s|}\right\}(4a^2+1)^{\frac{1}{2}}}{2a\left\{1+\left[\tan(\Theta_a-\Theta_s+\frac{\pi}{2}-\tan^{-1}\frac{1}{2a})\right]^2\right\}^{\frac{1}{2}}} - \frac{1}{2a} \qquad \text{(AP.66)}$$

Having knowledge of $|\rho_a|$, $|\rho_s|$ and $(\Theta_a-\Theta_s)$ from measurements,
the magnitudes of ε' and ε'' can be determined.

In practice the slotted-line is terminated with a characteristic
impedance Z_o (50 Ω) and this is used as the reference. Then an insertion
unit (e.g. Type 874-X) into which the sample can be introduced connected
between the termination and the slotted-line. The insertion unit can be
specially designed if needed. Such an insertion unit may have some stray
inductive and capacitive effects which would change the terminating
characteristic impedance. In order to overcome this, a three stub tuner
can be used to obtain the required match and hence standing wave ratio
of 1. This requires a great accuracy and its tuning must be precise.

This technique was not used in our project although from some
limited tests carried out it appeared to be   easy to use because of
lower VSWR's.

This method is especially useful in measuring dielectric prop-
erties of low loss materials.

To develop this method in order to get good results requires
extreme precision in making the insertion unit and using instruments.

REFERENCES

132.   Labuda, E.F. and Le Craw, R.C, Bell Telephone Laboratories

Incorp, Murray Hill, New Jersey (1961).

133.   Marcuvitz, N. (Ed), 'Waveguide Handbook', M.I.T. Radiation

Laboratories Series, Vol.10, New York, McGraw-Hill (1951).

PUBLICATIONS

'THE DIELECTRIC BEHAVIOUR OF SINGLE CRYSTAL MgO, Fe/MgO

AND Cr/MgO'

Journal of Materials Science - accepted for publication